Sediment storage in the Upper Rhone Valley, Switzerland

Dissertation

zur

Erlangung des Doktorgrades (Dr. rer. nat.)

der

Mathematisch-Naturwissenschaftlichen Fakultät

der

Rheinischen Friedrich-Wilhelms-Universität Bonn

vorgelegt von

Anna Fides Schoch-Baumann

aus Bietigheim-Bissingen

Bonn, Mai 2021

Angefertigt mit Genehmigung der Mathematisch-Naturwissenschaftlichen Fakultät der Rheinischen Friedrich-Wilhelms-Universität Bonn

1. Gutachter: Prof. Dr. Lothar Schrott

2. Gutachter: Jun.-Prof. Dr. Jan H. Blöthe

Tag der Promotion: 12.10.2021

Erscheinungsjahr: 2022

Acknowledgments

During the years of my PhD I was lucky to have the support of many people, including all my colleagues and friends from the Department of Geography at the University of Bonn, who all helped me and contributed to finishing this big project. I am glad so many of you were there to always ask the right questions, push me a bit further, discuss seemingly unsolvable problems and let me know that this can (still) be done.

First of all, I want to thank my supervisors Lothar Schrott and Jan Blöthe, who always acknowledged my work, believed in my ideas and challenged me not give up and finish my thesis.

I thank the Geomorphology and Environmental Systems research group, the British Society for Geomorphology and the Gesellschaft für Erdkunde zu Berlin for funding my research and field work, as well as the IDIP4all funding by the DAAD and the University of Bonn and the Arbeitskreis Geomorphologie for funding several conference visits during the course of my PhD.

A big (huge!) thank you goes to my dear research colleagues of the Geomorphology and Environmental Systems research group Thomas Hoffmann, Chris Halla, Simon Terweh, Tamara Köhler, Melanie Stammler, Gabriele Kraus, Nora Schneevoigt, Rainer Bell & Réné Kusdian for uncountable coffee and lunch breaks, support in the field, words of advice whenever needed, proof reading of papers and this work and some after work beers. I definitely could not have done any of this without you!

Manfred, Simone and Sonja – my colleagues from the department's administration – I cannot say how thankful I am for having had the opportunity to finish my dissertation in 2021. This would not have been possible without your urging, your creative way of giving me so much time and taking on all of my "every-day" tasks. This is still unbelievable!

I acknowledge all my co-authors Henry Munack, Thomas Hoffmann, Jens Hornung, Alexandru T. Codilean, Réka-H. Fülöp and Klaus Wilcken from whom I have learned a lot during the last years. A special thank you goes to Christoph Holst and Stefan Winkler, who gave me the opportunity to be part of their research projects and to co-author papers with them.

Thanks for the support and your hard work during field and lab work: Gerrit Heinmüller, Thomas Baumann, Nicola Schulte-Kellinghaus, Marcel Marx, Philipp Oeynhausen, Lorenz Banzer and all the students of my project seminar "Sediment dynamics in alpine geomorphic systems". I hope that Swiss cheese, chocolate and beer made up a little bit for all the sweat and sore muscles.

Last, but not least, I have to express my sincere gratitude to my family and friends who supported me in the last years, brought joy and love to my life every day and were always there for me.

Contents

Summary

High-mountain areas feature the largest potential energy gradients and are thus characterized by the highest sediment fluxes. Besides a large potential for erosion and transport, also vast amounts of sediment are stored in this environment on all spatial scales. These sediment storages are mostly of Postglacial age. Pleistocene glaciations led to the depletion of already stored sediment, transport of the material to the alpine foreland and further bedrock erosion. They left behind a system with "empty" sediment sinks, but at the same time a high availability of unconsolidated sediment.

Today, unconsolidated and potentially transportable sediment covers large shares of high-mountain areas. Investigating these storages is of utmost importance, since mountains cover one fourth of the Earth's terrestrial surface and are home to more than 10% of the global population. Nonetheless, little is known about the distribution, volumes, morphology and residence time of sediment storages. Triggers, such as strong rainfall, snowmelt or earthquakes, can cause rapid changes in sediment storage including erosion and deposition. Hence, sediment storages often rather boost than buffer extreme sediment transport and consequently pose a hazard to human society and infrastructure.

Due to often pointed out (up-)scaling issues in sediment budget studies and geomorphology in general, knowledge on sediment storages on larger scales is restricted. Several studies focus on sediment storage in smaller scale catchments (mostly up to 10^2 km^2) and emphasize their (long-term) importance. In contrast, larger scale studies mostly concenter on macro-scale sediment storages (e.g. valley fills), hence, neglecting the relevance of headwater sediment storage. In this thesis, I approach the problem of transferring knowledge and bridging the gap between different scales, by applying multiple methods on multiple scales in the large catchment of the Upper Rhone, Switzerland. I contribute to this aim with the ensuing objectives: (1) understanding and analyzing the formation of Postglacial landforms on the small scale, (2) investigating the landform assemblage in medium-sized tributaries within the Upper Rhone Basin, and (3) creating scale linkages for sediment distribution between smaller scales and a large catchment scale through a hierarchical upscaling.

On the small scale, three outsize fans, which are strikingly large fans with unlikely small feeder basins, are investigated to contribute to the gradualism vs. catastrophism debate in outsize fan formation, and therefore to a better quantitative understanding of these landforms and their effect on larger spatial scales. Morphometric analysis of the fans and their source areas, geophysical surveys of the subsurface material and cosmogenic radionuclide exposure dating are combined in a multi-method approach. This approach is used to quantify the volume of sediment eroded from feeder catchments and stored in the fans, to analyze the surface morphology of the fans and their source areas, to investigate the internal structure of one outsize fan and its interfingering with the underlying valley fill, as well as to determine its onset and period of formation. Outsize fan formation in the Upper Rhone valley was rapid, but incremental and non-catastrophic. In a first phase, beginning soon after deglaciation around 10.0 ka and terminating after full development of the feeder basin ~6.0 ka, the largest part of the fan was deposited through high-energy, high-magnitude debris flow processes with average yields of up to 73 kt km^{-2} yr^{-1}. In a second phase, lower-magnitude debris flows deposited a second sedimentary facies across the initial fan deposit. Over time, erosion and sedimentation rates strongly lessened, eventuating in a third phase, starting ~0.8 ka, with very limited geomorphic activity. Due to the initial delivery of extremely high sediment amounts to the main Rhone valley, where the outsize fans occupy the full valley width, they have a potent influence on sediment transfer, storage and therefore landscape evolution on a larger scale.

On the regional scale, the aims are to investigate sediment storage with a geomorphic mapping approach in five key sites, Goms, Lötschental, Turtmanntal, Val de la Liène and Val d'Illiez, and to map and geomorphometrically analyze sedimentary fans in the whole Upper Rhone catchment. Both approaches yield at bridging the gap between the regional and the large catchment scale. Overall, 360.3 km^{2} of sediment and bedrock cover, or 6.7% of the Upper Rhone catchment area, is mapped within the five key sites. For the Goms, Lötschental and Turtmanntal detailed sediment storage maps are created. Furthermore, 186 sedimentary fans are mapped from digital topographic data and remote sensing imagery. Morphometric analysis reveals the outstanding ratio between fan and catchment area for outsize fans. Both large datasets serve as valuable contributions in the upscaling approach. Geomorphic mapping proves to be a useful technique in sediment storage analysis on the regional scale.

On the large catchment scale, the Upper Rhone Basin, the aim is to investigate the spatial sediment distribution in great detail. This is achieved, through modeling the spatial distribution of sediment cover using a combined field-based and statistical modeling approach. Moreover, the quality of the model outcome and the effects of input data on this in a large scale geomorphic system is analyzed. The modeling results are interpreted in a geomorphic context with respect to the general pattern and the topographic position of sediment storages, the relevance of sediment storage in recently deglaciated areas as well as the spatial variability of sediment storage on different scales. Best prediction results with an excellent performance and both, a high spatial and non-spatial transferability, are achieved with a generalized additive model. Sediments cover 53.5 ± 21.7% of the land surface in the Upper Rhone catchment. However, the spatial distribution is by no means even. Small headwaters (< 5 km^{2}) feature a very strong variability in sediment coverage. While some are fully blanketed with sediments, sediment cover is quasi absent in others. More than 90% of the sediment cover is located outside the main valley, where the macro-scale sediment storages are situated. The majority of sediment cover account for a significant part of the sediment stored in large-scale

catchments (very conservative estimates: up to 16%), thus highlighting the importance of sediment storage in low-order catchments and headwaters.

Based on my observations, results and in-depth discussion of collected data from different spatial scales, I conclude that geomorphic systems have a nested hierarchical structure (de Boer, 1992). I utilize this structure to transfer knowledge on sediment storages to larger scales in the Upper Rhone catchment, resulting in a detailed analysis of all sediment storages in this geomorphic system. Each examined spatial scale has certain strengths and discernible properties of sediment storage. Qualitative and quantitative linkages to the higher scale are identified and applied. This is synthesized in a framework for resolving scaling issues in sediment storage analysis comprising conceptual and applied notions: (1) ordering the investigated systems and thinking across scales, (2) finding and identifying the linkages between scales, (3) applying a multi-scale and multi-method approach, (4) bringing together spatial scales – process, observation and modeling, (5) incorporating existing data, as well as (6) acknowledging the important role of high-resolution data and computational power. This framework is intended to serve as a guiding concept for further large-scale sediment storage analysis.

Zusammenfassung

Hochgebirgsregionen weisen die größten, potentiellen Energiegefälle auf und sind daher durch die höchsten Sedimentflüsse gekennzeichnet. Neben dem großen Potential für Erosion und Transport, werden in diesen Gebieten auch enorme Mengen an Sediment auf allen räumlichen Skalen gespeichert. Diese Sedimentspeicher sind meist Postglazialen Alters. Pleistozäne Vergletscherungen führten zur Entleerung von bereits bestehenden Speichern, zum Transport von Material ins Alpenvorland und zu weiterer Erosion von Festgestein. Zurück blieb ein System mit „leeren" Sedimentsenken und gleichzeitig einer hohen Verfügbarkeit von Lockersedimenten.

Nicht konsolidierte und potenziell transportierbare Sedimente bedecken heutzutage große Teile der Hochgebirgsregionen. Die Untersuchung dieser Speicher ist von größter Bedeutung, da Bergregionen ein Viertel der Erdoberfläche bedecken und mehr als 10 % der Weltbevölkerung beherbergen. Über Verteilung, Volumen, Morphologie und Verweilzeit von Sedimentspeichern ist jedoch wenig bekannt. Auslöser wie Starkregen, Schneeschmelze oder Erdbeben können zu schnellen Erosion oder Ablagerung der Sedimentspeicher führen. Sedimentspeicher fördern daher häufig eher extremen Sedimenttransport als ihn abzuschwächen und stellen folglich eine Gefahr für die menschliche Gesellschaft und Infrastruktur dar.

Aufgrund der häufig dargelegten (Hoch-)Skalierungsprobleme in Studien zu Sedimentbudgets und der Geomorphologie im Allgemeinen ist das Wissen über Sedimentspeicher auf größeren Skalen begrenzt. Mehrere Studien konzentrieren sich auf die Speicherung von Sedimenten in kleineren Einzugsgebieten (meist bis zu 10^2 km^2) und betonen deren (langfristige) Bedeutung. Im Gegensatz dazu konzentrieren sich groß-skalig angelegte Studien hauptsächlich auf makro-skalige Sedimentspeicher (z. B. Talfüllungen), wobei die Relevanz der Sedimentspeicherung im Quellgebiet vernachlässigt wird. In dieser Arbeit gehe ich auf das Problem des Wissenstransfers und der Schließung der Kluft zwischen verschiedenen Skalen ein, indem ich im Einzugsgebiet der Oberen Rhone in der Schweiz mehrere Methoden auf unterschiedlichen Skalen anwende. Ich trage hierzu mit den folgenden Zielen bei: (1) Verständnis und Analyse der Bildung Postglazialer Landformen auf der kleinen Skale, (2) Untersuchung der Anordnung von geomorphologischen Formen in mittelgroßen Nebenflüssen im Oberen Rhone Einzugsgebiet und (3) Schaffung von Skalenverknüpfungen im Bereich der Sedimentverteilung zwischen kleineren Skalen und einer großen Einzugsgebietsskala durch hierarchische Hochskalierung.

Auf der kleinen Skale werden drei übergroße Fächer untersucht, bei denen es sich um auffallend große Fächer mit unpassend kleinen Zulieferungsgebieten handelt, um zur Debatte ‚Gradualismus versus Katastrophismus' bei der Entstehung übergroßer Fächer beizutragen. Darüber hinaus wird ein Beitrag

zu einem besseren quantitativen Verständnis dieser geomorphologischen Formen und ihrer Auswirkungen auf größere räumliche Skalen geleistet. Eine morphometrische Analyse der Fächer und ihrer Einzugsgebiete, geophysikalische Untersuchungen des Untergrundmaterials und die kosmogene Radionuklid-Expositionsdatierung werden in einem Multi-Methoden-Ansatz kombiniert. Dieser Ansatz wird verwendet, um das Volumen des Sediments zu quantifizieren, das aus den Einzugsgebieten erodiert und in den Fächern gespeichert wurde, um die Oberflächenmorphologie der Fächer und ihrer Zulieferungsgebiete zu analysieren, um die interne Struktur eines übergroßen Fächers und dessen Verzahnung mit der darunterliegenden Talfüllung zu untersuchen sowie um den Beginn und die Dauer der Entstehung zu bestimmen. Die Entstehung der übergroßen Fächer im Oberen Rhonetal verlief sehr schnell, aber schrittweise und nicht katastrophal. In einer ersten Phase, die kurz nach der Enteisung um 10,0 ka begann und nach der vollständigen Anlage des Einzugsgebiets ~6,0 ka endete, wurde der größte Teil des Fächers durch hochenergetische Murgangprozesse großer Magnitude abgelagert. Durchschnittliche Sedimentaustragsraten von bis zu 73 kt km^{-2} yr^{-1} wurden erreicht. In einer zweiten Phase lagerten Murgänge geringerer Magnitude eine zweite Sedimentfazies über den initialen Fächer ab. Im Laufe der Zeit nahmen die Erosions- und Sedimentationsraten stark ab und resultierten in einer dritten Phase, beginnend ~0,8 ka, mit sehr eingeschränkter geomorphologischer Aktivität. Aufgrund der anfänglichen Lieferung extrem hoher Sedimentmengen in das Rhonetal, in dem die übergroßen Fächer die gesamte Talbreite einnehmen, haben sie einen starken Einfluss auf den Sedimenttransfer, die Speicherung und damit die Landschaftsentwicklung auf größeren Skalen.

Auf regionaler Skale besteht das Ziel darin, die Sedimentspeicherung mit einem geomorphlogischen Kartierungsansatz an fünf Schlüsselstandorten Goms, Lötschental, Turtmanntal, Val de la Liène und Val d'Illiez zu untersuchen und Sedimentfächer im gesamten Oberen Rhone-Einzugsgebiet zu kartieren und geomorphometrisch zu analysieren. Beide Ansätze zielen auf eine Schießung der Kluft zwischen der regionalen und der großen Einzugsgebiets-Skale ab. Insgesamt werden 360,3 km^2 Sediment- und Festgesteinsbedeckung oder 6,7 % des Einzugsgebiets der Oberen Rhone innerhalb der fünf Schlüsselstandorte kartiert. Für das Goms, das Lötschental und das Turtmanntal werden detaillierte Sedimentspeicherkarten erstellt. Darüber hinaus werden 186 Sedimentfächer aus digitalen topographischen Daten und Fernerkundungsbildern kartiert. Die morphometrische Analyse zeigt das auffällige Fächer-Einzugsgebiet-Verhältnis für übergroße Fächer. Beide großen Datensätze dienen als wertvolle Beiträge für den Hochskalierungsansatz. Die geomorphologische Kartierung erweist sich als nützliche Methode bei der Analyse der Sedimentspeicherung auf regionalen Skalen.

Auf der großen Einzugsgebiets-Skale, dem Einzugsgebiet der Oberen Rhone, soll die räumliche Sedimentverteilung detailliert untersucht werden. Dies wird durch die Modellierung der räumlichen Verteilung der Sedimentbedeckung mithilfe eines kombinierten feldbasierten und statistischen Modellierungsansatzes erreicht. Darüber hinaus werden die Qualität des Modellergebnisses und die

Auswirkungen von Eingangsdaten auf dieses in einem großen, geomorphologischen System analysiert. Die Modellierungsergebnisse werden in einem geomorphologischen Kontext mit Bezug auf das allgemeine Verteilungsmuster und die topographische Position von Sedimentspeichern, die Relevanz der Sedimentspeicherung in kürzlich entgletscherten Gebieten sowie die räumliche Variabilität der Sedimentspeicherung auf verschiedenen Skalen interpretiert. Die besten Vorhersageergebnisse mit einer hervorragenden Leistung und sowohl einer hohen räumlichen als auch einer nicht-räumlichen Übertragbarkeit werden mit einem Generalized Additive Model erzielt. Sedimente bedecken 53,5 ± 21,7 % der Landoberfläche im Einzugsgebiet der Oberen Rhone. Die räumliche Verteilung ist jedoch keineswegs gleichmäßig. Kleine Quellgebiete (< 5 km^2) weisen eine sehr starke Variabilität der Sedimentbedeckung auf. Während einige vollständig mit Sedimenten bedeckt sind, fehlt bei anderen die Sedimentbedeckung quasi komplett. Mehr als 90 % der Sedimentbedeckung befinden sich außerhalb des Haupttals, wo sich die makro-skaligen Sedimentspeicher befinden. Der Großteil der Sedimentbedeckung macht einen erheblichen Teil des in großen Einzugsgebieten gespeicherten Sediments aus (sehr konservative Schätzungen: bis zu 16 %), was die Bedeutung der Sedimentspeicher in Einzugsgebieten niedriger Ordnung und Quellgebieten unterstreicht.

Basierend auf meinen Beobachtungen, Ergebnissen und der eingehenden Diskussion gesammelter Daten von verschiedenen räumlichen Skalen schließe ich, dass geomorphologische Systeme eine verschachtelte hierarchische Struktur haben (de Boer, 1992). Ich nutze diese Struktur, um Wissen über Sedimentspeicher im großen Einzugsgebiet der Oberen Rhone auf höhere räumliche Skalen zu übertragen, was zu einer detaillierten Analyse aller Sedimentspeicher in diesem geomorphologischen System führt. Jede untersuchte räumliche Skale weist bestimmte Stärken und erkennbare Eigenschaften der Sedimentspeicherung auf. Qualitative und quantitative Verknüpfungen mit der höheren Skala werden identifiziert und angewendet. Dies wird in einem Rahmenkonzept zur Lösung von Skalierungsproblemen in der Sedimentspeicheranalyse zusammengefasst, das konzeptionelle und angewandte Ideen umfasst: (1) Ordnen der untersuchten Systeme und Denken über Skalen hinweg, (2) Finden und Identifizieren der Skalenverknüpfung, (3) Anwenden eines Multi-Skalen- und Multi-Methoden-Ansatzes, (4) Zusammenführen von räumlichen Skalen – Prozess, Beobachtung und Modellierung, (5) Einbeziehen vorhandener Daten sowie (6) Erkennen der wichtigen Rolle hochauflösender Daten und Rechenleistung. Dieses Rahmenkonzept soll als Leitlinie für weitere Sedimentspeicheranalysen auf großen räumlichen Skalen dienen.

List of Publications

Holst, C., Janßen, J., Schmitz, B., Blome, M., Dercks, M., Schoch-Baumann, A., Blöthe, J. H., Schrott, L., Kuhlmann, H. & Medic, T. (2021): Increasing spatio-temporal resolution for monitoring alpine solifluction using terrestrial laser scanners and 3D vector fields. Remote Sensing, 13(6), 1192.

DOI: https://doi.org/10.3390/rs13061192

Schoch-Baumann, A., Blöthe, J. H., Munack, H., Hornung, J., Codilean, A. T., Fülöp, R.-H., & Schrott, L. (2022): Postglacial outsize fan formation in the Upper Rhone Valley, Switzerland – gradual or catastrophic? Earth Surface Processes and Landforms, 47(4), 1032-1053.

DOI: https://doi.org/10.1002/esp.5301

The published article is reproduced in chapter 5 of the dissertation.

Schoch, A., Blöthe, J. H., Hoffmann, T., & Schrott, L. (2018): Multivariate geostatistical modeling of the spatial sediment distribution in a large scale drainage basin, Upper Rhone, Switzerland. Geomorphology, 303, 375-392.

DOI: https://doi.org/10.1016/j.geomorph.2017.11.026

The published article is reproduced in chapter 7 of the dissertation.

Winkler, S., Bell, D., Hemmingsen, M., Pedley, K. L., & Schoch, A. (2018): Disestablishing “Glacial Lake Speight”, New Zealand? An example for the validity of detailed geomorphological assessment with the study of mountain glaciations. E&Q Quaternary Science Journal, 67, 25-31.

DOI: https://doi.org/10.5194/egqsj-67-25-2018

List of Figures

List of Tables

List of Abbreviations

ACCLOG	Size of the contributing area
ACCSLP	Mean slope gradient of the contributing area
AIK	Akaike Information Criterion
AMS	Accelerator mass spectrometry
ASP	Aspect
ASP_EW	East-exposedness
ASP_NW	North-exposedness
AUROC	Area under the receiver operating characteristics curve
CMP	Common midpoint measurements
CRN	Cosmogenic radionuclide
CUR	Curvature
DEM	Digital elevation model
D-GPS	Differential global positioning system
DOI	Depth of investigation index
ERT	Electrical resistivity tomography
FN	False negatives
FP	False positives
GAM	Generalized additive model
GOF	Goms outsize fans
GPR	Ground penetrating radar
HI	Hypsometric index
IC	Index of connectivity
IQR	Interquartile range
LGM	Last Glacial Maximum
LIA	Little Ice Age

LR	Logistic regression model
NDR	Normalized distance to ridge
NDVI	Normalized difference vegetation index
OSL	Optically stimulated luminescence
PC	Principal component
PCA	Principal component analysis
PCLR	Principal component logistic regression model
PLC	Plan curvature
PRC	Profile curvature
REL	Local relief
ROU	Roughness
SCM	Surface classification model after Bowles and Cowgill (2012)
SD	Standard deviation
SLP	Slope gradient
SR	Solar radiation
SSY	Specific sediment yield
TL	Thermoluminescence
TN	True negatives
TNR	True negative rate
TP	True positives
TPI	Topographic position index
TPR	True positive rate
TSP	Topographic slope position
TWI	Topographic wetness index
URB	Upper Rhone Basin
VDC	Vertical distance to channel network
VF	Variable selection frequency

VIF	Variance inflation factor

1 Introduction

Featuring the largest potential energy gradients, high-mountain areas are characterized by the highest sediment fluxes (Barsch and Caine, 1984; Milliman and Syvitski, 1992; Church, 2010a). However, not only erosion and sediment fluxes are high, also the potential for sediment storage is large. Pleistocene glaciations augmented erosional intensity in nearly all mountain areas (Barsch and Caine, 1984) and led to the formation of vast sediment storages in valley positions (e.g. Pfiffner et al., 1997; Hinderer, 2001; Straumann and Korup, 2009), but also in the headwater catchments (e.g. Otto et al., 2009; Hoffmann et al., 2013; Messenzehl et al., 2014). These sediment storages are mostly of Late- and Postglacial age (e.g. Pfiffner et al., 1997; Hinderer, 2001; Otto et al., 2009), since glaciers effectively removed sediment from the inner-alpine areas and transported it to the alpine foreland during the last ice age (Preusser et al., 2010).

Major challenges concerning sediment storages in high-mountain areas and the motivation based on the relevance of this topic are pointed out in the introduction. This is followed by the objectives and the respective aims for the addressed scales. Finally, the chapters are outlined and summarized.

1.1 Challenges to address and major objectives

Early on it was recognized that mountain environments exist in a metastable state making them particularly vulnerable to disturbance (Barsch and Caine, 1984). Large portions of high-mountain areas are covered with unconsolidated, potentially transportable sediments. Their residence times vary between 10^0-10^6 years (Dunning et al., 2006; Davies and Korup, 2010; Blöthe and Korup, 2013; Hoffmann et al., 2013). High mean erosion rates in high-mountain areas are the product of events episodic in time and discontinuous in space (Barsch and Caine, 1984; Kirchner et al., 2001). These events are often triggered by e.g. seismic activity (e.g. Schwanghart et al., 2016) and extreme rain or snowmelt events (e.g. Lenzi et al., 2003). Long recurrence intervals (10^2-10^4 years) of processes imply that high-mountain systems are controlled by transient behavior (Brunsden and Thornes, 1979; Barsch and Caine, 1984). In high-mountain areas, which were repeatedly glaciated during the Pleistocene (Lang and Wolff, 2011), geomorphic processes, sediments, landforms and landscapes are directly conditioned by former glaciation and deglaciation (Church and Ryder, 1972; Ballantyne, 2002b). This is summarized in the concept of paraglacial geomorphology. The concept is primarily concerned with the long-term disturbance of landforms and landscapes through glaciations, thus putting the focus on transience and transition in geomorphic systems and their recovery (Slaymaker, 2009). Process rates and sediment transport rates can stay elevated due to their glacial inheritance for several 10^4 years (Church and Slaymaker, 1989). Hoffmann et al. (2013) point out that small headwater basins, the steepest parts of mountain environments, erode large amounts of Postglacial sediment, but the majority remains in storage during interglacial periods. Hence, these sediment storages do not affect the large scale sediment cascade. The paraglacial response time of sediment fluxes is estimated to 100-400 kyr, which is longer than the recurrence interval of major glaciations, leaving these systems in a transient state (Hoffmann, 2015).

Recent, ongoing deglaciation due to anthropogenic climate change since the Little Ice Age (LIA) (Mann, 2002; Grove, 2004; Zemp et al., 2015) exposes formerly glaciated areas to new conditions and geomorphic processes. Geomorphic responses to deglaciation include spatial and temporal changes in process activity, slope (in-)stability as well as deposition and erosion of sediment storages (Heckmann et al., 2019). These forefields feature many unstable sediment storages, which are of major interest for studies on sediment budgets (Hilger et al., 2019), natural hazards (Knight and Harrison, 2014; Heckmann et al., 2016b) as well as sediment connectivity and fluxes (Carrivick et al., 2013; Lane et al., 2017; Cavalli et al., 2019).

Investigating sediment, its distribution and volume in mountain areas is of global importance: Mountains cover 25% of the Earth’s terrestrial land surface (Meybeck et al., 2001) and were home to roughly 10% of the global population in 2010 (Jones and O'Neill, 2016; Hock et al., 2019) with increasing tendency (Gao, 2019; Hock et al., 2019). However, too little is known about the volumes, morphologies and residence times of sediment storages. This represents a major shortcoming, since rapid changes in sediment storage (e.g. catastrophic erosion or deposition) can pose a serious hazard to human society and infrastructure (Davies and Korup, 2010). Korup (2012) states sediment storages rather fuel than buffer high sediment transport rates. Thus, the highest sediment transport events largely involve the (re-)mobilization of sediment storage along the sediment cascade. Debris flows, geomorphic processes responding to seismic activity as well as flash floods, natural dam-burst floods and glacier lake outburst floods with sediment entrainment are among the natural hazards local populations are facing (Hewitt, 1992; Zimmermann and Haeberli, 1993; Hewitt, 2004; Glade, 2005). Moreover, sediment storages have important impacts on the propagation of seismic waves (Allen and Wald, 2009) and sediment transfer in mountain areas (e.g. Phillips, 2003a) influencing hydropower generation (Vörösmarty et al., 2003; Kummu and Varis, 2007; Syvitski and Milliman, 2007). Sediment storages can act as buffers, barriers and blankets strongly influencing (dis)connectivity along the sediment cascade (Fryirs et al., 2007; Fryirs, 2013), thus modulating mountain landscape evolution. Sediment cascades between storages are influenced by the sediment production rate and the characteristics of intermediate storage (longevity, liability to fail, recurrence interval of failure triggering events such as earthquakes, major storms or glaciations) (Davies and Korup, 2010).

Despite their relevance for society and related natural hazards, surprisingly few studies have systematically analyzed sediment distribution or quantified sediment storage in larger catchments or mountain belts. This is supposedly due to unsolved scaling issues in sediment budget studies (Slaymaker, 2006). While small scale studies highlight the importance of sediment storage in small (headwater) catchments (e.g. Schrott et al., 2003; Otto et al., 2009; Götz et al., 2013), large scale studies focus on large scale sediment storages (e.g. Hinderer, 2001; Straumann and Korup, 2009) or only partially include storages from smaller scales (e.g. Jordan and Slaymaker, 1991; Tunnicliffe and Church, 2011; Tunnicliffe et al., 2012) (Figure 1-1). The issue of transferring knowledge between systems of different magnitude is one of the most intransigent problems in geomorphology, concerning both temporal and spatial scale (Church, 1996).

Based on this discussion, I conclude that knowledge on the spatial pattern of sediment storage and material mobility along the sediment cascade in a large drainage basin is imperative to a better understanding of transient landscape evolution, Postglacial sediment evacuation, and connectivity from and within the tributaries of large-scale drainage basins. Incorporating the hitherto underrepresented sediment storage in headwaters into a regional assessment of sediment distribution remains “a major challenge of geomorphic studies in mountain environments” (Hoffmann, 2015, p. 625). This also needs to systematically include recently deglaciated areas inevitably located in the headwater areas. It is therefore essential to bridge the gap between spatial scales: Small-scale sediment storage analysis needs to be upscaled to a large catchment scale (Figure 1-1). This work will contribute to this aim with the following objectives:

(1) understand and analyze the formation of Postglacial landforms on a small scale using the examples of outsize fans in the Upper Rhone valley, Switzerland,

(2) investigate the landform assemblage in medium-sized tributaries within the Upper Rhone Basin, and

(3) create scale linkages for sediment distribution between smaller scales and a large catchment scale through a hierarchical upscaling approach based on predictive mapping.

The focus of this dissertation lies on the local and the catchment scale, which is manifested in the more detailed work published in two papers (chapters 5 and 7). Since research on sediment storage and budgets on the regional scale has been performed and published in many scientific papers before (examples in chapter 2), the methods and results for this scale are briefly described in chapter 6.

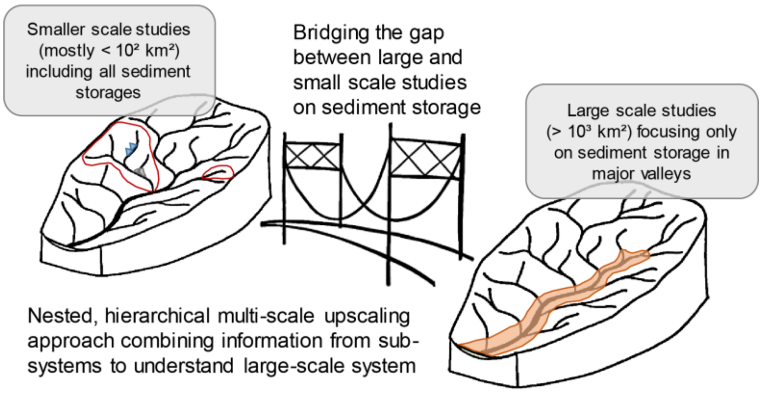

Figure 1-1: Schematic illustration of the scaling issue in sediment storage analysis and the approach to bridge the gap between different spatial scales. Underrepresented sediment storage in headwaters needs to be included in an assessment of sediment distribution on a larger scale. This can be addressed with a nested, hierarchical multi-scale, multi-method approach.

1.1.1 Aims on the local scale

Outsize fans in the Goms region, located in the uppermost part of the Upper Rhone valley near the Rhone Glacier (Figure 3-1), are studied in detail on a small, local scale. The three Goms outsize fans (GOF) are characterized by an anomalous relationship between fan and catchment area (up to > 1.0) (e.g. Crosta and Frattini, 2004; Jarman et al., 2011). The formation of these landforms and sediment storage forms in not yet fully understood, therefore their surface morphology, sedimentology, architecture and formative period is investigated in more detail.

On the small, local scale the aims are to

- quantify the volume of sediment eroded from the catchments and trapped in the fans,
- analyze the surface morphology of the fans and their source areas,
- investigate the internal structure of one outsize fan and the interfingering with the underlying valley fill, and
- determine the onset and period of fan formation.

1.1.2 Aims on the regional scale

Five key sites are investigated on the regional scale, i.e. Val d'Illiez, Val de la Liène, Turtmanntal, Lötschental and Goms (Figure 3-1). These key sites represent the heterogeneity of the Upper Rhone Basin (URB; Table 6-1), by covering all major tectonic units, many lithologies exposed within the study area and the full width of surface morphology, relief, Pleistocene glacial imprint and contemporary glacial cover as well as climatic conditions. Moreover, sedimentary fans and their characteristics are studied in the URB.

On the medium, regional scale the aims are to

- map and investigate the spatial distribution of sediment storage forms and sediment cover in different tributaries of the URB, and
- map all sedimentary fans and analyze the morphometric properties of the fans and their feeder basins within the URB.

1.1.3 Aims on the catchment scale

The large, catchment scale comprises the URB in this thesis. The catchment is located in the southwestern Swiss Alps between the Rhone Glacier and Lake Geneva, and is one of the largest inner-alpine basins with a size of c. 540 km^2 (Figure 3-1). The Rhone, originating at the Rhone glacier, drains the catchment and is fed by a large number of tributaries (c. 50 tributaries > 10 km^2).

On the catchment scale, the aims are to

- model the spatial distribution of sediment cover in the URB using a combined field-based and statistical modeling approach,
- analyze the quality of the model outcome and the effects of input data on this in a large scale geomorphic system, and
- interpret the modeling results in a geomorphic context with respect to the general pattern and the topographic position of sediment storages as well as the relevance of sediment storage in recently deglaciated areas and the spatial variability of sediment storage on different scales.

1.2 Chapter outline and chapter summary

Chapter 2: Sediment storage in high-mountain areas

Sediment fluxes in high-mountain areas are highly dynamic and complex. Changing climate since the Last Glacial Maximum (LGM) led to changing process regimes, producing a variable landscape with numerous types and generations of landforms at various scales. The strong imprint of Pleistocene glaciations is still observable in current processes, landforms and landscapes. In this transient setting, sediment storage as an integral part of high-mountain sediment budgets is discussed. Focusing on exemplary studies ranging from small to large spatial scales, I shed light on scale linkage problems and different upscaling approaches. It is pointed out that knowledge on the spatial sediment storage distribution and sediment fluxes along the sediment cascade in a large drainage basin are necessary to comprehend transient landscape evolution, Postglacial sediment evacuation and connectivity. Thus, methods to overcome scaling issues in sediment budget studies are urgently needed. The chapter concludes with a summary of methods to quantitatively study sediment distribution and volumes.

Chapter 3: Study area

Located in the southwestern Swiss Alps between the Rhone Glacier and Lake Geneva, the URB is one of the largest inner-alpine basins (c. 5400 km^2). The Rhone valley with a total length of c. 160 km dissects the western Swiss Alps with a general southwest trend, along regional tectonic structures. The tectonic and geologic setting, glaciation of the study area since the LGM, sediment storage and transient sediment fluxes as well as climatic conditions are described. The characteristics of the five key sites on the regional scale are briefly summarized.

Chapter 4: Conceptual and methodological approach

The conceptual framework of this thesis consists of a multi-scale approach within the nested, hierarchical structure of a geomorphic system. Observations and data from different scales are combined to model the spatial sediment distribution in a large scale catchment, the URB, with a predictive modeling upscaling approach. This hierarchical structure is acknowledged as an essential concept in geomorphology, since the properties of a larger scale consist of the sum of properties of smaller scales plus emergent properties and since the complexity grows with increasing spatial scale. Thus, data from different scales are indispensable and each scale has its own strengths, which can be combined. A multitude of different methods are used in this thesis to understand the formation of certain landforms on a small local scale, to observe the assemblage of sediment storage forms on a regional scale and to predict the spatial sediment distribution on a large catchment scale.

Chapter 5: Postglacial outsize fan formation in the Upper Rhone valley, Switzerland – gradual or catastrophic?

Outsize fans are characterized by seemingly disproportional, small feeder catchments in relation to their fan area. Often escaping rigorous scientific inquiry, the formative processes of these outstanding landforms remain inconclusive, ranging from catastrophic mass-wasting processes to gradual fluvial formation. Here we apply a multi-method approach to three outsize fans with hitherto unknown formation history in the Upper Rhone valley, Switzerland, combining morphometric analysis of the fans and their source areas with geophysical surveys of the subsurface material and cosmogenic radionuclide exposure dating. The fan feeder catchments are cut into sheer bedrock, hence in contrast to textbook examples of sedimentary fan formation, no unconsolidated material was available after deglaciation, let alone a pre-existing catchment.

We find a fan formation in three phases: In Phase I starting with full deglaciation ~10.0 ka and ceasing with full catchment development around ~6.0 ka, the major part of the fan was built up by the deposits of massive high-energy, high magnitude debris flows comparable to the current activity of the Illgraben. In Phase II lasting until ~0.8 ka, the feeder basin was affected by comparatively lower-magnitude debris flows depositing a second sedimentary unit characterized by debris flow channels, snouts and large boulders on the initial fan. In Phase III the fan-feeder basin transport system seized up with only isolated cases of geomorphic activity within the catchment. Thus, erosion and sedimentation rates of these fan systems were elevated soon after deglaciation and then decreased over time during the Holocene.

We conclude a rapid, but incremental formation of outsize fans in the Upper Rhone valley. The feeder basins export material at extremely high rates resulting in the disruption of longitudinal sediment connectivity in the main valley and hence on a larger scale.

Chapter 6: Mapping on the regional scale: sediment storage distribution in five key sites and sedimentary fans in the Upper Rhone Basin

Sediment storage distribution and quantification on the regional scale (mostly < 10^2 km^2) has been the subject of several studies, which have a geomorphic mapping approach in common. Geomorphic maps are holistic images or inventories of a landscape including information on processes, form and material (Smith et al., 2011; Otto and Smith, 2013). This chapter aims on the one hand at creating derivative geomorphic maps of the sediment storage distribution for the five key sites and on the other hand at mapping and analyzing sedimentary fans and their geomorphometric properties within the URB. Mapping and classification techniques for sediment storages are based on a process domain and landform approach. Overall, 360.3 km^2 of sediment and bedrock cover is mapped within the five key sites in the URB, equivalent to 6.7% of the total area. Furthermore, 186 sedimentary fans are mapped in the URB. I conclude, that geomorphic mapping of specific landforms or landform assemblages in the field and from remote sensing imagery is a useful technique to bridge the gap between different scales in an upscaling approach based on automated methods such as predictive mapping.

Chapter 7: Multivariate geostatistical modeling of the spatial sediment distribution in a large scale drainage basin, Upper Rhone, Switzerland

There is a notable discrepancy between detailed sediment budget studies in small headwater catchments (< 10^2 km^2) and large scale studies (> 10^3 km^2) in higher order catchments. While the former mainly focus on the identification of sedimentary landforms in the field (e.g. talus cones, moraine deposits, fans), the latter apply modeling and/or remote sensing based approaches for major sediment storage delineation. To bridge the gap between these scales, we compiled an inventory of sediment and bedrock coverage from field mapping, remote sensing analysis and published data for five key sites in the URB (Val d'Illiez, Val de la Liène, Turtmanntal, Lötschental, Goms). This inventory was used as training and testing data for the classification of sediment and bedrock cover with statistical models.

Our high-resolution classification shows 53.5 ± 21.7% of the URB are covered with sediment. This coverage is by no means evenly distributed: small headwaters (< 5 km^2) feature a very strong variability in sediment coverage. In contrast, larger watersheds predominantly show a bimodal distribution, with highest densities for bedrock being consistently lower than for sediment cover. Earlier studies quantifying sedimentary cover and volume focus on the broad glacially overdeepened Rhone valley accounting for c. 9% of our study area. While our data support its importance, we conservatively estimate the remaining 90% of sediment cover, mainly located outside trunk valleys, account for a volume of 2.6-13 km^3, i.e. 2-16% of the estimated sediment volume stored in the Rhone valley between Brig and Lake Geneva. We therefore conclude that sediment storage in low-order valleys, often neglected in large scale studies, constitutes a significant component of large scale sediment budgets that needs to be better included into future analysis.

Chapter 8: Synthesis

The analysis of sediment storage requires a deliberate consideration of spatial and temporal scales. Since a geomorphic system is the result of processes operating at all involved scales, the system can be seen as a nested, hierarchical structure (de Boer, 1992). A hierarchical scaling approach serves as a basis to upscale detailed knowledge on sediment storage in the large scale Upper Rhone catchment. This transferal of knowledge between different spatial scales has been identified as a major problem in sediment budget studies (Slaymaker, 2006), but also in geomorphology in general (Church, 1996). Based on the application of a multi-scale and multi-method approach, the major findings and conclusions from the three investigated scales are summarized and scale linkages explicitly pointed out. I synthesize a framework to resolving scaling issues in sediment storage analysis on this foundation including the following applied and conceptual ideas:

- ordering the investigated systems and thinking across scales,
- finding and identifying the linkages between scales,
- applying a multi-scale and multi-method approach,
- bringing together spatial scales – process, observation and modeling,
- incorporating existing data, and
- acknowledging the important role of high-resolution data and computational power.

These points should be taken into consideration and used as a guiding concept for further sediment storage and sediment budget studies on large scales. At last, future research needs are pointed out and discussed.

Appendix

The appendix consists of supplementary material to the published papers presented in this thesis (chapters 5 and 7).

2 Sediment storage in high-mountain areas

High-mountain areas and their geomorphic processes, forms and material are characterized by elevation, steep gradients, surficial bedrock and the presence of ice and snow. They are internally diverse and variable due to their elevation, relief and exposure, show signs of late Pleistocene glaciations, are tectonically active and in many cases exist in a metastable condition, making them especially prone to perturbation (Barsch and Caine, 1984). Impermanent climate since the LGM (Ivy-Ochs et al., 2009a) led to changing process regimes, producing a diverse landscape with legion types and generations of landforms at various scales (Otto et al., 2008). Today's palimpsest of relict, modern, overlapping and replaced landforms shows the influence of past processes on current landscapes (Chorley et al., 1985; Hewitt, 2002a; Hewitt, 2002b).

Sediment fluxes in high-mountain areas are highly dynamic and complex (Caine, 1974; Hinderer, 2001; Hinderer et al., 2013) and the strong imprint of Pleistocene glaciations is still observable in current sediment fluxes (e.g. Church and Ryder, 1972; Church and Slaymaker, 1989; Hinderer, 2001; Otto et al., 2009). Sediment fluxes can be conceptualized in a sediment cascade model describing the flow of material along a gravitational gradient (Caine, 1974; Slaymaker, 1991; Burt and Allison, 2010), i.e. an example of a cascading system (Chorley, 1962; Chorley and Kennedy, 1971). Sediment is eroded, transferred, stored, remobilized and accumulated through and in different subsystems (Caine, 1974). In these systems, sediment storages control the output of sediment from alpine catchments through (dis)connectivity (Fryirs et al., 2007) and changing process rates (Davies and Korup, 2010).

2.1 Controls on topography in high-mountain areas

The topography of the Earth's surface is created by the interplay of climate, tectonics, lithology and geomorphic processes (e.g. Molnar and England, 1990; Raymo and Ruddiman, 1992; Whipple et al., 1999; Kühni and Pfiffner, 2001; Champagnac et al., 2009; Whipple, 2009; Champagnac et al., 2012; Mey et al., 2016). The question if tectonics have driven long-term climate change or vice versa as well as their feedback and relative importance in landscape evolution and thus mountain height have been subject to a long debate (overviews in Molnar, 2009; Whipple, 2009; Champagnac et al., 2012). The erodibility of rocks and topography show a correlation in the Swiss Alps, where the highest peaks and water divides are characterized by lithologies of very low and low erodibility (Kühni and Pfiffner, 2001). Recent uplift rates from geodetic measurements in the Alps can be attributed to several factors including the isostatic response to erosional unloading (Champagnac et al., 2009) and glacial isostatic uplift (Gudmundsson, 1994; Mey et al., 2016). Mey et al. (2016) conclude the LGM ice load was much larger than the load of Postglacially eroded sediments that were for the most part stored within the Alps. Thus, ~90% of the recent uplift can be explained by the unloading due to LGM deglaciation.

Nonetheless, the interaction of endogenic and exogenic processes created mountain ranges with steep topographic gradients featuring some of the highest sediment fluxes on Earth (Caine, 1974; Barsch and Caine, 1984; Milliman and Syvitski, 1992). Sediment fluxes and hence sediment yields in the European Alps are quite variable. While glaciated catchments are characterized by the highest sediment yields of up to 7000 $\mathrm{t\,km^{-2}\,a^{-1}}$, those from non-glaciated catchments are much lower. Thus, repeated Quaternary glaciation as well as glacier retreat since the LIA led to a transient state in the European Alps (Hinderer et al., 2013).

2.2 Transient state of the Alps

Many high-mountain geomorphic systems are considered to be out of equilibrium or in a transient state in terms of the external driving forces, i.e. a shift from glacial to interglacial conditions, because their response to environmental changes is not immediate but buffered and delayed (Phillips, 2003a; Hoffmann, 2015). In systems out of equilibrium, the input into the system is not equal to the output (e.g. Hack, 1960; Chorley and Kennedy, 1971). However, a dynamic equilibrium state, meaning a single, stable equilibrium condition existing in a geomorphic system, has shortcomings and is generally not realistic. The dynamic equilibrium paradigm has been challenged by concepts of complexity and nonlinearity, in which landscape evolution is more chaotic and less predictable (Phillips, 2003b). The presence of non-equilibrium states, multiple equilibria and complex nonlinear dynamic behavior of a system including feedbacks are better concepts to understand the processes, forms and control factors of a geomorphic system such as high-mountain areas (Phillips, 1992).

Several cycles of ice advance and retreat during Pleistocene glaciations created a distinct topography in many mountain systems and produced, eroded and transported vast amounts of sediment (Penck, 1905; e.g. Hallet et al., 1996; Montgomery, 2002; Schlüchter, 2004a; Lisiecki and Raymo, 2005; Lang and Wolff, 2011; Valla et al., 2011). Furthermore, glacial erosion created overdeepened valleys (e.g. Hooke, 1991; Preusser et al., 2010; Prasicek et al., 2014; Haeberli et al., 2016), hanging valleys (e.g. Valla et al., 2010b), and glacial cirques (e.g. Hooke, 1991; Evans, 2006) potentially retaining vast amounts of sediment (Hoffmann et al., 2013). A conceptual model proposes that sediment yield over a glacial cycle is highly variable (Figure 2-1). Early phases of glacier (re-)advance lead to very strong increases in sediment yield, since pre-glacial sediments can be easily accessed and reworked. Sediment yields decrease over time during glacier advances and are mostly fed by glacial erosion. The initial phase of glacier advance (first glaciation) can result in very high sediment yields due to a combination of erosion of pre-glacial sediments, glacial erosion and adjustment of a fluvially conditioned landscape. Subsequent deglaciation phases were conceptualized in the paraglacial concept (see below), featuring very high sediment yields at the beginning due to the availability of easily erodible sediment followed by a decrease, since sedimentary sources are stabilized, exhausted or disconnected from the sediment cascade. Consequently, export rates are lowest (comparable to pre-glacial conditions) (Antoniazza and Lane, 2021). These systems are in a transient state most of the time, having a relaxation time longer than the recurrence interval of events. The response to changing environmental conditions is often related to the strength of coupling or the connectivity between the systems components. Thus, systems with a high degree of connectivity between the systems components through sediment fluxes can rapidly forward responses to environmental change, while sediment fluxes in systems with disconnected components cannot reach the outlet and transmit the signals (Brunsden and Thornes, 1979; Hoffmann, 2015). Regarding the alpine environment, the system is currently in an advanced deglaciation phase following the last Pleistocene glaciation, where stabilization, exhaustion and disconnection of sediment storages is important. However, the modern proglacial areas of the LIA glacier extent are in an early state of deglaciation, due to the active glacier retreat (Antoniazza and Lane, 2021). The following paragraphs focus on the adjustment of a transient landscape to deglaciation.

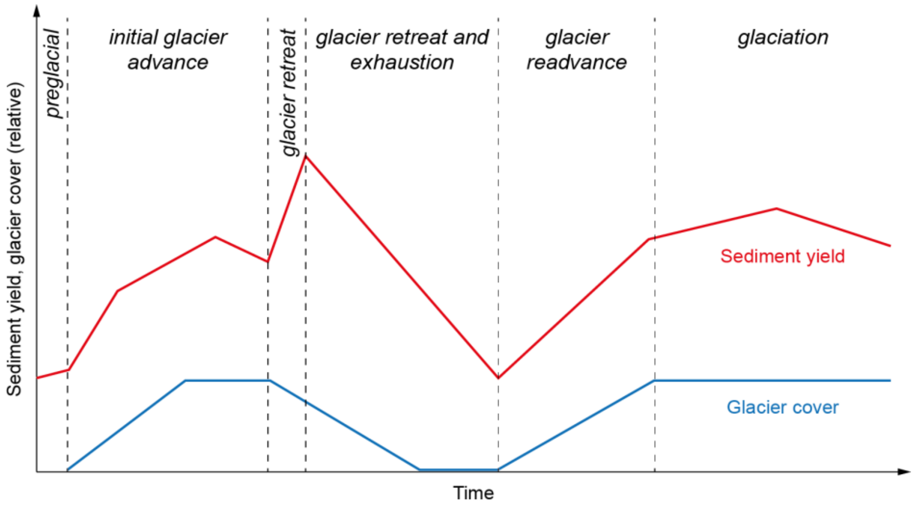

Figure 2-1: Conceptual model of change in sediment yield during phases of glacier advance, stagnation, retreat and re-advance. Sediment yield and glacier cover are plotted together over a glacial cycle. Rates are relative (adjusted after Antoniazza and Lane, 2021, p. 7).

The paraglacial concept comprises non-glacial Earth-surface processes, sediments, landforms, landsystems and landscapes directly conditioned by former glaciation and deglaciation (Ballantyne, 2002b). Accordingly, it is a prominent example of a non-equilibrium or transient geomorphic system. Formerly glaciated mountain regions are supposedly characterized by a disequilibrium between rates of post-glacial sediment yield from the headwaters, where steep hillslopes are prone to erosional processes, and fluvial sediment yield in the major fluvial river systems. Sediment yield in British

Columbian rivers increases with catchment sizes up to $3x10^4$ km^2, which is a result of the reworking of Pleistocene glacial deposits. Thus, it has been discussed that accelerated sediment fluxes stay elevated for several thousand years after deglaciation in large scale systems (Church and Ryder, 1972; Church and Slaymaker, 1989; Ballantyne, 2002b) (Figure 2-2).

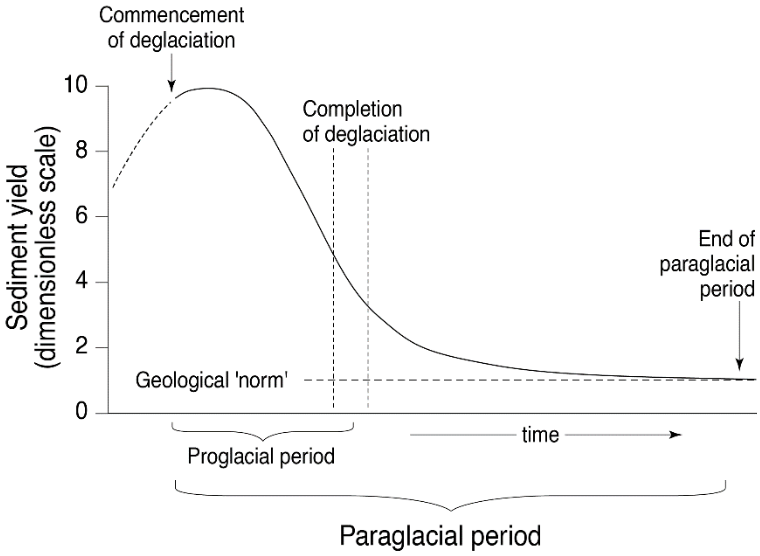

Figure 2-2: Schematic representation of the pattern of paraglacial sediment reworking. The ‘paraglacial period’ of enhanced sediment yield commences at deglaciation and terminates when sediment yield is indistinguishable from the ‘geological norm’ resulting from primary denudation of the land surface (Ballantyne (2002b, p. 1194); modified from Church and Ryder (1972, p. 3069)).

The unifying concept of paraglacial adjustment refers to glacially conditioned sediment availability and encompasses the release of primary in situ glacigenic sediment and the reworking of secondary paraglacial sediment stores (e.g. talus or debris cones, but also re-entrainment of glacigenic sediment) (Ballantyne, 2002b; Ballantyne, 2002a). In primary paraglacial systems the sediment release is directly glacially conditioned. Therefore, it does not involve the reworking of sediments mobilized by non-glacial processes before. These systems can be described with an exhaustion model. The rate of sediment release declines through time and is related to the proportion of available sediment at time since deglaciation (Figure 2-3). Several assumptions are made in this model: (1) the only constrain on the rate of sediment release is the availability of potentially unstable sediment, (2) no further processes perturb the paraglacial system and (3) the sediment release is reduced due to stability or depletion of sediment sources (Cruden and Hu, 1993; Ballantyne, 2002a).

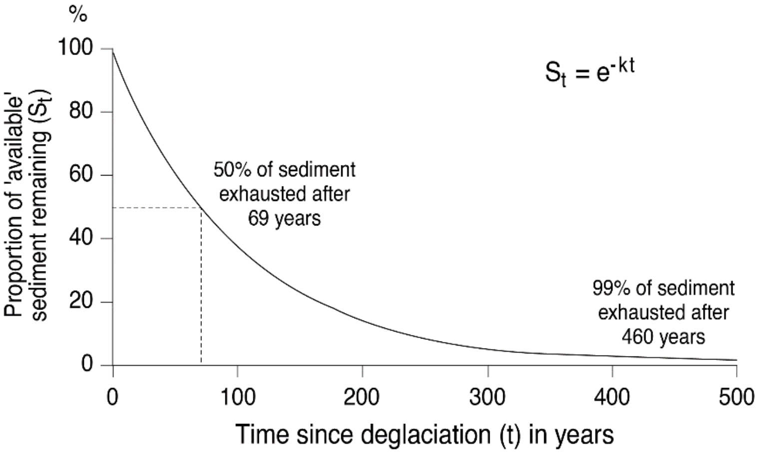

Figure 2-3: Exponential exhaustion model of paraglacial sediment reworking, which assumes that rate of sediment removal (k) is dictated by the proportion of 'available' sediment remaining for transport (S_t) according to the relation St = e^{-kt}, where t is the time since deglaciation and e is a constant. In the example shown, k = 0.01 (i.e. 1% of remaining 'available' sediment is removed per year); the 'half life' of the system (the time taken to evacuate 50% of 'available' sediment) is 69 years, and 99% of sediment has been evacuated after 460 years, thus defining the approximate length of the 'paraglacial period' of enhanced sediment reworking (Ballantyne, 2002b, p. 1995).

Secondary paraglacial systems are more complex, because the rate of sediment release is further conditioned by the reworking of paraglacial sediment storages (Ballantyne, 2002a). Harbor and Warburton (1993) suggest the pattern of fluvial paraglacial sediment transport can be described by different curves depending on the spatial scale of the basin (Figure 2-4). While specific sediment yields from the smallest catchments peak directly after deglaciation, those for larger basins peak gradually later. Yet, a deficit of the model is its implication of a limited reworking of in situ glacigenic sediment in larger basins immediately after deglaciation.

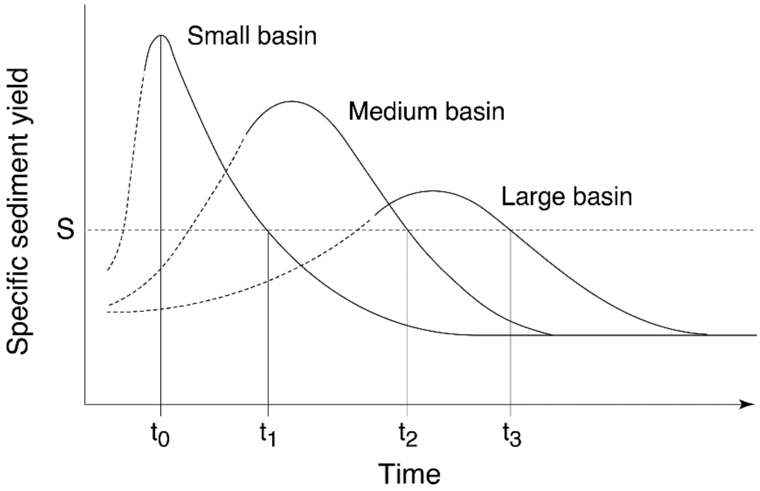

Figure 2-4: Paraglacial sedimentation cycles for catchments of different scale, given as hypothetical sediment yield variations over time. Timing of deglaciation is denoted by t_0: Comparative sediment yield at particular times (t_1; t_2; t_3) is strongly conditioned by basin size. Conversely, basins of different size may have a similar sediment yield (S) at different times (t_1; t_2; t_3) after deglaciation. The diagram demonstrates why comparison of sediment yield for deglaciated basins of different sizes is likely to reflect stage in the cycle of paraglacial sediment reworking rather than primary catchment denudation (Ballantyne (2002b, p. 1974); modified from Harbor and Warburton (1993, p. 3)).

Ballantyne (2002a) proposes that secondary paraglacial systems can also be described with an exhaustion model. This is the case, if initial sediment availability and rates of sediment release are larger in small basins due to the steep topography, and if the rate of change in sediment removal declines with increasing basin size. This decline is due to a maintained sediment transport in larger basins by reworked sediment from smaller catchments. The exhaustion model is generally based on a steady state assumption, which cannot be valid over millennial time scales and on large spatial scales. Therefore, the idealized model and the constant decline of sediment release are subject to perturbations prolonging or rejuvenating sediment release. This implies the paraglacial period extends far beyond the initial cycle of paraglacial adjustment (Ballantyne, 2002a). Nevertheless, both paraglacial landscape models suggest a shorter response and thus adjustment time in small drainage basins, while the time lag in large scale drainage basins may be up to several tens of thousands of years (Harbor and Warburton, 1993; Ballantyne, 2002a). However, Hoffmann (2015) reveals, headwaters in an alpine environment with distinct Pleistocene glacial imprint still respond to the change from glacial to interglacial conditions due to reduced lateral and longitudinal connectivity. The residence times of sediment is in the order of 100-400 kyr, indicating the response time of these geomorphic systems to environmental changes (i.e. Pleistocene glaciation) is longer than past interglacials. Blöthe and Korup (2013) identify millennial lag times in the sediment routing systems of the Himalayas where valley fills may reach residence times of > 100 kyr. Both studies suggest paraglacial adjustment could be more complex than previously assumed. Therefore, the investigation of sediment storage in high-mountain areas on different spatial scales should be the focus of future research.

2.3 Sediment storage as an integral part of high-mountain sediment budgets

"The sediment budget is defined as the accounting of sources, sinks and redistribution pathways of sediments in a unit region over unit time" (Slaymaker, 2003, p.71). Hence, sediment budgets represent a holistic view of geomorphic sediment erosion, transport and deposition in a system (Dietrich et al., 1982; Reid and Dunne, 1996; Slaymaker, 2003; Hilger and Beylich, 2019). It is a mass balance based approach of sediments (incl. bedload and solutes) that can be described by the continuity equation of mass

$$I \pm \Delta S = O \qquad (1)$$

stating a change in storage (S) is equal to an excess of inflow (I) over outflow (O) or an excess of outflow over inflow. The input is sediment produced by weathering or from dynamic sediment sources, the storage is sediment stored e.g. on slopes, floodplains, channels, in lakes or ice and the output is the sediment exported. If input and output are not equal, it means the area of interest is eroding or depositing (Slaymaker, 2003). Often a sedimentologically closed or semi-closed system (e.g. alluvial fan, glacial valley, lake) is chosen for sediment budget studies, since mass conservation is fulfilled (Hinderer, 2012). First pioneering sediment budget studies were performed by Jäckli (1957) who studied sediment sources in the Upper Rhine valley and Rapp (1960) studying the sources, sinks and movements of sediment in the alpine/arctic Kärkevagge catchment.

The storage term is of high importance in sediment budgets, since it determines erosion or deposition for a defined area. Sediment storages need to be identified, quantified (Dietrich et al., 1982; Slaymaker, 2003; Otto et al., 2008), and their age, which is the time since deposition of material, can be determined with different methods (Dietrich et al., 1982) (chapter 2.5). Changes in sediment storage over time require knowledge on the age of the sediment to calculate its virtual velocity through the catchment (Slaymaker, 2006). Measuring recent sediment fluxes only gives information on sediment transport under current conditions, but quantifying sediment storage reveals information on sediment transport regimes and rates over a longer time scale, i.e. the Postglacial period (e.g. Hinderer, 2001; Otto et al., 2009; Tunnicliffe et al., 2012; Götz et al., 2013). Walling (1983) focuses on the effects of storage on the non-delivery of sediment to basin outlets. A simple sediment delivery ratio concept is not able to solve the associated problems including temporal and spatial lumping of data on sediment transport and yield as well as the neglect of influencing and explanatory factors. De Vente et al. (2007) refer to the non-predictability of a simple relationship between catchment area and area-specific sediment yield because of opposing trends from different driving forces and non-linear relationships due to internal and external factors (e.g. lithology, land cover, topography, climate and human influence). Fryirs (2013) presents a conceptual framework for the analysis of (dis)connectivity within a catchment integrating the spatial and temporal variability of blockages, and their characteristics regarding sediment residence time and linkage disruptions of sediment transfer. These reviews highlight the importance of a site-specific approach with (field) investigations. Not considering sediment storage in a catchment by only measuring sediment output cannot give information on actual denudation and sediment fluxes within the system, since the system is treated as a black box.

Despite substantial potential energy in mountain environments, sediment flux in large river systems is frequently disconnected from alpine headwaters, due to intermittent storage along the flow path from the bedrock source to large sedimentary sinks in major alpine valleys (e.g. Otto et al., 2009; Hoffmann et al., 2013; Messenzehl et al., 2014). Thus, the sediment delivery to the outlet is in these regions by no means a simple and consistent relationship between drainage area and sediment yield as only a small fraction of sediment eroded within the catchment is delivered to its outlet (Hoffmann et al., 2013). Therefore, detailed studies on the spatial distribution of sediments are needed to explain the discrepancy (Walling, 1983; Phillips, 1986; Church and Slaymaker, 1989; Phillips, 1991; de Vente et al., 2007; Hinderer, 2012; Fryirs, 2013) and to better understand sediment routing in alpine environments (Otto et al., 2008). Sediment storage is ultimately linked to the concept of geomorphic connectivity, since they are buffers, barriers and blankets of the lateral, longitudinal and vertical fluxes of sediment and energy. The residence time of sediment storages therefore determines the time scale of (dis)connectivity (Brierley et al., 2006; Fryirs et al., 2007; Hoffmann, 2015).

Moreover, the spatial pattern of sediment storage has important implications for the prediction, mitigation and management of natural hazards (Zimmermann and Haeberli, 1993; Glade, 2005), the analysis of seismic wave propagation (Allen and Wald, 2009), the effects of land use changes (Reid and Dunne, 1996) and the management of hydropower reservoirs in mountain regions (Vörösmarty et al., 2003; Kummu and Varis, 2007; Syvitski and Milliman, 2007). In times of global warming, changes in sediment storage and sediment transport in high-mountain areas can result in a threat to humans and their infrastructure (Hilger and Beylich, 2019).

2.4 Scaling issues in sediment storage analysis

The distribution of sediment storages has been investigated on different spatial and temporal scales. Applying the sediment budget approach and hence analyzing sediment storage needs a careful consideration of spatial and temporal scales (review by Hinderer, 2012). However, only few studies address the gap between scales and present approaches to interlink methods on different scales (Otto et al., 2008). Especially on larger scales, the volume quantification is problematic and challenging (Slaymaker, 1991; Otto et al., 2008). The term scale has different meanings (e.g. Schlummer et al.,

2014) (see also chapter 4), but here I refer to the spatial scale as the size or extent of the area under consideration and the temporal scale as the time period investigated.

Scaling issues concern the transfer of knowledge between systems of different magnitude. The core problem is the scale linkage referring to the transfer of findings from one scale to another (Phillips, 1999; Slaymaker, 2006). For sediment budgets this is crucial, since drainage basins are characterized by different properties at different scales of investigation (Figure 2-5). Each scale level includes the cumulative effects of lower levels but also new, emergent properties (Slaymaker, 2006). Emergence describes how patterns arise from interactions among system components, but emergent properties and behaviors are not predictable from the laws governing interactions among components or the structure and function of the system (Phillips, 2011).

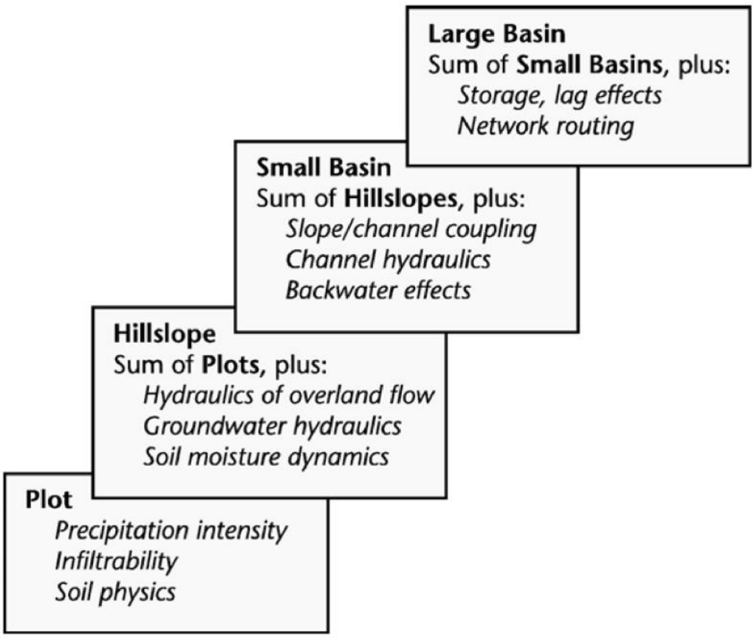

Figure 2-5: The scale linkage problem (Slaymaker (2006, p. 9); modified from Phillips (1999, p. 131)).

Spatial and temporal scales are inevitably linked (Figure 2-6). On small spatial scales the investigated temporal scale is assumed to be rather short, while on large spatial scales the temporal scale is supposedly longer (Hinderer, 2012). Schumm (1991) approaches the question of scale and scale linkage by evaluating the historical component required to explain events of increasing magnitude and age (Figure 2-7). Smaller and younger geomorphic processes and landforms differ concerning their importance of historical legacy compared to larger and older ones. However, I need to point out that sediment budget studies and the investigation of sediment storage (forms) in high-mountain areas often span the time since deglaciation after the Würmian ice age independent of the spatial scale (e.g. Hinderer, 2001; Otto et al., 2009; Hornung et al., 2010; Götz et al., 2013; Kober et al., 2019).

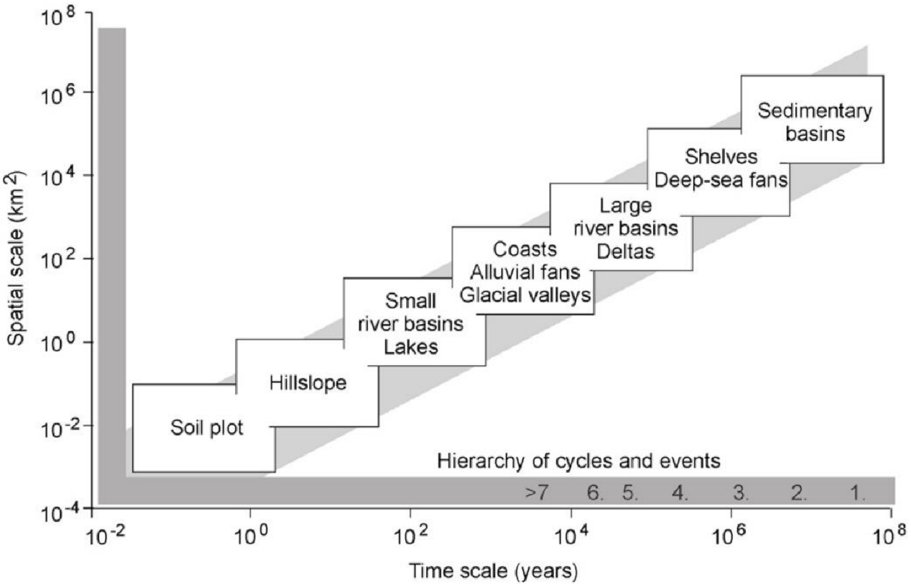

Figure 2-6: Arrangement of different sedimentary (sub-) systems in terms of spatial and temporal scales (Hinderer, 2012, p. 26).

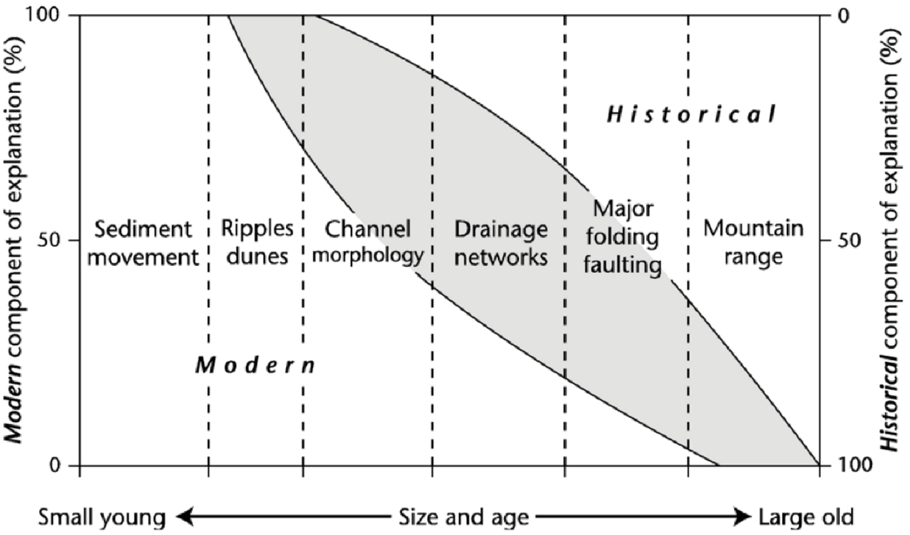

Figure 2-7: The component of historical explanation required to explain events of increasing magnitude and age (Slaymaker (2006, p. 10); modified from Schumm (1991, p. 53)).

Detailed sediment budget studies based on storage quantification are mainly available for small scale drainage basins (< 10^2 km^2) (e.g. Schrott and Adams, 2002; Otto et al., 2009; Götz et al., 2013), whereas studies in larger drainage basins (> 10^3 km^2) rather focus on large scale sedimentary landforms such as valley fills (e.g. Hinderer, 2001; Straumann and Korup, 2009). However, the crossing of scales and therefore up- and downscaling still remain widely unresolved issues (Slaymaker, 2006).

Small scale studies often quantify sediment storage in great detail with geomorphic, geomorphometric, geophysical and coring methods. These (multi-method) approaches have been applied in various small alpine catchments (4.5-17.0 km^2) (e.g. Schrott and Adams, 2002; Schrott et al., 2003; Götz et al., 2013). Geophysical methods proved useful, since their quantitative measurement showed geomorphometric estimations can overestimate sediment thickness and thus sediment volume (Hoffmann and Schrott, 2002). Furthermore, the spatial distribution of different sediment storage types, connectivity and alpine sediment transfer on this scale has been subject to detailed studies (e.g. Otto and Dikau, 2004; Messenzehl et al., 2014). Hoffmann et al. (2013) investigate sediment storage and catchment morphology of small catchments (< 10 km^2) in the Rocky Mountains, where Postglacial sediment still remains in storage. Hence, there is no significant coupling in the sediment cascade to larger-scale mountain river systems (Hoffmann et al., 2013). Otto et al. (2009) quantify sediment storage in a catchment of c. 100 km^2 in great detail by combining geomorphic mapping of sediment storage types, geophysical surveying to determine mean thicknesses for each sediment storage type and geomorphometric estimations of sediment volumes from digital elevation data.

The quantification and analysis of sediment storage in alpine areas on larger scales has been performed in several studies, since it is a crucial link between rates of erosion and sediment yield. Hinderer (2001) maps 16 valley fills in major valleys and lake basins in the European Alps and quantifies their volume based on existing geophysical data and a geomorphological approach extrapolating the hillslopes into the subsurface. Extrapolating this data to the entire Alps yields denudation rates of 620 mm kyr^{-1} averaged over the last 17 kyr compared to modern denudation rates of 125 mm kyr^{-1}. Denudation rates were highest during in the Late Glacial in the order of 1100-2900 mm kyr^{-1}, resembling the paraglacial cycle (Hinderer, 2001). Jaboyedoff and Derron (2005) propose an approach based on parabolic valley cross sections to estimate valley fill volumes of glacial valleys from DEMs and apply this method to the Rhone valley. Straumann and Korup (2009) use an automated region-growing algorithm based on a slope-gradient criterion to detect areas of Postglacial fluvial and lacustrine valley fills from DEMs at the mountain-belt scale. Based on this, they set up an empirical volume-area-scaling to quantify volumes. Mey et al. (2015) use artificial neural networks to estimate valley fill thickness and bedrock topography from the geometric properties of the landscape. Their estimated cross-sectional areas differ only by 21.5% from seismic surveys. Despite quantifying not only the largest intra-montane valley fills, the latter two approaches can solely include valley fill sediment storage in their quantification.

Information on the distribution, thickness and volume of valley fills is an integral part of sediment budgets (Hinderer, 2001; Straumann and Korup, 2009; Mey et al., 2015). Further, this information is crucial when investigating the sediment fluxes and (dis)connectivity along the sediment cascade in high-mountain areas (Caine and Swanson, 1989; Burt and Allison, 2010; Davies and Korup, 2010). More information on the catchment is nonetheless needed to fully understand these large-scale systems.

Few studies on these larger scales include more details on the stored sediment. Jordan and Slaymaker (1991) investigate the sediment sources, storage and yield of clastic sediment in the Lillooet River catchment (3150 km^2), British Columbia. Here, storage quantification is limited to alluvial storages of floodplains, fans and terraces as well as colluvial storages including landslide deposits, debris flow fans and terraces. Due to a discrepancy between sediment sources and output, they point out that more quantitatively precise data on sediment storage is needed. Tunnicliffe and Church (2011) and Tunnicliffe et al. (2012) investigate sediment erosion, storage and yield in the Chilliwack Valley catchment (1230 km^2), British Columbia. Deposited sediment at so called scale linkages (e.g. fans or cones) is estimated from the reconstruction of landforms using geometric methods, but sediment storages on hillslopes (e.g. talus) are considered a sediment source. They observe discrepancies between eroded and deposited material, which is probably due to not quantified sedimentation along the sediment cascade and over- or underestimation of eroded or deposited material. Furthermore, they find a high percentage of sediment being deposited at the numerous low order stream linkages. Low order catchments make up c. 50% of the whole catchment area, highlighting the importance of headwater sediment storage. However, this within-catchment storage is not regarded (Tunnicliffe and Church, 2011).

These examples highlight that the coupling of different scales remains a major challenge addressed with different up- and downscaling techniques (e.g. Blöschl and Sivapalan, 1995; Harvey, 2000; de Boer, 2001; Slaymaker, 2006; Otto et al., 2008; Schlummer et al., 2014). Upscaling is the transfer of knowledge from a specific site to a larger, e.g. regional or catchment, scale. Thus, larger-scale information is created from small scale data (e.g. point data) (Harvey, 2000; Zhang et al., 2004; Schlummer et al., 2014). Sediment budget studies and models cannot be scaled up linearly (Tunnicliffe and Church, 2011), therefore new approaches for the investigation of sediment storages on large scales are needed. Different system properties cause uncertainties associated with the transfer of knowledge between spatial scales (Zhang et al., 2004; Schlummer et al., 2014). These system properties and scaling issues need to be known and acknowledged:

(1) scale dependency of the characteristics of objects or processes and identifying their characteristic scale (Phillips, 1999; Harvey, 2000; Zhang et al., 2004),

(2) linkage of the characteristic scale and the intended scale of observation and modeling (Phillips, 1999),

(3) emergent properties arising at larger spatial scales (Harvey, 2000; de Boer, 2001; Zhang et al., 2004; Slaymaker, 2006; Phillips, 2011),

(4) feedbacks associated with process interactions at various scales (Harvey, 2000; Zhang et al., 2004),

(5) spatial heterogeneity of objects and process nonlinearities (Harvey, 2000; Phillips, 2003b; Zhang et al., 2004),

(6) time lags of system response to external perturbation (Chorley and Kennedy, 1971; Harvey, 2000; Zhang et al., 2004),

(7) historical and spatial contingency is strongly related to spatial heterogeneity, nonlinearity and scale dependency and leads to locally unique features (Phillips, 2001),

(8) scale linkages concerning operational problems such as up- and downscaling (Phillips, 1999; Slaymaker, 2006), and

(9) problems of dimensionality and similarity relating to a range of scales at which patterns or relationships are constant and thus the rules for up- and downscaling within such ranges (Phillips, 1999).

Slaymaker (2006) infers scale invariance of sediment budgets is improbable and scale distortions are common due to a lack of continuity in space and time. This discontinuity is observed e.g. by Hoffmann et al. (2013) who find out that more sediment is stored in headwaters with a strong glacial imprint than in headwaters with no glacial imprint.

Based on this, knowledge on the spatial pattern of sediment storage and fluxes in large catchments is urgently required to attain better understanding of transient landscape evolution, Postglacial sediment evacuation and connectivity. Incorporating the yet underrepresented sediment storage in small-scale catchments into larger-scale studies continues to be “a major challenge of geomorphic studies in mountain environments” (Hoffmann, 2015, p. 625).

As exemplarily shown, very few of these larger-scale studies include different sediment storage types in their budgets (e.g. Jäckli, 1957; Jordan and Slaymaker, 1991; Phillips, 1991; Tunnicliffe and Church, 2011; Tunnicliffe et al., 2012). Due to this fact, the scaling of erosion, transport and storage and their controlling factors are insufficiently understood (Otto et al., 2008; Tunnicliffe and Church, 2011). Tributaries and headwaters are often portrayed to act as sediment sources without substantial sediment storage (Schumm, 1977; Hinderer, 2001). Hinderer (2012) states, at long time scales, ultimate sinks win over intermittent storage, but the actual temporal scale is not defined more precisely. The simplistic model of a river system by Schumm (1977) divides the system into three zones with dominant processes: (1) The source region is dominated by erosional processes (e.g. landslides, fluvial incision). (2) The transport zone features sediment transfer typically in a fluvial channel. (3) The accumulation zone is characterized by deposition of transported sediment for example in fans, lakes or valley fills (Figure 2-8). This model of a river system neglects the significance of headwaters and smaller catchments as sediment storage areas, but their significance is reported in various studies (e.g.

Otto et al., 2009; Tunnicliffe and Church, 2011; Götz et al., 2013; Hoffmann et al., 2013). Systematically neglecting these small scale sediment storages might introduce notable error into sediment budgets (Hoffmann, 2015). Consequently, treating sediment storage as a black box in large drainage basins is problematic.

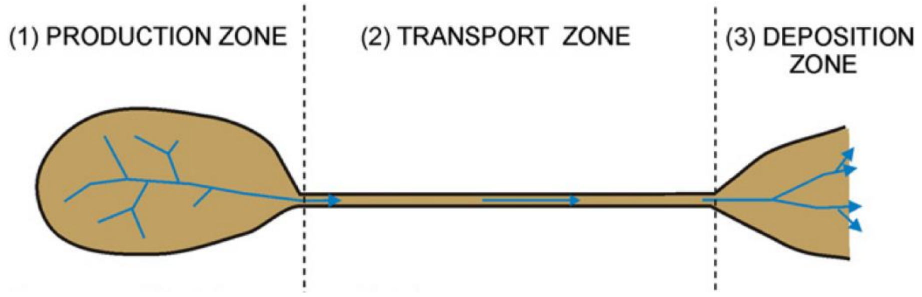

Figure 2-8: Zones of a river system (Hinderer (2012, p. 30); modified from Schumm (1977, p. 3)).

To face this error when constructing large scale sediment budgets, upscaling approaches can be a useful tool. They include methods such as pattern recognition, interpolation and extrapolation, paleo-surface models, conceptual models, empirical models, predictive models, process-based/physical models, numerical models and implicit upscaling. Overviews of the different methods can be found in e.g. de Boer (1992) (focus on geomorphology), Blöschl and Sivapalan (1995) (focus on hydrology), Harvey (2000) (focus on global change research), Wainwright and Mulligan (2004) (focus on environmental research) and Schlummer et al. (2014) (focus on archaeology and geomorphology). I refer the reader to Schlummer et al. (2014), who give a comprehensive and synoptic overview of upscaling categories including pattern recognition, interpolation and extrapolation, predictive modeling, process-based modeling as well as implicit upscaling.

Different approaches have been used to quantify sediment storage including headwater storage, leading to a quantification of smaller sediment storage forms on larger scales in high-mountain settings. Jordan and Slaymaker (1991) only include certain storage types in their budget, omitting certain colluvial or glacial storages. Otto et al. (2008) use a simple, hierarchical approach to estimate the complete storage volume in the Upper Rhone catchment based on storage quantification from the Turtmanntal (Otto et al., 2009) and valley fill quantification in the Rhone valley (Finckh and Frei, 1991; Pfiffner et al., 1997; Hinderer, 2001). A division of the large scale catchment into small subsystems of the sediment cascade based on stream order, followed by a quantification of the stored sediment in each part, yields a complete volume of 39 km^3 of sediment stored in the tributaries (Otto et al., 2008) compared to 106 km^3 stored in the main valley fill (Hinderer, 2001). Tunnicliffe and Church (2011) focus on sediment storage at scale linkages, i.e. stream junctions, while neglecting sediment storage in the uppermost catchment parts and from non-fluvial/non-flow processes. Hence, none of these approaches put their focus on quantifying all sediment storages within a large scale catchment including talus and glacial sediment storages, either by excluding certain parts of the catchment or certain storage types, or by only using data from a limited and potentially not representative sub-catchment.

2.5 Overview of common methods to study sediment storages

Studying sediment budgets including the sediment storage component is a challenging and time-consuming task. Information on (i) the sediment distribution, (ii) the 3-D geometry of the sediment body, (iii) its age and, if applicable, internal stratigraphy and (iv) the coupling or (dis)connectivity within a modern or past sediment cascade is needed to fully quantify and understand the storage component (Hinderer, 2012). I will shortly summarize different methods applied to study the distribution, volume quantification, internal architecture, age and coupling of sediment storages (Table 2-1). This summary is not intended to fully cover methods for sediment budget studies in general, but only the most common methods applied in (high-)mountain settings within the last decades. A broader overview of methods applied in sediment budget studies on different scales can be found in Hinderer (2012).

Table 2-1: Overview of common methods to study the distribution, volume quantification, internal architecture, age and coupling of sediment storages.

Method	**Short description**	**Exemplary studies**
Distribution		
Geomorphological mapping	Geomorphological mapping is a key tool for the initial analysis of a geomorphic system and serves as a basis to understand catchment configuration (Otto and Dikau, 2004). Geomorphic maps are graphical inventories of the landscape including landforms, surfaces and subsurface material. In sediment budget studies the distribution of sediment storages is mapped in the field and/or based on remote sensing data (Smith et al., 2011; Otto and Smith, 2013).	Otto and Dikau (2004), Otto et al. (2009), Götz et al. (2013), Messenzehl et al. (2014)
Semi-automated (geomorphological) mapping	(Semi-)automated mapping approaches in geomorphology can be used for the detection of landforms and thus sediment storages. Due to the benefits of repeatable and time-saving methods, this is highly desirable. However, the results are often of low to moderate accuracy. The method can be used for upscaling approaches (Seijmonsbergen et al., 2011; Otto and Smith, 2013).	van Asselen and Seijmonsbergen (2006), Schneevoigt et al. (2008), Straumann and Korup (2009)
Predictive (geomorphological) mapping	Predictive geomorphological mapping is the development of a statistical model of the functional relationship between environmental variables (available spatial information) and geomorphic processes and/or landforms. This model is then applied to create a predictive map. Models include for example logistic regression, generalized linear models, generalized additive models or machine learning techniques. The method can be used for upscaling approaches (Luoto and Hjort, 2005; Schlummer et al., 2014).	Marmion et al. (2008), Brenning (2009), Schoch et al. (2018)
Volume quantification and internal sedimentological architecture		
Geometric and statistical approaches	Well defined sediment bodies (e.g. fans, valley fills) can be quantified with geometric methods based on, for instance, the surface area and a defined geometric body (Giles, 2010), cross section modeling using power laws or polynomial regression (Hoffmann and Schrott, 2002), an iterative sloping local base level routine (Jaboyedoff and Derron,	Hinderer (2001), Hoffmann and Schrott (2002), Jaboyedoff and Derron (2005), Straumann and

Method	Short description	Exemplary studies
	2005), volume-area scalings (Straumann and Korup, 2009) or artificial neural networks (Bishop, 1995).	Korup (2009), Blöthe and Korup (2013), Mey et al. (2015)
High-resolution surface data	The generation of high-resolution surface data with terrestrial and airborne laser scanning (TLS and ALS) as well photogrammetry can be used for sediment storage quantification with a high level of precision. Furthermore, this data enables semi-automated mapping, predictive modeling and quantification of changes (Höfle and Rutzinger, 2011).	van Asselen and Seijmonsbergen (2006), Carrivick et al. (2013), Götz et al. (2013)
Geophysical surveying	Geophysical methods, including electrical resistivity tomography, ground penetrating radar and seismic refraction, are used to detect boundary surfaces (e.g. sediment-bedrock, between landforms) and the internal sedimentary architecture. In many cases it is recommendable to use a combination of at least two methods to yield good results and to avoid misinterpretation (Schrott and Sass, 2008; Hinderer, 2012).	Hinderer (2001) (with data from Finckh and Frei (1991) and Pfiffner et al. (1997)), Schrott et al. (2003), Otto et al. (2009), Schoch-Baumann et al. (under review)
Core drilling	Core drilling can be applied to detect sediment thickness, internal sedimentary architecture and stratigraphic sequences at single point locations (Schrott et al., 2013).	Schrott et al. (2002), Schrott and Adams (2002), Götz et al. (2013)
Age		
Radiocarbon dating (^{14}C)	Radiocarbon dating is one of the most widely used and was one of the first available absolute dating techniques in Earth sciences. The upper age limit for radiocarbon dating is c. 50 ka and organic material must be present in the sediment. In sediment storages for example peat or soil layers as well as charcoal fragments can be dated (Walker, 2005).	Schrott and Adams (2002), Hornung et al. (2010), Götz et al. (2013), Ratnayaka et al. (2019)
Cosmogenic radionuclide dating	Cosmogenic radionuclides include the often used members ^{10}Be, ^{26}Al, ^{36}Cl and ^{14}C (see above) in Earth sciences, due to their well suited half-life length and wide range of applications. Cosmogenic nuclides can be used for (i) surface exposure dating and (ii) burial dating in sediment storage analysis. (i) Every geologic surface can in general be	(i) Savi et al. (2016), Ratnayaka et al. (2019), Schoch-Baumann et al. (under review)

Method	**Short description**	**Exemplary studies**
	dated by measuring the amount of accumulated cosmogenic nuclide in surficial rocks (f.i. depositional surfaces of fans or erosional surfaces of landslide scarps) or in a depth profile. (ii) Burial dating relies on the differential decay of cosmogenic nuclides where previously exposed samples become shielded from cosmic rays (e.g. burial by subsequent deposition) (Granger and Muzikar, 2001; Ivy-Ochs and Kober, 2008; Dunai, 2010).	(ii) Balco and Rovey (2008), Balco et al. (2013)
Optically stimulated luminescence (OSL) dating	Luminescence dating techniques are subdivided based on the energy supplied for stimulation: by light for OSL and by heat for thermoluminescence (TL). Only light sensitive electron traps are stimulated during measurement of the luminescence signal. This is an advantage of OSL over TL for dating sediment. It results in a higher dating precision and enables dating of sediments only briefly exposed to light before burial. OSL can be used with very common quartz and feldspar minerals and it is applicable to a wide range of materials and sedimentary systems such as fluvial, colluvial, glacial, Aeolian or coastal. OSL dating is an absolute dating technique, dating sediments and thus landforms or sediment storages directly by detecting the time elapsed since grains were last exposed to daylight. The age range comprises few years to > 100,000 years (Lang et al., 1999; Stokes, 1999; Mellett, 2013).	Preusser et al. (2007), Chen et al. (2008), Blöthe et al. (2014)
Further dating methods	Other dating methods e.g. dendrochronology, varve chronology, lichenometry, palynology and relative dating methods such as rock surface weathering and pedogenesis (van der Knaap et al., 2000; Walker, 2005) are less common in sediment storage analysis.	
(Dis)Connectivity and coupling along the sediment cascade		
Index of connectivity (IC)	The IC is a distributed geomorphic index focusing on the influence of topography on sediment connectivity, i.e. it can be used to investigate landform distribution and sediment fluxes in mountain areas. It is a hydro-geomorphic approach based on slope gradient, flow length, surface roughness and contributing area (Borselli et al., 2008; Cavalli et al., 2013).	Messenzehl et al. (2014), Cavalli et al. (2019)

Method	Short description	Exemplary studies
Graph theory for sediment cascade analysis	Mathematical graph theory is applied to explore the network structure of coarse sediment pathways. Numerical models for geomorphic processes, such as rockfall, debris flow and fluvial processes, are used to set up a spatially explicit graph model of sediment sources, pathways and sinks. Raster cells of a DEM are the nodes of this graph and simulated sediment pathways are the corresponding edges (Heckmann and Schwanghart, 2013; Heckmann et al., 2015).	Heckmann et al. (2016a)
Toposequences	Toposequences can be detected from geomorphic sediment storage maps to assess the (de)coupling state of landforms/sediment storages along the sediment cascade and sediment connectivity. This approach is based on manual mapping (Rasemann, 2004; Messenzehl et al., 2014).	Otto et al. (2009), Messenzehl et al. (2014)

3 Study area

The URB is located in the southwestern Swiss Alps between the Rhone Glacier and Lake Geneva, and is one of the largest inner-alpine basins with a size of c. 5400 km^2 (Figure 3-1). The Rhone valley with a total length of c. 160 km dissects the western Swiss Alps with a general southwest trend, along regional tectonic structures. The valley abruptly changes to a north-northwest direction at Martigny. It shows an asymmetry whereby the tributaries draining the area north of the main valley are smaller than the tributaries in the south. The drainage basin is a closed system for suspended and clastic sediment transport with Lake Geneva acting as a sediment sink. The basin is located between 372 and 4634 m asl, with dozens of peaks reaching elevations of more than 4000 m.

In this chapter relevant information on the study area is given, including the tectonic and geologic setting, the glacial history since the Pleistocene, sediment storage and transient sediment fluxes as well as the past and present climate.

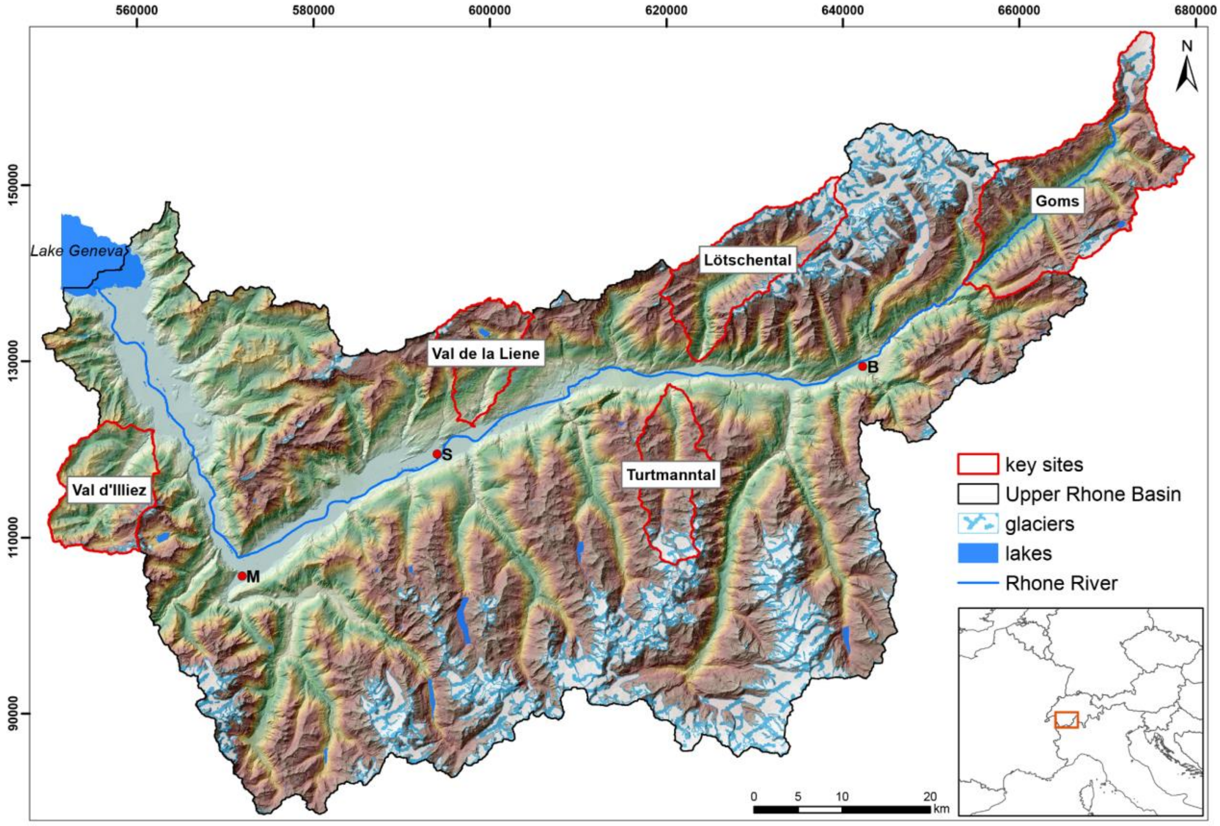

Figure 3-1: Location of study area and key sites (chapter 6) within the Upper Rhone Basin (URB) (M = Martigny, S = Sion, B = Brig). Glacier extent from Swiss glacier inventory 2010 (Fischer, 2013). Lakes classified based on digital elevation model (DEM) with a semi-automated surface classification model (Bowles and Cowgill, 2012; DEM from swisstopo, projection: CH1903).

3.1 Tectonic and geologic setting

The geologic structure of Switzerland between the Po Basin and the Molasse Basin is characterized by nappe systems derived from the continental margins of Europe and Adria (promontory of Africa) and the ocean basins existing between the two. Plate tectonic movements during mountain building involved the breakup of the supercontinent Pangea and the opening of the Alpine Tethys. This ocean subsequently subducted underneath the Adriatic continent, finally followed by the collision of the Adriatic and the European continent. The nappe systems consist of crystalline basement rocks and cover sediments deposited on top. The Penninic and the Helvetic nappes, i.e. thin sheets of rocks, were transported over long distances (50-200 km). Over the last 30 Ma, most of the nappe pile (c. 30 km) has been eroded and underlying crystalline bedrock was exposed (e.g. the Aar massif) (Pfiffner, 2021). The bedrock geology of the URB is dominated by three major tectonic units: the Penninic unit (areal cover c. 52%), the Helvetic unit (areal cover c. 16%) and the crystalline basement bedrock (Aar and Gotthard massifs, areal cover c. 22%) (Figure 3-2). The rest of the URB is covered by minor units and unconsolidated Quaternary sediments (c. 6%). For a detailed overview of the architecture of the Alps the reader is referred to Schmid et al. (2004) and Pfiffner (2021). The southwest oriented Rhone valley marks a major active tectonic boundary (Rhone-Simplon fault) between the Penninic and the Helvetic units. The Penninic units, derived from the marine basins formed between the two continental margins in the Mesozoic, cover the largest area of the catchment mainly located south of the Rhone and consist of Penninic basement nappes and Mesozoic sediments. Thus, folding involved the crystalline basement rocks (mainly metamorphic rocks: gneiss, schists, and metasedimentary rocks). The Helvetic and Ultrahelvetic nappes are part of the former European continental margin and are located north of the Rhone-Simplon fault or the Rhone valley. The unit is dominated by nappes consisting of (meta)sedimentary rocks (mainly Mesozoic and Tertiary limestone dominated cover nappes). The crystalline basement bedrock includes the Aar Massif, the largest of the Swiss massifs, the Gotthard Massif (Allochthone massifs and Infra-Penninic crystalline nappes) occurring upstream of Brig and in the Goms and Aletsch region, as well as the Mt. Blanc and Aiguilles Rouges Massifs underlying the area near Martigny and the Mt. Blanc region. The crystalline basement rocks represent the oldest rock types. The lithology comprises mainly granitic rocks as well as gneiss, schists and metagranitoids (Schmid et al., 2004). The erodibility of the lithologies found within the study area is investigated by Kühni and Pfiffner (2001) based on a geotechnical map and regional geomorphic studies. Erodibility controls topography, accordingly higher mean elevations and slopes are found in regions with lithologies of low erodibility. The lithologies of the Helvetic and Ultrahelvetic nappes are characterized by medium and high erodibility, while the Penninic nappes and the external massifs (i.e. the Gotthard and Aar massif) have a low or very low erodibility, respectively. The Rhone river follows the Rhine-

Simplon fault, which is at the same time a contact zone between a more and a less erodible unit (Kühni and Pfiffner, 2001).

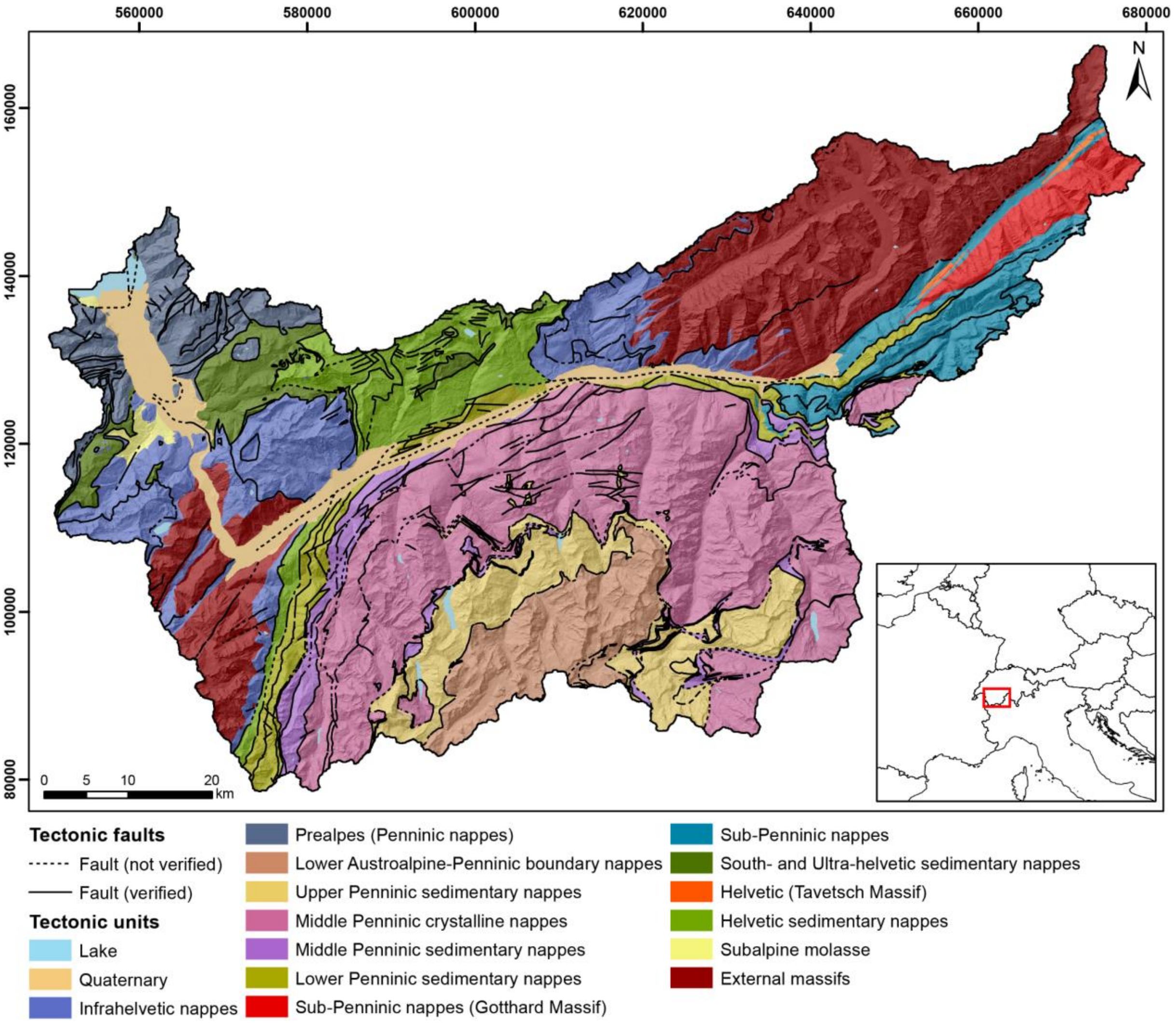

Figure 3-2: Simplified geologic map of the URB showing the major litho-tectonic units and tectonic faults (swisstopo, 2011; DEM from swisstopo, projection: CH1903).

Fission track ages show spatially variable uplift rates in the Western Alps over a longer time scale. Apatite fission track ages range between 1.5 and 20 million years within the URB. The northern areas (Helvetic unit), the Aar Massif and the southwestern part of the basin have considerably lower ages (1.5-8.0 Ma), than the area south of the Rhone valley (Penninic unit) and the area close to Lake Geneva (8-20 Ma). Thus, long term uplift rates are highest in the area with low apatite fission track ages (Vernon et al., 2008). Recent uplift rates in the study area are some of the highest in the Alps and generally show a similar picture as long-term exhumation rates. Levelling and geodetic surveys show uplift rates of up to 1.3 mm a^{-1} in the eastern part of the URB, but decrease to < 0.3 mm a^{-1} near Lake

Geneva (Kahle et al., 1997; Schlatter et al., 2005). High uplift rates occur due to erosion (Champagnac et al., 2009), glacial isostasy (Gudmundsson, 1994; Mey et al., 2016) and collisional processes (Persaud and Pfiffner, 2004).

3.2 Glaciation since the Last Glacial Maximum

The topography in the URB is strongly impacted by repeated Pleistocene glaciations (Lang and Wolff, 2011) and is thus characterized by U-shaped valleys, cirques, hanging valleys and steep peaks (Penck, 1905; Sternai et al., 2011). Glacial erosion produced a high-mountain landscape with peaks over 4000 m and contrasting glacial overdeepenings up to 1000 m in depth (Pfiffner et al., 1997). During the LGM of the Würmian Ice Age (LGM, 22.1 ± 4.3 ka) the whole basin, with the exception of some ridges and peaks, was covered with glacial ice (Bini et al., 2009; Schlüchter et al., 2021) (Figure 3-3). The ice thickness was > 2000 m based on a sediment and ice free topography (Mey et al., 2016). The glaciers in the study area were influenced by at least four centers of ice accumulation: the Rhone ice dome, the Aletsch ice field, the southern Valais icefield and the Mt. Blanc region (Kelly et al., 2004). The Rhone ice dome with radial outflow following the pre-existing valley system but also flowing over the high passes (Grimsel and Furka Pass) was located in the headwaters of the Rhone valley (Florineth and Schlüchter, 1998). The LGM Rhone Glacier filled the Rhone valley, outflowed onto the foreland and was the main component of the LGM transection glaciers in the western Alps, an interconnected system of valley glaciers. It reached a thickness of as much as 2300 m near Martigny. Around Brig and Martigny, ice diffluences existed and ice exited the Rhone valley towards the south across Simplon Pass and Gd. St. Bernard Pass as well as towards southwest, north of present-day Glacier d'Argentière. Ice confluences were located south of the Aletsch icefield, north of the Southern Valais icefield and north of the Mt. Blanc region near Martigny (Kelly et al., 2004). The Rhone Glacier expanded into the alpine foreland after 30 ka (Ivy-Ochs et al., 2006b). This is further confirmed by a mammoth tusk recovered from fluvioglacial gravel deposited in front of the advancing Rhone Glacier yielding an age of 30.2-28.5 ka (recalibrated; near Finsterhennen) (Schlüchter, 2004b). Luminescence dating of sediments from the same site shows similar ages (Preusser et al., 2007). Deglaciation (retreat from LGM position) began in 21.1 ± 0.9 ka and ice collapse already initiated between 16.8 and 17.4 ka, indicating the onsetting of the Lateglacial period (Ivy-Ochs et al., 2004; Ivy-Ochs et al., 2006b; Ivy-Ochs et al., 2008). This period lasted until alpine glaciers reached the dimensions of the Holocene maximum extent, i.e. in most places the LIA maximum (Ivy-Ochs et al., 2008). Deglaciation was an "environmental catastrophe", since it was rapid. Radiocarbon dates from organic material in the southern and northern foreland as well as inner-alpine areas are synchronous and there are no moraines deposited in the main valleys in between the LGM moraines and the high-mountain valley (Schlüchter, 1988; Schlüchter et al., 2021). By 18 ka more than 80% of the LGM ice volume had melted (Ivy-Ochs et al., 2008). Some inner-alpine regions were ice-free by around 15-14 ka (Welten, 1982; Maisch, 1987). During the Lateglacial period, lasting only until around 10 ka, glaciers advanced several times to successively smaller positions (stadials: Gschnitz, Clavadel, Daun and Egesen) and deposited moraines (Ivy-Ochs et al., 2006b; Ivy-Ochs et al., 2008). Moraines, formed during the Gschnitz stadial, can be found in many tributary valleys, but are missing in the main valley, where glaciers at that time were still large (Ivy-Ochs et al., 2006a).

Data from the Valais do not feature such old ages for deglaciation as other inner-alpine areas. Lac du Mont d'Orge near Sion (640 m asl) was, based on pollen analysis, a shallow lake above dead ice during the Oldest Dryas based on pollen analysis. Thus, this area was ice-free by at least 13 ka. A depression (today peat Zeneggen-Hellelen, 1510 m asl) south of the Rhone valley in the Visp Valley was supposedly filled with dead ice after deglaciation until end of the Younger Dryas. Oldest radiocarbon ages within the peat are c. 12.3 ka BP old. Hence, the area was probably ice-free by around 13 ka. Lower parts of the Aletsch region (Bitsch-Naters, 1030 m asl) were ice-free by at least 10.0-9.7 ka BP (Welten, 1982). Regional studies based on cosmogenic nuclide exposure ages of bedrock within the URB reveal more details on post-LGM deglaciation. At the Grimsel Pass (2164 m asl, northeast of URB) deglaciation took place at least from about 14.0 to 11.3 ka, indicated by ^{10}Be exposure dates on Nägelisgrat (E of Grimsel Pass) below 2500 m asl (Kelly et al., 2006). Deglaciation of the Simplon region (~2000 m asl, southeast of URB) took place between 13.5 ± 0.6 and 15.4 ± 0.6 ka, therefore the Simplon Pass became ice-free at 14.1 ± 0.6 ka. The high valley glaciers melted during the Bølling-Allerød interstadial after the Oldest Dryas (Dielforder and Hetzel, 2014). This is supported by palynostratigraphy and radiocarbon ages of 14.0-15.6 ka BP (recalibrated) from Lake Hopchu at Simplon Pass (Welten, 1982; Dielforder and Hetzel, 2014). Exposure ages from higher elevations of 17.8 ± 0.6 and 18.0 ± 0.6 ka reflect the downwasting of the Rhone ice dome and the termination of ice transfluence across the Simplon Pass towards the southern foreland (Dielforder and Hetzel, 2014). Directly investigating the deglaciation of the Rhone valley and the retreat of the valley glaciers is difficult, since the valley is filled with a thick Postglacial valley fill and no bedrock is exposed. The Pleistocene-Holocene boundary is dated at 11.7 ka, which represents the end of the Younger Dryas cold spike (Schlüchter et al., 2021).

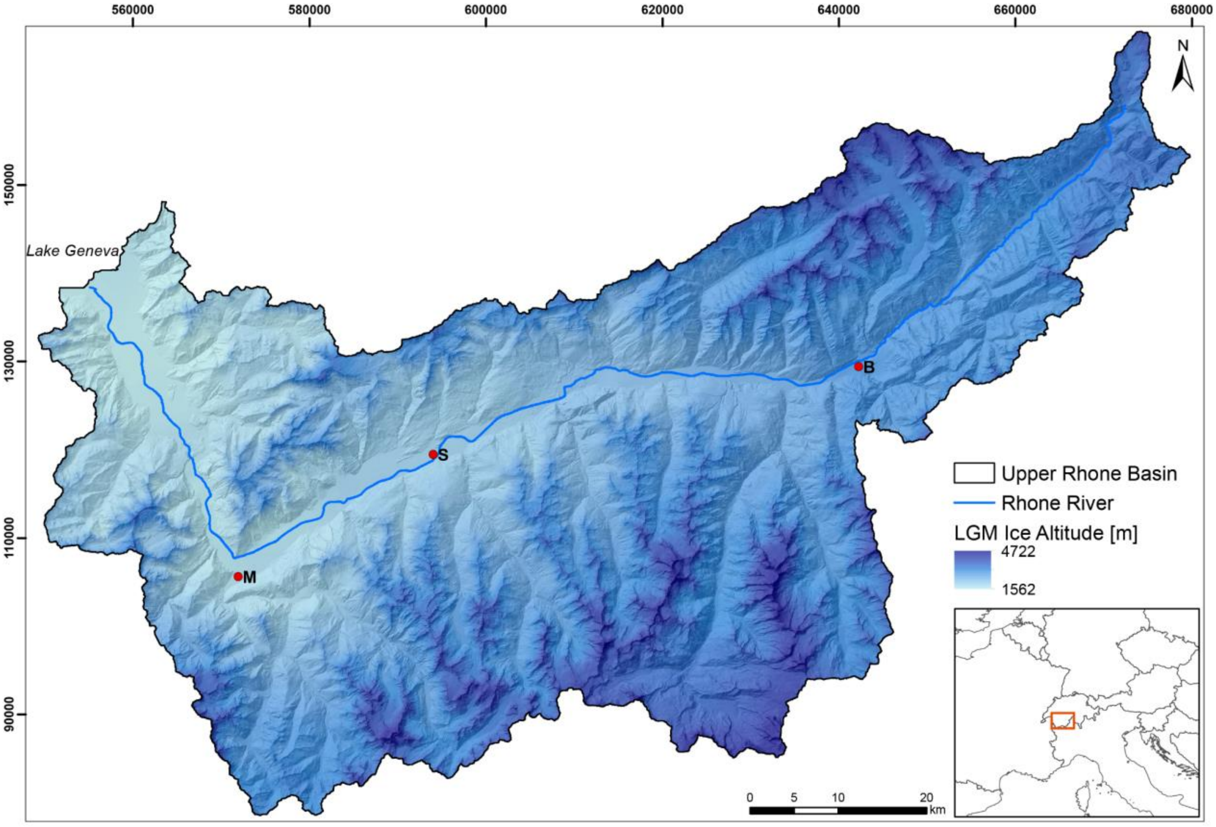

Figure 3-3: Last Glacial Maximum ice altitude within the URB (Bini et al., 2009) (M = Martigny, S = Sion, B = Brig). (DEM from swisstopo, projection: CH1903).

Compared to other regions in the Alps, glaciers are still widespread in the URB due to high elevations and precipitation from (north)westerly and south/southwesterly atmospheric circulation patterns (Kelly et al., 2004). Approximately 569 km^2 (c. 10.6%) of the land surface was covered with glacial ice in 2010 (Fischer, 2013; Fischer et al., 2014). The highest glacier cover is located in the Aletsch region, in the southern part of the study area, the Valais Alps and especially the Mattertal, the Mont Blanc massif and in the Goms region with the Rhone Glacier (Penninic unit and crystalline basement rock). In the Helvetic unit the glacial cover is comparably low. This is conditioned by the substantially higher elevations in the Penninic unit and crystalline basement rock. During the LIA, c. 929 km^2 were covered with glacial ice (Maisch, 2000), hence the deglaciated areas since 1850 comprise 360 km^2 within the URB. The glaciers within the study area lost c. 39% of their areal extent within the time period 1850-2010 (Figure 3-4).

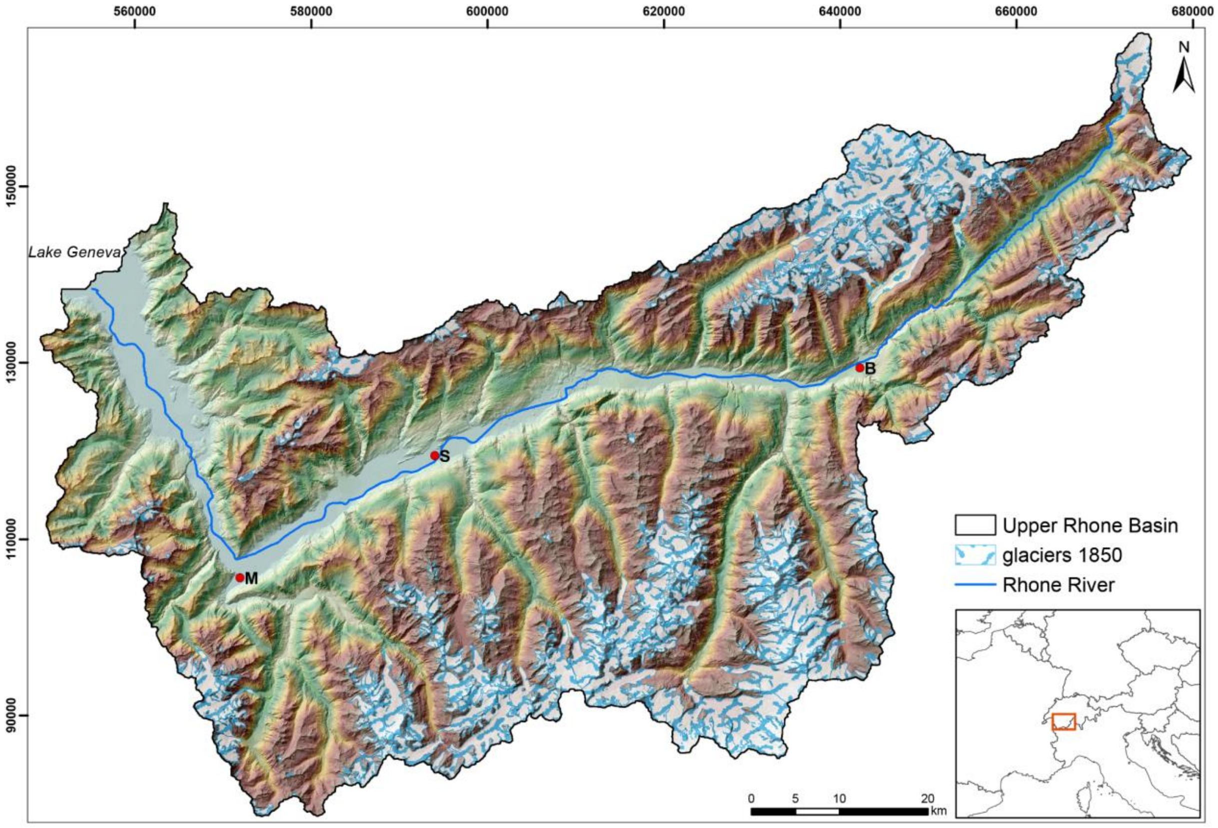

Figure 3-4: Glacier extent c. 1850 (Maisch, 2000) during the Little Ice Age in the URB (M = Martigny, S = Sion, B = Brig). (DEM from swisstopo, projection: CH1903).

3.3 Sediment storage and transient sediment fluxes in the Upper Rhone Basin

The landscape of the URB was mainly formed by Pleistocene glaciations (Pfiffner et al., 1997). Currently, the glacially conditioned landscape is adjusting to fluvial conditions (Ballantyne, 2002b) through e.g. fluvial incision (Valla et al., 2010b), mass wasting (McColl, 2012), and sediment transport (Church and Slaymaker, 1989), i.e. the landscape is in a transient state (Brunsden and Thornes, 1979; Schlunegger and Norton, 2013). The adjustment from a glacial to a fluvial landscape is prominent at the so called transition zones between the Rhone valley and the tributaries, often forming hanging valleys. Transitions zones are characterized by knickpoints, steep gradients and V-shaped valleys. They are dominated by river incision and unstable slopes. Within the URB, these knickpoints are located close to the trunk stream because lithologies with low erodibility are widespread (e.g. Schlunegger and Hinderer, 2003; Norton et al., 2010a; Valla et al., 2010a; Valla et al., 2010b).

The architecture and thickness of the valley fill of the Upper Rhone valley between Vouvry (near Lake Geneva) and Turtmann was investigated with nine high resolution seismic surveys (Finckh and Frei, 1991; Pfiffner et al., 1997). The Rhone valley is strongly overdeepened, reaching as deep as 500 m below sea level near Martigny (Pfiffner et al., 1997) and near Vouvry (Finckh and Frei, 1991). Hence, the valley fill is c. 1000 m thick. The valley is U-shaped at the bottom, but has less steep side walls than an idealized glacial valley profile. The sedimentary units of the sediment body were deposited during glaciation (sub-glacial channel deposits, lodgement till) and deglaciation (melt-out till) as well as Postglacial sediments (glacio-lacustrine deposits from a proglacial setting, lacustrine/deltaic sediments). The sediments were mostly accumulated during one single deglaciation event of the Last Glacial Maximum. Deposition of the Postglacial sediments during the last deglaciation was rapid with a maximum interval of 5 kyr between 18 and 13 ka BP. Sedimentation rates in this period were ~6 cm a^{-1}, i.e. 300 m of sediment were deposited within 5 kyr (Pfiffner et al., 1997).

Based on this geophysical data and a geomorphological approach that extrapolated the hillslope into the subsurface, Hinderer (2001) estimates the sediment volume of the valley fill in the Rhone valley between Brig and Lake Geneva to ~106 km^3. Additional 35 km^3 of sediment are stored in Lake Geneva. Rosselli and Olivier (2003) use gravimetric measurements and estimated the valley fill volume between 80-100 km^3. Jaboyedoff and Derron (2005) propose a volume of 118 km^3 with parabolic valley cross sections. Information on the valley fill thickness in the Rhone valley is complemented by data based on the geometric properties of the landscape using artificial neural networks. The total estimated sediment volume yields 97 ± 11 km^3 based on this method. The mean deviation of cross-sectional area between measurements from seismic surveys and model estimates is 21.5% (Mey et al., 2015). This dataset is further extended to the Goms region and also the tributaries of the Rhone. The capability of applying the method easily to larger spatial scales and other areas is a big advantage of this method. The estimated valley fill thickness in the Goms region is up to 270 m with an average thickness of 100 m (pers. communication, J. Mey). This yields an additional sediment volume of c. 1.5 km^3 stored in the Goms valley fill.

Sediment yields for the URB were estimated with these sediment volumes. In general, sediment yields in the Alps reached a maximum during deglaciation when large amounts of unconsolidated sediment were available, vegetation cover was low and transport capacities were high. Sediment yields decreased over time during the Holocene by one order of magnitude. While the modern sediment yield from the Rhone Basin is 380 kt km^{-2} yr^{-1}, the average post-LGM sediment yield was 2370 kt km^{-2} yr^{-1} (Hinderer, 2001), exceeding modern rates by a factor of > 7. Mean post-LGM denudation rate was 1010 mm kyr^{-1}. However, the effective Late Glacial denudation rates must have been even higher (2870 mm kyr^{-1}), because mean denudation rates during the Holocene were supposedly in the order of modern denudation rates (240 mm kyr^{-1} calculated from river sediment loads) (Hinderer, 2001; Hinderer et al., 2013). Late-glacial denudation rates are comparable to catchment-wide denudation rates from ^{10}Be analysis in glaciated basins (Figure 5-13).

Denudation rates for alpine catchments from ^{10}Be abundances in stream samples covering a millennial time scale are some of the highest in the URB compared to other regions in the European Alps (Wittmann et al., 2007; Norton et al., 2010b; Stutenbecker et al., 2018; Delunel et al., 2020). The denudation rate for the whole catchment (sample location near Vouvry) is 1603 ± 319 mm kyr^{-1}, but spatially averaged denudation rates are highly variable along the Rhone river ranging between 178 ± 38 near Sion and 1933 ± 434 mm kyr^{-1} near Granges, Sierre (Wittmann et al., 2007; Codilean et al., 2018; Stutenbecker et al., 2018). Averaged denudation rates for the tributaries are also very variable (101 ± 20 for the Wilerbach, Goms, to 9051 ± 2454 mm kyr^{-1} for the Illgraben) (Wittmann et al., 2007; Norton et al., 2010b; Codilean et al., 2018; Stutenbecker et al., 2018). The characteristics of these tributary catchments are very diverse with large differences in mean gradient, glacier cover, size, lithology and uplift rates. Especially for highly glaciated catchments (up to 50%) or catchments dominated by gravitational mass movement processes, the analyzed denudation rates need to be questioned. Delunel et al. (2020) observe a high variability in catchment denudation rates across the Alps with a strong control of slope and a correlation to recent uplift rates. An analysis of all catchment-wide denudation rates of areas draining ultimately into Lake Geneva show also a strong correlation to slope as well as glacier cover. In general, catchments with no or very low glacier cover have considerably lower denudation rates (Figure 5-13).

Modern denudation rates for the URB calculated from sediment and dissolved yield of the Rhone at Porte du Scex near Lake Geneva yield a denudation rate of 240 mm kyr^{-1}. Certain tributaries within the URB or sub-catchments of tributaries have very variable denudation rates varying between 128 to 2869 mm kyr^{-1} (Hinderer et al., 2013). Their relation to longer-term denudation rates has been discussed before. Modern denudation rates are in general lower, due to human impact including reservoir construction, sediment extraction, sediment storage and climate change (Hinderer et al., 2013; Stutenbecker et al., 2018)

3.4 Climatic conditions in the Upper Rhone Basin since the end of the Pleistocene glaciations

After the end of the last glaciation, called Würm in the Alps, the climate in Switzerland was characterized by several variations during the Late Glacial and Postglacial periods (end of the Pleistocene at 11.7 ka). Cold phases, so called stadials, during the Late Glacial (i.e. Gschnitz, Clavadel, Daun and Egensen; Oldest and Younger Dryas) were significantly stronger and colder than during the subsequent Postglacial/Holocene. Each cold phase resulted in advancing glaciers. The Bølling-Allerød phase (13-11 ka BP) featured a warmer period with a glacier retreat possibly close to today’s glacier extent (Maisch, 2000; Ivy-Ochs et al., 2008). During the Postglacial, climatic fluctuations were shorter and had smaller amplitudes. The relatively stable climate is revealed by different proxys, e.g. oxygen isotopes from Greenland icecores (Andersen et al., 2004) and lake sediments (von Grafenstein et al., 1999) on a larger scale. More local proxys such as laminated lake sediments (Nussbaumer et al., 2011), remains of wood and peat in glacier forefields (Joerin et al., 2006), tree line positions (Tinner and Theurillat, 2003), dendrochronology (Nicolussi et al., 2009) and seed production of certain plants, pollen and macrofossil records (Haas et al., 1998) show more detailed and local climatic oscillations. For example, the periods from c. 9-5 ka BP (Holocene climatic optimum), 4.5-3.5 ka BP and around 3 and 2 ka BP were distinguished by warmer periods, while the phases in between were characterized by colder conditions, such as the Misoxer, Piora, Löbben and Göschener cold phases (overview in Maisch, 2000; Joerin et al., 2006; Ivy-Ochs et al., 2009a; Schlüchter et al., 2021).

Since there is no detailed areal climatic data available for the time after the end of the Pleistocene glaciations, I need to regard the current climatic conditions. I assume, they are in their basic distribution representative for the heterogeneous climate within the study area over a longer timescale. The current climate in the URB is very heterogeneous. While annual precipitation is less than 600 mm within the Rhone valley, it reaches > 2500 mm in high elevations, reaching up to ~3500 mm in the Jungfrau Massif (north of Brig) representing the peak value in Switzerland (Figure 3-5). Inner-alpine valleys are located in shielded positions, resulting in the lowest precipitation values of Switzerland in the Rhone valley between Martigny and Brig. Precipitation is mainly driven by an orographic effect, while a simple relation between precipitation and height does not exist (Frei and Schar, 1998). The mean annual temperature ranges between c. -10 and 10°C. Highest temperatures are recorded in the Rhone valley at low elevations and decrease towards higher elevations. However, a linear vertical dependence does not exist. Deviations are for instance cold-air pools or maximum recorded temperatures during the summer in alpine valleys (Figure 3-5) (Frei, 2014).

The datasets RnormY8110 and TnormY8110 show the yearly precipitation [mm] and the mean annual temperature [°C] averaged over the period 1981-2010, respectively (Figure 3-5) (SwissMeteo, spatial resolution 2 km). The spatial analysis of the mean yearly precipitation is based on RhiresY, which uses a high-resolution rain gauge network (currently c. 420 stations). Details on the analysis and interpolation methods (PRISM approach) can be found in Schwarb (2000) and Schwarb et al. (2001). The spatial distribution of the mean annual temperature is based on temperature norm values (1981-2021) from c. 90 climatological stations in Switzerland. The interpolation methods are described in detail in Frei (2014).

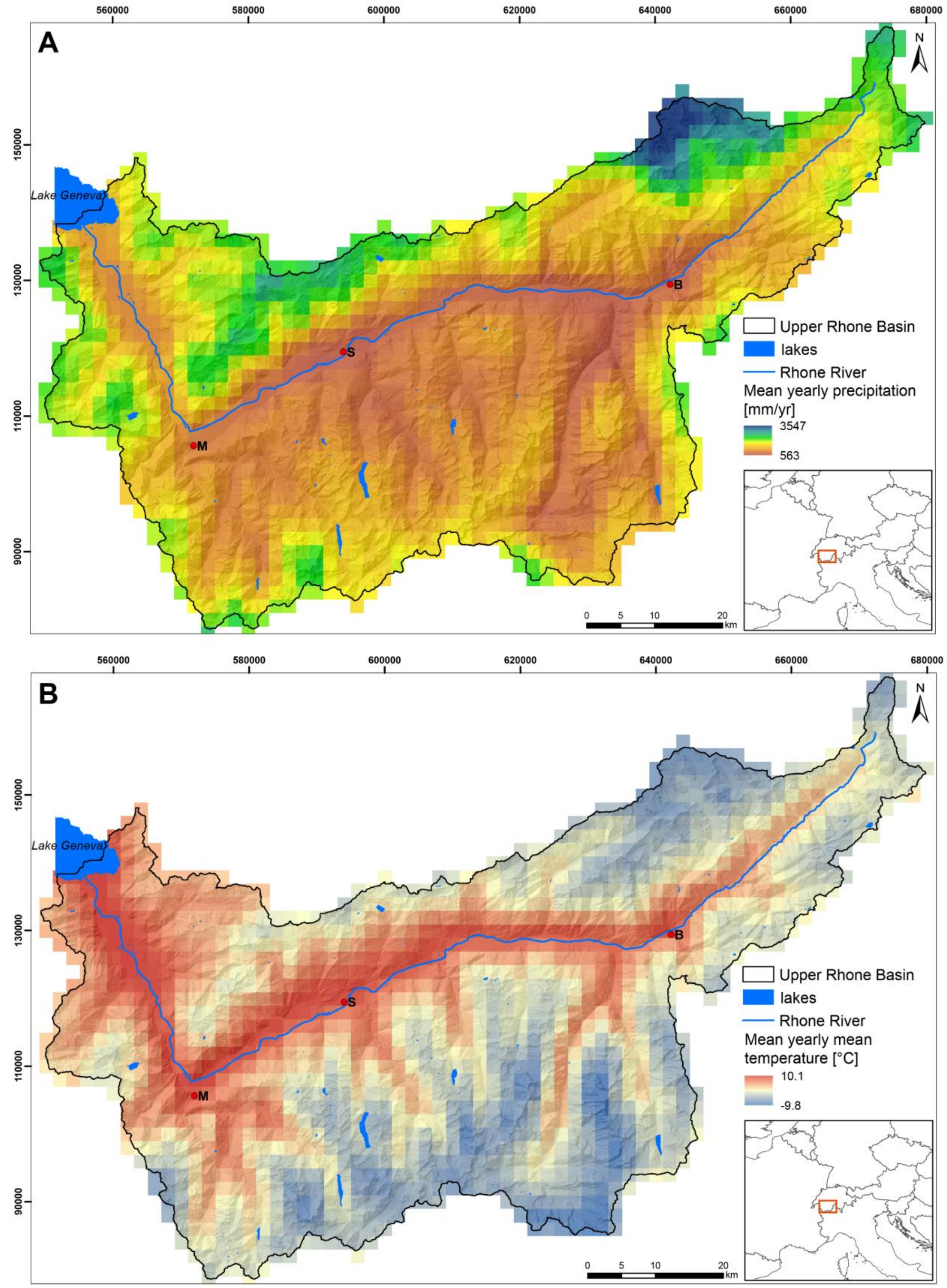

Figure 3-5: A: Spatial distribution of yearly precipitation [mm] averaged over the period 1981-2010 (norm value, RnormY8110). B: Spatial distribution of the yearly mean temperature [°C] averaged over the period 1981-2010 (norm value, TnormY8110) (MeteoSwiss).

4 Conceptual and methodological approach

Analyzing sediment storage needs a careful consideration of spatial and temporal scales (Hinderer, 2012). De Boer (1992) points out that any geomorphic system, its form and functioning is the product of processes operating at all scales. The nested, hierarchical structure of geomorphic systems needs to be acknowledged to understand the effect of scale in process geomorphology. Every geomorphic system consists of smaller, lower level systems and is part of larger, higher-order systems. Thus, a hierarchical approach to study geomorphic systems is sensible. However, to understand a system not every scale has to be considered, but depending on the objective of the study and the studied scale, certain scale levels will be dominant (de Boer, 1992).

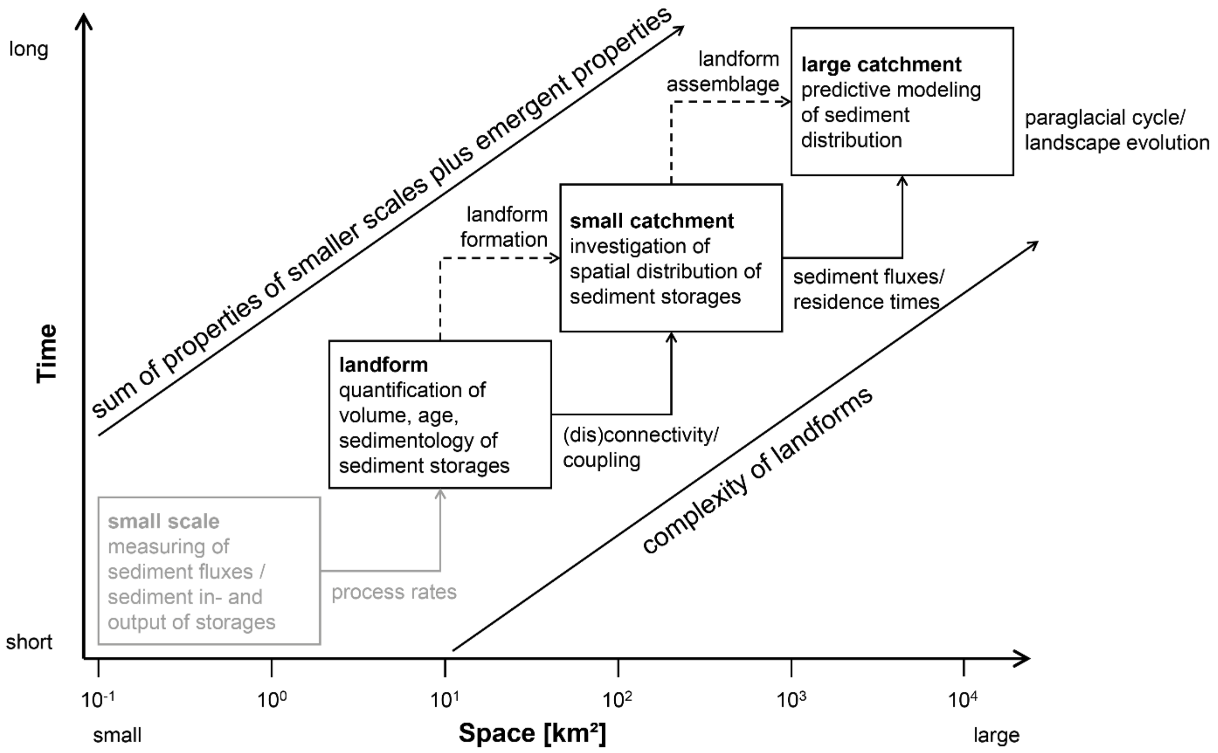

Figure 4-1: Conceptual approach: scaling relationships for the sediment storage analysis in the URB. Solid arrows show the sediment-related relations existing between the scales. Dashed arrows show the conceptual scale linkages and the data transfer between scales. For each scale the most relevant analyses are listed (see boxes). More details on applied methods in text and Table 4-1. Modified from Phillips (1999, p. 131), Slaymaker (2006, p. 9) and Otto et al. (2008, p. 259).

In this thesis a hierarchical scaling approach was established (Figure 4-1), meaning that different kinds of knowledge can be produced on each scale level in this hierarchy. Knowledge from each scale is mutually exclusive but not contradictory. This is based on the assumption, that a larger system can be understood by studying subsystems at all levels. However, one needs to recognize scale invariance, i.e.

the consistency of properties on one scale, may not exist (Phillips, 2001; Slaymaker, 2006). Furthermore, the complexity of single landforms increases with increasing spatial scale and the characteristics on each scale consist of the sum of properties of the smaller scales plus new, emergent properties (Phillips, 1999). Larger alpine catchments contain a complex pattern of sediment storage. Landforms are located at different positions along a sediment cascade, where sediment is transferred. Sedimentary deposits are often decoupled through climatic (i.e. permafrost), vegetative or topographic (for example hanging valley) conditions and thereby preserved from erosion (Otto et al., 2008). While sediment storage forms in alpine headwaters are often deposited by one (dominant) process (talus deposits by rock fall processes, debris flow cones by debris flows), sediment deposits e.g. in valley fills on a larger scale are more complex comprising the deposits of several processes, such as glacial, (glacio-)fluvial and gravitational mass movements, interfingering with each other. These landform assemblages of relict, overlapping and replaced landforms reflect the active processes over time (Hewitt, 2002a).

I argue, scaling issues can only be overcome by applying a multi-scale approach. The strengths of each scale need to be highlighted and data need to be available or produced at each scale that can then be linked to other scales through appropriate methods. Thus, data from different smaller scales is needed to comprehend sediment storage on a larger scale. Each scale has certain strengths and geomorphic characteristics determining the applicable methods (Figure 2-5). Certain properties associated with scales need to be carefully considered. On the one hand, the observation scale and the targeted modeling scale need to be brought together by overcoming the discrepancies between these two scales. On the other hand, the observation scale needs to fit the process scale, meaning the scale at which processes operate (Blöschl and Sivapalan, 1995; Zhang et al., 2004; Schlummer et al., 2014).

Sediment storages and their distribution are studied with a multi-scale approach in this thesis. Three spatial scales are covered comprising the URB with a size of c. 5400 km^2 on a large, catchment scale; five tributaries within the basin of c. 90-230 km^2 on a medium, regional scale and three outsize fans in the Goms with a catchment size of c. 1 km^2 on a small, local scale (Figure 4-1, overview of applied methods in Table 4-1). The investigated, temporal scale is roughly consistent on all three spatial scales and spans the time since LGM deglaciation, i.e. the Late Glacial and in particular the Postglacial period. In the following paragraphs I point out the conceptual strengths of each studied scale and the relevant sediment related properties.

4.1 Conceptual and methodological approach on the local scale

On the local scale, the focus lies on single landforms. The strength of this scale is to investigate in detail certain characteristics of landforms to better comprehend their formation, including the volume quantification, age and sedimentary architecture. Observational scale and process scale are the same on this hierarchy level. The gathered information can be used as input for the next higher spatial scale, the small catchment scale, where these details can be used to understand the spatial distribution of different sediment storages and their assemblage.

Outsize fans in the Goms region are examined in detail on a small, local scale. The three outsize fans are characterized by an anomalous relationship between fan and catchment area (up to > 1.0) (e.g. Crosta and Frattini, 2004; Jarman et al., 2011). Knowledge on the formation of these landforms and sediment storage forms is not thorough, therefore their surface morphology, sedimentology, and formative period are studied explicitly.

A multi-method approach combining morphometric analysis of the fans and their source areas based on a high-resolution DEM with ground-penetrating radar and electrical resistivity tomography measurements of the subsurface material (e.g. Otto and Sass, 2006; Schrott and Sass, 2008; Hornung et al., 2010) and cosmogenic radionuclide exposure dating (e.g. Ivy-Ochs and Kober, 2008; Ivy-Ochs et al., 2013) is applied. These methods are described in more detail in chapter 5.

4.2 Conceptual and methodological approach on the regional scale

On the regional scale the spatial distribution of sediment storage and bedrock are investigated. As I assume scale invariance is highly unlikely, I produce data in five different key sites: Val d'Illiez, Val de la Liène, Turtmanntal, Lötschental and Goms (Figure 3-1). These key sites are chosen to represent the high spatial heterogeneity within the large Upper Rhone catchment concerning e.g. geology and lithology, surface morphology, relief, climate, Pleistocene glacial imprint and contemporary glacial cover. On this spatial scale (~100 km^2) it is still possible to make observations in the field and from remote sensing data, which is the main strength since process and observational scale are equal. Additionally, sedimentary fans are mapped within the URB and then the fans and their feeder catchments are geomorphometrically analyzed.

I use a combined geomorphological mapping approach based on field mapping campaigns and mapping from high-resolution remote sensing data. Furthermore, I include existing data for the Turtmanntal hanging valleys (Otto et al., 2009). Geomorphic mapping is a fundamental technique producing a landscape inventory that can be used for further analysis (Smith et al., 2011; Otto and Smith, 2013). Details on the methods can be found in chapter 6.

4.3 Conceptual and methodological approach on the catchment scale

The large, catchment scale comprises the URB located in the southwestern Swiss Alps. It is one of the largest inner-alpine basins. The Rhone, originating at the Rhone Glacier, drains the catchment into Lake

Geneva and is fed by a large number of tributaries (c. 50 tributaries > 10 km^2) (Figure 3-1). More details on the study area are presented in chapter 3.

Since it is not possible to observe the spatial distribution of sediment storage on this scale (> 1000 km^2), upscaling techniques are needed. Data from the regional scale is used as input to model the spatial sediment (and bedrock) distribution. The hierarchical, methodological approach consists of (1) an analysis of the spatial distribution of sediment storage on the regional scale (chapter 6) and (2) statistically modeling the spatial distribution of sediment storage in the large scale URB using logistic regression, principal component logistic regression, and generalized additive models (Hastie and Tibshirani, 1990; Atkinson et al., 1998; Brenning, 2005; Aguilera et al., 2006; Hastie et al., 2009; Hosmer et al., 2013). One solution to upscaling is adjusting the resolution of spatial data (Harvey, 2000; Tunnicliffe and Church, 2011). High resolution data allows to upscale data from a smaller to a larger scale, which I apply by using a high-resolution digital elevation model as input data.

Predictive mapping (e.g. Luoto and Hjort, 2005; Brenning, 2009; Hoffmann et al., 2014; Petschko et al., 2014) is applied to bridge the gap between detailed sediment budget studies in small headwater catchments (< 10^2 km^2) and large scale studies (> 10^3 km^2) in higher order catchments. The applied models are validated and their performance is analyzed in detail (e.g. Sing et al., 2005; Goetz et al., 2011; Brenning, 2012; Petschko et al., 2014). Finally, the spatial distribution of sediment is analyzed in a geomorphic context. More details on the applied methods are presented in chapter 7.

Table 4-1: Overview of applied methods of the multi-scale approach.

Scale	Method
Local/landform Outsize fans plus feeder catchments in the Goms region (c. 2 km^2)	• **Morphometric analysis** including volume estimation of the fans and their source areas based on a high-resolution DEM • **Geophysical surveying**, i.e. ground-penetrating radar and electrical resistivity tomography measurements, of the subsurface material • **Cosmogenic radionuclide exposure dating** of boulders on the fan surface and bedrock cliffs in the catchment
Regional/small catchment Tributaries of Upper Rhone valley (c. 90-230 km^2)	• Analysis of the spatial distribution of sediment storage based on a **geomorphic mapping** approach • **Mapping and morphometric analysis** of sedimentary fans within the URB
Large catchment Upper Rhone Basin (c. 5400 km^2)	• **Predictive mapping** of spatial distribution of sediment storage using statistical models (i.e. logistic regression, principal component logistic regression and generalized additive models) • Detailed model validation and evaluation of model performance/quality • **Geomorphic analysis** of modeled spatial distribution of sediment based on geomorphometric parameters (e.g. slope, elevation and topographic position index)

5 Postglacial outsize fan formation in the Upper Rhone valley, Switzerland – gradual or catastrophic?

This chapter is based on the publication “Schoch-Baumann, A., Blöthe, J. H., Munack, H., Hornung, J., Codilean, A. T., Fülöp, R.-H., & Schrott, L. (2022): Postglacial outsize fan formation in the Upper Rhone Valley, Switzerland – gradual or catastrophic? Earth Surface Processes and Landforms, 47(4), 1032-1053.”.

DOI: https://doi.org/10.1002/esp.5301

It addresses thesis objective (1): Understanding and analyzing the formation of Postglacial landforms on a small scale using the examples of outsize fans in the Upper Rhone valley, Switzerland.

Further information for this chapter can be found in appendix A.

Abstract

Outsize fans are characterized by seemingly disproportionately small feeder catchments in relation to their fan area. Often having escaped rigorous scientific inquiry, the formative processes of these landforms remain inconclusive, supposedly ranging from catastrophic mass-wasting processes to gradual fluvial formation. Here we apply a multi-method approach, combining morphometric analysis with geophysical subsurface surveys and cosmogenic radionuclide exposure dating, to three outsize fans with hitherto unknown formation history in the Upper Rhone valley, Switzerland. Their feeder catchments are cut into bedrock hillslopes with a lack of indication of both pre-existing catchment structures and/ or unconsolidated material that was available after deglaciation.

Focusing our study on the largest of these fans, our findings suggest a fan formation in three phases: In Phase 1, commencing after deglaciation at ~10 ka and ceasing with full catchment development ~6.0 ka, bulk fan bodies were established by deposits of massive high-energy, high-magnitude debris flows exporting sediment with average yields of up to 73 kt km^{-2} yr^{-1}. In Phase 2, feeder basins were affected by comparatively lower-magnitude debris flows that distributed a sedimentary facies of debris flow channels, snouts and large boulders across the initial fan. Over time, deposition rates quickly decayed and finally ceased ~0.8 ka, when the system entered the present Phase 3, during which the fan-surface consolidated and fan aggradation terminated. Low gradient and abundant still-water deposits upstream of the fan still attest to the disruption of longitudinal sediment connectivity in the trunk valley.

We conclude that outsize fan formation by massive debris flows in the upper Rhone valley was rapid and massive, but incremental and non-catastrophic. Given the delivery of material at extremely high

rates, outsize fans are capable of having a sustained impact on geomorphic systems and, during phases of activity, potentially endangering human livelihoods.

5.1 Introduction

Sedimentary fans are ubiquitous landforms, especially in mountainous terrain. Yet, their occurrence is by no means limited to subaerial high-relief environments but also comprises the subaquatic realm and even extraterrestrial environments, e.g., Mars (Kraal et al., 2008) and Titan (Radebaugh et al., 2013) surfaces, attesting to past sediment transport there. Typical fan area proportions, when related to their catchment source areas, remain at ratios well below 0.5. There is, however, a range of disturbed ratios beyond the latter observation with sedimentary fans often occupying the full width of the main valley floor, but featuring seemingly disproportionally small feeder catchments. A prominent, modern example is the Illgraben fan, Switzerland (fan: 6.97 km^2, catchment: 11.39 km^2). Though lacking clear quantitative definition, such outsized fans operate outside of the 'normal' allometric fan-area to catchment-area relationship and are nourished by catchments of about similar size. Also referred to as anomalous fans (Crosta and Frattini, 2004), further differentiation into outsize fans and megafans (Jarman et al., 2011) seems somewhat confusing, as the term megafan is reserved for large-scale fan systems along mountain fronts (e.g. Harvey et al., 2005; Bowman, 2019). In our study we use the term 'outsize fan' to emphatically address a striking mismatch of the size of a sedimentary fan in relation to the (under)size of its feeder basin.

Outsize fan formation has been associated with deep-seated slope deformation and catastrophic mass movements, with extreme sediment yields delivered by one or multiple high-magnitude events as the main process of fan build-up (Crosta and Frattini, 2004; Jarman et al., 2011). Despite their position as outstanding landforms in many (high-)mountain settings, outsize-fan formation has rarely been examined in depth. Yet outsize fans, though not explicitly labelled as such, have been reported from different continents (e.g. Jarman et al., 2011; Brardinoni et al., 2018; Winkler et al. 2018; Ratnayaka et al., 2019) and planetary settings alike (Moore and Howard, 2005). We study three outsize fans in the Upper Rhone valley to contribute to a better understanding of formation processes, timing and the sedimentology of these potentially indicative landforms.

In most mountain areas, paraglacial fans and valley fills evolved rapidly following the last Pleistocene glaciation (Church and Ryder, 1972; Hinderer, 2001; Brardinoni et al., 2018). Outsize fans were proposed to be postglacial features due to their location 'on top' of late-glacial valley fills – a plausible reasoning, although lacking quantitative foundation (Jarman et al., 2011).

Previous research on sedimentary fans supports the notion of their gradual formation (e.g. Hooke, 1968; Bull, 1977; Harvey, 2011), yet Lecce (1990) sparked a 'gradualism vs. catastrophism' debate in fan research. However, considerations dealing with the relative importance of rare, catastrophic vs. more frequent events of smaller magnitude in the formation of specific landscape features are a longer-standing investigation topic in geomorphology (Wolman and Miller, 1960). Although several fan deposits were described as the result of few, possibly catastrophic events (e.g. Derbyshire and Owen, 1990; Crosta and Frattini, 2004), comprehensive assessment of the factors controlling a catastrophic formation is still missing.

Fan shape is supposedly conditioned by the runout path. Hence, the upstream debouchure – a distinct bottle-neck shaped catchment-fan transition – might play an essential role in constraining downslope material trajectory (Jarman et al., 2011). Yet, little is known about the sedimentological architecture, the timing and the processes of outsize fan formation.

The internal structure of sedimentary fans can be investigated using electrical resistivity tomography or ground penetrating radar (e.g. Ekes and Friele, 2003; Hornung et al., 2010; Franke et al., 2015), allowing for insights into depositional structures and, hence, processes. Therefore, fans can be valuable sedimentological archives recording environmental conditions during deposition in mountain sediment-source areas (Harvey et al., 1999). Structural fan data can be complemented with results from dating methods, to further constrain controls on sediment fluxes and the timing of fan formation (Hornung et al., 2010). Cosmogenic radionuclide (CRN) dating has been applied in several studies on fans (overview in Ivy-Ochs et al., 2013), though application of this method can be problematic due to potential complex pre-exposure history of surfaces and/or their nuclide inheritance (Nishiizumi et al., 1993; Ivy-Ochs and Kober, 2008). Nonetheless, surface exposure dating was used to identify climatic controls on debris flow activity and lobe chronologies in fan environments (e.g. Dühnforth et al., 2007; Schürch et al., 2016; D'Arcy et al. 2019, Ratnayaka et al., 2019). Since the formation of outsize fans is potentially catastrophic (Crosta and Frattini, 2004; Jarman et al., 2011), apparent surface exposure ages not only from the deposition zone, but also from the source area should help to better constrain the onset and main period of fan formation (Ivy-Ochs and Kober, 2008; Ivy-Ochs et al., 2009b).

Sedimentary fans can play key roles in landscape evolution and sediment fluxes in mountain areas (Costa and Schuster, 1988; Crosta and Frattini, 2004). In general, the presence of a fan can increase, but also decrease – or even stop – the sediment transport within the fluvial system of the main valley (Savi et al., 2020). Since outsize fans often occupy large parts of the valley floor, they may act as efficient upstream sediment traps on the valley scale. In addition, outsize fans may govern fluvial reworking of the valley fill and incision, and form geomorphic barriers, which limit sediment connectivity and cause fragmentation of the river longitudinal profile including knickpoints (Fryirs et al., 2007; Brardinoni et al., 2018; De Finis et al., 2018). Furthermore, fans can promote lake formation and aggradation of thick lacustrine deposits due to natural damming (Costa and Schuster, 1988; Phartiyal et al., 2005). From a natural hazards perspective, outsize fans have been proposed to be generated by catastrophic processes, such as debris-flows and landslides with large destructive potential (Crosta and Frattini, 2004; De Finis et al., 2018). In the light of climate change, future increases in extreme precipitation patterns likely favor the generation of large debris-flows, putting human livelihoods in alpine regions at increased risk (Stoffel et al., 2014).

In the Swiss Goms Region, Central Alps, three conspicuously large fans with hitherto unknown formation history occupy the Upper Rhone valley floor, dominating the overall appearance of the valley (Figure 5-1). All three fans originate from feeder catchments < 1 km^2 that are cut into steep bedrock hillslopes. We focus on the largest of these Goms outsize fans (GOFs) and analyze its surface morphology, sedimentology, architecture and formative period in detail (GOF #3, Figure 5-1). Due to their obvious similarity, we project these findings onto GOF #1 and GOF #2, but include a morphometric analysis for all three outsize fans. Our study contributes to the 'gradualism vs. catastrophism' debate in fan formation based on the following analytical steps:

- volume quantification of sediment eroded from feeder catchments and stored in the fans,
- analysis of the surface morphology of the fans and their source areas,
- investigation of the internal structure of one outsize fan (GOF #3) and its interfingering with the underlying valley fill, and
- determination of the onset and period of fan formation for GOF #3.

We combine morphometric analysis of the fans and their source areas with geophysical surveys of the subsurface material and CRN exposure dating.

5.2 Study area

Three noticeably large fans are located in the Goms region in the Upper Rhone valley, Switzerland. The valley floor between Niederwald and Oberwald, at an elevation of ~1350 m asl, is wide enough (0.8-0.9 km) to accommodate those large fan systems. In the past, these fan deposits have been referred to as rock avalanche deposits (Gemeinde Münster, 1992) and their source areas have been described as landslide-debris flow scars shaped by very low frequency, but large-scale deep seated failures (Norton et al., 2010).

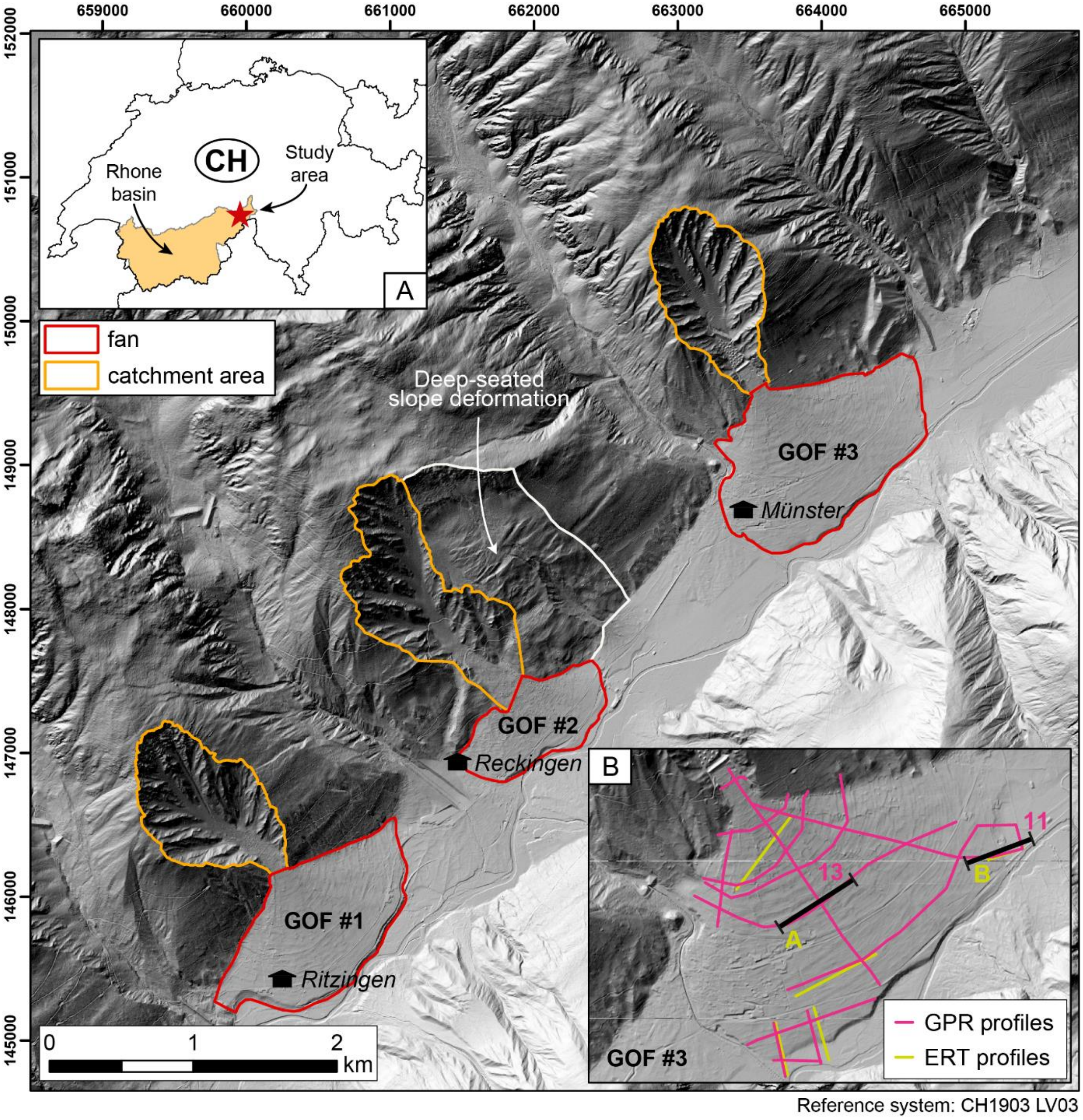

Figure 5-1: Location of the Goms outsize fans (GOFs; red outlines) and their catchments (orange outlines) in the Upper Rhone valley, Switzerland. Inset A shows location of the study area (red star) within the national boundaries of Switzerland (black) and within the Upper Rhone catchment. Inset B shows surface of GOF #3 with the location of GPR and ERT transects in pink and yellow, respectively. Transects discussed in the text and shown in figures are labelled and highlighted in bold (swisstopo DEM, EPSG:21781).

The three GOFs and their source areas are of comparable general appearance, suggesting similar formative processes. All three catchment-fan systems are located on the northwestern valley flank, where deeply incised Rhone tributaries have modelled steep interfluves that form triangular facet-like surfaces facing the Rhone valley (Figure 5-1). Their small catchment areas, together with the absence of any indication of fluvial activity that could feed their very large fan systems, are particularly striking, making these catchment-fan systems outstanding in an environment of many others that sustain perennial streams, but develop considerably smaller fans. Other interfluves of the Upper Rhone valley, with otherwise similar morphology, show no indications of comparable erosion. While there is evidence for just one noticeable deep-seated gravitational mass movement on the south-facing hillslopes (Figure 5-1), i.e., the valley flanks hosting GOFs #1-3, hillslopes on the opposite, north-facing Rhone valley flanks are affected by large deep-seated slope deformation more frequently (Tonini et al., 2014). In all three cases (GOFs #1-3), the catchment-fan transition is characterized by a debouchure.

GOF #3 (Figure 5-2A) must have formed more than 700 years ago, as settlement on the fan started at least in the 14th century (W. Lagger, pers. communication). Since then, the fan surface is under anthropogenic influence including agricultural boulder clearance. Large exposed boulders (a-axis up to 4 m) appear to be concentrated in the upper parts of the fan (Figures 5-3D & E, 11), presumably due to their depletion as construction material on the lower fan. Exposure of subsurface material is confined to construction sites that indicate a dominance of sub-rounded boulders of 0.5-1.5 m in diameter in the upper part of GOF #2 (Figure 5-3A-C), whereas the distal part of GOF #3 showed sub-rounded to well-rounded gravel-sized clasts.

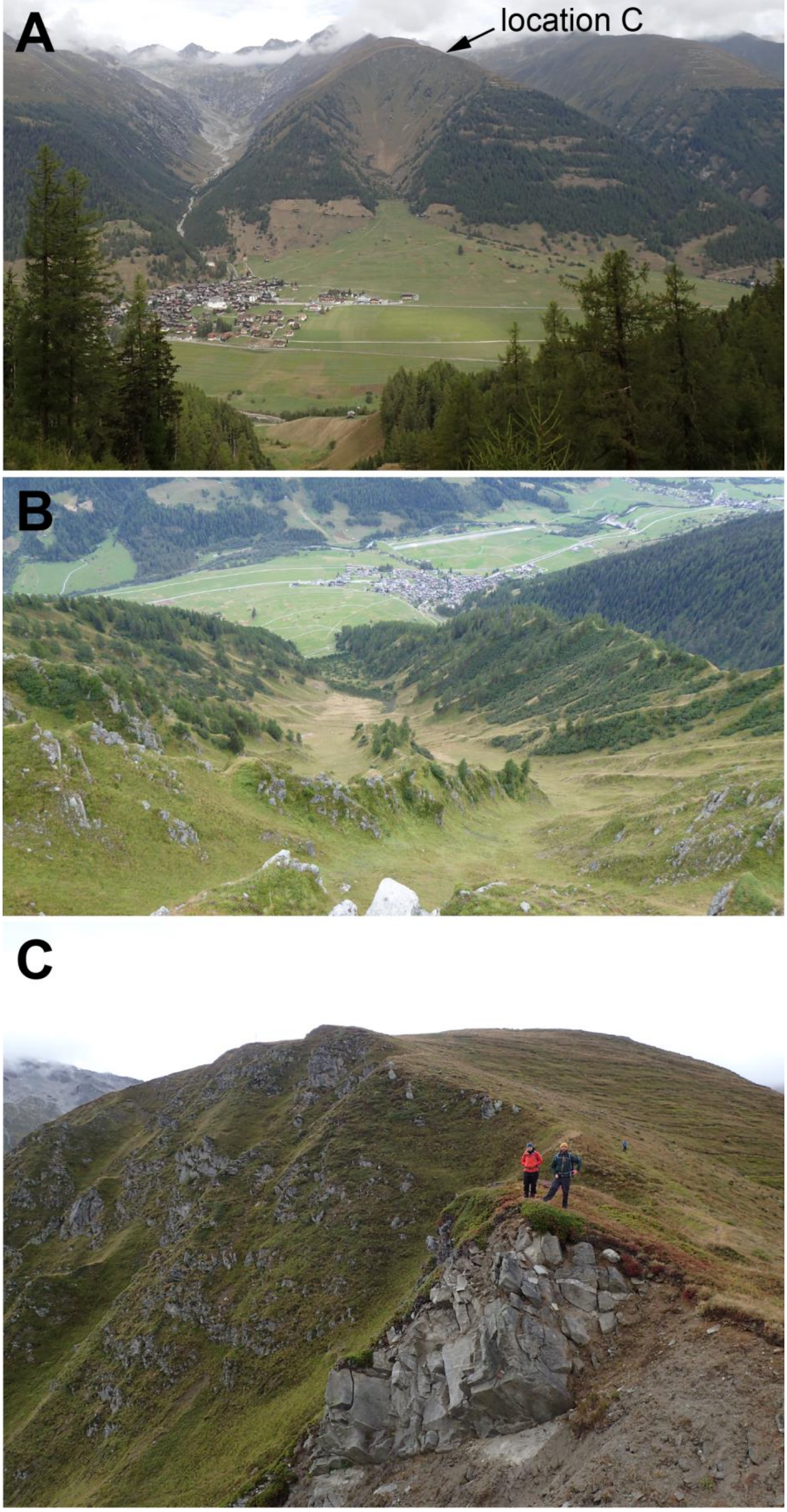

Figure 5-2: GOF #3. A: Münster-Geschinen catchment-outsized fan system. B: Feeder catchment. C: Debris flow initiation zone in the uppermost catchment.

Figure 5-3: A and C: Boulders exposed during construction of avalanche defense structure in 2008 on GOF #2. B: Construction site on GOF #2. D: ^{10}Be sample SE9 on GOF #3. E: ^{10}Be sample SE11 on GOF #3. Boulder flipping is unlikely due to their size and large burial depth.

The lithology of the Goms is dominated by the NE-SW striking Aar and Gotthard massifs (Schmid et al., 2004) (see geological map in appendix A, Figure A). These rock masses are structurally separated by the Goms zone. Both crystalline-basement rock massifs belong to the European basement, placing them among the oldest rock types in Switzerland (Pfiffner, 2021). Our feeder-basins under investigation, lying within the Aar massif, are mainly built up by augen gneiss and migmatite of the Ausserberg-Avat Zone (Labhart, 1977; swisstopo, 2013; Berger et al., 2017), which are generally characterized by a very low erodibility (Kühni and Pfiffner, 2001). The contact between the Gotthard and Aar massifs runs along-strike the Rhone valley, right at the base of the northwestern valley flank, but is overlain with sediments. A tectonic fault is presumed at this location (swisstopo, 2011; Berger et al., 2017), but has not seen thorough investigation. The opposite valley flank, meanwhile – where no outsize fans are present – is built up by metasedimentary gneisses, amphibolites and ultramafic rocks of the Gotthard massif (swisstopo, 2013; Berger et al., 2017), which have a generally low erodibility (Kühni and Pfiffner, 2001).

The U-shaped Rhone valley was sculpted by repeated Pleistocene glaciations (e.g. Lang and Wolff, 2011). The “Rhone ice dome”, one of two major ice accumulation areas during the Last Glacial Maximum (LGM) in the European Alps, with radial outflowing ice outlets mainly following the pre-existing valley system, was located in the Rhone headwaters and filled up the Rhone valley (Florineth and Schlüchter, 1998; Kelly et al., 2004). The Rhone glacier, during its greatest extent, reached into the alpine foreland until deglaciation commenced by 21.1 ± 0.9 ka. The valley glacier finally collapsed by 16.8 to 17.4 ka (Ivy-Ochs et al., 2004; Ivy-Ochs et al., 2006b). Deglaciation happened rapidly, as indicated by synchronous radiocarbon ages from the forelands and the inner Alps and a lack of prominent moraines in the main valleys (Schlüchter, 1988; Schlüchter et al., 2021). By 18 ka more than 80% of the LGM ice volume had melted (Ivy-Ochs et al., 2008). Further dating from the Grimsel Pass area and the Aletsch region allow constraining the timing of deglaciation in the study area (Welten, 1982; Kelly et al., 2006). While some inner-alpine regions were ice-free by ~15-14 ka (Welten, 1982; Maisch, 1987), Goms proximal data suggest a later deglaciation timing. After final deglaciation (presumably after the Egesen stadial/Younger Dryas, post 12.8 to ~11 ka) a thick valley fill accumulated in the overdeepened U-shaped Rhone valley (Pfiffner et al., 1997; Ivy-Ochs et al., 2009a). Using artificial neural networks, Mey et al. (2015) estimated the valley fill thickness in the Goms region to be up to 270 m.

5.3 Methods and data

To investigate outsize fan formation in the Goms region, we combine geomorphometric analyses with geophysical surveying and cosmogenic radionuclides. Using ground penetrating radar (GPR) and electrical resistivity tomography (ERT), we explore the sedimentological fan architecture. We further use ^{10}Be and ^{26}Al concentrations to reconstruct the chronology of fan formation.

5.3.1 Geomorphometric analysis of fans and source areas

Within the Upper Rhone catchment upstream of Lake Geneva (~5400 km^2), we map sedimentary fans from high-resolution digital topography and optical imagery (swissALTI3D DEM, 2 m resolution, ©swisstopo; GoogleEarth) (appendix A, Figure B), delineating catchments automatically with a D8 flow direction algorithm. For all fans > 0.015 km^2, we derive a set of morphometric parameters, such as fan and catchment planimetric area, as well as their mean gradients. We use these data to establish a regional fan-catchment area relationship and compare this to the GOFs, favouring 2D planimetric area over 3D slope-corrected area to maintain comparability to earlier studies (e.g. Bull, 1977; Lecce, 1991; Jarman et al., 2011).

For our three outsize fans under investigation, we further estimate sediment volumes eroded from the catchments and deposited in the fans based on a morphometric approach using a DEM (swissALTI3D DEM, resampled to 10 m resolution, ©swisstopo). To conservatively quantify fan volumes, we assume fan formation on top of the valley floor (Giles, 2010), and use extrapolated U-shaped valley side-walls based on contour lines of undisturbed adjacent triangular facets for lateral constriction. We acknowledge that fan volumes may be underestimated by this approach, due to interfingering with the fluvial deposits by the Rhone or burial (Hooke, 1968; Hoffmann and Schrott, 2002).

To estimate eroded volumes from the source areas, we rely on the circum-basin remnants of pre-erosion surfaces (Small and Anderson, 1998). We do not consider denudational surface lowering of the surrounding area of the catchment, thus our calculations might be subject to underestimation (Brocklehurst and Whipple, 2002). We decide to calculate two different scenarios: for a conservative estimate of eroded volume, contour lines intersecting with the source-area boundaries were connected forming a pre-erosion surface with a straight hillslope profile (Figure 5-4, scenario A). For an even more realistic scenario, we construct a convex hillslope profile that resembles the morphology of intact adjacent interfluves (Figure 5-4, scenario B). We convert eroded and deposited volumes to mass using a bulk-density span of 2.5-2.9 g cm^{-3} for gneiss (Schön, 2004) and a bulk-density span of 1.8-2.53 g cm^{-3} for debris flow deposits (Costa, 1984).

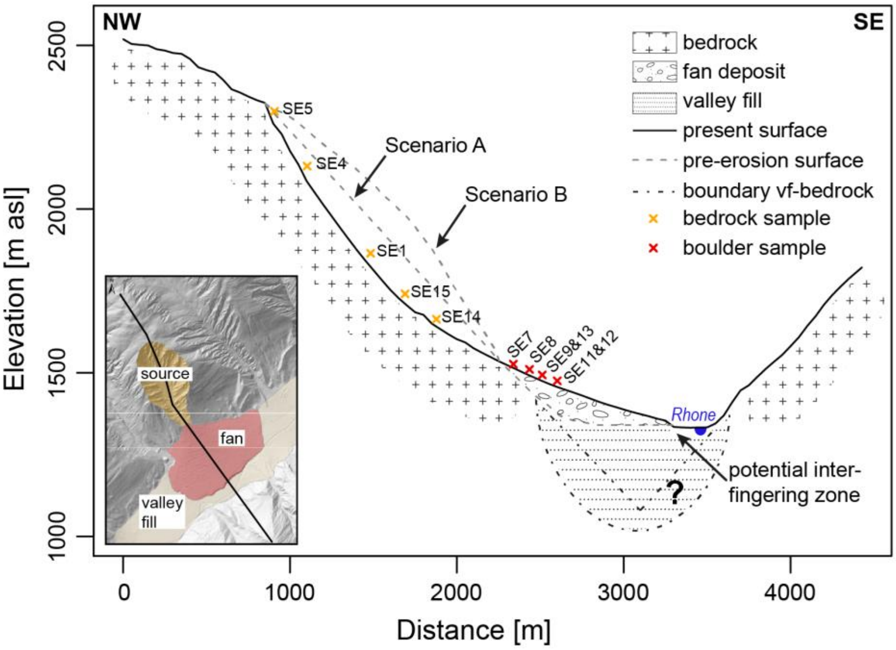

Figure 5-4: Schematic Upper Rhone valley cross profile at GOF #3 including details on the reconstructed surfaces for morphometric volume estimations. Locations of bedrock and boulder samples for surface exposure dating (SE) are indicated. Question mark below valley floor indicates uncertain position and shape of valley fill-bedrock boundary (DEM from swisstopo, reference system: CH1903).

5.3.2 Geophysical surveying

We conducted GPR and ERT measurements to investigate the near-surface underground of GOF #3. While GPR is suitable for the detection of small scale sedimentary features and the sediment-bedrock boundary, ERT is a powerful tool to analyze material characteristics, particularly in environments with strong contrasts in electrical resistivity. Combined data from these two complementary methods can be used to gather detailed information of the subsurface material (Schrott and Sass, 2008).

5.3.2.1 Ground penetrating radar

By detecting changes in the dielectric property of materials, GPR measurements produce continuous, high-resolution data of the shallow subsurface. Differences in dielectric properties are mainly due to changes in water content caused by e.g. sediment type, grain size, porosity, compaction and clay mineral content. Hence, GPR is well suited for high-resistivity sediments (Jol and Bristow, 2003; Schrott and Sass, 2008). We used an unshielded, bistatic 40 MHz multi low frequency (MLF) antenna (length ~240 cm, parallel broadside) from Geophysical Survey Systems Inc. (GSSI) and a shielded, bistatic GSSI 200 MHz antenna (perpendicular broadside) with a GSSI SIR 3000 and SIR 4000 control unit. All surveys were carried out in distance mode with a survey wheel, enabling a high-resolution data collection with a fixed antenna geometry and a step size of 0.01-0.033 m. Depth control on GOF #3 revealed an average penetration depth of 15 m (200 MHz antenna) to > 30 m (40 MHz antenna) established by ten common midpoint (CMP) measurements determining electromagnetic wave velocities in the subsurface. Vertical resolutions are 0.11-0.23 m (200 MHz antenna) and 0.56-1.13 m (40 MHz antenna) (Jol and Bristow, 2003).

We process our radar data using the ReflexW software (Sandmeier Scientific; processing sequences summarized in appendix A, Table K; more details on processing steps in Cassidy, 2009). We analyze and interpret our radar transects based on common terminology for radargram-analysis (Mitchum et al., 1977; Neal, 2004) and reference radar facies linked to sedimentary facies from outcrops in alluvial fan systems (e.g. Mitchum et al., 1977; Hornung et al., 2010; Franke et al., 2015).

5.3.2.2 Electrical resistivity tomography

Geoelectrical sounding provides a two-dimensional profile of the electrical resistivity distribution of the subsurface. We used a multi-electrode, multi-channel device (ABEM Terrameter LS) with four cables with 21 electrodes each in a roll-along mode. We set up our ERT device to spacings of 1 to 5 m in Wenner and Gradient arrays (Milsom, 2003), aiming for resulting profile lengths of 80 to 400 m and yielding a penetration depth of ~13 to 67 m.

To ensure high survey data quality, we excluded data points from the original data set with a standard deviation ≥ 3% following stacking operations on the measured voltage to current ratio, and we paid attention to keeping the number of deleted data points < 10% (Hilbich et al., 2009). Furthermore, we excluded data points with negative resistivity and filtered data points in RES2DINV (Geotomo Software) based on the RMS error statistics that calculate the misfit between the measured and calculated apparent resistivity values (Loke, 2017), choosing a cut-off value of 50%.

We conducted inversion of the apparent resistivity values using RES2DINV, a software iteratively producing a two-dimensional subsurface model from the measured pseudosection by minimizing the deviation between the measured apparent resistivity and the model results (Loke and Barker, 1995; Loke and Barker, 1996; Loke and Dahlin, 2002). We included topography as part of data processing and chose a damping factor of 0.15, a convergence limit of 5% and the robust inversion method for all datasets (Loke et al., 2003).

Ranges of resistivities for different materials overlap significantly (appendix A, Table W) and depend strongly on factors such as water content, chemical properties of rock and pore fluid, pore size and distribution as well as jointing (e.g. Kneisel and Hauck, 2008). A challenge for the interpretation of ERT results are high resistivity contrasts between materials, which typically complicate data inversion (Marescot et al., 2003). We use the depth of investigation (DOI) to identify unreliable resistivity areas in our model. Thus we can drop areas unsupported by measured data and avoid over-interpretation of our ERT-derived results (see appendix A for details on the method) (Oldenburg and Li, 1999; Hilbich et al., 2009).

5.3.3 Cosmogenic ^{10}Be and ^{26}Al analysis

We collected samples (Figure 5-4) from five bedrock outcrops within the source area and from six large boulders on the fan surface to derive apparent surface exposure ages from cosmogenic ^{10}Be and ^{26}Al abundances. Following the sampling considerations of Ivy-Ochs and Kober (2008), sample thickness was kept below 5 cm. Rock samples were predominantly augen gneiss with high portions of quartz. We sampled partially submerged large boulders with diameters of up to four meters that were not evenly distributed across the fan surface. In the field, we recorded topographic shielding at all sampling locations and determined elevation and geographic position using a D-GPS device (Table 5-1).

We crushed and ground our samples to 125-500 µm grainsize. We then isolated and purified quartz following standard procedures for in-situ cosmogenic ^{10}Be and ^{26}Al analysis (Kohl and Nishiizumi, 1992), using froth-flotation to remove feldspars from quartz. Be and Al were separated at the University of Wollongong following procedures described in von Blanckenburg et al. (1996) with the modification that Al was separated from Be and Ti using pH sensitive precipitation before Be cation exchange chromatography (Child et al., 2000). Samples were spiked with ~300 µg of ^{9}Be from a low-level beryl carrier solution added prior to complete HF dissolution. The native Al concentrations of the samples ranged from 53-264 ppm (median = 130 ppm) and were determined via ICP-OES with a precision of 3-4% (Fujioka et al., 2015). ^{26}Al measurements of the Co-QTZ-N (Binnie et al., 2019), and CRONUS-A and CRONUS-N (Jull et al., 2015) laboratory intercomparison materials prepared at the University of Wollongong between 2017 and 2020 yield results in agreement with consensus values suggesting that our Al chemistry procedures are robust and there is no systematic loss of ^{27}Al during sample processing.

We measured ^{10}Be /^{9}Be and ^{26}Al /^{27}Al ratios at ANSTO's 6MV SIRIUS accelerator (Wilcken et al., 2019), and normalized results to KN-5-2 and KN-5-3 (Nishiizumi et al., 2007) and KN-4-2 standards (Nishiizumi, 2004), respectively. Analytical uncertainties for the final ^{10}Be and ^{26}Al concentrations (atoms g^{-1}) include AMS measurement uncertainties (larger of counting statistics or standard deviation of repeats and blank corrections) in quadrature with 1-2% for ^{10}Be and 2-3% for ^{26}Al standard reproducibility (depending on the individual AMS measurement conditions), 1% uncertainty in the ^{9}Be carrier concentration and 4% uncertainty in the ICP-OES Al measurements.

Table 5-1: Location data and summary of ^{10}Be and ^{26}Al data for samples analyzed at ANSTO (see Figure 5-4). Blank IDs UOWBLK2-8 and UOWBLK-Al4, respectively.

Sample ID	Type	Latitude [°]	Longitude [°]	Elevation [m]	Total Qtz. [g]	Blank corrected ^{10}Be/^{9}Be [10^{-15}]	Blank corrected d(^{10}Be/^{9}Be) [10^{-15}]	Blank ^{10}Be/^{9}Be [10^{-15}]	^{9}Be spike [µg]	^{10}Be SRM-4325 [atoms*g^{-1}]	d(^{10}Be) [atoms*g^{-1}]	Blank corrected ^{26}Al/^{27}Al [10^{-15}]	Blank corrected d(^{26}Al/^{27}Al) [10^{-15}]	Blank ^{26}Al/^{27}Al [10^{-15}]	^{27}Al native [µg]	^{26}Al KNSTD [atoms*g^{-1}]	d(^{26}Al) [atoms*g^{-1}]
SE1	bedrock	46.5008	8.2631	1881	40.213	100.317	3.21922	0.483 ± 0.165	270.2	45041	1762	90.4572	14.2102	8.537 ± 8.537	5249.85	263582	42728
SE4	bedrock	46.5039	8.2618	2150	40.246	138.417	4.6799	0.483 ± 0.165	268.4	61688	2501	-	-	-	-	-	-
SE5	bedrock	46.5052	8.2619	2272	40.008	226.917	6.99894	0.483 ± 0.165	268.8	101864	3881	582.463	21.3143	8.537 ± 8.537	2134.76	693677	37607
SE7	boulder	46.4933	8.2678	1515	39.960	71.7069	2.69104	0.483 ± 0.165	268.7	32222	1408	-	-	-	-	-	-
SE8	boulder	46.4924	8.2683	1491	36.035	63.1169	2.25602	0.483 ± 0.165	268.2	31395	1324	-	-	-	-	-	-
SE9	boulder	46.4916	8.2687	1471	40.262	66.2469	2.5633	0.483 ± 0.165	269.7	29650	1325	-	-	-	-	-	-
SE11	boulder	46.4918	8.2719	1440	40.035	23.6569	1.17559	0.483 ± 0.165	269.6	10645	580	-	-	-	-	-	-
SE12	boulder	46.4933	8.2728	1439	40.139	116.717	3.80257	0.483 ± 0.165	268.8	52223	2064	-	-	-	-	-	-
SE13	boulder	46.4935	8.2705	1471	40.232	105.217	5.08467	0.483 ± 0.165	268.6	46934	2499	129.103	14.9805	8.537 ± 8.537	4343.54	311101	38183
SE14	bedrock	46.4962	8.2659	1648	40.091	152.317	6.20319	0.483 ± 0.165	268.2	68089	3163	139.643	14.2983	8.537 ± 8.537	6343.12	493137	54209
SE15	bedrock	46.4985	8.2644	1765	40.159	34.1169	1.63531	0.483 ± 0.165	268.7	15256	807	-	-	-	-	-	-

Using version 3 of the Balco et al. (2008) online calculators (https://hess.ess.washington.edu; Balco et al., 2008) – there choosing the LSDn production rate scaling (Lifton et al., 2014; Balco, 2020) that is based on the calibration data set of Borchers et al. (2015) and using a half-life of 1.387 * 10^6 a for ^{10}Be (Chmeleff et al., 2010; Korschinek et al., 2010) and 7.05 * 10^5 a for ^{26}Al (Nishiizumi, 2004), respectively – we calculated apparent exposure ages, accounting for topographic shielding following Codilean (2006) and assuming a bulk density of 2.75 g cm^{-3}, and an erosion rate of 3 mm kyr^{-1} (Ivy-Ochs et al., 2004; Ivy-Ochs et al., 2006b). We further calculated snow shielding following Gosse and Phillips (2001):

$$S_{snow} = \frac{1}{12}\sum_{i}^{12} e^{-(z_{snow,i}\rho_{snow,i}/\Lambda_f)} \qquad (2)$$

where zsnow is the average thickness of snow cover for each month of the year [cm], ρsnow is the average density of snow [g cm^{-3}], and Λf is the attenuation length for fast neutrons in snow [g cm^{-2}]. We estimated median monthly snow thickness from long-term average monthly data recorded at the MeteoSwiss station ‘Ulrichen’ (N46.50 E8.30, 1345 m, SYNOP 067450) between October 1999 and July 2020 (appendix A, Figure X). We used an average snow density of 0.3 g cm^{-3}, and 109 g cm^{-2} as the attenuation length of fast neutrons in snow (Zweck et al., 2013).

5.4 Results

5.4.1 Geomorphometry of fans and source areas and field observations

We mapped 186 fans from digital topographic data and remote sensing imagery (Figure 5-5, Figure 6-8) and calculated their planimetric areas. We note here that using slope-corrected area instead of planimetric area does not introduce significant shifts in the ratio between fan and source area in our data (appendix A, Figure C). In comparison to the general distribution of fans and their feeder basins in the Upper Rhone catchment, the three large GOFs (stars in Figure 5-5) can clearly be labelled as outsize fans, with their fan area roughly equaling their catchment area. Those three fans have spatial extents of 0.48 to 1.29 km^2. In contrast to GOFs #1 and #3 that show little signs of distal erosion, GOF #2, the smallest one, was considerably trimmed by the Rhone river. All three fan toes are characterized by ~20 m high fluvially eroded cliffs. The mean slope angle of all three fans is ~10°. Fan source areas range from 0.69 to 0.94 km^2, with high-angle slopes (mean 37.6-40.8°) and sharp cliff/ridge fringes (Table 5-2). The feeder catchments are dominated by exposed bedrock, partially covered with a thin soil veneer, and backfilled valley floors that grade into the fan apices. Exposed bedrock ridges stand high above the valley floor; grassy vegetation predominates the valley bottom and soil-covered parts of bedrock ridges. There are no indications of active higher-magnitude gravitational mass movement processes, with the exception of a vegetation free debris flow source area on the northeastern crest of the catchment feeding GOF #3 that is detectable in early airphotos of 1940 (© swisstopo) (Figure

5-2). The most obvious anthropogenic alteration within the catchment-fan systems was the construction of avalanche barriers.

Our geomorphometric estimates of material eroded from the catchments of the three outsize fans yield volumes between 63 and 65 * 10^6 m^3 for GOF #1, between 51 and 52 * 10^6 m^3 for GOF #2, and between 55 and 69 * 10^6 m^3 for GOF #3, depending on the scenario (Table 5-2). Though the approximated material volume stored in GOFs #1 and #3 roughly matches these numbers, the volume of GOF #2 is significantly smaller than the volume eroded from the catchment, which we attribute to distal erosion.

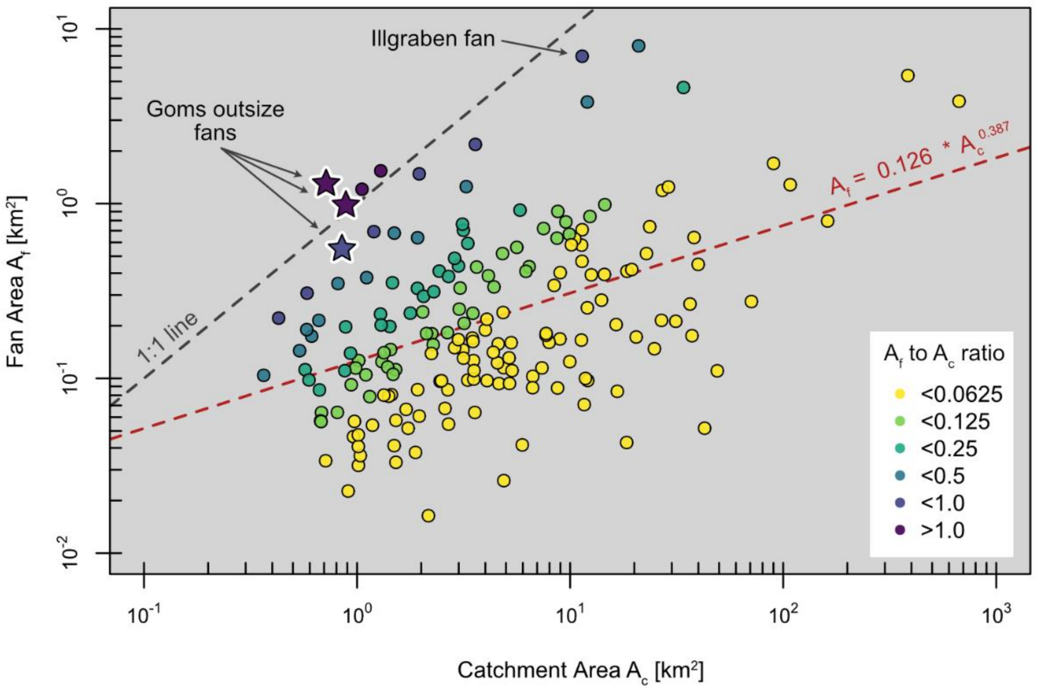

Figure 5-5: Log-log plot of planimetric fan area vs. planimetric catchment area for 186 fans located in the Upper Rhone catchment, color-coded to their fan-to-catchment area ratio. The three investigated fans in the Goms region are highlighted with stars. Red dashed line = regression model. Grey dashed line = 1:1 line (see Figure 6-8 for map showing the locations of all mapped fans).

Table 5-2: Characteristics of GOFs and their feeder catchments, approximated volumes and masses deposited in fans and eroded from catchment. Scenario A and B are calculated for catchments (source area, Figure 5-4). Gneiss and debris flow deposit densities from Schön (2004) and Costa (1984) respectively.

GOF	Fan area [km²]	Catchment area [km²]	Mean fan slope [°]	Fan height [m]	Debouchure width [m]	Mean catchment slope [°]	Approx. fan volume [10^6 m³]	Approx. fan mass (ρ = 1.8-2.5 t*m^{-3}) [10^6 t]	Approx. source volume - scenario A [10^6 m³]	Approx. source mass - scenario A (ρ = 2.5-2.9 t m^{-3}) [10^6 t]	Approx. source volume - scenario B [10^6 m³]	Approx. source mass - scenario B (ρ = 2.5-2.9 t m^{-3}) [10^6 t]
#1	1.01	0.69	10.58 ± 5.83	185	190	40.17 ± 9.82	66.06	118.92-165.16	62.52	156.29-181.30	65.24	163.09-189.19
#2	0.48	0.94	10.45 ± 5.32	113	330	37.64 ± 11.03	19.39	34.90-48.47	50.75	126.88-147.18	52.33	130.81-151.74
#3	1.29	0.74	9.76 ± 4.64	213	230	40.79 ± 9.82	86.66	155.98-216.64	55.40	138.50-160.66	69.06	172.66-200.29

5.4.2 Sedimentological architecture of the fan

We recorded ~8 km of GPR profiles using a 40 MHz antenna and ~1.8 km with a 200 MHz antenna on GOF #3 (appendix A, Figure B, Table D). In addition, we surveyed six ERT profiles – with different arrays and spacings – to back our GPR results (appendix A, Figure B, Table L).

Here we focus on three GPR profiles measured in the center of GOF #3 as well as right at the interface between fan and fluvial Rhone deposits at the upstream distal part of the fan (profile #13 (40 and 200 MHz antenna) and #11 (40 MHz antenna), respectively, Figure 5-1B). Due to ideal fieldwork conditions in December 2016 (dry and frozen ground), our GPR survey yielded good results. We further draw on two ERT profiles, measured September 2017, taken at the same locations (profile A, B, Figure 5-1B). We give further geophysical survey results and details in appendix A (Figures & Tables E-W).

Our geophysical survey results and the general depositional situation indicate a mixed subsurface material composition of sediments of various sizes (boulders, gravel, sand, some silt). Common midpoint (CMP) measurements indicate a propagation signal velocity of 0.09 m ns^{-1} (appendix A Figures G-J), used here for the depth-time conversion of our radar data.

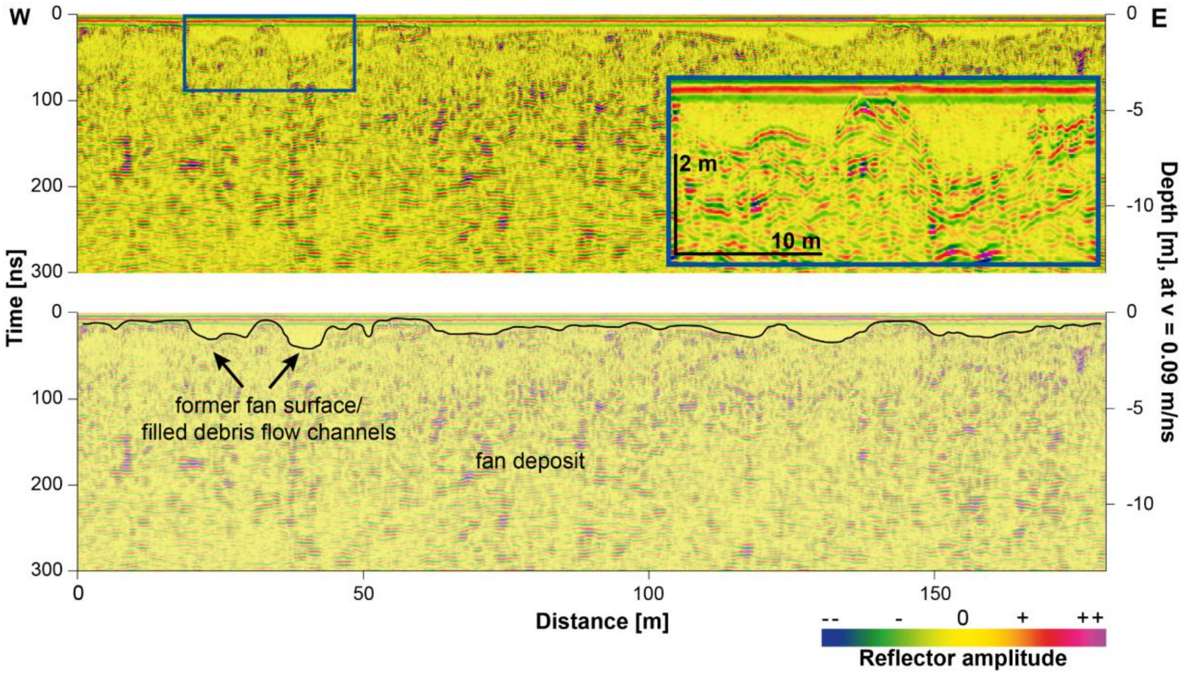

Figure 5-6: 200 MHz GPR profile #13 from central GOF #3 (see Figure 5-1B for location). The former fan surface can be identified. Debris flow channels are filled with homogenous (nearly reflection free) material most likely due to human modification/smoothing of fan surface. Penetration depth is ~15 m.

GPR profile #13 from the center of GOF #3 (Figure 5-6, penetration depth ~15 m) shows a uniform radar facies with the exception of the upper meters. Here, the continuous, wavy reflector marks the irregular fan surface with former debris flow channels that are now filled with nearly reflection free infillings, likely related to human activity. We interpret this material as relatively fine grained and homogeneous while strong reflectors below indicate large boulders (up to several meters in diameter, majority 0.5-1.5 m) that float in a finer matrix.

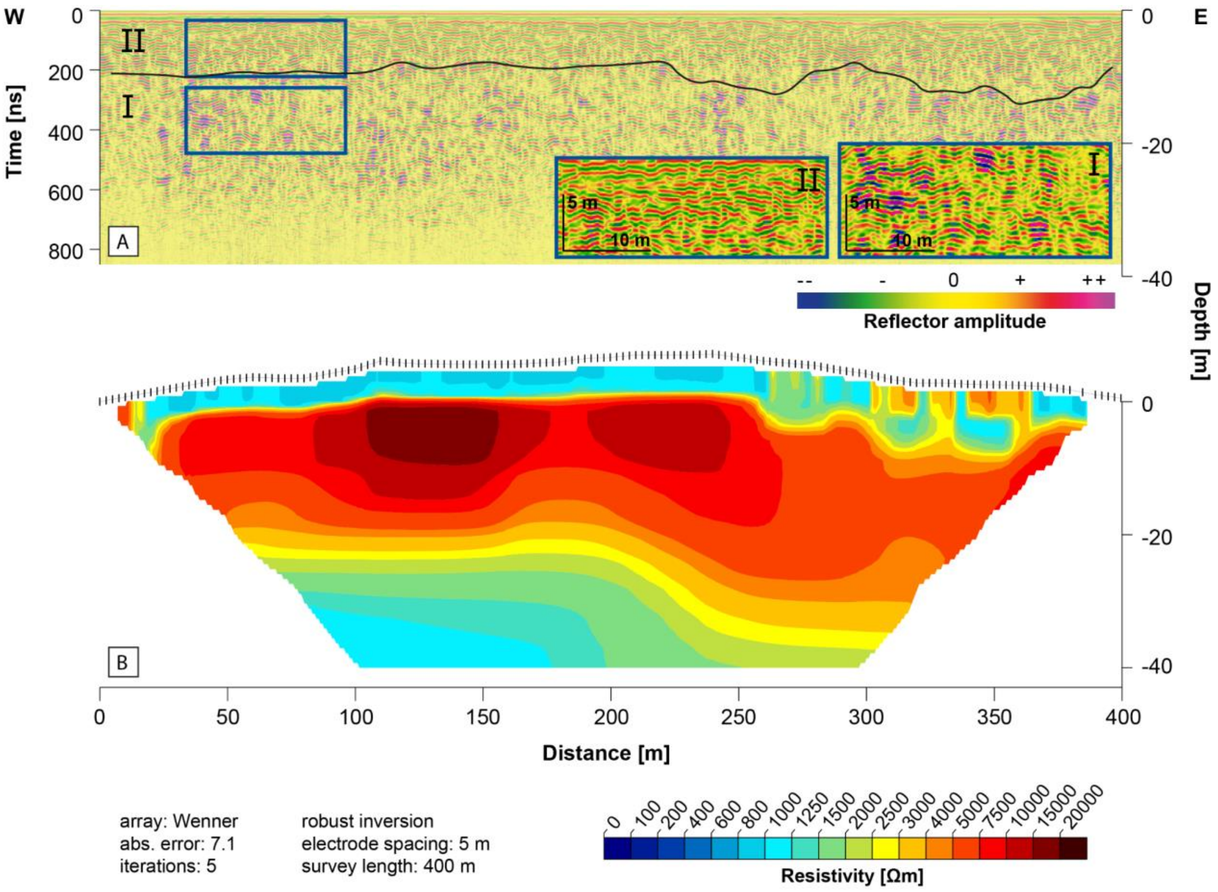

Figure 5-7: A: 40 MHz GPR profile #13 from central GOF #3 (see Figure 5-1B for location). The two radar facies of the fan deposit are clearly distinguishable (I & II). Enlargements show the two radar facies in more detail (for plain profile see appendix A, Figure E). B: ERT cross profile at the same location (Profile A, 0-400 m, but truncated at 40 m depth) where red = high and blue = low resistivity. Full-depth profile see appendix A, Figure M. DOI see appendix A, Figure N.

Two radar facies can be distinguished in GPR profile #13, located within central GOF #3 (Figure 5-7A; penetration depth > 30 m), with the upper facies II being ~10 m thick and characterized by moderately continuous, mid-amplitude, wavy and subparallel reflectors. We identify debris flow channels, and associated levees, with their channel bed as continuous reflectors in many locations in the upper radar facies II (Figure 5-8A). These channels were filled with debris flow material from successive events. The debris flow channel in Figure 5-8A, for instance, is ~30 m wide and several meters deep. The underlying radar facies I (below ~10 m depth) has stronger, less continuous reflectors. Facies I features more angular reflector patterns and, therefore, appears more heterogeneous. An assemblage of many debris flow channels, levees, fillings and stacked debris flow snouts as well as large boulders can be identified. The blocky and heterogeneous material is poorly structured (Figure 5-8B). Total thickness of facies I cannot be determined from our radargrams since the lower boundary is below 30 m of depth. We interpret the strong reflectors of facies I as very large boulders (up to several meters in diameter) in a coarse-grained matrix and note that the additional 40 MHz profiles show similar patterns (Figures 5-9A, 5-10).

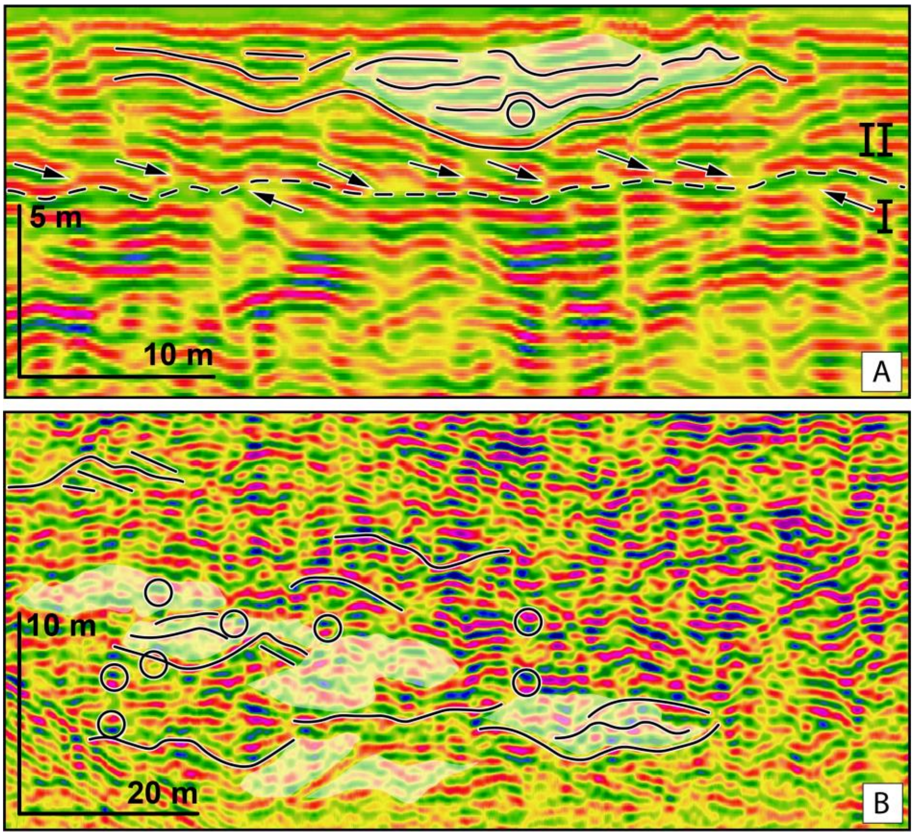

Figure 5-8: 40 MHz GPR profile #13 detail examples. A: Debris flow channel with levees and subsequent filling (white shading) in radar facies II. Channel is ~30 m wide and several meters deep. The lower half of the section displays radar facies I. B: Stacked debris flows snouts and channels with levees in radar facies I. Filling/snouts indicated for several channels (white shading). Representative large boulders highlighted with circles. Blocky and heterogeneous material, which is poorly structured.

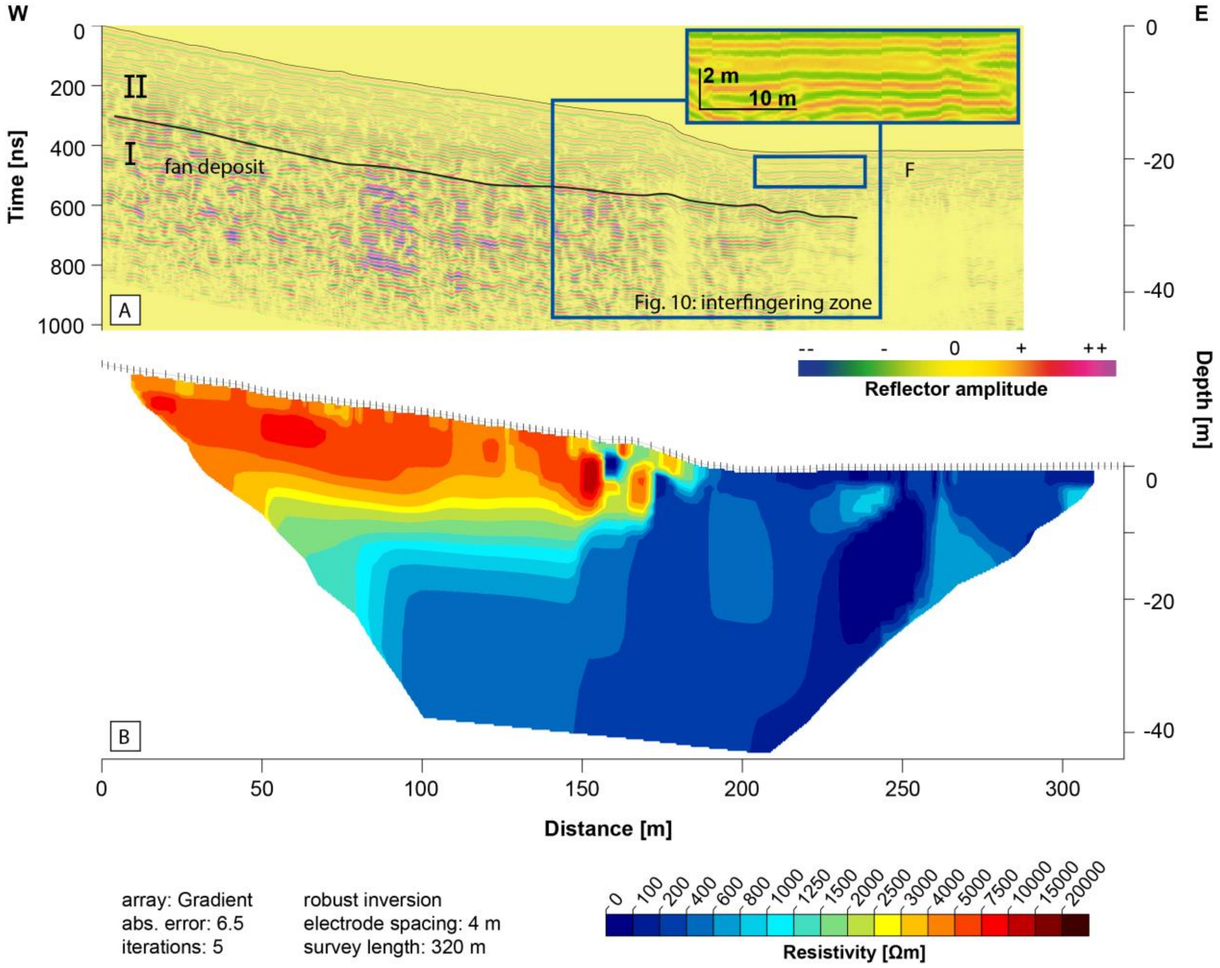

Figure 5-9: A: 40 MHz GPR profile #11 measured at the interface between GOF #3 and fluvial Rhone deposit (see Figure 5-1B for location). Enlargement shows fluvial radar facies (F) in the valley fill zone. Onlapping deposition of fluvial material (F) on fan and vice versa. The two radar facies of the fan deposit are clearly distinguishable (I & II). Fan topography is included to correct reflector positions and to clearly identify the transition zone. Enlargement of interfingering zone shown in Figure 5-10 (for plain profile see appendix A, Figure F). B: ERT profile at the same location (Profile B, 0-320 m) where red = high and blue = low resistivity. Full profile see appendix A, Figure O. DOI see appendix A, Figure P.

GPR profile #11 shows the transition from GOF #3 to the fluvial Rhone deposit at the distal, eastern part of the fan (Figure 5-9A; penetration depth > 30 m). Radar facies I and II can be identified here, too. The fluvial Rhone deposits are different and show less intense, but continuous, horizontal and planar, parallel reflectors. The fluvial Rhone deposits is dominated by finer grained material and increased ground water influence promoting signal attenuation (penetration depth ~10 m). A more detailed look at the fan-Rhone deposit transition (Figure 5-10) reveals interfingering structures of the two sediment facies. Fan deposits extend into river gravel and vice versa. In addition, the fluvial radar facies has onlap structures onto the fan radar facies I and II.

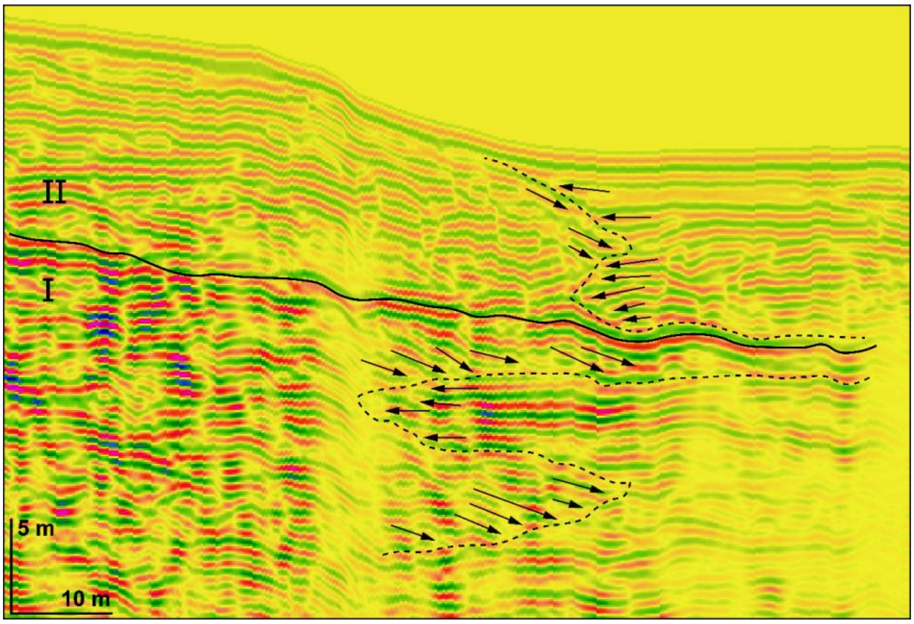

Figure 5-10: Enlargement of interfingering zone from 40 MHz-GPR profile #11 (Figure 5-9). Arrows show on- and downlap structures of the fluvial radar facies onto the fan radar facies and vice versa clearly representing interfingering of the two radar facies.

The ERT cross profile A (Figure 5-7B) from central GOF #3 (same location as GPR profile #13) is 400 m long and was measured with 5 m spacings and a Wenner array. Measured resistivity ranges from ~1 kΩm to > 20 kΩm and penetration depth is up to 67 m in the center of the profile. The DOI (appendix A, Figure N) supports the notion that apparent resistivities in the pseudosection are reliable. Profile A is characterized by an upper layer of lower resistivities with a depth of 5-10 m, which corresponds to radar facies II. This upper layer shows variations with small areas of resistivities up to 5 kΩm that we interpret as a finer grained sedimentary deposit with higher resistivities being remains of the "original" fan surface. Underneath lies a more continuous layer with high resistivities of 5-20 kΩm indicating very coarse material, matching radar facies I. This second layer is ~20 m thick and shows decreasing resistivities with depth, potentially related to higher moisture contents. However, it remains difficult to measure comparably lower resistivities underneath a continuous and thick high-resistivity sediment layer. Moreover, we find no supporting indication for a change in material composition within radar facies I in our GPR data, though we acknowledge the lower penetration depth. ERT cross profiles C and D show a similar picture with an upper layer of lower resistivities that matches radar facies II and an underlying layer of much higher resistivities, matching radar facies I (appendix A, Figures Q, U).

ERT profile B (Figure 5-9B, DOI in appendix A, Figure P) is located at the transition from GOF #3 to the flat valley fill at the distal, eastern part of the fan. The fan interior (left side of pseudosection, 0-180 m) has high resistivities up to 10 kΩm here. This is in contrast to the fluvial Rhone deposits (right side of pseudosection, 180-320 m) which are characterized by resistivities largely remaining below 0.6 kΩm. This clear contrast corresponds well to different geological units: while the subsurface of the fan consists of large boulders in a matrix, the fluvial deposit is finer grained material (mainly clay, silt, sand) with groundwater influence.

5.4.3 Surface exposure ages from ^{10}Be and ^{26}Al

We determined cosmogenic radionuclide abundances for eleven samples, six of which we collected from bedrock outcrops within the feeder catchment of GOF #3, the remaining five samples collected from boulders deposited on the fan surface (Figure 5-11). We generally determined apparent exposure ages relying on ^{10}Be abundances, but for four samples we also measured ^{26}Al to back up our ^{10}Be data. Overall, our ^{10}Be and ^{26}Al -derived result pairs are in good agreement (Figure 5-11, Table 5-3).

Obtained ^{10}Be -derived exposure ages range from 0.82 to 6.09 ka (Table 5-3). For comparison, we also provide exposure ages assuming zero erosion and/or neglecting snow shielding (Table 5-3). While apparent exposure ages are generally younger for the no erosion case, excluding snow shielding results in negligibly younger ages that remain within ± 1σ error (Table 5-3).

Three of the five bedrock exposure ages from the source area cluster around an age of ~6 ka. The samples were collected in the uppermost part of the catchment (SE4, SE5), and in vicinity to the catchment outlet on the narrowest part of the debouchure (SE14). The remaining two source area samples yielded ages of ~1.1 and ~3.9 ka (SE15, SE1). We note that the apparent-age difference between the ^{10}Be and ^{26}Al results for sample SE1 is ~0.8 ka, though errors are still overlapping.

Apparent boulder exposure ages from the fan surface range from 4.56 to 0.82 ka. Three samples, collected along a vertical transect from a boulder field on the central fan (SE7, SE8, SE9), cluster around ~2.4 ka (Figure 5-11). Furthermore, two samples from boulders of a linear cluster on the eastern part of the fan give ^{10}Be apparent exposure ages of ~3.9 and ~4.6 ka (SE13, SE12), respectively, that have overlapping errors. Finally, one sample taken from a third cluster of boulders in the southeastern part of the fan yields the youngest age of ~0.8 ka (SE11). For one sample on the fan surface (SE13), we also obtained an ^{26}Al exposure age that does not match the ^{10}Be estimate exactly, but overlaps within error (Figure 5-11, Table 5-3).

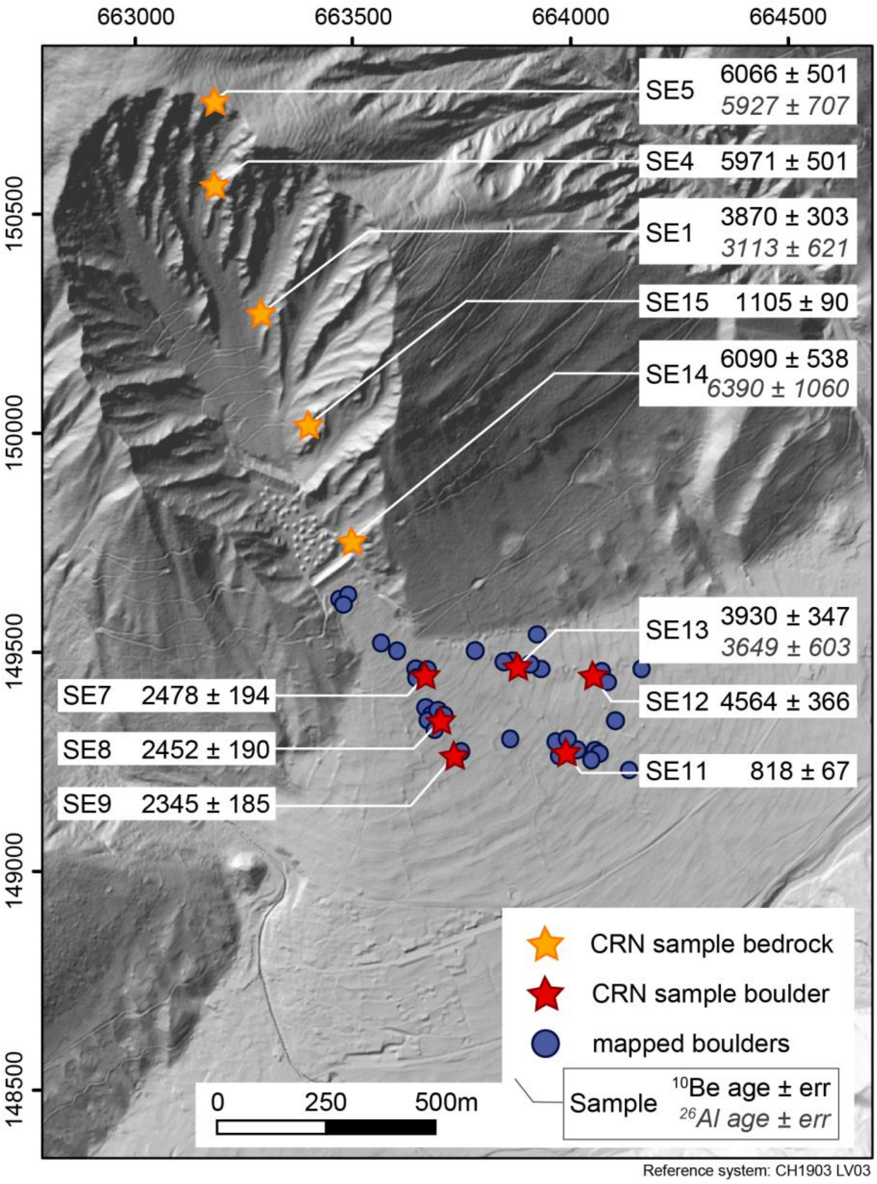

Figure 5-11: Münster-Geschinen feeder catchment and outsized fan system (GOF #3) – apparent ^{10}Be and ^{26}Al (italic) surface exposure ages (in years) of source-area bedrock outcrops (yellow) and of boulders (red) covering the depositional fan surface. Sampling strategy aimed at (a) vertically covering the feeder catchment and (b) capturing conspicuous fan boulder clusters. Regular structures above fan head are man-made avalanche barriers (swisstopo DEM, EPSG: 21781).

Table 5-3: ^{10}Be and ^{26}Al apparent surface exposure ages (LSD production rate scaling from Lifton et al. (2014)). Our preferred apparent exposure age estimates are 'Exposure age E $S_{TopoSnow}$' (bold). Errors given as '(int)' and 'ext', with the latter including both measurement and production rate uncertainty whilst '(int)' includes uncertainties on the nuclide concentration measurement only. * Snow data: MeteoSwiss (Ulrichen, SYNOP 067450).

Sample ID	Sample type	Topo shielding	Topo + Snow* shielding	Nuclide	Exposure age E S_{Topo}				Exposure age E $S_{TopoSnow}$				Exposure age E_{null} S_{Topo}				Exposure age E_{null} $S_{TopoSnow}$			
					3 mm kyr^{-1} erosion, topo shielding only				3 mm kyr^{-1} erosion, topo + snow shielding				0 mm kyr^{-1} erosion, topo shielding only				0 mm kyr^{-1} erosion, topo + snow shielding			
					yrs		*ext*	*(int)*	*yrs*		*ext*	*(int)*	*yrs*		*ext*	*(int)*	*yrs*		*ext*	*(int)*
SE1	bedrock	0.672	0.672	^{10}Be	3869	±	303	-168	**3870**	**±**	**303**	-168	3445	±	244	-135	3445	±	244	-135
				^{26}Al	3113	±	621	-548	**3113**	**±**	**621**	-548	2888	±	531	-469	2888	±	531	-469
SE4	bedrock	0.520	0.520	^{10}Be	5971	±	501	-284	**5971**	**±**	**501**	-284	5167	±	370	-210	5167	±	370	-210
SE5	bedrock	0.778	0.778	^{10}Be	6066	±	501	-272	**6066**	**±**	**501**	-272	5238	±	368	-200	5238	±	368	-200
				^{26}Al	5927	±	707	-377	**5927**	**±**	**707**	-377	5127	±	523	-279	5127	±	523	-279
SE7	boulder	0.977	0.962	^{10}Be	2438	±	191	-114	**2478**	**±**	**194**	-116	2298	±	169	-100	2332	±	171	-102
SE8	boulder	0.980	0.965	^{10}Be	2412	±	186	-108	**2452**	**±**	**190**	-110	2275	±	165	-96	2310	±	168	-97
SE9	boulder	0.982	0.967	^{10}Be	2309	±	182	-110	**2345**	**±**	**185**	-111	2178	±	161	-97	2214	±	164	-99
SE11	boulder	0.983	0.968	^{10}Be	801	±	66	-45	**818**	**±**	**67**	-46	783	±	63	-43	797	±	64	-43
SE12	boulder	0.979	0.964	^{10}Be	4487	±	359	-200	**4564**	**±**	**366**	-204	4007	±	285	-159	4073	±	290	-161
SE13	boulder	0.976	0.961	^{10}Be	3848	±	339	-227	**3930**	**±**	**347**	-232	3431	±	273	-183	3497	±	278	-186
				^{26}Al	3576	±	590	-483	**3649**	**±**	**603**	-494	3234	±	485	-398	3283	±	493	-404
SE14	bedrock	0.835	0.835	^{10}Be	6090	±	538	-333	**6090**	**±**	**538**	-333	5256	±	395	-244	5256	±	395	-244
				^{26}Al	6390	±	1060	-835	**6390**	**±**	**1060**	-835	5449	±	763	-601	5449	±	763	-601
SE15	bedrock	0.842	0.811	^{10}Be	1068	±	87	-58	**1105**	**±**	**90**	-60	1041	±	83	-55	1077	±	85	-57

5.5 Discussion

We discuss the sedimentological architecture of GOF #3, the chronology of fan formation based on our apparent ^{10}Be exposure ages and the fan's influence on sediment fluxes in the Upper Rhone valley. We conclude outlining how our results can contribute to a better understanding of outsize fan formation in general.

5.5.1 Sedimentological architecture

Taken together, the high resistivities and strong reflectors in our geophysical data indicate a heterogeneous texture for both sedimentary units identified for GOF #3, pointing to gravitational processes. However, units I and II show distinct differences: For unit I, geophysical data point to depositional processes, which facilitated the sedimentation of coarse material including very large blocks of several meters in diameter. Sediment routing took place in small-scale channels, showing distinct blocking and filling of channels with frequent avulsions indicating a highly dynamic depositional environment, characteristic of debris flow processes. Similarly, debris flow channels, boulders and debris flow snouts also point to a dominance of gravitational processes in unit II (Figures 5-6, 5-8). In contrast to unit I, however, channels appear shallower and more persistent, filled with more uniform material indicating a calmer and more confined pattern of deposition. Clusters of boulders stand out of the anthropogenically smoothed fan surface, further supporting the notion of a dominance of gravitational processes during the entire fan formation.

In the context of other studies conducting GPR on alluvial fans in alpine environments, the radar facies observed for sedimentary unit I proves exceptional (e.g. Ekes and Friele, 2003; Hornung et al., 2010; Franke et al., 2015). However, in a similar setting, Hornung et al. (2010) identified two distinct radar facies on an alpine alluvial fan in Switzerland that correspond to debris flows and fluvial processes, using material outcrops to validate radargrams. Their debris flow radar facies, as well as similar results obtained for the Illgraben fan (Franke et al., 2015), are comparable to our sedimentary unit II. Yet the very pronouncedly heterogeneous reflectors found for sedimentary unit I, as well as their very high resistivities, have not been reported from other alpine fans and point to an even coarser material composition. Sass (2006) reports resistivities of up to 20 kΩm for coarse, loose debris deposited by gravitational mass movements. Further studies found resistivities ranging from 14 to > 36 kΩm for (catastrophic) rock slope failure deposits (coarse grained dry sediments) (Hilger et al., 2018), while reported values for debris flow deposits range below 10 kΩm (Sass, 2006; Silhan and Panek, 2010; Dietrich and Krautblatter, 2017). Drawing a general picture of sedimentary fan architecture, we interpret the upper sedimentary unit II as the deposit of intermediate-magnitude debris flows, while the very high resistivities and very distinct reflectors of sedimentary unit I point to a generally coarser deposit associated with more energetic, higher-magnitude debris flow processes.

We conducted our GPR soundings at a very high resolution, allowing for a detailed investigation of the fan's internal structure. However, uncertainties of indirect geophysical measurements remain, and data should therefore be interpreted with caution, or checked against in-situ data. Here we take advantage of 28 boreholes located on and near the three outsize fans. Their core material (https://geocadast.crealp.ch/, appendix A, Figure Y for borehole locations) suggests a very similar internal structure for all three GOFs, with m-sized boulders in a matrix consisting of sand, gravel and boulders, thus supporting our indirect geophysical measurements. Cores from GOF #1 and #2 show fan sediments reach ~30 m below the present-day elevation of the glacio-fluvial Rhone deposits that are distinctly different from the fan material. Drillings proximal to the steep valley flanks of the U-shaped Rhone valley reach bedrock, supporting the notion of several decameters thick fan deposits. These drillings, which have greater penetration depth than the geophysical surveys, along with our geomorphometric volume estimations, suggest that sedimentary unit I makes up most of the fan deposit. In the case of GOF #3, we estimate the minimum deposited volume of sedimentary unit I and II to $73.75 * 10^6$ m^3 and $12.91 * 10^6$ m^3 (assuming a uniform thickness of 10 m for unit II), respectively, resulting in ~85% of the material stored in unit I. This number is a minimum estimate, as our approximated volume of fan material assumes a flat deposition on top of the Rhone sediments, disregarding any burial or interfingering evidenced by GPR data (Figures 5-9, 5-10) and drillings.

5.5.2 Apparent ^{10}Be exposure ages – chronology of fan formation

Despite an age spread from ~1.1 to ~6.1 ka (bedrock in GOF #3 feeder catchment) and from ~0.8 to ~4.6 ka (boulders on GOF #3 surface), our established chronology allows us to infer some general information on catchment-fan system development. We take the cluster of three ages (SE4, SE5 & SE14) spanning the whole elevation profile of the source area as an indication that the feeder catchment was completely established, in close-to present-day size and shape, by ~6 ka. In this sense, younger ages within the catchment (SE1 & SE15) represent ongoing geomorphic activity of smaller magnitude that modulated the catchment surface and contributed to the deposition of sedimentary unit II, but the bulk of material had been evacuated before. The latter interpretation is in line with the distribution of boulder ages on the fan surface that are all significantly younger than ~6 ka. All sampled boulders on the fan surface, amongst them a cluster of three boulder exposure ages around ~2.4 ka, are part of larger boulder fields that are oriented radially across the fan surface (Figure 5-11), marking former debris-flow trajectories. We interpret their exposure ages as indicators of continued activity that modulated the surface after the fan and its feeder basin had largely been established.

Taken together, we infer from our chronological and geophysical data that fan formation happened in three distinct phases (Figure 5-12). In a preparatory Phase 0 after final LGM deglaciation, ice retreat exposed stripped rock walls at the steep, triangular interfluves, which were then prone to non-glacial erosion. During Phase 1 that ceased with the full development of the catchment around ~6.0 ka, the fan interior (sedimentary unit I) was built up by the deposits of massive high-magnitude debris flows sourced from the feeder catchment. Geophysical reflector patterns for ~30 m depth, paired with local borehole data, allow for an interpretative rejection of rockslides or rock avalanches as formative processes, since they would have caused a chaotic reflector pattern. The i) narrow debouchure, ii) lacking runup deposits on the opposite valley flank and iii) prominent bedrock ridges within the source area further attest against a fan formation in a single event and particularly against a deep-seated slope failure. In Phase 2, the feeder basin was affected by intermediate-magnitude debris flows that deposited sedimentary unit II on the initial fan. Numerous debris flow channels that shaped the fan surface during this phase are still identifiable in the geophysical data as well as in the distribution of large boulders on the fan surface (Figures 5-6, 5-8, 5-11). Taking our CRN ages at face value, Phase 2 lasted until ~0.8 ka, indicated by the youngest boulder exposure age that we found on the fan surface. Continued debris-flow activity beyond this time seems unlikely, given the lack of documented events during at least 700 years of, otherwise well documented, local settlement history (W. Lagger, pers. communication). During the most recent Phase 3, the fan-feeder catchment transport system ceased with only isolated cases of geomorphic activity within the catchment not reaching the fan, as documented in aerial photographs. Whether this fan consolidation was caused by material exhaustion, by sufficient stress release, by ceased tectonism, or by changes in climatic boundary conditions – as well as any information about synchronism of events between the three catchments – currently remains elusive.

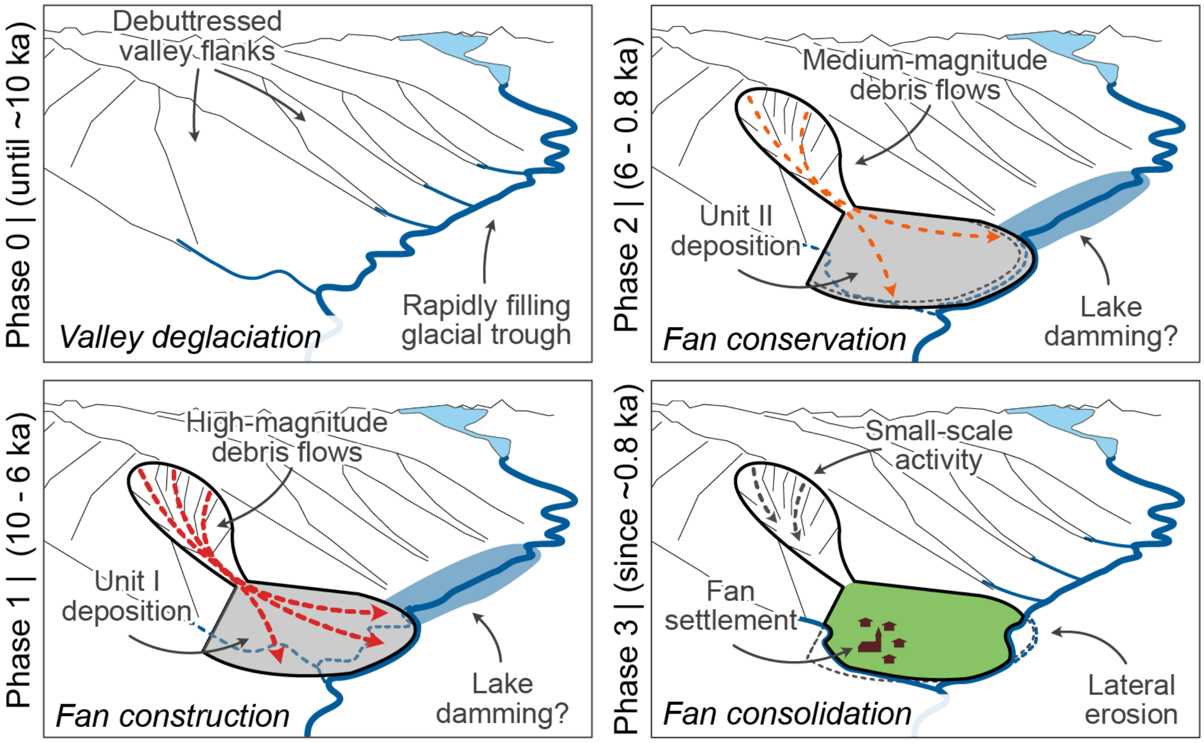

Figure 5-12: Conceptual framework. Phases of outsize fan formation in the Upper Rhone valley. Phase 0: valley deglaciation, Phase 1: fan construction, Phase 2: fan conservation, Phase 3: fan consolidation.

Further, our absolute age control cannot resolve the onset point of fan formation. However, given the inner-alpine setting and the late Pleistocene local regime of the Rhone glacier, fan development must have commenced after final deglaciation of the Goms presumably following the Egesen stadial, i.e., post 12.8 ka to ~11 ka (Ivy-Ochs et al., 2009a). In the absence of fan-proximal age control, we rely on data from the nearby Grimsel Pass (Kelly et al., 2004) and Aletsch region (Welten, 1982) to narrow down the earliest possible onset of fan formation. Just ~9 km upstream of our study area, the Grimsel Pass (2164 m asl; Figure 5-13), a transfluence pass of the Rhone glacier to the northward Aare catchment, became ice-free between 14.0-11.3 ka (Kelly et al., 2004). Farther downstream (~27 km), where the Aletsch glacier (Figure 5-13) entered the Rhone valley, the area around Naters (~1000 m asl) was ice-free by at least 10-9.2 ka BP (Welten, 1982). Given the altitude of our study area (1350 m asl), we infer that fan formation in the Goms Rhone valley is unlikely to have started before ~10 ka, leaving a time window of ~4 kyr until the feeder catchment of GOF #3 was established. Still, this is a conservative estimate, as large parts of the fluvial deposits of the Rhone must have been deposited prior to fan formation, as indicated by borehole data, geophysical soundings and the close match of estimated fan and source area mass (Table 5-2).

For the above scenario of ~4 kyr for incipient fan formation (Phase 1), in line with the regional constraints on the timing of deglaciation and our apparent bedrock exposure ages, we calculate average specific sediment yields (SSY) for the feeder basin of GOF #3 that range from 51-73 kt km^{-2} yr^{-1} (scenarios A and B, Table 5-2) placing them among the highest SSY documented (Korup, 2012). The close-by Illgraben catchment with a SSY of 25-50 kt km^{-2} yr^{-1} (McArdell and Hirschberg, 2020), might serve as a modern analogue, yet its catchment and fan area are one order of magnitude larger.

Denudation rates can be used to the timescale of fan formation, given the volume of dated sediment. Across the European Alps and uplifted forelands (OCTOPUS database; n samples = 301, dataset not filtered for disturbances as for instance debris flows, landslide occurrence, or catchment glaciation), CRN-derived catchment-averaged denudation rates are highly variable, ranging across three orders of magnitude from < 14 mm kyr^{-1} (sample 'GO1' in Buechi et al., 2014) to > 9780 mm kyr^{-1} (sample 'G1 1012' in Brardinoni et al., 2020). For the Upper Rhone valley upstream of Lake Geneva – including both tributary and trunk samples (Figure 5-13) – catchment-wide denudation rate estimates vary from 84 mm kyr^{-1} (sample 'WIL' in Norton et al., 2010) to > 9000 mm kyr^{-1} (Illgraben in Stutenbecker et al., 2018), with a median value of 1276 mm kyr^{-1}. Focusing our analysis on the Goms region, maximum and median rates reduce to 2831 mm kyr^{-1} and 673 mm kyr^{-1}, respectively.

Apart from the Illgraben, denudation rates tend to be higher with increasing glacial cover (Figure 5-13C & D). We therefore use a subset of catchments with less than 3% glacial cover (Figure 5-13B) to compare against average denudation rate estimated for the GOF #3 feeder basin. Assuming constant rates over a 4 kyr-period of bulk catchment and fan formation, our estimates of eroded volumes from the feeder catchment of GOF #3 would translate to average denudation rates of $18.7\text{-}23.3*10^3$ mm kyr^{-1}, ranging more than twice as high as basin wide denudation rates for the Illgraben (Stutenbecker et al., 2018; McArdell and Hirschberg, 2020) and 16 to 20-times higher than 1.5 times the interquartile range (IQR) of denudation rates from the Goms region (Figure 5-13). From a different angle, applying a denudation rate of $\sim 1.2*10^3$ mm kyr^{-1} (1.5 IQR) and a 90% trapping efficiency, deposition of sedimentary unit I of GOF #3 alone would take nearly 100 kyr. Based on this, the denudation from the small feeder catchments nourishing the Goms fan systems must have happened at outstanding rates, even exceeding the highest measured denudation rates in the region and involving similar or even higher-magnitude debris-flow processes than the modern Illgraben fan system.

From our geophysical survey results we infer that formative processes behind (outsize) fan formation were by no means continuous over time – a basic assumption that is backed by other studies (e.g. Hornung et al., 2010; Brardinoni et al., 2018; Ratnayaka et al., 2019). It is striking that Brardinoni et al. (2018) find a very similar time window for the generation of the Gadria fan, where postglacial sediment yield peaked around 9 ka and bulk fan deposition ended around 6 ka. CRN-derived denudation rates, however, are inherently non-informative in this regard because they integrate over the time period of their validity. Models of postglacial landscape evolution suggest elevated erosion and sedimentation rates soon after deglaciation that decreased or ceased during the Holocene. This is a core notion of paraglacial sedimentation theory in fan environments (Church and Ryder, 1972), and part of the concept of paraglacially conditioned sediment yields (Church and Slaymaker, 1989; Hinderer, 2001), which pertains to the observations made for the three GOFs. Furthermore, the magnitude of sediment yields and denudation rates estimated for Phase 1 of GOF #3 formation indicate the predominance of high-energy and high-magnitude gravitational debris flows.

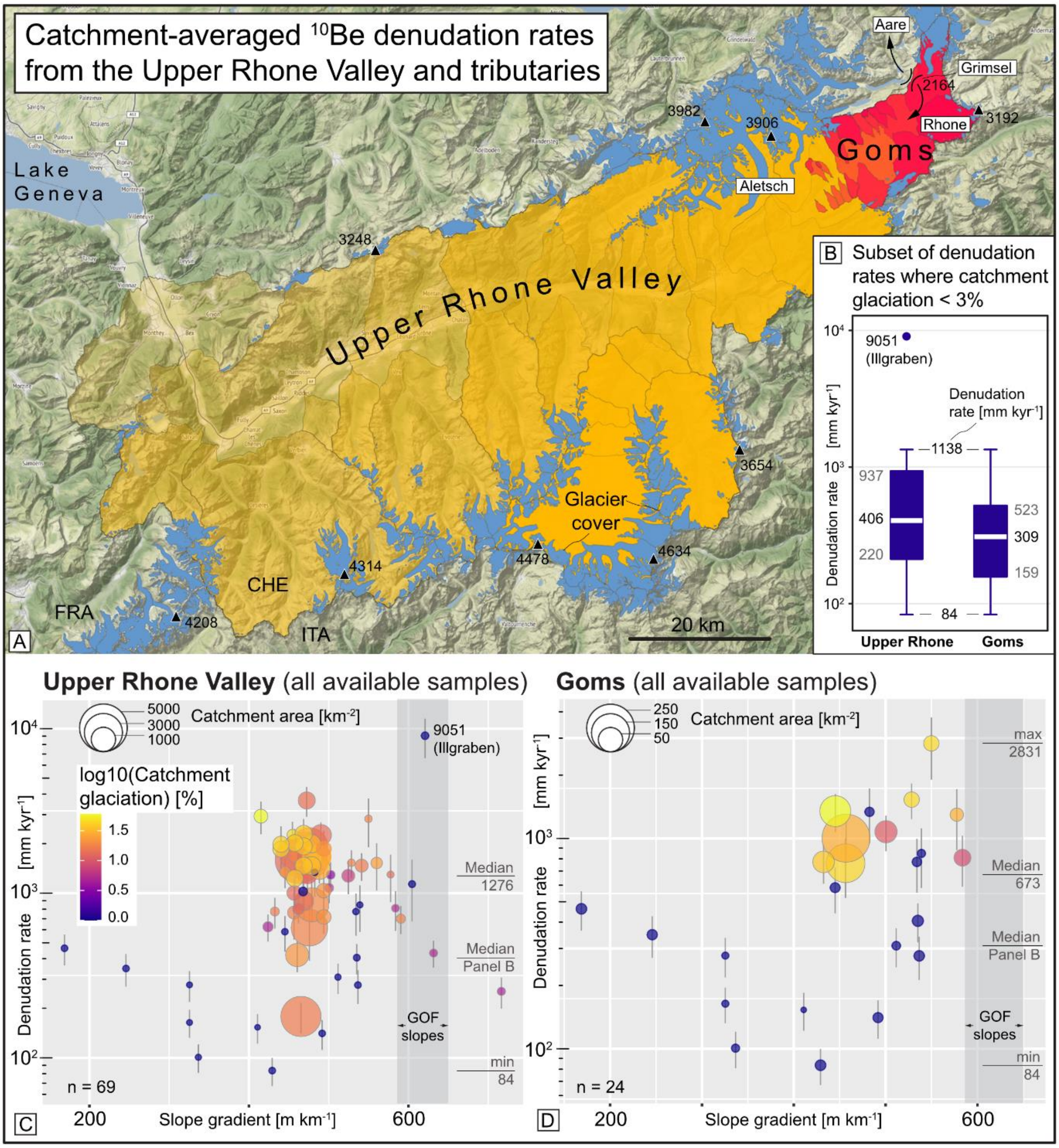

Figure 5-13: Catchment-averaged denudation rates in the Upper Rhone valley and tributaries. A: Terrain map (http://maps.stamen.com/terrain/) with catchment outline overlay where intensity of catchment color increases with level of nesting (i.e., sampled sub-catchment in catchment), or number of sample repeats (e.g. yearly repeats) on one and the same catchment area. Catchment polygons and recalculated rates taken from OCTOPUS DB (Codilean et al., 2018); therein Wittmann et al. (2007), Norton et al. (2010), Stutenbecker et al. (2018) and Delunel et al. (2020). Yellow polygons = Upper Rhone valley catchments, Red polygons = Goms catchments, which are part of the Upper Rhone valley. Blue polygons = Glacier outlines from RGI 6.0 (RGI-Consortium, 2017). Black triangles = outstanding peaks; number is elevation. 'Grimsel' = former transfluence pass with flow directions 'Aare' and 'Rhone' indicated. B: Box- and whisker plots of ^{10}Be denudation rates from catchments with < 3% glacial cover exclusively. Left - Entire dataset (median = 406 mm kyr^{-1}), right - Goms catchments only (median = 309 mm kyr^{-1}). Whiskers extend to 1.5 IQR (interquartile range). Outlier (Illgraben catchment) is heavily disturbed by high-magnitude and -frequency debris flow occurrence (Schlunegger et al., 2009; McArdell and Hirschberg, 2020). C: Available ^{10}Be catchment-averaged denudation rates for the Rhone catchment upstream Lake Geneva (yellow + red polygons on A over slope gradient. Data points scaled to catchment size and colored according to percentage of glaciation. Grey vertical boxes border slope-gradient bin covered by outsize fan feeder catchments (GOFs #1-#3). Min, max and median values indicated right-hand;

'Median Panel B' refers to matching median on panel B. D: Available catchment-averaged denudation rates for the Goms region. The rules for C do apply. Note different Y- and point-size scaling.

5.5.3 Influence on sediment fluxes in the Upper Rhone valley

The Rhone valley long profile between Oberwald and Niederwald (Figure 5-14) indicates strong control of GOF #3 on trunk channel gradient. Apparently, GOF #3 forced the Rhone River to the southern valley side and promoted upstream aggradation. This is reflected by the broad and gently sloping valley floor with a gradient of ~0.4% upstream of GOF #3 that contrasts with a distinctly steeper channel gradient of ~1.4% below GOF #3.

Furthermore, stillwater deposits recovered from shallow sediment cores (~6-20 m) upstream of GOF #3 (appendix A, Figure Y), dominated by clay, silt and sand intercalated with thick organic layers, support early interpretations of a complete or at least partial blockage of the Rhone valley by GOF #3 (Bögli, 1941). Whether three ^{14}C samples with ages between 3705 ± 55 and 3961 ± 55 a BP recovered from excavations upstream of GOF #3 (M. Schmidthalter, pers. communication) point to upstream deposition well beyond the emplacement of the incipient fan around ~6 ka, or merely indicate a short episode of damming during Phase 2 of fan development remains inconclusive. In any case, outsize fans in the Goms region functioned as effective and persistent barriers, interrupting longitudinal sediment connectivity at the valley scale (Fryirs et al., 2007). A similar situation has been reported from the Venosta Valley, Italy, where outsize fans and their deposits cause upstream deposition of fine material and/or damming of a lake (Brardinoni et al., 2018). Based on the above, outsize fans are capable of attenuating sediment fluxes and inducing knickpoints along the valley profile, further delaying postglacial landscape adjustment.

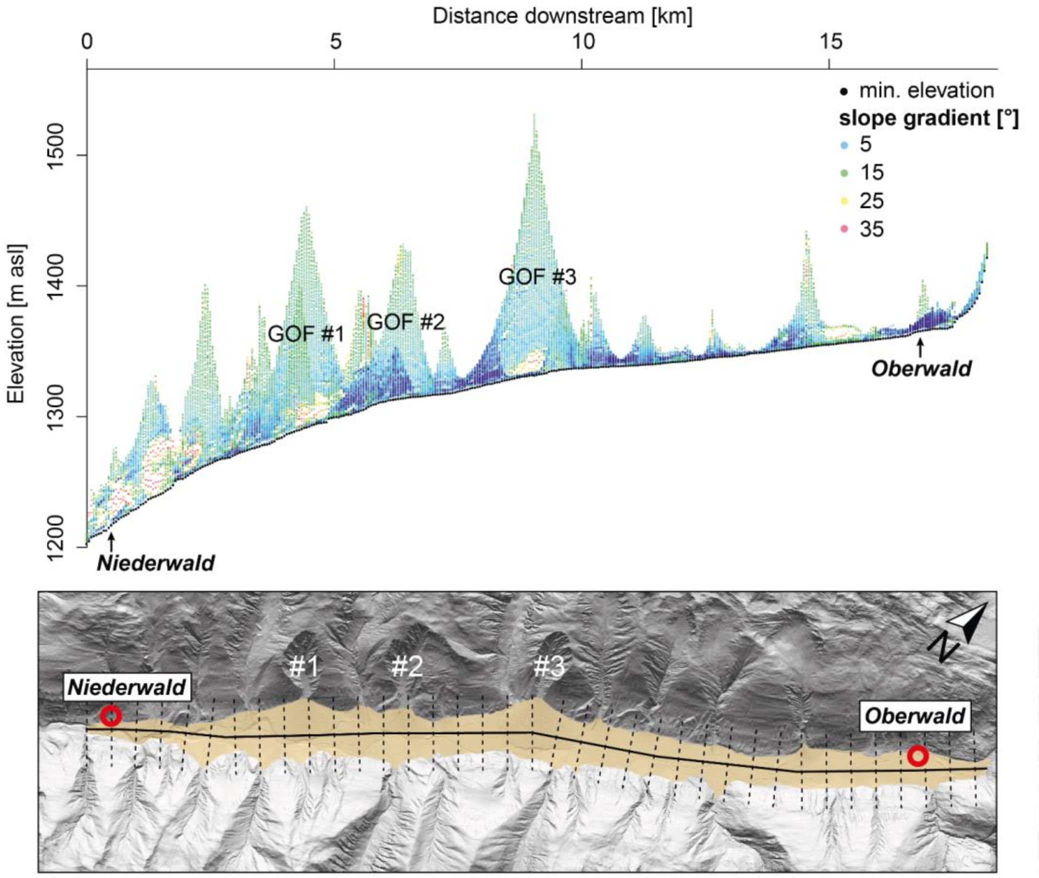

Figure 5-14: Longitudinal profile (see solid line in inset for location) of the valley floor including fans of the Upper Rhone valley from Oberwald to Niederwald with stacked slope/elevation pixels (color coded dots) along 750 m wide swath cross profiles every 50 m respectively (see dashed lines in inset). Black dots show minimum elevation and thus the long profile of the valley floor. The Quaternary valley fill is shaded in yellow (see inset) (swisstopo DEM, EPSG:21781).

5.5.4 Outsize fan formation and controls

In line with earlier studies on outsize fans (Jarman et al., 2011; Brardinoni et al., 2018; Ratnayaka et al., 2019), the GOFs have steep surfaces of ~10° (Table 5-2), comparable to inclinations typical for debris flow cones (e.g. Derbyshire and Owen, 1990). With respect to the formative processes we find no indication that the studied fans were (mainly) formed by single catastrophic events. Moreover, our data do not support earlier inferences that outsize fan formation is bound to or conditioned by the presence of large-scale slope instabilities (Lecce, 1990; Crosta and Frattini, 2004; Jarman et al., 2011). By contrast, large deep-seated slope deformation can mainly be found on the opposite valley flank of the Rhone valley (Tonini et al., 2014), where only very small fan systems have developed. Instead, our quantitative data on the subsurface material and the exposure ages from the catchment area and fan surface rather point to a rapid, but incremental formation of outsize fans in the Upper Rhone valley. This is in accordance with other studies on alluvial fans (e.g. Ekes and Friele, 2003; Hornung et al., 2010;

Brardinoni et al., 2018; Ratnayaka et al., 2019) and raises the question, whether outsize fan formation is fundamentally different from the formation of non-outsize fan systems after all.

However, in contrast to these examples, the three GOFs originate from very small catchments carved into bedrock hillslopes where the availability of large amounts of unconsolidated sediment was unlikely, let alone the presence of an initial catchment, i.e., we imagine the valley slopes under investigation as post-glacial blank triangular facets rather than considerable reservoirs of ready-to-transport material. Nonetheless, we cannot completely rule out the pre-existence of catchments that were preserved during the last glacial cycle, acting as traps for glacigenic sediments readily available for erosion after deglaciation (Bögli, 1941). However, this scenario seems unlikely, given the absence of significant sediment storage within the catchments, the very young surface exposure ages obtained and the absence of comparable catchments on other interfluves in the Rhone valley.

In this setting, paraglacial rock slope instabilities following deglaciation and concomitant stress-field changes might play a key role for initially high rates of sediment production (e.g. Derbyshire and Owen, 1990; Ballantyne, 2002; Crosta and Frattini, 2004; Jarman et al., 2011; McColl, 2012), but tectonic and/or climatic conditioning of catchment initiation and fan formation seems equally likely (e.g. Bull, 1977; Densmore et al., 2007; Ratnayaka et al., 2019). Furthermore, the absence of perennial streams that would allow material to be reworked and ultimately exported might facilitate the generation of large fans from developing catchments in this setting. Ultimately, the question what caused high rates of sediment delivery from these catchments to quickly drop and finally cease over the course of the Holocene remains unresolved. In any case, outsize fans are witnesses of their formation by high-magnitude processes, giving rise to concerns that a future reactivation of their steeply inclined feeder basins by shifts in precipitation patterns might pose local communities at elevated risk (De Finis et al., 2018; Stoffel et al., 2014).

5.6 Conclusion

We present a multi-method study of three prominent outsize fans in the Upper Rhone valley of the Swiss Alps. In contrast to other sedimentary fan systems, outsize fans are characterized by a ratio of fan to source area of > 0.5, steep hillslope gradients and a bottle-neck transition between fan surface and feeder basin. The fans under our investigation are fed by catchments of just about similar size, which are carved into bedrock hillslopes. Interestingly, presence of pre-existing catchment structures at the positions of the three catchment-fan systems under investigations appears unlikely. Thus, no considerable amounts of unconsolidated sediment could have been available here.

Fan architecture, absolute ages and morphometric considerations suggest a fan formation in three major phases (Figure 5-12). In a Phase 0 directly following deglaciation, intact rock walls were left prone to erosion. During Phase 1 that ceased with the full development of the catchment around ~6.0 ka, the fan interior (sedimentary unit I) was built up by deposits of massive high-energy, high-magnitude debris flows sourced from the feeder catchment. In Phase 2 lasting until ~0.8 ka, feeder basins were affected by comparatively lower-magnitude debris flows that deposited sedimentary unit II characterized by debris flow channels, snouts and large boulders on the initial fan. During the most recent Phase 3, the feeder basin-fan transport system slackened with only isolated cases of geomorphic activity within the catchment not reaching the fan. We conclude a rapid, but incremental formation of outsize fans in the Upper Rhone valley.

Erosion and sedimentation rates of these fan systems were remarkably elevated soon after deglaciation and then decreased or ceased over time during the Holocene, which is a core notion of paraglacial sedimentation theory in fan environments. However, besides paraglacial rock slope instabilities we acknowledge that tectonic and/or climatic conditioning of catchment initiation and fan formation might have (also) conditioned initially high rates of sediment production. The magnitude of averaged denudations rates in Phase 1 of fan formation was exceptionally high, ranging 16 to 20-times higher than 1.5 IQR of the basin wide denudation rates from the Goms region and Upper Rhone valley. In other words, this means that the geomorphic work that was done right after deglaciation in just ~4 kyr would take ~100 kyr to be done under recent environmental conditions. This enhanced activity following deglaciation is at least comparable to the current Illgraben activity.

We conclude that outsize fans are conspicuous landscape features, that rapidly – however, not necessarily catastrophically – evolve from feeder basins of similar size. These basins would otherwise produce smaller fans, but export material at extremely high rates in response to environmental disturbance, as for example climatic shifts. Due to rapid delivery of exceptional material amounts outsize fans have the potential to overwhelm (downstream) geomorphic systems. As a result, outsize fans are particularly capable of disrupting longitudinal sediment connectivity not only in terrestrial mountain regions.

6 Mapping on the regional scale: sediment storage distribution in five key sites and sedimentary fans in the Upper Rhone Basin

This chapter addresses thesis objective (2): Investigating the landform assemblage in medium-sized tributaries within the Upper Rhone Basin.

6.1 Introduction

Sediment storage on the regional scale in high-mountain areas is investigated in several studies in the European Alps, but also in other locations worldwide. These studies have different foci, e.g. on studying geomorphic systems (Otto and Dikau, 2004; Lambiel et al., 2016), quantifying sediment storage in a sediment budget approach (Otto et al., 2009), analyzing the spatial distribution of sediment storage and quantifying valley fill deposits (Schrott et al., 2003), quantifying Postglacial sediment storage and reconstructing rates of Postglacial rock wall retreat and mechanical denudation (Götz et al., 2013), as well as analyzing sediment connectivity (Messenzehl et al., 2014). Most of these studies were carried out in catchments < 10^2 km^2, however, Otto et al. (2009) utilize a novel upscaling approach to extend their detailed analysis on sediment storage quantification to the Turtmanntal (~110 km^2) by combining geophysical surveys and topography-based modeling techniques.

All of the aforementioned studies have in common that they are based on a geomorphic mapping approach. Geomorphic mapping creates a holistic image or inventory, i.e. a map, of an area including information on processes, forms and (subsurface) material (Smith et al., 2011; Otto and Smith, 2013). It is an essential tool for the initial analysis of a geomorphic system and serves as a basis to understand catchment configuration (Otto and Dikau, 2004).

Since manual, geomorphic mapping in the field and from remote sensing data is very time consuming, several (semi-)automated approaches are established and applied to a variety of geomorphic studies and settings (e.g. Luoto and Hjort, 2005; van Asselen and Seijmonsbergen, 2006; Klingseisen et al., 2008; Schneevoigt et al., 2008; Brenning, 2009; Theler et al., 2010; Petschko et al., 2014; Goetz et al., 2015). These approaches can be pixel- or object-based. Pixel-based classifications were used while the resolution of remote sensing data was coarser than or the same resolution as the studied object. Increasing spatial resolution facilitated the detection of objects consisting of multiple pixels. Object-based classifications use image segmentation and object classification techniques. Then these objects are further classified based on a combination of distinct characteristics (e.g. spectral information, geomorphometric properties, textural information) (Dragut and Blaschke, 2006; Blaschke, 2010; Otto et al., 2018). Predictive geomorphic mapping, also a pixel-based approach, is “the development of a statistical model of the relationship between environmental variables and geomorphologic processes and/or landforms, which is then applied to a geographic data base to create a predictive map" (Luoto and Hjort, 2005, p. 300). All of these classifications have the benefits of repeatable and time-saving methods, which is highly desirable. However, the results are often of low to moderate accuracy (Seijmonsbergen et al., 2011; Otto and Smith, 2013; Otto et al., 2018). Both methods, pixel- and object-based classifications, have been applied successfully in upscaling approaches.

This chapter aims on the one hand at creating derivative geomorphic maps of the sediment storage distribution for the five key sites, Goms, Lötschental, Turtmanntal, Val de la Liène and Val d'Illiez, and on the other hand at mapping and analyzing sedimentary fans and their geomorphometrical properties within the URB. Both approaches yield at bridging the gap between the regional and the large catchment scale.

6.2 Study areas

Five key sites, Goms, Lötschental, Turtmanntal, Val de la Liène and Val d'Illiez, are chosen for investigating sediment storage on the regional scale. They are selected to reflect the heterogeneity of the URB and its tributaries (Table 6-1). The five key sites cover all three major tectonic units and many lithologies exposed within the study area (chapter 3.1; Figure 3-2). Highly variable climatic conditions within the URB are exemplified (chapter 3.4). Further, the full width of surface morphology, relief, Pleistocene glacial imprint and contemporary glacial cover are represented. Each key site spans across different spatial scales. Mean elevations of the key sites vary between 1650 and 2500 m, although the surface morphology is comparable with mean slope gradients between 26 and 32%. The most important characteristics of the key sites are summarized in Table 6-1 and the following chapters.

Table 6-1: Characteristics of the five key sites in the URB. Glacier extent from Swiss glacier inventory 2010 (Fischer, 2013). Erodibility after Kühni and Pfiffner (2001).

Key site	Total area [km²]	Min. elevation [m]	Max. elevation [m]	Mean elevation [m] ± 1SD	Glacier cover [%]	Lake cover [%]	Mean slope gradient [%] ± 1SD	Lithology	Erodibility	Absolute and relative mapped area [km²/% of URB]	
										Bedrock	**Sediment**
Goms	233.27	1309	3629	2305 ± 484	11.66	0.43	28.92 ± 14.43	granites and metamorphic rocks	very low - low	51.12/0.95	62.78/1.17
Lötschental	164.73	649	3962	2393 ± 584	14.23	0.04	32.31 ± 14.52	granites and metamorphic rocks	low	57.43/1.07	21.52/0.40
Turtmanntal	107.95	638	4152	2517 ± 552	10.81	0.14	29.14 ± 13.12	metamorphic rocks	low	40.91/0.76	18.05/0.34
Val de la Liène	90.90	506	3248	1921 ± 627	1.22	0.94	26.11 ± 14.21	limestone	medium	28.25/0.52	26.88/0.50
Val d'Illiez	135.59	427	3254	1647 ± 472	1.22	0.02	29.18 ± 13.64	flysch, limestone	medium	25.87/0.48	27.49/0.51
total										**203.58/3.78**	**156.72/2.91**

6.2.1 Goms

The Goms region is located in the uppermost part of the Upper Rhone valley and stretches from the Furka Pass, Grimsel Pass and the Rhone glacier to Fiesch. The drainage basin has a size of ~230 km^2 and can be divided into different entities: The Rhone glacier and its surrounding areas including the LIA glacier forefield stretching until Gletsch, the main valley with its adjacent slopes between Oberwald and Niederwald as well as many tributaries of variable sizes northwest and southeast of the Rhone valley. The main valley is dominated by a thick valley fill (thickness up to 270 m, Mey et al., 2015) and three distinct outsize fans originating from conspicuously small feeder basins located on the northwestern valley slopes (chapter 5). The gradient of the main valley is low (0.78%). A bedrock knickpoint at the valley outlet, between Fiesch and Brig, hinders base level lowering of the valley.

Glaciers cover c. 12% of the study area: The Rhone glacier (14.6 km^2), the Gries glacier (4.8 km^2) and the Minstiger glacier (2.3 km^2) are the largest glaciers in this area (Fischer, 2013; Fischer et al., 2014). During the Pleistocene, the wide glacial trough of the main valley was formed. The LGM ice thickness reached at least 1500 m (Florineth and Schlüchter, 1998; Kelly et al., 2004). The tributaries have varying degrees of glacier cover. The Bieligertal, Bächital and Minstigertal to the northwest have the strongest glacial imprint and are most deeply incised. Most other tributaries exhibit a less strong glacial character (Norton et al., 2010b). The region is located within the crystalline basement bedrock, which consists of the Aar and Gotthard massifs northwest and southeast of the Rhone valley, respectively. The two massifs are separated by a tectonic fault. The crystalline basement rocks represent the oldest rock types within the URB. The lithology comprises mainly granitic rocks as well as gneiss, schists and metagranitoids (Schmid et al., 2004; swisstopo, 2005; swisstopo, 2011).

6.2.2 Lötschental

The Lötschental is situated north of the Rhone valley at Gampel. It has a size of ~165 km^2 and is drained by the Lonza, a tributary of the Rhone. It is characterized by a high-alpine morphology and a high glacier cover of > 14% including the Lang glacier and several smaller glaciers within the tributaries northwest and southeast of the main valley. The valley features a strong north-south contrast in topography. Thus, the valley can be subdivided into the Lang glacier (covering 8.2 km^2, Fischer, 2013; Fischer et al., 2014) and its extensive glacier forefield, the tributaries northwest and southeast of the main valley, respectively, the main valley between the Lang glacier and Ferden as well as the main valley between Ferden and Gampel. Between Gampel and Ferden, the main valley has a V-shaped cross section and steep valley slopes. Upstream of Ferden, it is characterized by a broad glacial trough with many, exceptionally large debris flow cones, mostly originating from the tributaries to the southeast. These steep tributaries are characterized by extensive moraine deposits and several small glaciers. Of the tributaries situated northwest of the main valley, the four to be located closest to the Lang glacier are deeply incised, U-shaped hanging valleys with much sediment is deposited in the valley floor areas.

The Lötschental is mostly located within the Aar massif and thus underlain by crystalline basement rocks consisting mainly of gneiss, mica schists, granites and amphibolites. The Infrahelvetic nappes only crop out in the southernmost part of the catchment (Schmid et al., 2004; swisstopo, 2005; swisstopo, 2011).

6.2.3 Turtmanntal

The Turtmanntal is a high-alpine catchment with a size of ~110 km^2. It is located between the Mattertal and the Val d'Anniviers south of the Rhone valley, roughly opposite the Lötschental. It is an approximately 20 km long and up to 7 km wide basin drained by the Turtmänna river. The valley can be structured into 14 hanging valleys, the Turtmann and Brunegg glaciers (5.2 and 5.3 km^2, respectively) with their forefields, and the main valley with its slopes (Otto et al., 2009). The main valley as well as the hanging valleys were sculpted by repeated Pleistocene glaciations (Lang and Wolff, 2011) resulting in a distinct U-shaped glacial trough of the main valley. The hanging valleys are characterized by high alpine landforms including a large number of relict and active rock glaciers and talus deposits (Otto and Dikau, 2004; Nyenhuis, 2006). The two main glaciers and some remnants within the hanging valleys cover c. 11% of the surface (Fischer, 2013; Fischer et al., 2014). The Turtmanntal is located in the Penninic units, which originate from the marine basins formed between the two continental margins in the Mesozoic and consist of Penninic basement nappes and Mesozoic sediments (Schmid et al., 2004; swisstopo, 2011). The lithology is dominated by metamorphic rocks including gneiss and mica schist. Mesozoic dolomites, limestones and marbles are found in the western and south-eastern parts of the valley (swisstopo, 2005).

6.2.4 Val de la Liène

The Val de la Liène is c. 90 km^2 and a northern tributary to the Rhone. The catchment is drained by the river La Liène. A large hydropower dam built in 1957 impounds Lac de Tseuzier in the upper part of the valley. Elevation and hence glacier cover (1.2%) are much lower than in the three previously described study areas (Fischer, 2013; Fischer et al., 2014). The valley is characterized by a deeply incised gorge in the lower, southern part of the catchment and a widening valley in the upper northern part. The upper valley has plateau-like flats at high elevations (~2500-2900 m). The only glacier is located in the northwestern-most area exhibiting the highest elevations. Val de la Liène is located in the Helvetic nappes featuring (meta-)sedimentary rocks, e.g. schist, limestone and sandstone (Schmid et al., 2004; swisstopo, 2005; swisstopo, 2011).

6.2.5 Val d'Illiez

The Val d'Illiez, a western tributary to the Rhone at Monthey, is drained by the river La Vièze and has a northeast-southwest orientation. The catchment with a size of ~135 km^2 lies at similar elevations as the Val de la Liène and thus features a similar glacier cover (1.2%) in the southern part of the catchment where elevations are highest (up to 3250 m). Here, the prominent mountain ranges Dents du Midi and Les Dents Blanches consisting of limestone are located. Situated in the Infrahelvetic and Helvetic nappes, the study area exhibits mostly flysh and limestone (Schmid et al., 2004; swisstopo, 2005; swisstopo, 2011). The catchment can be divided into the mentioned, outstanding mountain ranges in the southeast, the roughly U-shaped main valley, a small tributary valley (Val de Morgins) in the northwest, and less noticeable drainage divides in the western part of the basin. The glacial imprint is less pronounced in comparison to the three at first described study areas.

6.3 Methods

6.3.1 Geomorphic mapping

The geomorphic maps of sediment storage forms in this thesis are produced as base data for an upscaling approach. Thus, these derivative geomorphic maps have a clear purpose to which the applied method was adjusted (Dramisa et al., 2011; Otto and Smith, 2013). An inventory of sediment storages and bedrock cover is mapped in the field and complemented with data mapped from high-resolution remote sensing data. The SwissAlti3D DEM (2 m resolution, swisstopo) and the derived hillshade and slope raster as well as satellite imagery (available on GoogleEarth) serve as a mapping basis (Figure 6-1). Lakes within the URB are delineated semi-automatically with a surface classification model based on the DEM data combining slope and surface roughness characteristics (Bowles and Cowgill, 2012). Furthermore, the Swiss glacier inventory 2010 is used to identify currently glaciated areas (Fischer, 2013; Fischer et al., 2014). In addition, existing data on sediment storage distribution from the hanging valleys in the Turtmanntal are included in the dataset (Otto and Dikau, 2004; Otto, 2006; Otto et al., 2009). This data is expanded to the glacier forefield area and parts of the main valley of the Turtmanntal.

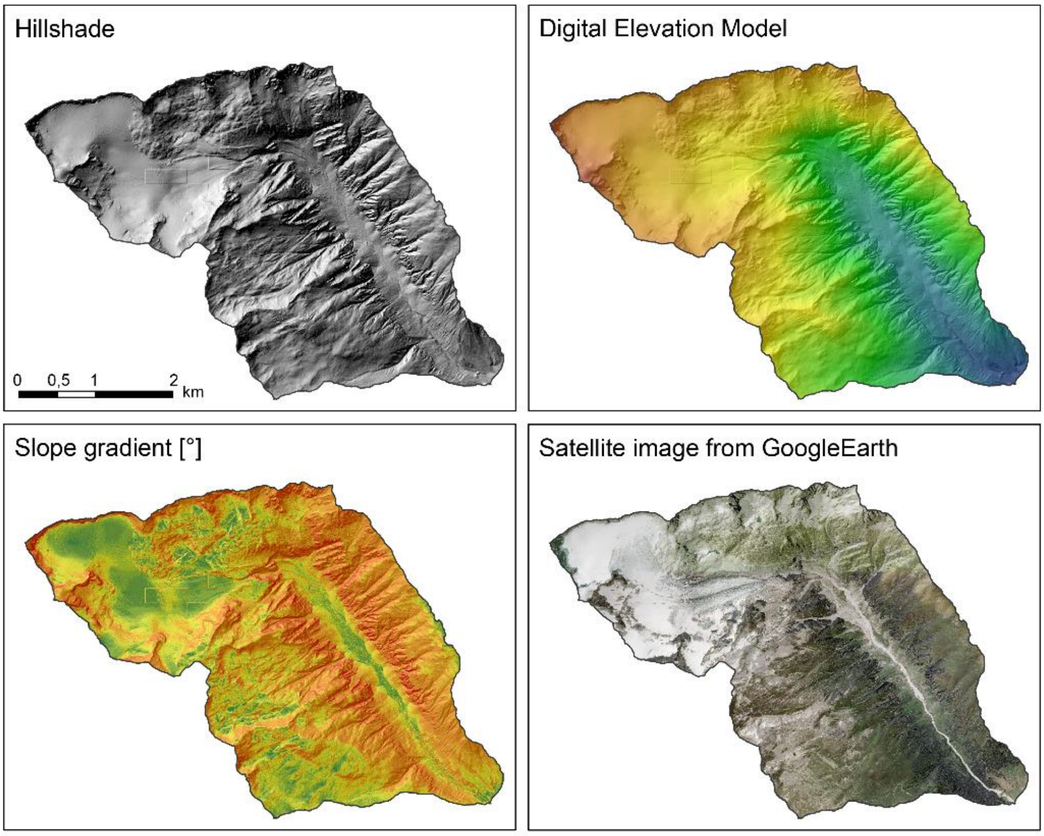

Figure 6-1: Mapping basis for the identification of sediment storages. Hillshade (swisstopo) and satellite imagery available from GoogleEarth were used in the field. It was complemented with the DEM and the slope raster for the geomorphic mapping from remote-sensing data. Exemplary catchment is the Minstiger Valley in the Goms region, Upper Rhone valley (DEM from swisstopo, projection: CH1903).

The inventory of sediment storages within the five key sites is classified based on process domains and sediment storage forms of the according process domain (Table 6-2). The process domains comprise alluvial, colluvial, debris flow, gravitational, glacial, periglacial, complex, other (lakes, glaciers, anthropogenic), bedrock and undefined units. This classification follows existing classifications by Ballantyne and Harris (1994) and Otto and Dikau (2004). Detailed descriptions of sediment storage forms can be found in Ballantyne and Harris (1994), Otto (2006) and Davies and Korup (2010).

Table 6-2: Classification of sediment storage forms into process domains and landforms.

Unit #	Process domain (unit)	Description of process domain	Subunit #	Landform (subunit)
1	alluvial	Deposits of fluvial processes including alluvial fans dominated by fluvial processes and fluvial valley fills	11	alluvial valley fill
			12	alluvial deposit
			13	alluvial fan
2	colluvial	Deposits of slope processes, e.g. creep or in situ weathering, resulting in colluvial deposits at lower slopes or block slopes	21	colluvial deposit/cover (foot of slope)
			22	block slope (bedrock with thin colluvial cover)
3	debris flow	Deposits of debris flow processes	31	debris flow cone
			32	debris flow deposit
4	gravitational	Deposits of gravitational mass movement processes after e.g. Cruden and Varnes (1996), not including debris flow processes	41	talus (slope, cone, etc.)
			42	talus (with creep structures)
			43	deposit by other gravitational processes
5	glacial	Deposits of glacial processes (LGM, LIA, recent) mainly consisting of moraine material, e.g. side and base moraines	51	side moraine
			52	base moraine
			53	moraine undefined
6	periglacial	Deposits of periglacial origin, including the most striking features of rock glaciers, but also other small-scale, cryogenic landforms (e.g. solifluction lobes, patterned ground, protalus ramparts)	61	rock glacier active/undefined
			62	protalus rampart
			63	rock glacier intact
			64	rock glacier fossil
7	complex	Sediment storages, which cannot be ascribed to one single process: e.g. complex valley fills, sedimentary cones deposited by debris flow and fluvial processes as well as cones deposited by several processes (nival, fall/gravitational, debris flows)	71	talus-debris flow complex
			72	alluvial-debris flow deposit
			73	alluvial-debris flow fan
			74	talus-moraine complex
			75	valley fill
			76	complex (general)
8	other	Includes other land surface features such as lakes, glaciers and anthropogenically modified areas.	81	lake
			82	glacier
			83	anthropogenic
9	bedrock	Exposed bedrock with no sedimentary cover	91	bedrock
0	undefined	Sedimentary cover, which cannot be ascribed to a certain process	0	

6.3.2 Predictive geomorphic mapping

The mapping results from the regional scale are further used in an upscaling approach, which serves as a scale linkage between the regional and the large-catchment scale, i.e. the URB (chapter 7). For the statistical, predictive geomorphic mapping approach, I use the compiled dataset on sediment storage and bedrock distribution (dependent variable) as well as a set of 22 independent, predictor variables (Table 7-1, Figure 6-2). These are intended to explain the differences in local morphometry (or surface morphology), topography and position, characteristics of the contribution area as well as biotic and climatic variations between the two classes. The prerequisite for these models is a functional/statistical relationship between the studied objects and the available spatial information (Schlummer et al., 2014).

Three different statistical models are applied and compared to identify areas where the occurrence of sediment or bedrock cover is very likely. These techniques include a logistic regression model (LR), a principal component logistic regression model (PCLR) and a generalized additive model (GAM). More details on the independent variables and the predictive models are described in chapters 7.3.1 and 7.3.2.

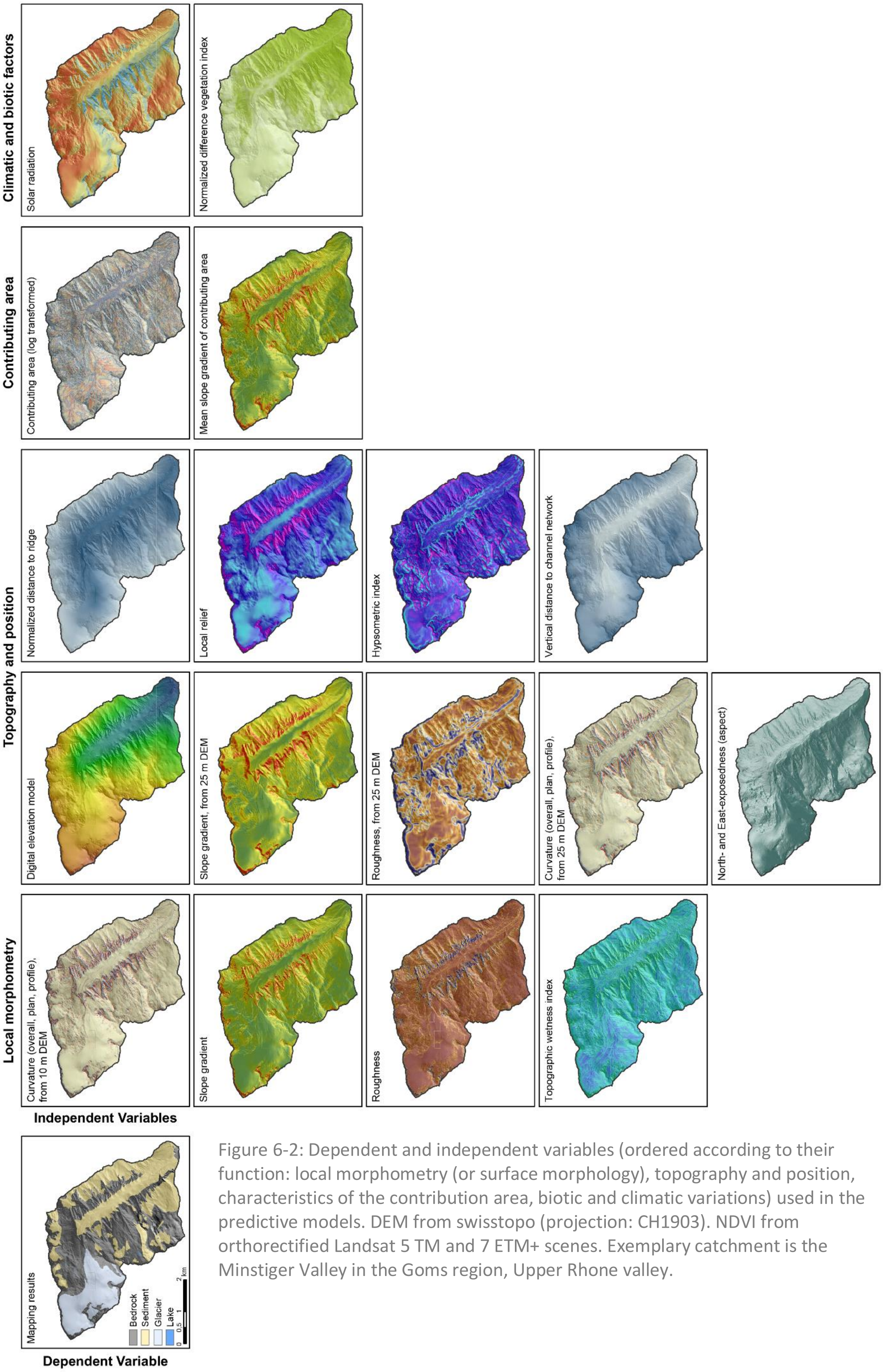

Figure 6-2: Dependent and independent variables (ordered according to their function: local morphometry (or surface morphology), topography and position, characteristics of the contribution area, biotic and climatic variations) used in the predictive models. DEM from swisstopo (projection: CH1903). NDVI from orthorectified Landsat 5 TM and 7 ETM+ scenes. Exemplary catchment is the Minstiger Valley in the Goms region, Upper Rhone valley.

6.3.3 Mapping of sedimentary fans

In addition to the mapped sediment storages in the five key sites, I mapped all sedimentary fans, also called alluvial fans – a misleading term concerning the involved processes, within the Upper Rhone catchment from high-resolution digital topography and optical imagery (swissALTI3D DEM, 2 m resolution, ©swisstopo; GoogleEarth). Alluvial fans are cone-shaped depositional landforms that preferentially develop where steep tributaries enter wide trunk valleys and stream power is greatly reduced (Harvey et al., 2005). For these fans (min. area > 0.015 km^2), I derive a set of morphometric parameters, e.g. fan and catchment area as well as their mean gradients, from a void-filled DEM with 30 m resolution (SRTM, ©NASA). This dataset is used to investigate a regional fan-catchment area relationship and compare this to the morphometric characteristics of the outsize fans in the Goms region (chapter 5).

6.4 Results and discussion

6.4.1 Sediment storage maps for the five key sites

In total, an area of 360.3 km^2 of sediment and bedrock cover is mapped within the five key sites in the URB, corresponding to 6.7% of the total area (Table 6-1). The mapped areas do not cover the full area of the key sites, since they are not intended for stand-alone maps but for data input in an upscaling approach (chapters 4, 7). Initially, sediment storages classified according to their process domain and landform (Table 6-2) are mapped in the Goms, Turtmanntal (including data from Otto et al., 2009) and Lötschental (Figure 6-3, Figure 6-4, Figure 6-5). These datasets are used for first predictive mapping tests, which revealed that modeling the spatial distribution of all landforms or process domains results in poor predictions, due to their overlapping properties. Thus, no clear statistical relationship between the large number of different, studied objects and the available spatial information can be established.

This problem has been pointed out in other studies before, where the classification of entire areas or different, specific landforms is only in parts successful. Earth's surface is highly complex: specific processes produce landforms with variable semblance and landforms with alike appearance can be formed by different processes, which is termed equifinality or convergence (Chorley, 1962; Thorn, 1988; Otto et al., 2018). Furthermore, the landforms one can observe today are an assemblage of relict, overlapping and replaced landforms reflecting past and present processes (Chorley et al., 1985; Hewitt, 2002a). Ascribing landforms in alpine environments to one formative or dominant processes is a challenging and in many cases futile intention. Even landforms in the headwaters are often not built up of material deposited by a single process. Talus cones, which collect eroded material from rockwalls located above, are the first storage form in alpine sediment cascades, but yet often a combination of at least rockfall, nival, debris flow and other processes (Ballantyne and Harris, 1994). Thus, they are complex landforms which provide evidence of past environmental changes. The relative importance of individual processes cannot always be inferred from surface investigations (Sass and Krautblatter, 2007). In addition, the complexity of landforms increases with spatial scale (chapter 4). Sediment storages in larger scale catchments are more complex and the deposits originating from several processes interfinger with each other (e.g. valley fills) (Phillips, 1999; Otto et al., 2008).

While talus cones or valley fills have in most cases a distinct morphometric signature, other geomorphic forms or process domains, such as moraines (glacial), have no marked morphometric properties. Schneevoigt et al. (2008) detect 20 different alpine landforms from remote sensing imagery combining topographic and spectral data. They observe good results for talus slopes, rock faces, and cirque walls, but are less efficient in the classification of fluvial, glacial, and debris flow deposits.

In contrast, predictive mapping (or (semi-)automated mapping) of single landforms yields good results. These studies are successful in detecting landslide hazard (Petschko et al., 2014; Goetz et al., 2015), the spatial distribution of permafrost landforms (Brenning, 2009) and active patterned ground (Luoto and Hjort, 2004).

Based on my observations, testing and published results, I decide to focus on a classification into of the land surface cover sediment and bedrock cover (chapter 7) in the remaining two key sites, Val de la Liène and Val d’Illiez (Figure 6-6, Figure 6-7), which results in better modeling results and hence a higher geomorphic plausibility of the results (Steger et al., 2016). The modeled sediment covered areas of the whole URB are later analyzed with a geomorphological approach based on their location and topographic slope position (chapter 7.5.2). Since the regional scale is not the focus of this dissertation, the following mapping results from the key sites are not be described and analyzed in further detail.

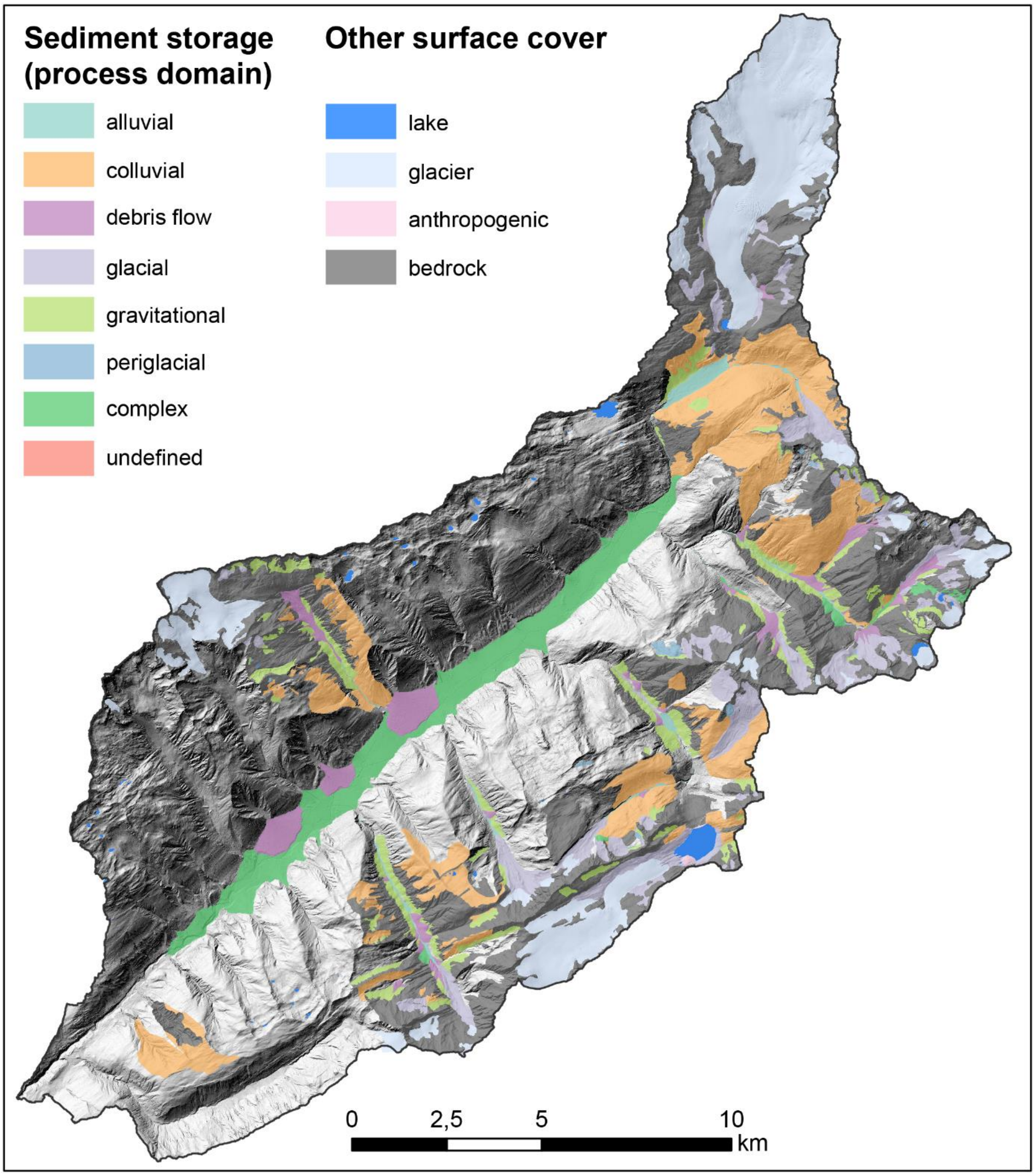

Figure 6-3: Geomorphic map of sediment storages classified according to their process domain (Table 6-2) for the Goms region (for location see Figure 3-1). Mapping basis illustrated in Figure 6-1. (DEM from swisstopo, projection: CH1903).

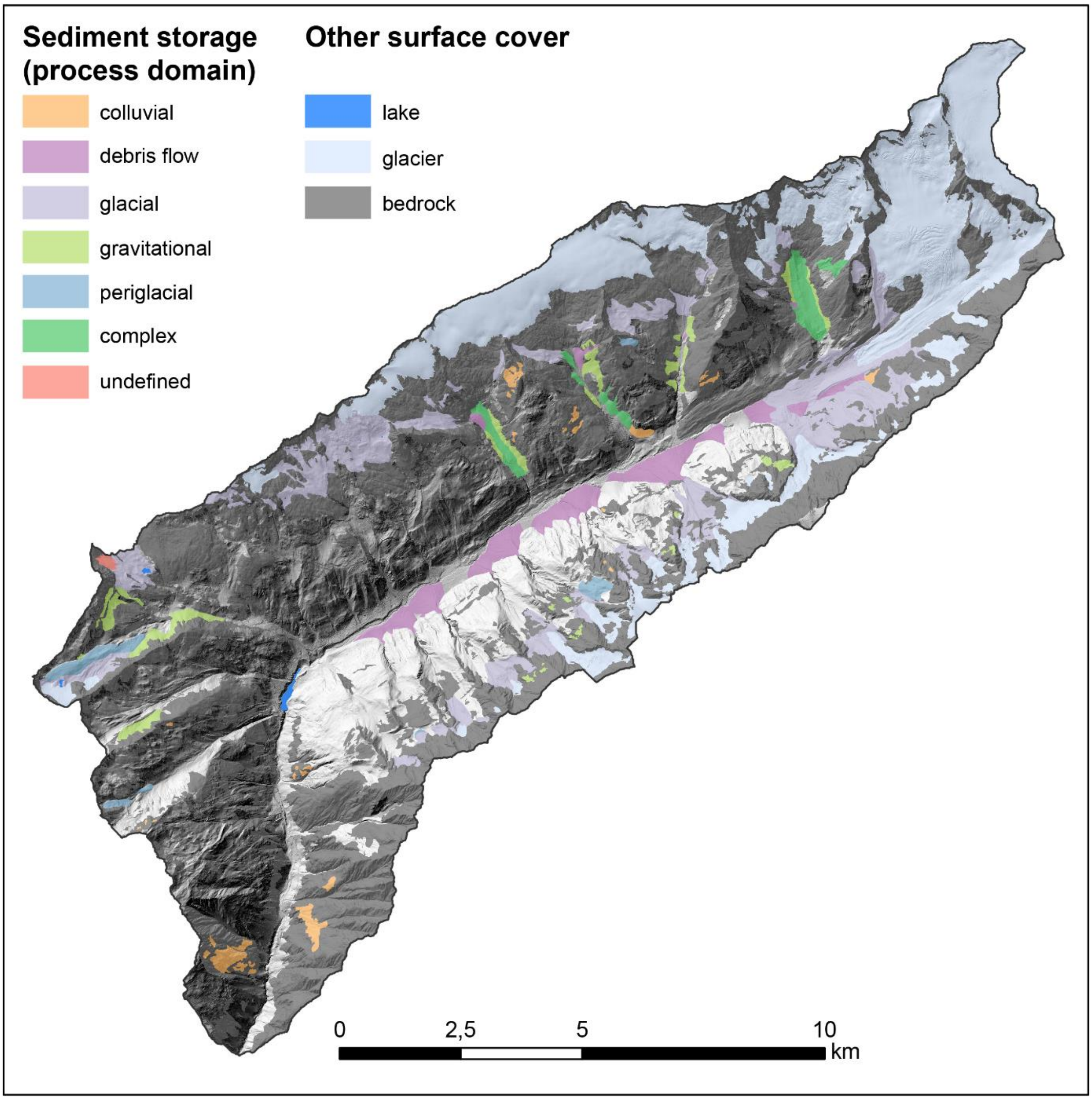

Figure 6-4: Geomorphic map of sediment storages classified according to their process domain (Table 6-2) for the Lötschental (for location see Figure 3-1). Mapping basis illustrated in Figure 6-1. (DEM from swisstopo, projection: CH1903).

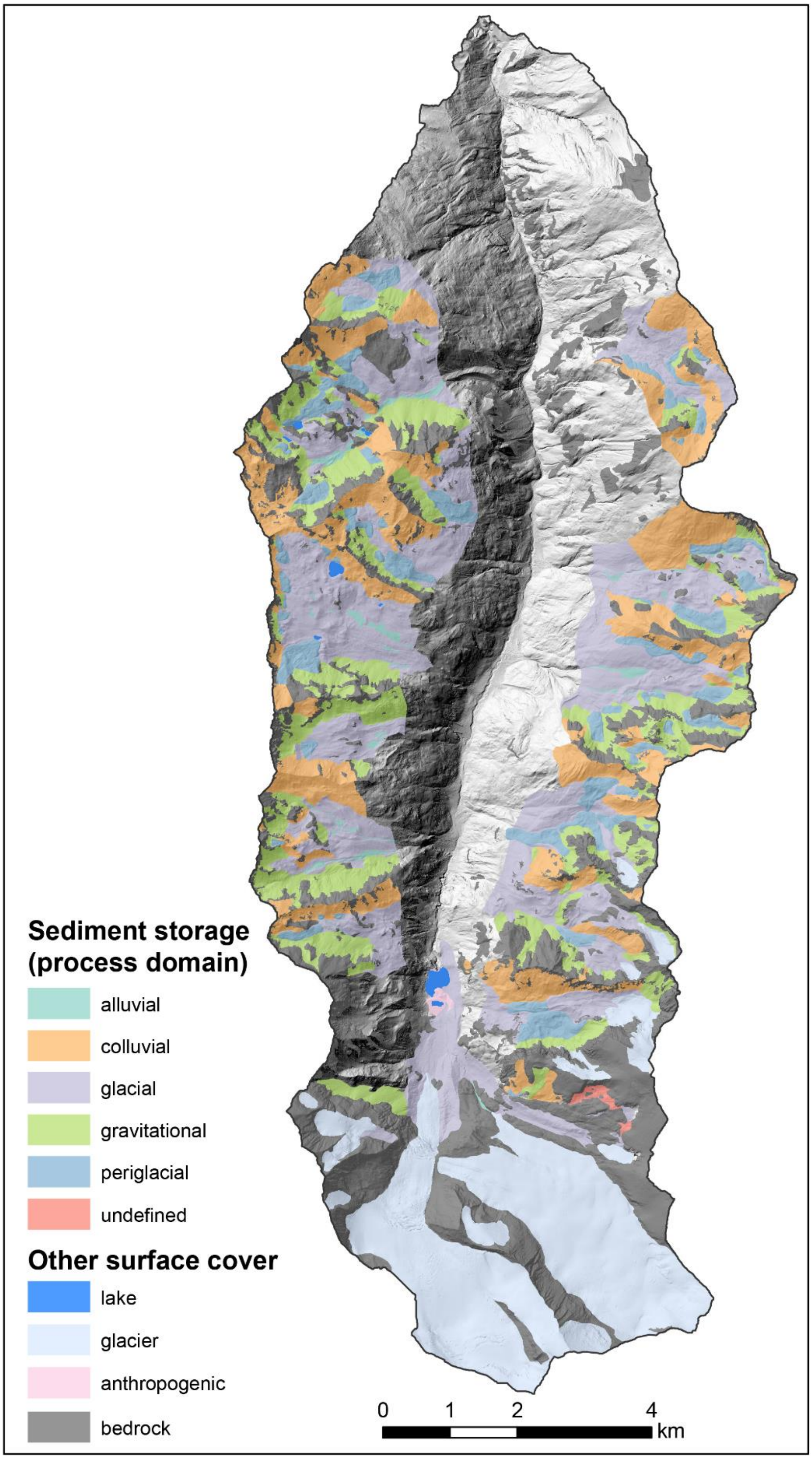

Figure 6-5: Geomorphic map of sediment storages classified according to their process domain (Table 6-2) for the Turtmanntal (for location see Figure 3-1) (including data from Otto et al., 2009). Mapping basis illustrated in Figure 6-1. (DEM from swisstopo, projection: CH1903).

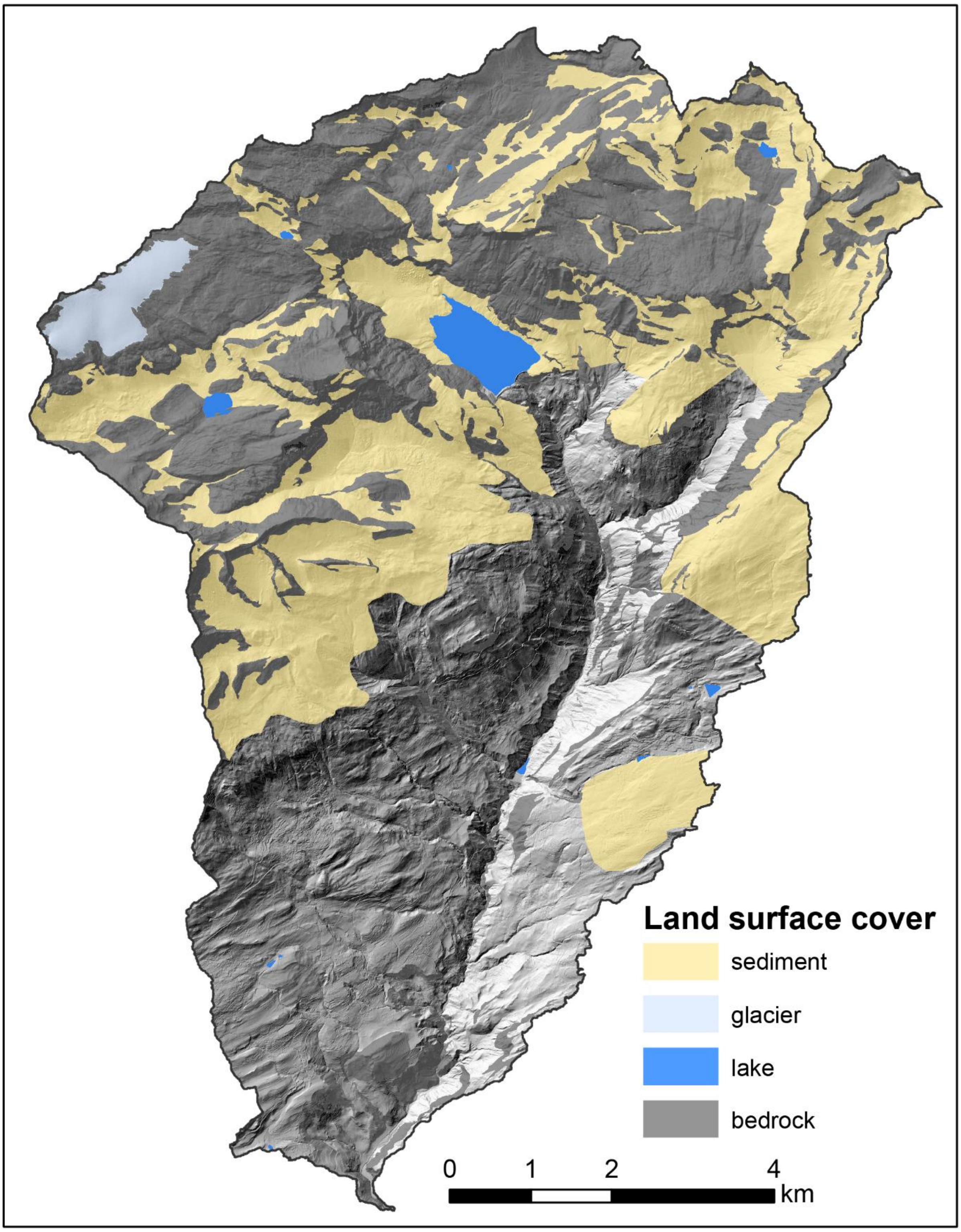

Figure 6-6: Map of land surface cover for the Val de la Liène (for location see Figure 3-1). Mapping basis illustrated in Figure 6-1. (DEM from swisstopo, projection: CH1903).

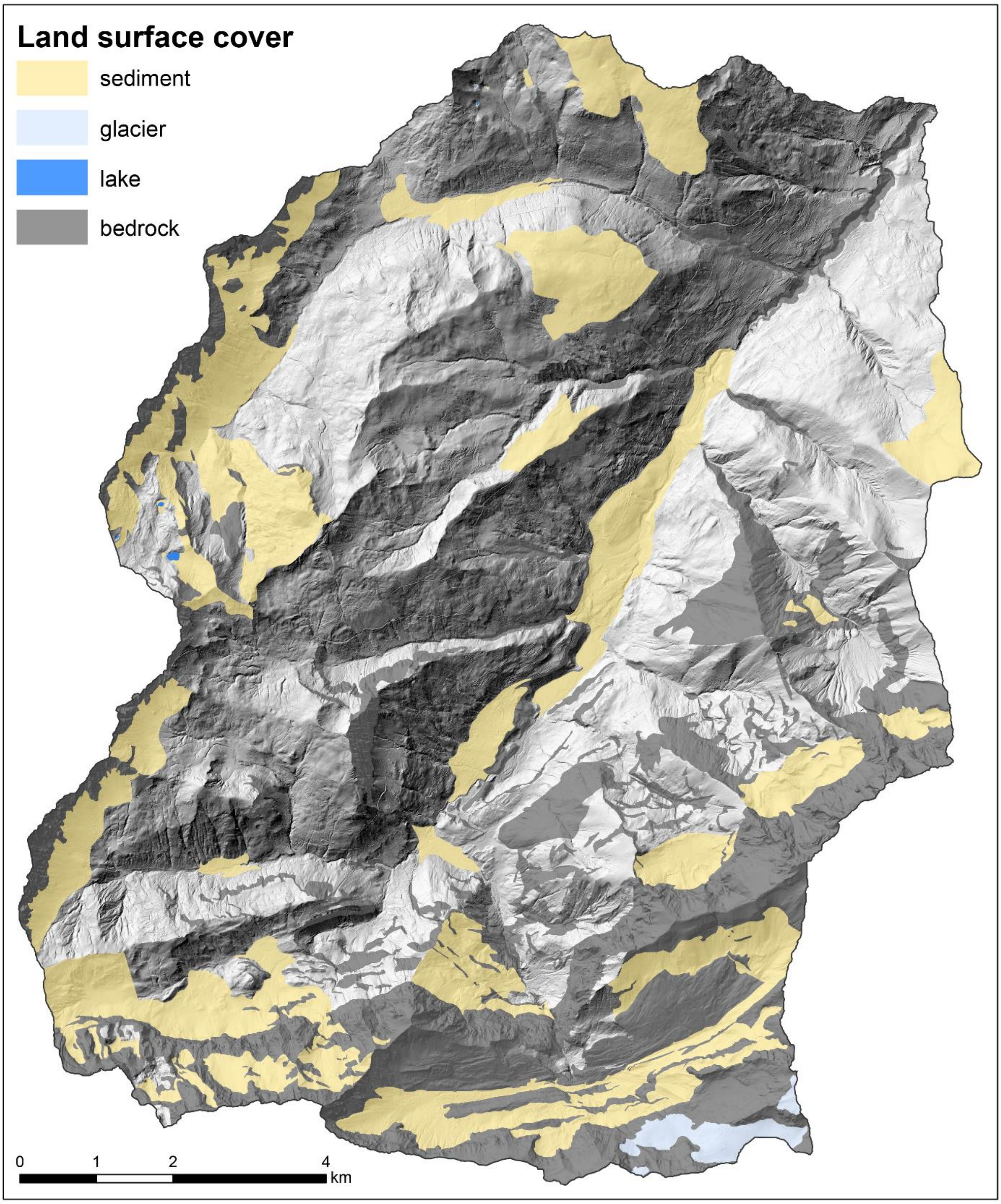

Figure 6-7: Map of land surface cover for the Val d'Illiez (for location see Figure 3-1). Mapping basis illustrated in Figure 6-1. (DEM from swisstopo, projection: CH1903).

6.4.2 Mapping and geomorphometric analysis of sedimentary fans

I mapped 186 fans from digital topographic data and remote sensing imagery (Figure 6-8). These sedimentary fans are deposited in the Rhone valley as well as in larger tributaries with valley floors that are wide enough (e.g. Lötschental, Mattertal, Val de Bagnes and Val d'Entremont). These fans are often complex landforms deposited by more than one specific process. In alpine environments, alluvial and debris flow processes are involved, but also other processes such as gravitational mass movements, earth flows and sheetfloods can associated. Depending on dominant formative process, denudation rate and accommodation space, deposits vary in size, slope, sedimentary facies and morphology (Blair and McPherson, 2009).

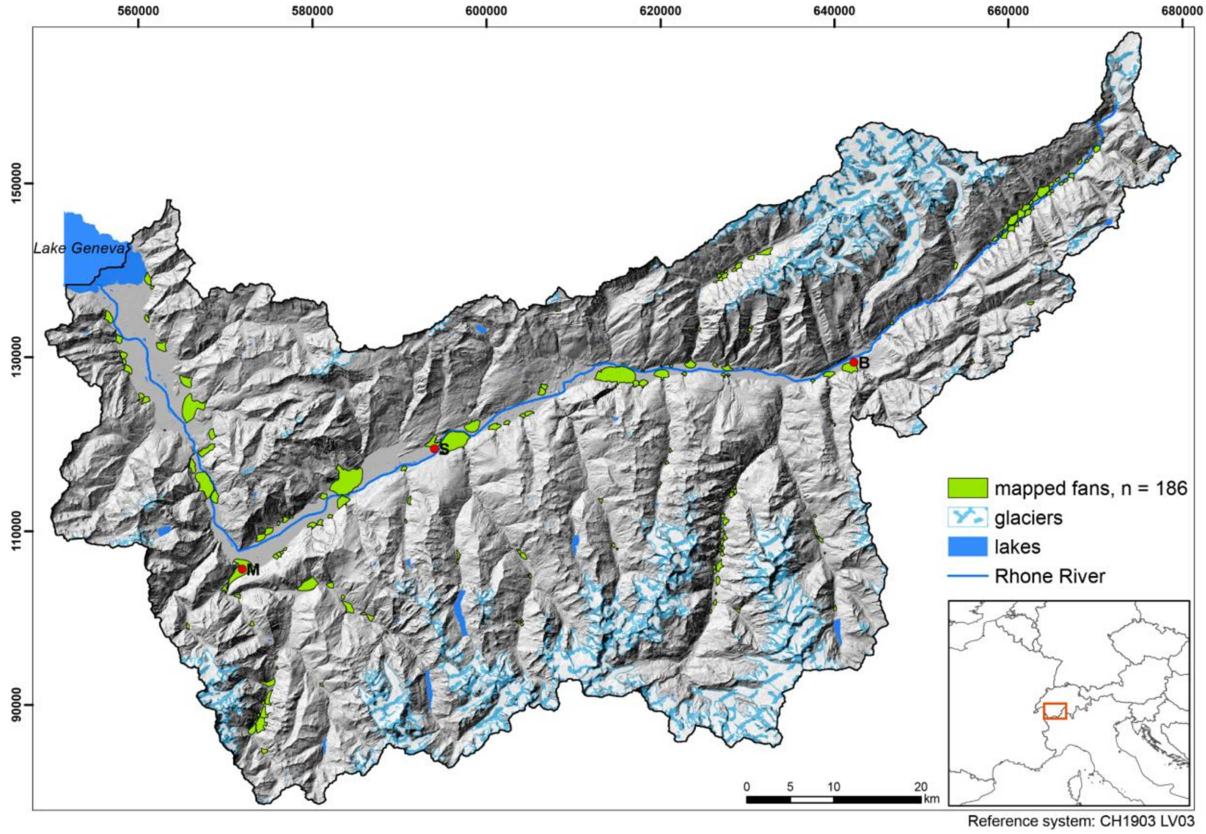

Figure 6-8: Location of mapped fans in the Upper Rhone catchment for morphometric analysis of fan area vs. catchment area. Glacier extent from Swiss glacier inventory 2010 (Fischer, 2013). Lakes classified based on digital elevation model (DEM) with a semi-automated surface classification model (Bowles and Cowgill, 2012) (swisstopo DEM, EPSG:21781).

Analyzing fan and catchment area (Figure 5-5) reveals that most sedimentary fans within the URB exhibit fan area to catchment area ratios well below 0.5. However, in comparison to the general distribution of fans and their feeder basins, the three large GOFs (red stars in Figure 5-5) can clearly be labelled as outsize fans, with their fan area roughly equaling their catchment area. Most of the mapped fans within the study area have steep catchments (mean gradients between 40 and 80%, or between 22 and 39°, respectively; Figure 6-9). Mean fan gradients range from 4 to 45% (~2-24°). As typical slope gradients, Derbyshire and Owen (1990) report < 10° (~17%) for fluvially-dominated and < 15° (~27%) for debris flow-dominated fans. Pointing out, that these categories broadly overlap, 46 of the mapped fans fall into the category of debris flow-dominated fans and 74 fans are within the category of fluvially-dominated fans. Regarding the GOFs, no clear signature of mean fan and catchment gradients are discernible (Figure 6-9). Hence, it could be useful to further investigate the morphometric properties of a large fan dataset and their catchments. Not only morphometric parameters from the fan itself are useful to distinguish between debris flow-dominated and fluvially-dominated fans as well as to refine the characteristics of outsize fans. Furthermore, a number of morphometric parameters such as catchment length, mean catchment slope and Melton's roughness index have been used to differentiate between catchments susceptible to debris flows and catchments more prone to fluvial processes (e.g. Stolle et al., 2015) and could be useful in a more concise definition of outsize fans.

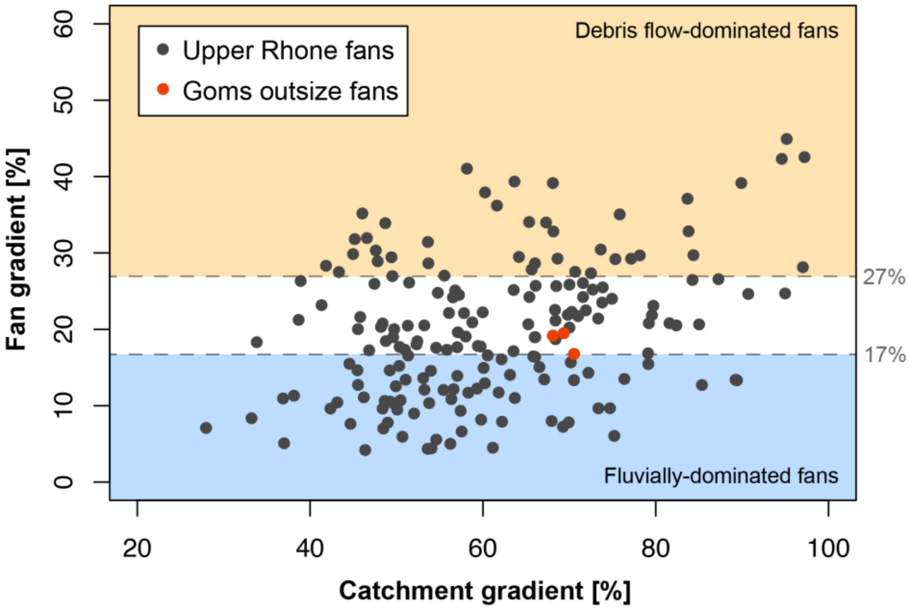

Figure 6-9: Plot of mean fan gradient vs. mean catchment gradient for 186 fans located in the URB. Typical ranges of slopes for fluvially- and debris flow-dominated fans are marked in blue and orange, respectively (Derbyshire and Owen, 1990). The three investigated fans in the Goms region (chapter 5) are highlighted with red dots (see Figure 6-8 for map showing the locations of all mapped fans).

6.5 Conclusion

Geomorphic mapping of specific landforms or landform inventories can be well performed on the regional scale. A combination of field mapping and mapping from high-resolution and remote sensing data has proven to be useful, when larger areas need to be covered in a time-saving procedure. Thus, an exceptionally large dataset of sediment and bedrock cover (process domain/landform inventory) is created, making it a valuable contribution to an upscaling approach in sediment storage analysis. Furthermore, mapping of single landforms and analyzing their morphometric parameters allow a more concise definition of specific categories, i.e. outsize fans. I conclude, that geomorphic mapping, creating a holistic image of an area, is an indispensable method in sediment storage analysis and sediment budgets, since processes and landforms are identified and, furthermore, linkages between system compartments can be investigated.

7 Multivariate geostatistical modeling of the spatial sediment distribution in a large scale drainage basin, Upper Rhone, Switzerland

This chapter is based on the publication "Schoch, A., Blöthe, J. H., Hoffmann, T., & Schrott, L. (2018): Multivariate geostatistical modeling of the spatial sediment distribution in a large scale drainage basin, Upper Rhone, Switzerland. Geomorphology, 303, 375-392.".

DOI: https://doi.org/10.1016/j.geomorph.2017.11.026

It addresses thesis objective (3): Creating scale linkages for sediment distribution between smaller scales and a large catchment scale through a hierarchical upscaling approach based on predictive mapping.

Further information for this chapter can be found in appendix B.

Abstract

There is a notable discrepancy between detailed sediment budget studies in small headwater catchments ($< 10^2$ km^2) focusing on the identification of sedimentary landforms in the field (e.g. talus cones, moraine deposits, fans) and large scale studies ($> 10^3$ km^2) in higher order catchments applying modeling and/or remote sensing based approaches for major sediment storage delineation.

To bridge the gap between these scales, we compiled an inventory of sediment and bedrock coverage from field mapping, remote sensing analysis and published data for five key sites in the Upper Rhone Basin (Val d'Illiez, Val de la Liène, Turtmanntal, Lötschental, Goms; 360.3 km^2, equivalent to 6.7% of the Upper Rhone Basin). This inventory was used as training and testing data for the classification of sediment and bedrock cover. From a digital elevation model (2×2 m ground resolution) and Landsat imagery we derived 22 parameters characterizing local morphometry, topography and position, contributing area, and climatic and biotic factors on different spatial scales, which were used as inputs for different statistical models (logistic regression, principal component logistic regression, generalized additive model). Best results with an excellent performance (mean AUROC: 0.8721 ± 0.0012) and both a high spatial and non-spatial transferability were achieved applying a generalized additive model. Since the model has a high thematic consistency, the independent input variables chosen based on their geomorphic relevance are suitable to model the spatial distribution of sediment.

Our high-resolution classification shows that 53.5 ± 21.7% of the Upper Rhone Basin are covered with sediment. These are by no means evenly distributed: small headwaters (< 5 km^2) feature a very strong variability in sediment coverage, with watersheds drowning in sediments juxtaposed to watersheds

devoid of sediment cover. In contrast, larger watersheds predominantly show a bimodal distribution, with highest densities for bedrock (30-40%) being consistently lower than for sediment cover (60-65%). Earlier studies quantifying sedimentary cover and volume focus on the broad glacially overdeepened Rhone Valley that accounts for c. 9% of our study area. While our data support its importance, we conservatively estimate that the remaining 90% of sediment cover, mainly located outside trunk valleys, account for a volume of 2.6-13 km^3, i.e. 2-16% of the estimated sediment volume stored in the Rhone Valley between Brig and Lake Geneva. Furthermore, our data reveal increased relative sediment cover in areas deglaciated since the Little Ice Age, as compared to headwater regions without this recent glacial imprint. We therefore conclude that sediment storage in low-order valleys, often neglected in large scale studies, constitutes a significant component of large scale sediment budgets that needs to be better included into future analysis.

7.1 Introduction

The topography of the earth's surface is created by the interplay of climate, tectonics, and geomorphic processes (e.g. Molnar and England, 1990; Whipple, 2009). This interaction of endogenic and exogenic processes created mountain ranges with steep topographic gradients featuring some of the highest sediment fluxes on earth. The transport of eroded material through a geomorphic system has been described as a sediment cascade connecting source to sink, involving a chain of subsystems dynamically linked by the transfer of mass or energy (Chorley and Kennedy, 1971; Caine, 1974; Slaymaker, 1991; Milliman and Syvitski, 1992; Burt and Allison, 2010).

Many high-mountain geomorphic systems are considered to be out of equilibrium or in a transient state in terms of the external driving forces, i.e. a shift from glacial to interglacial conditions, because the response to environmental changes is not immediate but buffered and delayed (Phillips, 2003a; Hoffmann, 2015). Several cycles of ice advance and retreat during Pleistocene glaciations created a distinct topography in many mountain systems (Penck, 1905) and produced, eroded and transported vast amounts of sediment (e.g. Hallet et al., 1996; Montgomery, 2002; Schlüchter, 2004a). Furthermore, glacial erosion created overdeepened valleys (e.g. Preusser et al., 2010; Prasicek et al., 2014; Haeberli et al., 2016), hanging valleys (e.g. Valla et al., 2010b), and glacial cirques (e.g. Hooke, 1991; Evans, 2006) that potentially retain vast amounts of sediment (Hoffmann et al., 2013). Despite substantial potential energy in mountain environments, sediment flux in large river systems is frequently disconnected from alpine headwaters, due to intermittent storage along the flow path from the bedrock source to large sedimentary sinks in major alpine valleys (e.g. Otto et al., 2009; Hoffmann et al., 2013; Messenzehl et al., 2014). Thus, the sediment delivery to the outlet is by no means a simple and consistent relationship between drainage area and sediment yield as only a small fraction of sediment eroded within the catchment is delivered to its outlet (Hoffmann et al., 2013). Therefore, detailed studies on the spatial distribution of sediments are needed to explain the discrepancy (Walling, 1983; Phillips, 1986; Church and Slaymaker, 1989; de Vente et al., 2007; Hinderer, 2012; Fryirs, 2013) and to better understand sediment routing in alpine environments (Otto et al., 2008).

Moreover, the spatial pattern of sediment storage has important implications for the prediction, mitigation and management of natural hazards (Zimmermann and Haeberli, 1993; Glade, 2005), the analysis of seismic wave propagation (Allen and Wald, 2009), and the management of hydropower reservoirs in mountain regions.

Sediment storage and flux along sediment cascades is controlled by scale specific system properties including (1) scale dependency of processes, (2) emergent phenomena arising at larger spatial scales, (3) feedbacks associated with process interactions at various scales, and (4) spatial heterogeneity (of objects) (Zhang et al., 2004). Thus, results from sediment budgets at small spatial scales cannot be simply transferred (Phillips, 1999; Slaymaker, 2006; Tunnicliffe and Church, 2011) and call for new approaches for the investigation of sediment storages on large scales.

The distribution of sediment storages has been investigated on different spatial and temporal scales (comprehensive review by Hinderer, 2012). Detailed studies are mainly available for small scale drainage basins (< 10^2 km^2) (e.g. Otto et al., 2009; Götz et al., 2013; Messenzehl et al., 2014), whereas studies in larger drainage basins (> 10^3 km^2) rather focus on large scale sedimentary landforms such as valley fills (e.g. Hinderer, 2001; Straumann and Korup, 2009). Very few of the large scale studies included different sediment storage types in their budgets (e.g. Jäckli, 1957; Jordan and Slaymaker, 1991; Phillips, 1991; Tunnicliffe and Church, 2011; Tunnicliffe et al., 2012). Thus, the scaling of erosion, transport and storage and their controlling factors are insufficiently understood (Otto et al., 2008; Tunnicliffe and Church, 2011) because tributaries and headwaters are often portrayed to act as sediment sources without substantial sediment storage (Schumm, 1977; Hinderer, 2001). However, the significance of headwaters and smaller catchments as sediment storage areas has been reported in various studies (e.g. Otto et al., 2009; Götz et al., 2013; Hoffmann et al., 2013). Systematically neglecting these small scale sediment storages might introduce notable error into sediment budgets (Hoffmann, 2015). Thus, treating sediment storage as a black box in large drainage basins is problematic and needs to be addressed.

Therefore, knowledge on the spatial pattern of sediment storage and the mobility of material along the sediment cascade in a large drainage basin are imperative to a better understanding of transient landscape evolution and Postglacial sediment evacuation and connectivity from and within the tributaries of large scale drainage basins. While direct geomorphic mapping in the field and from remote sensing data has shown to be useful in small scale studies (e.g. Schrott et al., 2003; Hoffmann et al., 2013), it is not suitable for large scale drainage basins. Predictive spatial models have been used to regionalize geomorphic processes or landforms mapped in smaller areas (e.g. Luoto and Hjort, 2005; Marmion et al., 2008; Brenning, 2009).

Here we use predictive modeling to incorporate the hitherto underrepresented sediment storage in headwaters into a regional assessment of sediment distribution, “a major challenge of geomorphic studies in mountain environments” (Hoffmann, 2015, p. 625). To address this shortcoming, we investigate the spatial distribution of sediment storage in a large alpine drainage basin, the Upper Rhone Basin (URB), and aim to:

- model the spatial distribution of sediment cover in the URB using a combined field-based and statistical modeling approach,
- analyze the quality of the model outcome and the effects of input data on this in a large scale geomorphic system, and

- interpret the modeling results in a geomorphic context with respect to the general pattern, the topographic position of sediment storages, the relevance of sediment storage in recently deglaciated areas and the spatial variability of sediment storage on different scales.

We apply a hierarchical approach where the spatial distribution of sediment storage is studied in five key sites in catchments up to a scale of 10^2 km^2. This data is then used to statistically model the spatial distribution of sediment storage in the large scale URB using logistic regression, principal component logistic regression, and generalized additive models.

7.2 Study area

The URB is located in the Swiss Alps between the Rhone Glacier and Lake Geneva, and is the largest inner alpine basin with a size of c. 5400 km^2 (Figure 3-1). The Rhone Valley with a total length of c. 160 km dissects the western Swiss Alps with a general southwest trend, along regional tectonic structures. The valley abruptly changes to a north-northwest direction at Martigny. It shows an asymmetry whereby the tributaries draining the area north of the main valley are smaller than the tributaries in the south. The drainage basin is a closed system for suspended and clastic sediment transport with Lake Geneva acting as a sediment sink. The basin is located between 372 and 4634 m asl, with dozens of peaks reaching elevations of more than 4000 m.

7.2.1 Tectonic and geological setting

The bedrock geology of the URB is dominated by three major tectonic units: the Helvetic unit, the Penninic unit and the crystalline basement bedrock (Figure 3-2). For a detailed overview of the architecture of the Alps we refer to Schmid et al. (2004). The southwest oriented Rhone Valley marks a major tectonic boundary (Rhone-Simplon fault) between the Penninic and the Helvetic units. The Penninic units cover the largest area of the catchment mainly located south of the Rhone and consists of Penninic basement nappes and Mesozoic sediments. Thus, folding involved the crystalline basement rocks (mainly metamorphic rocks: gneiss, schists, and metasedimentary rocks). The Helvetic and Ultrahelvetic nappes are part of the former continental margin and located north of the Rhone-Simplon fault, i.e. the Rhone Valley. The unit is dominated by nappes consisting of (meta)sedimentary rocks (mainly Mesozoic and Tertiary limestone dominated cover nappes). The crystalline basement bedrock includes the Aar Massif, the largest of the Swiss massifs, the Gotthardt Massif (Allochthone massifs and Infra-Penninic crystalline nappes) occurring upstream of Brig and in the Goms and Aletsch region, as well as the Mt. Blanc and Aiguilles Rouges Massifs underlying the area near Martigny and the Mt. Blanc region. The lithology comprises mainly granitic rocks as well as gneiss, schists and metagranitoids (Schmid et al., 2004).

The bedrock geology of the URB is dominated by three major tectonic units: the Helvetic unit, the Penninic unit and the crystalline basement bedrock (Figure 3-2). For a detailed overview of the architecture of the Alps we refer to Schmid et al. (2004). The southwest oriented Rhone Valley marks a major tectonic boundary (Rhone-Simplon fault) between the Penninic and the Helvetic units. The Penninic units cover the largest area of the catchment mainly located south of the Rhone and consists of Penninic basement nappes and Mesozoic sediments. Thus, folding involved the crystalline basement rocks (mainly metamorphic rocks: gneiss, schists, and metasedimentary rocks). The Helvetic and Ultrahelvetic nappes are part of the former continental margin and located north of the Rhone-Simplon fault, i.e. the Rhone Valley. The unit is dominated by nappes consisting of (meta)sedimentary rocks (mainly Mesozoic and Tertiary limestone dominated cover nappes). The crystalline basement bedrock includes the Aar Massif, the largest of the Swiss massifs, the Gotthardt Massif (Allochthone massifs and Infra-Penninic crystalline nappes) occurring upstream of Brig and in the Goms and Aletsch region, as well as the Mt. Blanc and Aiguilles Rouges Massifs underlying the area near Martigny and the Mt. Blanc region. The lithology comprises mainly granitic rocks as well as gneiss, schists and metagranitoids (Schmid et al., 2004).

7.2.2 Pleistocene glaciation, Little Ice Age and current glacier extent

The topography is strongly impacted by the Pleistocene glaciations and thus characterized by U-shaped valleys, cirques, hanging valleys and steep peaks. Glacial erosion produced a high-mountain landscape with peaks over 4000 m and glacial overdeepenings up to 1000 m (Pfiffner et al., 1997). During the Last Glacial Maximum (LGM) the glaciers in the study area were influenced by at least four centers of ice accumulation: the Rhone ice dome, the Aletsch ice field, the southern Valais icefield and the Mt. Blanc region (Kelly et al., 2004). The Rhone ice dome with radial outflow following the pre-existing valley system but also flowing over the high passes was located in the headwaters of the Rhone Valley (Florineth and Schlüchter, 1998). The LGM Rhone Glacier filled the Rhone Valley, outflowed onto the foreland and was the main component of the LGM transection glaciers in the western Alps, an interconnected system of valley glaciers. It reached a thickness of as much as 2300 m near Martigny (Kelly et al., 2004). The Rhone Glacier extended into the alpine foreland after 30 ka and deglaciation (retreat from LGM position) began in 21.1 ± 0.9 ka and ice collapse already initiated between 16.8 and 17.4 ka (Ivy-Ochs et al., 2004; Ivy-Ochs et al., 2006b). Currently the glacially conditioned landscape is adjusting to fluvial conditions through e.g. fluvial incision (Valla et al., 2010b), mass wasting (McColl, 2012), and sediment transport (Church and Slaymaker, 1989), i.e. the landscape is in a transient state (Brunsden and Thornes, 1979; Schlunegger and Norton, 2013). The adjustment from a glacial to a fluvial landscape is prominent at the so called transition zones between the Rhone Valley and the tributaries, often forming hanging valleys. Transitions zones are characterized by knickpoints, steep gradients and V-shaped valleys. They are dominated by river incision and unstable slopes. Within the

URB, these knickpoints are located close to the trunk stream because lithologies with low erodibility are widespread (e.g. Schlunegger and Hinderer, 2003; Norton et al., 2010a; Valla et al., 2010a; Valla et al., 2010b).

Compared to other regions in the Alps, glaciers are widespread in the URB due to high elevations and precipitation from (north)westerly and south/southwesterly atmospheric circulation patterns (Kelly et al., 2004). Approximately 569 km^2 (c. 10.6%) of the land surface was covered with glacial ice in 2010 (Fischer, 2013; Fischer et al., 2014). The highest glacier cover is located in the Aletsch region, in the southern part of the study area, the Valais Alps and especially the Mattertal, the Mont Blanc massif and in the Goms region with the Rhone Glacier (Penninic unit and crystalline basement rock). In the Helvetic unit the glacial cover is comparably low. This is conditioned by the substantially higher elevations in the Penninic unit and crystalline basement rock. During the Little Ice Age (LIA) c. 929 km^2 were covered with glacial ice (Maisch, 2000), hence the deglaciated areas since 1850 comprise 360 km^2 within the URB. The glaciers within the study area lost c. 39% of their areal extent within the time period 1850-2010.

7.2.3 Key sites

Five key sites, Val d'Illiez, Val de la Liène, Turtmanntal, Lötschental and Goms, have been selected to reflect the heterogeneity of the URB and its tributaries (Figure 3-1, Table 6-1). They cover all three major tectonic units (Figure 3-2), many lithologies exposed within the study area and the full width of surface morphology, relief, Pleistocene glacial imprint and contemporary glacial cover are represented. Each key site spans across different spatial scales. Mean elevations of the key sites vary between 1650 and 2500 m, however the surface morphology is comparable with mean slope gradients between 26 and 32%. Within the URB a total area of 360.3 km^2 of bedrock and sediment was mapped in the five key sites corresponding to 6.7% of the total basin area.

7.3 Methods

Our main goal is to investigate the spatial distribution of sediment and bedrock within the URB at various scales. The distribution of sediment and bedrock was mapped in five key sites on a spatial scale of up to > 200 km^2 and then upscaled to the large scale URB using a statistical predictive modeling approach (Figure 7-1). We focus on a distinction between bedrock and sediment in general, which encompasses all sediment accumulation forms, including as valley fills, fans, debris cones, terraces, talus deposits, moraines, and debris mantled slopes. A requirement for the application of a predictive model is a statistical relation between the studied objects and the available spatial information (predictive variables) to create a spatial probability model (Schlummer et al., 2014). The final output is a detailed map of the spatial sediment/bedrock distribution in the URB.

7.3.1 Dataset

An inventory of sediment storage and bedrock, compiled from field mapping, remote sensing imagery analysis and published data, was created for the five key sites and used as training and testing data for the classification of sediment and bedrock cover applied to the whole URB. Sediment storage and bedrock were mapped in the field, complemented by the interpretation of satellite imagery available on GoogleEarth, as well as a digital elevation model (DEM, 2 m resolution, swissALTI3D, ©swisstopo). The geomorphic map of the hanging valleys from the Turtmanntal was taken from Otto et al. (2009) and extended to the trunk valley. In total, an area of 360.3 km^2 was mapped, equivalent to 6.7% of the total area of the URB (Table 6-1). Mapped areas were classified into a binary raster (1=bedrock, 0=sediment/non-bedrock). Furthermore, the Swiss glacier inventory 2010 was used (Fischer, 2013; Fischer et al., 2014) to exclude areas covered by glaciers with a minimum area of 0.01 km^2. Lakes were classified based on the DEM data and a semi-automated surface classification model (Bowles and Cowgill, 2012). Both, glacier and lake areas were masked from the input data for modeling.

We compiled a set of predictor (independent) variables that are anticipated to explain the differences in surface morphology, topography and position, characteristics of the contributing area as well as biotic and climatic differences between sediment storages and bedrock. Since all input parameters need a comparable resolution, no data on lithology, erodibility or other rock mechanics or tectonics related input parameters could be included directly in the modeling approach, since no high resolution data for these parameters is available for the entire study area. The chosen input parameters conceptually explain the differences between bedrock and sediment on different scales (Table 7-1). These 22 variables were derived from the high-resolution DEM and orthorectified Landsat 5 TM and 7 ETM+ scenes following the approach by Brenning (2009), who combined process-related terrain attributes and multispectral remote-sensing data. Data were processed using the raster package in the open-source statistical software R (Hijmans, 2014; r-project.org), SAGA GIS (saga-gis.org) and Esri ArcGIS (esri.com).

Local surface morphology predictor variables include slope gradient, roughness, curvature and the topographic wetness index (Beven and Kirkby, 1979; O'Callaghan and Mark, 1984). Topography and position are represented by the elevation, slope gradient, roughness, curvature (the latter three from 25 m DEM), aspect, normalized distance to ridge, hypsometric index, local relief and vertical distance to channel network. Aspect variables were split into directional components resulting in “east-exposedness” and “north-exposedness” variables (Brenning, 2009). Normalized distance to ridge was calculated by semi-automatically extracting the ridgelines from the watershed boundaries (2nd-5th order watershed based on 1 km^2 stream head threshold) and the stream network (same threshold) representing the relative position within the sediment cascade (Messenzehl et al., 2014). The contributing area was delineated based on the D8-flow algorithm (O'Callaghan and Mark, 1984) and log transformed due to the extremely skewed distribution of the data (Brenning, 2009). The mean slope of the contributing area was calculated using a slope weighted flow accumulation divided by the unweighted flow accumulation. Climatic and biotic factors encompass solar radiation and the normalized difference vegetation index (NDVI) respectively. Landsat scenes (path 195, row 28, acquisition dates in June, July, August, September, one from October, see appendix B, Table Z) were used to compute the maximum NDVI for each cell.

Table 7-1: Candidate variables representing local morphometry, topography and topographic position, contributing area, climatic and biotic factors on different scales.

Name	Variable	Description	Formula	Scale
Local morphometry				
PLC10	plan curvature	calculated from resampled 10 m DEM (bilinear interpolation) due to noisy character of small scale curvature (Heckmann et al., 2014)		small
PRC10	profile curvature	calculated from resampled 10 m DEM (bilinear interpolation) due to noisy character of small scale curvature (Heckmann et al., 2014)		small
CUR10	overall curvature	calculated from resampled 10 m DEM (bilinear interpolation) due to noisy character of small scale curvature (Heckmann et al., 2014)		small
SLP	slope gradient [%]	calculated from original 2 m DEM		small
ROU	roughness	standard deviation of slope [°] in a 3x3 cell moving window, calculated from original 2 m DEM		small
TWI	topographic wetness index	calculated from original 2 m DEM *A*… upslope contributing area A (D8-flow algorithm) *B*… slope raster in radians (Beven and Kirkby, 1979; O'Callaghan and Mark, 1984)	$TWI = \ln(\frac{A}{\tan(\beta)})$	small
Topography and position				
DEM	digital elevation model	elevation [m]		large
SLP25	slope gradient [%]	calculated from resampled 25 m DEM (bilinear interpolation)		meso
ROU25	roughness	calculated from resampled 25 m DEM (bilinear interpolation) standard deviation of slope [°] in a 3x3 cell moving window		meso
PLC25	plan curvature	calculated from resampled 25 m DEM (bilinear interpolation)		meso
PRC25	profile curvature	calculated from resampled 25 m DEM (bilinear interpolation)		meso
CUR25	overall curvature	calculated from resampled 25 m DEM (bilinear interpolation)		meso
ASP_NS	north-exposedness	cosine of the original aspect raster [°]		small

Name	Variable	Description	Formula	Scale
ASP_EW	east-exposedness	sine of the original aspect raster [°]		small
NDR	normalized distance to ridge	relative position within the sediment cascade (ridgeline: NDR = 1, channel: NDR = 0) (Messenzehl et al., 2014)		large
REL40	local relief	calculated in moving window with a radius of 40 m *Z*… elevation [m]	$REL40 = Z_{max} - Z_{min}$	meso
HI40	hypsometric index	Calculated in moving window with a radius of 40 m *Z*… elevation [m] (Brocklehurst and Whipple, 2004)	$HI40 = \frac{Z_{mean} - Z_{min}}{Z_{max} - Z_{min}}$	meso
VDC	vertical distance to channel network	*DEM*… digital elevation model [m] CN_{int}… interpolated surface from the channel network [m]	$VDC = DEM - CN_{int}$	large
Contributing area				
ACCLOG	size of the contributing area [m^2]	D8-flow algorithm, log transformed (O'Callaghan and Mark, 1984; Brenning, 2009)		large
ACCSLP	mean slope [%] of the contributing area	slope weighted D8-flow algorithm divided by unweighted flow accumulation		large
Climatic and biotic factors				
SR	solar radiation	potential annual incoming solar radiation 2015 [Wh m^{-2}]		small
NDVI	normalized difference vegetation index	Landsat TM scenes converted to Landsat ETM+ values (Vogelmann et al., 2001) Atmospheric and illumination corrections applied to receive top of atmosphere reflectance values (Chander et al., 2009).		meso

7.3.2 Predictive modeling

We applied and compared three different statistical classification techniques, a logistic regression model (LR), a principal component logistic regression model (PCLR) and a generalized additive model (GAM). Classifiers are used to match a pixel based on the independent variables and the observation of the mapping results to a class (1=bedrock, 0=sediment/non-bedrock), i.e. they predict the probability of class membership to class 1. Further, we evaluated the predictive power of each classifier to quantify which model predicts the spatial distribution of sediment storages in the URB best. LR and PCLR are parametric techniques, i.e. they can only model linear relations between dependent and independent variables, while a GAM is a non-parametric classifier allowing non-linear relationships. For each model a dataset consisting of equal number of cases (bedrock pixels) and controls (sediment/non-bedrock pixels) was used (event/non-event ratio of 1) (Heckmann et al., 2014). In all three modeling approaches, a combined forward and backward stepwise model selection based on the Akaike Information Criterion (AIC) is applied (Akaike, 1974; Atkinson et al., 1998; Brenning, 2005; Petschko et al., 2014).

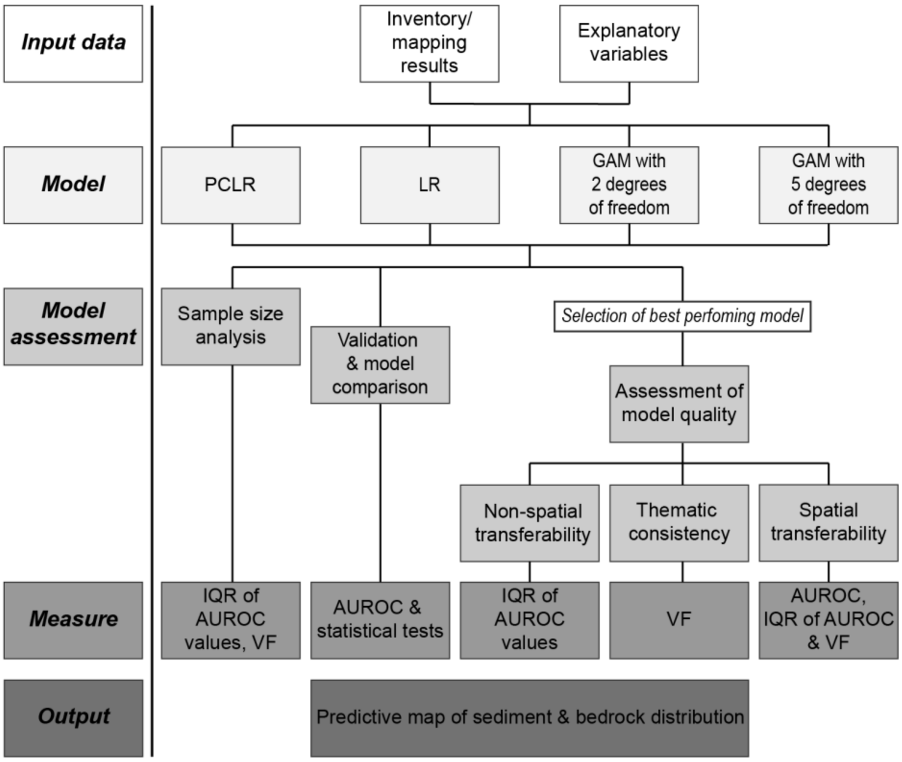

Figure 7-1: Flow chart of applied statistical methods to model the spatial distribution of sediment cover in the large scale URB based on geomorphic maps of sediment storages and bedrock cover from key sites (PCLR = principal component logistic regression model, LR = logistic regression model, GAM = generalized additive model, AUROC = area under the receiver operating characteristics curve, IQR = interquartile range of the AUROC values, VF = variable selection frequency).

7.3.2.1 Logistic regression model

LR are one of the most widely applied models in geomorphology (Brenning, 2005) to predict system properties described by a binary variable. The LR is a generalized linear model based on the logistic function. The logit or log-odds is calculated by:

$$\mathrm{Y} = \log\left(\frac{p(X)}{1-p(X)}\right) = \beta_0 + \beta_1 X_1 + \cdots + \beta_n X_n \qquad (3)$$

where Y is the dependent (response) binary variable (bedrock vs. sediment), p(X) is the probability of bedrock occurrence, β are the coefficients, X are the independent input variables and n is the number of independent input variables (Atkinson et al., 1998; Hosmer et al., 2013).

The coefficients of the model are estimated using a randomly sampled training dataset. Only non-collinear predictor variables should be used in a LR. Multicollinearity makes the interpretation of the model results difficult. Thus, multicollinearity was tested using the variance inflation factor for all 22 candidate variables (Aguilera et al., 2006; James et al., 2013). Overall curvature (calculated from 10 and 25 m DEM), local relief and topographic wetness index were excluded from the dataset used in the LR and the GAM (see appendix B, Table Table AA) because variance inflation factor values larger than 10 indicate a problematic amount of collinearity (Heckmann et al., 2014). The remaining 18 variables, all having variance inflation factor values below 5, were used as independent variables.

7.3.2.2 Principal component logistic regression model

PCLR is firstly a principal component analysis (PCA) to produce independent principal components (PCs) as predictors to prevent multicollinearity between the input datasets. Secondly, the PCs are used as input variables in a LR (Hengl et al., 2004; Aguilera et al., 2006; James et al., 2013; Hoffmann et al., 2014; Messenzehl et al., 2017). The key idea is that a smaller number of PCs are sufficient to explain most of the variability of the dataset and thus the relation to the response variable. Furthermore, the reduction of input variables in the model can mitigate overfitting (Aguilera et al., 2006; James et al., 2013). The PCA was performed with the psych package in R (Revelle, 2015; r-project.org). To analyze the PCs more easily and intuitively the factors must be rotated. The varimax rotation is an orthogonal rotation of the PC axes. Thus, the PCs have large or small loadings on any of the input variables (Kaiser, 1958). The number of PCs used in the PCLR was limited by a visual analysis of the knickpoint in an eigenvalue plot. Although eigenvalues under 1 are equal to the information explained by a single variable, these minor PCs with little explained variance may still be correlated to the dependent variable (Aguilera et al., 2006).

The PCA was performed by selecting random samples from all five key sites for all 22 input variables. From each key site c. 1% of all mapped pixels were selected (c. 140000 to 290000 pixels per site). The large dataset produced for this study is ideal for statistical modeling as the selection of only a small fraction of all data prevents overfitting and allows validation (James et al., 2013). The stability of the PCA was tested by applying a full PCA ten times to independent datasets and investigating the variance.

7.3.2.3 Generalized additive model

A GAM is considered a good compromise between the non-linear flexibility of machine learning techniques and the linear predictions of LR (Brenning, 2005; Brenning, 2008; Goetz et al., 2011). GAMs extend the LR by allowing linear and non-linear transformations of the independent variables utilizing smoothers but keeping the additive structure that is easily interpreted. Thus, they are more data-driven while the LR is more model-driven (Hastie and Tibshirani, 1990; Brenning, 2008; Hastie et al., 2009).

In a GAM the response variable is not modeled directly, but as in the “ordinary” LR the logit of the occurrence probability of bedrock p(X) is the result:

$$\mathrm{Y} = \log\left(\frac{p(X)}{1-p(X)}\right) = \beta_0 + \beta_1 f_1 X_1 + \cdots + \beta_n f_n X_n \tag{4}$$

where Y is the dependent (response) binary variable (bedrock vs. sediment), f are non-parametric smoothing functions, β are the coefficients, X are the independent input variables and n is the number of independent input variables (Hastie and Tibshirani, 1990). Two variations of the GAM were applied. In the GAM2df each variable can be selected as a linear (not transformed) or a non-linear (transformed with a smoothing spline with two degrees of freedom), or not at all included in the model. In the second version GAM5df the transformed variables may be entered not at all, untransformed or transformed with up to five degrees of freedom, thus allowing more flexibility of the model. GAM modeling was conducted with the gam package in R (Hastie, 2015; r-project.org).

7.3.3 Validation and assessment of model quality

We applied non-spatial and spatial validation approaches (using ten times a 25-fold validation) to investigate quality and transferability of the models (Brenning, 2012). Spatial validation tests a model in an independent site, thus accounting for the presence of spatial autocorrelation. This is not incorporated in the more widely used non-spatial equivalent (Brenning, 2012). Furthermore, we analyzed the thematic consistency (Goetz et al., 2011; Petschko et al., 2014) and the impact of spatial heterogeneity for the best performing model.

All four models were validated based on the area under the receiver operating characteristics curve (AUROC), the accuracy (sum of the true positive and the true negative rate), the error rate (opposite of accuracy) and the interquartile range (IQR) of the AUROC values in a non-spatial validation, i.e. data from all five key sites were used to train and test the models. These measures investigate the quality of the model, which is the ability to discriminate between bedrock and sediment locations. Test and training dataset have the same size and replicate data points were pre-empted. The larger the AUROC the better is the model and thus the classification. A model classifying the data comparable to coincidence would have an AUROC of 0.5 and a model separating the classes perfectly of 1.0 (Sing et al., 2005; Fawcett, 2006; Hosmer et al., 2013). The AUROC was calculated using the ROCR package in R (Sing et al., 2005; r-project.org). The IQR is used as a measure of the transferability of the models (Petschko et al., 2014).

To validate and evaluate the classifier, we determined a probability threshold (cutoff value) using a compromise between sensitivity (true positive rate) and 1-specificity (false positive rate). This cutoff value was used to classify the modeled probabilities of bedrock/sediment occurrence of the best performing model into the classes bedrock and sediment. This model selected based on the highest median AUROC and mean accuracy values was applied to the whole area of the URB using the raster package in R (Hijmans, 2014; r-project.org). To test if the performance of the individual models (LR, PCLR, GAM) is significantly different, the Kruskal-Wallis rank sum and the Wilcoxon signed rank tests were used (overall and pairwise model comparison respectively, 5% significance level) (Hollander et al., 1999; Goetz et al., 2011).

Additionally, the results of the validation were used to estimate thematic consistency and variable importance. Thematic consistency shows the sensitivity of the model to sample variation. A high thematic consistency means a good quality and high robustness of the model. The importance of each variable is represented by the variable selection frequency calculated from the ten models fitted for the best performing model (Goetz et al., 2011; Petschko et al., 2014). It can be interpreted as a measure for the thematic consistency of the model (Guzzetti et al., 2006). A high thematic consistency is indicated by a variable selection frequency either close to 0% or close to 100%, which means the variable is never or always chosen.

Spatial transferability, i.e. spatial validation, was tested for a GAM2df (sample size: 51200 pixels). The classifier was trained with 5 different input datasets, each consisting only of data points from four of the five key sites and then tested in the fifth, completely independent key site. Data from this site were not included when training the model. For each model the median AUROC and the IQR were estimated.

Furthermore, the impact of spatial heterogeneity within the study area and hence the input dataset in general on the model outcome were tested for a GAM2df (sample size: 20000 pixels). The classifier was trained with six different input datasets, one comprised of data from all key sites and five only of data from one site. These six classifiers were tested in all key sites and in each single site, of which four are completely independent. For each model the median AUROC and the IQR were calculated.

7.3.4 Geomorphic analysis of modeled spatial distribution of sediment

The spatial distribution of sediment storages was further analyzed with the topographic position index (TPI) that is used to semi-automatically classify topographic slope position (TSP) and thus the position of the modeled sediment distribution:

$$TPI = z_0 - \bar{z} \tag{5}$$

where z_0 is the elevation at the central point of the annulus and $\bar{z}$ is the mean elevation of the annulus area (Guisan et al., 1999; Weiss, 2000). Positive TPI values indicate locations higher than the mean elevation of the surrounding area (e.g. hilltops and ridges), while negative TPI values are locations lower than the surroundings (e.g. valleys). TPI values around zero represent flat areas or locations with constant slope (Figure 7-10). An outer and inner radius of 2000 and 1600 m of the annulus were chosen respectively to determine major landscape units (e.g. mountains, major ridge lines and major valleys). Six TSPs were classified based on the standard deviation of the TPI and the slope (Table 7-2) (Weiss, 2000). Based on this classification, the modeled sediment distribution was further classified and the portion of sediment cover per class calculated.

Table 7-2: Classification of topographic slope position (TSP) based on the topographic position index (TPI) after Weiss (2000). Sketch of TSP see Figure 7-10.

Topographic slope position class	Threshold based on standard deviation (SD) of TPI	Slope [°]
ridge and uppermost slope	> 1 SD	
upper slope	> 0.5 SD, ≤ 1 SD	
(middle) slope	> −0.5 SD, ≤ 0.5 SD	> 10
valley fill (main valley) and flat slopes	> −0.5 SD, ≤ 0.5 SD	≤ 10
lower slope	≥ −1 SD, ≤ −0.5 SD	
valley fills in tributaries	< −1 SD	

7.4 Results

7.4.1 Model performance and comparison

Model comparison, i.e. non-spatial validation of LR, PCLR, GAM2df and GAM5df, reveals that the GAM5df achieves the highest AUROC values and thus the best results (Figure 7-2). The PCLR yields the lowest accuracy and AUROC values, while the LR and GAM2df perform better. The median AUROC values of all four models, all between 0.8 and 0.9, indicate good performance and hence an excellent discrimination between sediment covered areas and bedrock areas (Hosmer et al., 2013).

The Kruskal-Wallis rank sum test, which compares the overall model outputs, shows significant differences between the AUROC and the accuracy values of the investigated models ($p < 0.0001$). Furthermore, the pairwise comparison of the models using the Wilcoxon signed rank test also results in p-values < 0.0001 for each test concerning the accuracy and the AUROC values. This indicates that significant differences exist between all four models, although the absolute differences in the median AUROC values and thus the quality of the models are small. However, the GAM5df performs significantly better than the other three models. IQR range between 0.0021 and 0.0025 and indicate good quality, high robustness and transferability of all models.

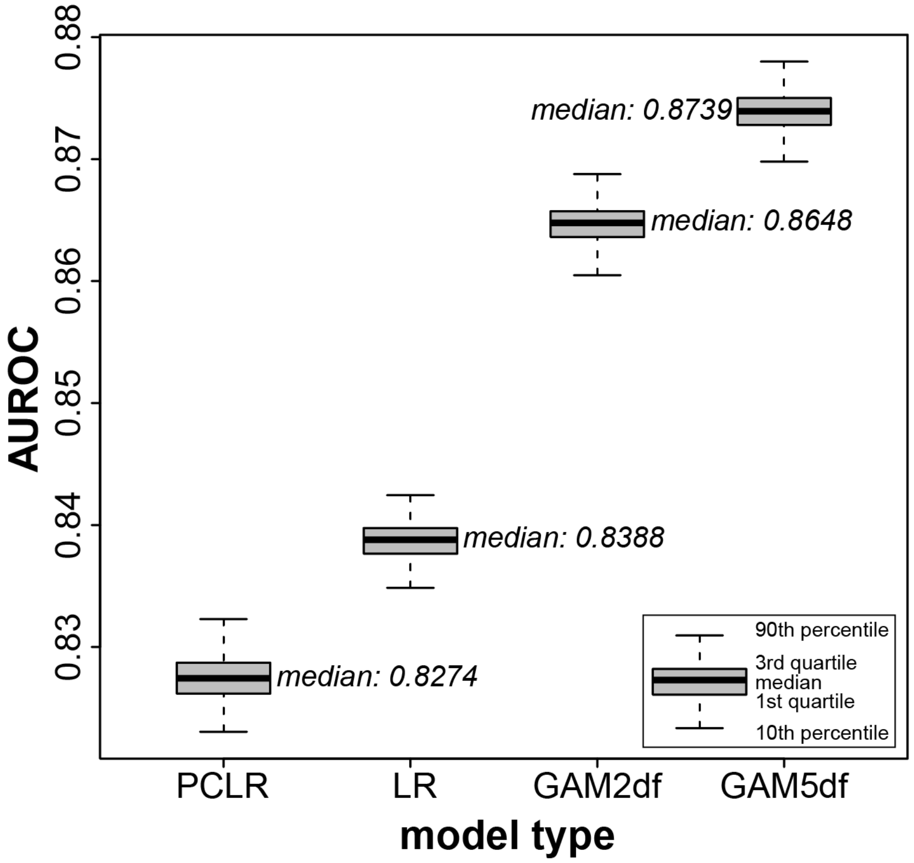

Figure 7-2: Boxplots of area under the receiver operating chracteristics curve (AUROC) values for all four applied models (sample size for all models 51200 pixels, equal number of cases and controls): principal components logistic regression model (PCLR), logistic regression model (LR) and generalized additive model (GAM) with input variables transformed with a smoothing spline with two and five degrees of freedom respectively. AUROC values are derived from 25-fold non-spatial validation analysis performed ten times for each model (i.e. 250 values).

7.4.1.1 Influence of sample size on model performance

The selection and quality of predictive models is sensitive to different sample sizes, i.e. pixels, because the sample size has to be large enough to cover the variability of the predictor variables and to produce stable and reproducible results. However, the sample size should not be too large because it is probable to neglect the assumption of independent observations due to spatial autocorrelation and overparametrization, overfitting might arise (Heckmann et al., 2014) and computation times become very long. Therefore, we analyzed the sample size for the models using equal number of cases and controls (N = 100, 200, 400, 800, 1600, 3200, 6400, 12800, 25600, 51200). The quality of the models (i.e. the ability to discriminate between bedrock and sediment locations) and its stability was analyzed based on the effect of sample size reduction on the AUROC and the IQR. Moreover, the thematic consistency of the GAM2df was investigated for all sample sizes (Goetz et al., 2011; Petschko et al., 2014).

The sample size analysis shows similar results for all three models tested (PCLR, LR, GAM2df,Figure 7-3). The PCLR returns stable AUROC values (median 0.8269) and narrow IQR (0.0020) with a sample size of only 6400 pixels that only slightly improve towards larger sample sizes. The LR also reaches relatively stable AUROC values (median 0.8374) with a sample size of 6400 pixels, but the IQR still declines from 0.0068 to 0.0023 (sample size 51200 pixels) indicating a better transferability of the model. The GAM2df needs larger sample sizes of 51200 pixels to reach a similar plateau with AUROC values increasing from 0.8607 to 0.8648 for sample sizes of 6400 to 51200 pixels. This is probably associated with the model setup that is more data driven than the LR and the PCLR, which only model linear correlations between the dependent and the independent variables. The generally high AUROC values indicate a good quality of the model. A low IQR of 0.0021 for the GAM2df implies a good transferability of the model. However, the results of the GAM2df are better than the results of the other two models likewise for smaller sample sizes and thus a GAM should be the preferential model even if only a smaller dataset is available. Based on these results, a sample size of 51200 pixels was chosen for each modeling approach achieving a better comparability. Furthermore, the thematic consistency, which was only investigated for the GAM2df (i.e. best performing model in sample size analysis), improves substantially with an increase of the sample size (see appendix B, Table BB). The total variable selection frequency in the GAM increases to 100% for most independent variables at a sample size of 51200 pixels, thus the ten models built are very similar and the thematic consistency of the GAM model is high. Only two input variables, mean slope of the contributing area (accslp) and profile curvature (10 m resolution, prc10), have a variable selection frequency of 50% and 60% respectively signifying a low thematic consistency, thus their relevance in the model is interpreted as relatively low. On the other hand, slope gradient (calculated from resampled 25 m DEM) yields a high variable selection frequency (100%) at a sample size of 400 pixels indicating a high importance of this variable in the model as well as the relevance of slope gradient for sediment erosion, transport and deposition.

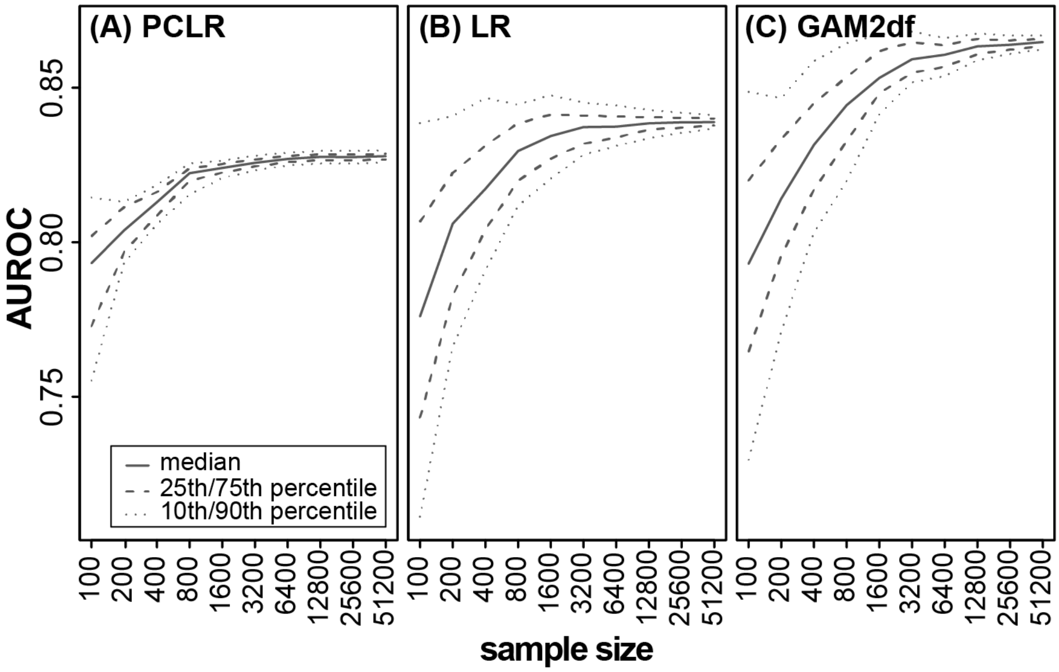

Figure 7-3: Median, 10th, 25th, 75th and 90th percentile of AUROC (area under the receiver operating characteristics curve) values derived from ten times 25-fold validation of A: the principal components logistic regression model (PCLR), B: the logistic regression model (LR) and C: the generalized additive model (GAM2df) for different sample sizes, i.e. number of pixels (equal number of cases and controls).

7.4.1.2 Model performance of generalized additive model

The GAM5df (sample size: 51200 pixels) as the best performing model is further analyzed and spatial prediction realized for the whole URB. The validation of the GAM5df shows an excellent performance (Hosmer et al., 2013) and a high transferability (median AUROC: 0.8739, IQR: 0.0022; Figure 7-2). The thematic consistency of all but three variables (i.e. accslp, plc10, prc10) is very high indicated by a total variable selection frequency of 100%. This means all ten independent and individually created models are very similar and comprise mostly the same input variables (Table 7-3). Most variables are chosen in every model run with a high number of degrees of freedom, thus the relation between the dependent and the independent variables is clearly non-linear.

Table 7-3: Thematic consistency of generalized additive model with input variables transformed with a smoothing spline with five degrees of freedom (GAM5df) based on ten individual models build. Relative variable selection frequencies as well as the variable selection frequencies of non-transformed (N) and transformed (S) variables are calculated for each independent input variable.

Variable	Variable selection frequency [%]	Non-transformed	Transformed (2df)	Transformed (3df)	Transformed (4df)	Transformed (5df)
acclog	100	-	1	-	2	7
accslp	40	-	-	-	-	4
asp_ew	100	-	-	-	-	10
asp_ns	100	-	6	2	2	-
dem	100	-	-	-	-	10
hi40	100	-	-	-	-	10
ndr	100	-	-	-	-	10
ndvi	100	-	-	-	-	10
plc10	70	-	-	-	-	7
plc25	100	-	-	-	-	10
prc10	50	-	-	5	-	-
prc25	100	-	-	-	-	10
rou	100	-	-	-	-	10
rou25	100	-	-	-	-	10
slp	100	-	-	-	-	10
slp25	100	-	-	-	-	10
sr	100	-	-	-	-	10
vdc	100	-	-	-	-	10

One of the ten independent and individually created models was applied to the URB due to the high thematic consistency and the high transferability of the models. The mean accuracy is 78.35 ± 0.18%, which means on average 78.35% of all pixels are correctly classified based on cutoff values ranging between 0.4403 and 0.5109. A mean cutoff value of 0.4768 was chosen for the application of the model to the whole URB. The mean AUROC is 0.8721 ± 0.0012. Further measures illustrating the quality of the model are listed in Table 7-4.

Table 7-4: Evaluation and confusion matrix of generalized additive model with input variables transformed with a smoothing spline with five degrees of freedom (GAM5df) based on 25fold validation (AUROC= area under the receiver operating characteristics curve, SD = standard deviation, TPR = true positive rate, TNR = true negative rate, TP = true positives, FP = false positives, FN = false negatives, TN = true negatives).

Evaluation		
Mean AUROC ± 1SD		0.8721 ± 0.0012
Mean accuracy ± 1SD [%]		78.3519 ± 0.1838
Range of cutoff values		0.4403 - 0.5109
Mean cutoff value ± 1SD		0.4768 ± 0.0156
Mean odds ratio ± 1SD		13.2769 ± 0.2876
TPR/sensitivity ± 1SD [%]		76.1375 ± 1.3600
TNR/specificity ± 1SD [%]		80.5663 ± 1.2783
Confusion matrix [%]		
	Predicted bedrock cover (1)	**Predicted sediment cover (0)**
Actual bedrock cover (1)	TP: 0.3807 ± 0.0068	FN: 0.1193 ± 0.0068
Actual sediment cover (0)	FP: 0.0972 ± 0.0064	TN: 0.4028 ± 0.0063

7.4.2 Modeled spatial sediment distribution

The model was applied to all areas of the URB (total area 5382.3 km^2) that are not covered by glaciers or lakes (Bowles and Cowgill, 2012). The current glacier extent comprises an area of 569.8 km^2 of the URB (Fischer, 2013) corresponding to 10.6%, while lakes only cover 34.2 km^2 or 0.6%. Of the remaining 4778.3 km^2 sediment covers 2876.9 ± 622.8 km^2 (53% of the URB) and bedrock comprises 1901.4 ± 411.6 km^2 (35%) (Table 7-5). A visual comparison of the mapped sediment and bedrock distribution and the modeled sediment and bedrock classification in the five key sites shows good accordance (exemplary for the Minstigertal, Goms; Figure 7-4). The overall spatial distribution of sediment in the URB shows a high degree of variability at different scales. However, the basic pattern of sediment-filled valley floors and bedrock in the location of peaks and the highest elevations is apparent. The valley fill of the Upper Rhone Valley is also correctly classified as sediment, while bedrock is exposed on the very steep sides of the U-shaped valley.

Table 7-5: Modeled surface extent of bedrock and sediment within the URB based on generalized additive model (GAM) with smoothing spline transformation of input variables and up to five degrees of freedom. Results were classified based on an optimal compromise between sensitivity and 1-specificity of the predicted probabilities. Glacier extent from Swiss glacier inventory 2010 (Fischer, 2013). Lakes classified based on digital elevation model (DEM) with a semi-automated surface classification model (Bowles and Cowgill, 2012).

Class	Modeled surface extent [km^2]	Modeled surface extent [%]
Sediment	2876.93 ± 622.80	53.45 ± 21.65
Bedrock	1901.37 ± 411.61	35.33 ± 21.65
Glacier (data from Fischer, 2013)	569.78	10.59
Lakes (based on SCM algorithm by Bowles and Cowgill, 2012)	34.22	0.64
Total area	**5382.30**	**100.00**

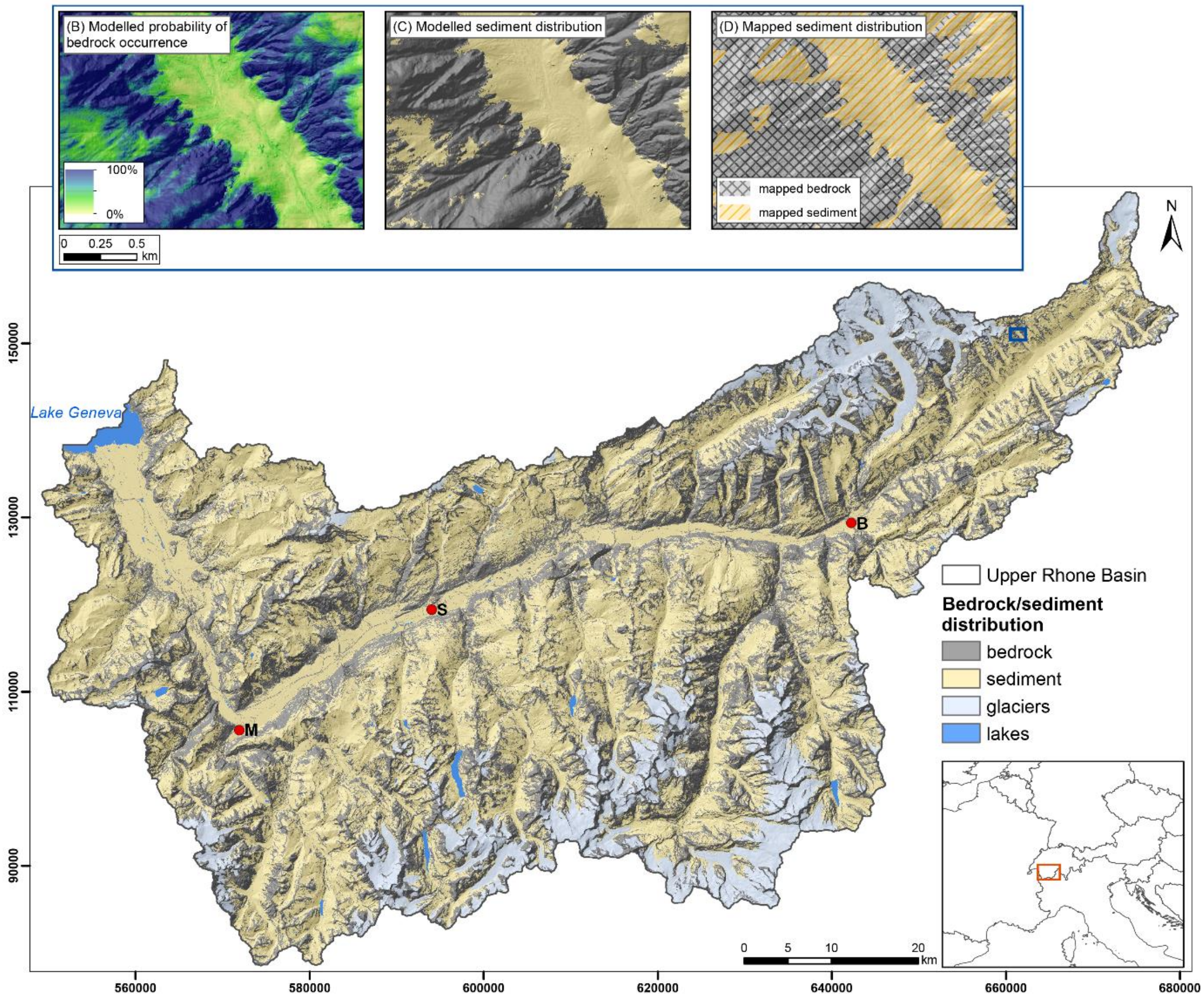

Figure 7-4: A: Modeled bedrock and sediment distribution within the URB (M=Martigny, S=Sion, B=Brig) based on generalized additive model (GAM) with smoothing spline transformation of input variables and up to five degrees of freedom. Results were classified based on an optimal compromise between sensitivity and 1-specificity of the predicted probabilities. Glacier extent from Swiss glacier inventory 2010 (Fischer, 2013). Lakes classified based on digital elevation model (DEM) with a semi-automated surface classification model (Bowles and Cowgill, 2012). (DEM from swisstopo, projection: CH1903). B: modeled probability of bedrock occurrence, C: modeled bedrock and sediment distribution and D: mapped bedrock and sediment distribution in detail for the Minstigertal, Goms.

The spatial variability of the modeled sediment coverage in the URB was additionally analyzed by calculating the relative sediment cover in watersheds on different spatial scales (Figure 7-5). The considered watersheds are characterized by glacier and lake coverage of < 50% and a valley fill cover of < 40% (Bowles and Cowgill, 2012; Blöthe and Korup, 2013; Fischer, 2013). At small spatial scales (< 5 km^2), areal sediment cover varies between 0 and 100%. However, no clear pattern is apparent, and watersheds with high sediment coverage are often located next to those with low sediment coverage (Figure 7-5). With increasing spatial scale (5 - 100 km^2), and a decreasing absolute number of watersheds in the respective class, overall variability decreases and peaks for bedrock and sediment coverage become more pronounced, with highest densities for bedrock (30-40%) being consistently lower than for sediment cover (60-65%) (Figure 7-5).

Figure 7-5: A: Map of the spatial variability of the modeled sediment cover [%] in watersheds with a spatial scale of 1 - < 5 km^2 in the URB. Glacier extent from Swiss glacier inventory 2010 (Fischer, 2013). Lakes classified based on digital elevation model (DEM) with a semi-automated surface classification model (Bowles and Cowgill, 2012) (DEM from swisstopo, projection: CH1903). B: Probability density functions show the density [%] of modeled sediment and bedrock cover for each spatial scale of watersheds (0.1 - < 1 km^2, 1 - < 5 km^2, 5 - < 10 km^2, 10 - < 25 km^2, 25 - < 50 km^2, 50 - < 100 km^2).

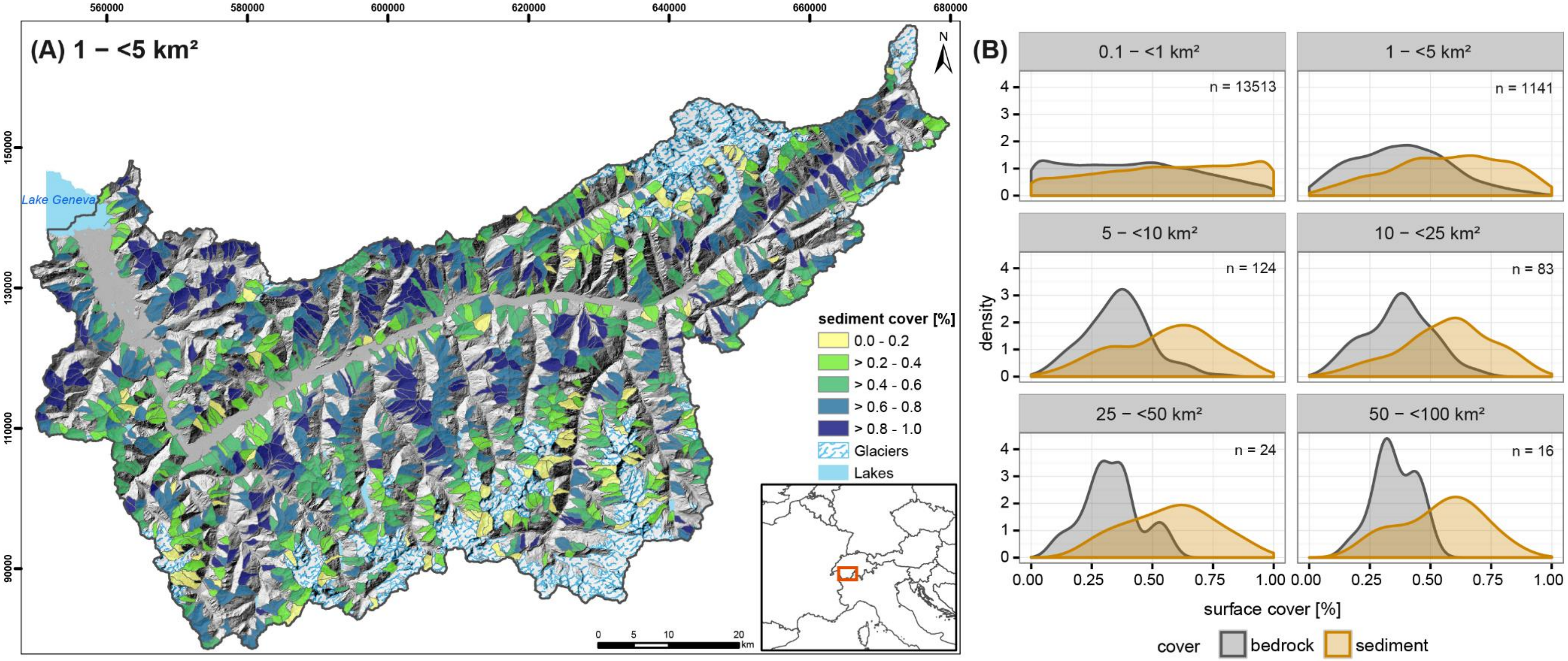

7.5 Discussion

7.5.1 Predictive modeling of spatial sediment distribution

Predictive models have been applied in a variety of geomorphological studies including landslide hazard analysis (Petschko et al., 2014; Goetz et al., 2015), the spatial distribution of permafrost landforms (Brenning, 2009), geomorphological mapping (Luoto and Hjort, 2005), and the spatial variability of soil organic carbon stocks (Hoffmann et al., 2014). In the present study, we used predictive modeling to distinguish between sediment and bedrock and, judging from the AUROC values, all applied models showed satisfying results (Figure 7-2), though differences of the models' quality are significant. Moreover, model robustness and transferability, both crucial model properties when modeling natural phenomena, are high, as indicated by the low IQR. However, small differences between the performance of different statistical and machine learning models is not exceptional (e.g. Luoto and Hjort, 2005; Marmion et al., 2008; Goetz et al., 2011; Goetz et al., 2015), thus model evaluation should not solely be based on the estimated error rate or other quantitative performance measures such as AUROC (Steger et al., 2015). Instead, other qualitative and quantitative measures more in line with research questions and aims should be included in model evaluation and selection (Luoto and Hjort, 2005; Goetz et al., 2015; Steger et al., 2016). These measures include for example the geomorphic plausibility of a predictive map, which means the results should demonstrate no bias related to input data, show no algorithm artifacts, and have high AUROC values (Steger et al., 2016). We thus focus on several configurations that are important for our aims, e.g. the spatial and non-spatial validation, influence of input parameters, sample size, robustness of model, and variable importance.

The three different models applied were chosen due to their good interpretability (Goetz et al., 2011; Goetz et al., 2015), their wide application in geomorphic research and reliable results in earlier studies. Besides, machine learning techniques, such as random forest or support vector machine, are more prone to overfitting, difficult to interpret ("black boxes") and produce a rather noisy and heterogeneous prediction surface (Brenning, 2005; Goetz et al., 2015; Steger et al., 2016). Generalized linear and generalized additive models are continuous functions of the predictors (Formula 1, 2), thus they produce smooth and visually appealing prediction surfaces, i.e. prediction maps without single pixels classified incorrectly in an otherwise heterogeneous area and without artifacts from the algorithm (Figure 7-4). This is of high importance, as our aim is to deliver a geomorphic interpretation of the spatial distribution of sediments. Based on the median AUROC the best performance (0.8739) was obtained with the GAM5df (Figure 7-2), which is in good agreement with other studies (e.g. Marmion et al., 2008; Brenning, 2009; Petschko et al., 2014; Goetz et al., 2015).

7.5.1.1 Spatial validation and heterogeneity within a large scale drainage basin

Besides the non-spatial validation (Figure 7-2), we apply a spatial validation procedure by training and testing five models with different input datasets. Training datasets were taken from four of the five key sites. This model is tested and errors are estimated in the fifth key site. The datasets from the five key sites are assumed to be completely independent as they are far enough apart to avoid spatial autocorrelation (Brenning, 2005; Brenning, 2012) and exhibit differing characteristics (Figure 3-1, Table 6-1). This allows us to check how the model performs in areas where no sampling took place (Figure 7-6). In contrast, the commonly used approach to select a model is a non-spatial validation performed by splitting the dataset into training and test datasets (often without repeated or cross-validations). This approach has considerable drawbacks due to the dependence of training and test data (Brenning, 2005): it produces results too overoptimistic, underestimates error rates, causes overfitting, and does not allow an estimation of the model robustness because only one error rate or AUROC can be estimated especially when applying flexible machine learning methods.

Overall, the results of the non-spatial validation (Figure 7-2) are better than of the spatial validation (Figure 7-6). However, the performance estimates from the spatial validation are more realistic and do not overestimate the ability of the predictor (Brenning, 2005; Petschko et al., 2014). In the Val d'Illiez and the Turtmanntal, the models performs better than the GAM2df, trained and tested in all key sites (Figure 7-2). The models in the Goms and the Lötschental perform only slightly poorer. However, the results of the spatial validation in the Val de la Liène are strikingly low. In the four key sites where the spatial validation yields median AUROC values above 0.8, the IQR are very low (0.0019-0.0028), indicating high model robustness and transferability, which is also lower in the Val de la Liène (0.0160). These results suggest that further investigation of the differing site conditions in the key sites and the heterogeneity within the URB is necessary (Table 6-1).

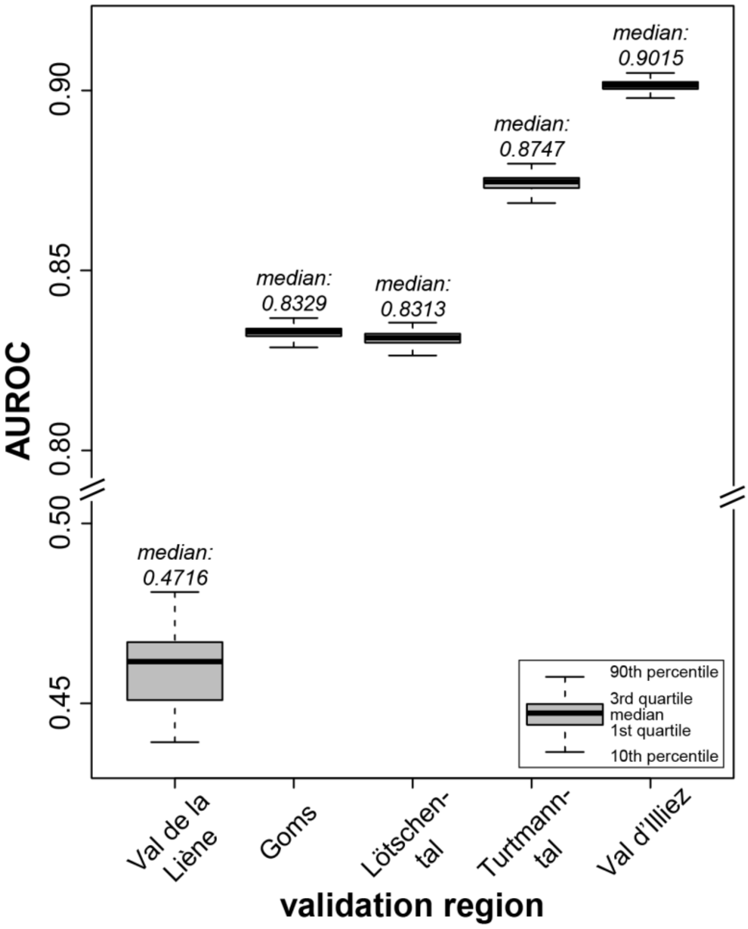

Figure 7-6: Spatial validation: training datasets consist of data from four of the five key sites and the model, a generalized additive model with input variables transformed with a smoothing spline with two degrees of freedom (GAM5df), is then tested and AUROC values are estimated in the fifth site (sample size for all models 51200, equal number of cases and controls). AUROC values are derived from ten times 25-fold validation.

The poor performance of the GAM2df for the Val de la Liène using a spatial validation can be associated with a variety of factors, including lithology, erodibility, topography, and glacial imprint. The Val de la Liène features mostly Mesozoic limestones of the Helvetic sedimentary nappes distinguished by a medium erodibility (Kühni and Pfiffner, 2001) and is situated north of the Rhone Valley. It is located at lower elevations, where contemporary glacial extent is low (c. 1.2%) (Fischer, 2013). Pleistocene glacial imprint is less pronounced due to the absence of an ice dome in this region (Kelly et al., 2004), the asymmetry of the URB with smaller tributaries in the north, the lower elevations and thus the formation of a major valley glacier. These site conditions distinguish the Val de la Liène strongly from the Goms, the Turtmanntal and the Lötschental. The Val d'Illiez, however, located in the westernmost part of the URB where the Rhone Valley is oriented in a NNW direction, has some conditions in common. It is dominated by the Infrahelvetic nappes and the South- and Ultrahelvetic sedimentary nappes consisting dominantly of flysch, and Mesozoic and Tertiary limestone with a low to medium erodibility (Kühni and Pfiffner, 2001). Only the NW part is underlain by the non-metamorphic Prealps (detached Upper and Middle Penninic nappes). The Val d'Illiez is also located at relatively low elevations, resulting in only minor glacial extent today (c. 1.2%). Albeit, the Val d'Illiez is characterized by a distinct glacial topography left behind by Pleistocene valley glaciers flowing from the SW (Kelly et al., 2004). The remaining three key sites have a higher contemporary glacial extent (10.8-14.2%), are dominated by lithologies with a low erodibility (metamorphic and plutonic rocks) and are located at higher elevations (Table 6-1). These lithological differences find their expression in the chemical denudation that is responsible for one third of total denudation in the sedimentary units of the Alps as opposed to only 10% in regions dominated by crystalline rocks (Hinderer et al., 2013). Hence, lithology might set upper boundaries to storage of clastic sediment. Besides lithology, differing Pleistocene glacial imprint seems to have an influence on the performance of the model in the URB. Schlunegger and Norton (2013) concluded the inheritance of Pleistocene glaciations have the strongest influence on current erosional forces and the landscape in the Central Alps and thus possibly on the spatial distribution of sediment. Future studies should further investigate these and other influential factors with heterogeneous distribution within a large scale area, e.g. current uplift rates (Kahle et al., 1997; Schlatter et al., 2005) and long-term exhumation ages (Vernon et al., 2008).

7.5.1.2 *Influence of data input and potential sources of error*

Analysis of the influence of the input dataset on the performance of the model (Figure 7-7) show that models trained with data from all key sites perform best when tested in all key sites (median AUROC = 0.8655). However, these models do not perform as good in the single key sites with median AUROC values ranging between 0.7454 in the Val d'Illiez and 0.8385 in the Turtmanntal (Figure 7-7). If only one site would have been sampled for model training purposes, the performance in the remaining URB would be less good. Not surprisingly, the highest median AUROC values are obtained when a model is trained and validated with data from only one key site. These key sites are on the one hand characterized by a low heterogeneity, on the other hand training and testing dataset are presumably not independent due to spatial autocorrelations (Brenning, 2005). Again, we point out site conditions in the Val de la Liène must be distinctly different from the other sites since models trained with data from this site perform weakly in the other four key sites.

Both results (Figure 7-6, Figure 7-7) indicate the importance of local site conditions, which has been pointed out in previous studies (Blahut et al., 2010; Petschko et al., 2014). As overall topographic and morphological characteristics do not vary notably throughout the URB (Table 6-1), we decided to train one model for the whole URB with one large input dataset from all five key sites representing the heterogeneity, instead of training individual models for homogeneous regions (Petschko et al., 2012). This attempt yields good results in the URB. Training several models produces problems such as subjective subdivision, more data input, and more model training validation and application runs with longer computation times. Our results highlight the importance of a sensible selection of key sites and thus the sampling design, which are both vital for the model performance. Spatial transferability can only be achieved when the input dataset reflects the properties and heterogeneity of the region.

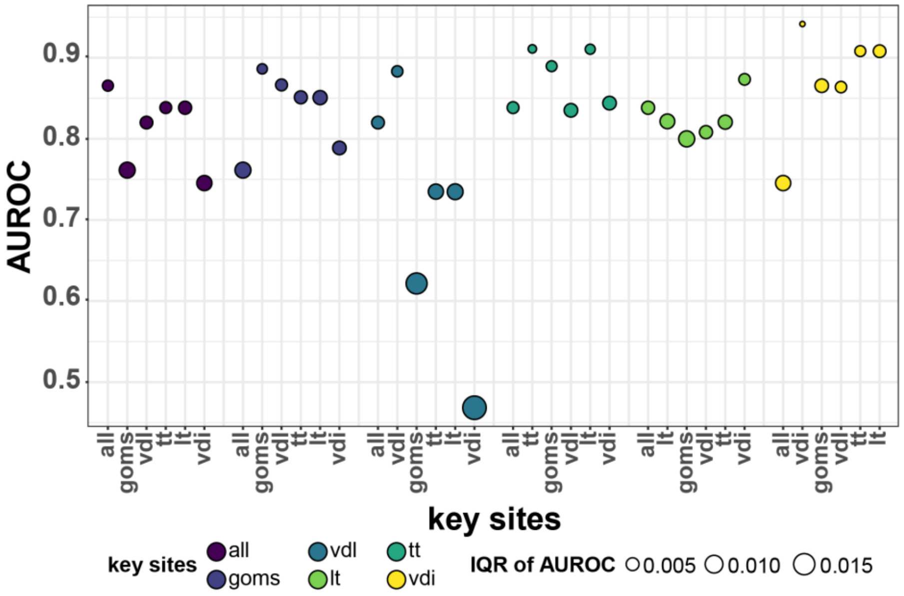

Figure 7-7: Spatial heterogeneity and spatial transferability of generalized additive model with smoothing spline transformation of input variables and up to two degrees of freedom (GAM5df). Models were trained with data from all and each single key site and then tested in all sites and each single site. Testing consists of applying ten times a 25-fold validation. Sample size for all training and testing datasets is 20000 (equal number of cases and controls). Color of bubbles indicates the spatial origin of the input data for model training. AUROC values signify the quality of the models. Bubble size represents the IQR (interquartile range of the AUROC) values, which are used as a measure of the transferability of the models. (all = all key sites, vdl = Val de la Liène, goms = Goms, lt = Lötschental, tt = Turtmanntal, vdi = Val d'Illiez).

Based on the sample size analysis (chapter 7.4.1.1) and quality assessment of the applied model, we infer that a minimum sample size of at least 25600 pixels (2 m resolution) of sediment cover and bedrock each needs to be mapped to set up a robust GAM. This would be equivalent to an area of c. 0.2 km^2 distributed across the five key sites with the pixels spread far apart to minimize spatial autocorrelation. However, this only includes setting up one model without validation, i.e. ten times a 25fold validation in this study corresponds to 10.7 km^2 of mapped area. Moreover, the samples need to capture not only the spatial heterogeneity within the URB represented by the five key sites but also several characteristics within the key sites, e.g. different spatial scales, elevations, slope gradients and topographic slope positions as well as the possibly occurring sediment storage types. Further spatial validation in this study required a total of 2.1 km^2 of sediment cover and bedrock each mapped in every key site, summing up to 20.8 km^2 in the URB. Even though a relatively small area of 20.8 km^2 (c. 0.4% of the URB) could be sufficient to achieve the presented modeling results, the pixels would have to be spread out relatively even across the five key sites and a point-based mapping would be much more time consuming than an area-covering mapping approach. Based on our results, we can recommend for future studies to map the spatial distribution of a geomorphic feature, e.g. sediment distribution, in different key sites representing the heterogeneity of the whole study area and to map an area spread out evenly and representing the relevant system characteristics. Nevertheless, a smaller area than the mapped 6.7% of the URB, i.e. 360.3 km^2 (Table 6-1), should be sufficient to model the spatial sediment distribution of a large scale drainage basin.

Besides the error rate of the applied model (Table 7-4, 21.7% for the GAM5df), other errors are more difficult to quantify. First, errors arise during mapping of sediment storages in the five key sites and due to uncertainties in the digital elevation model, which is the basis for most of the predictors. Furthermore, only areas presently free of glacial ice can be modeled (c. 90% of URB), as the underlying material (sediment/bedrock) of glaciers cannot be analyzed. We assume that the five key sites represent the heterogeneity of the URB and that the predictive model performs well in both sampled and not sampled sites. However, error quantification with validation procedures is not possible in regions which were not considered by field mapping. Even though the selected candidate predictors incorporate a large variety of processes influencing the distribution of sediment, we cannot rule out the possibility to have missed out influencing factors.

7.5.2 Geomorphic implications of modeled sediment distribution

Slope gradient, as one of the key factors driving sediment erosion, transport and deposition and thus sediment cover, constitutes an important variable in the applied models (chapter 7.4.1.1). Hence, it was used to compare the mapped and modeled spatial distribution of sediment cover in the five key sites (Figure 7-8). While the prediction performs well with an accuracy of c. 78% and displays the overall pattern of sediment distribution correctly, relative sediment cover in areas with slope gradients < 30° tends to be overestimated by the applied model in comparison to the field mapping results. This is especially the case in limestone dominated, deglaciated areas located in the north of the URB, where other erosional processes, i.e. carbon dissolution, might cause a difference in surface morphology. Furthermore, very flat bedrock-dominated glacier forefields are affected by misclassification. Sediment coverage is slightly underestimated in areas with slope gradients > 50°. These are often the ridges of steep side moraines. Apart from these special situations, even steep sediment storages types, i.e. talus and sediment-filled couloirs, were correctly classified and precisely delineated from the bordering bedrock.

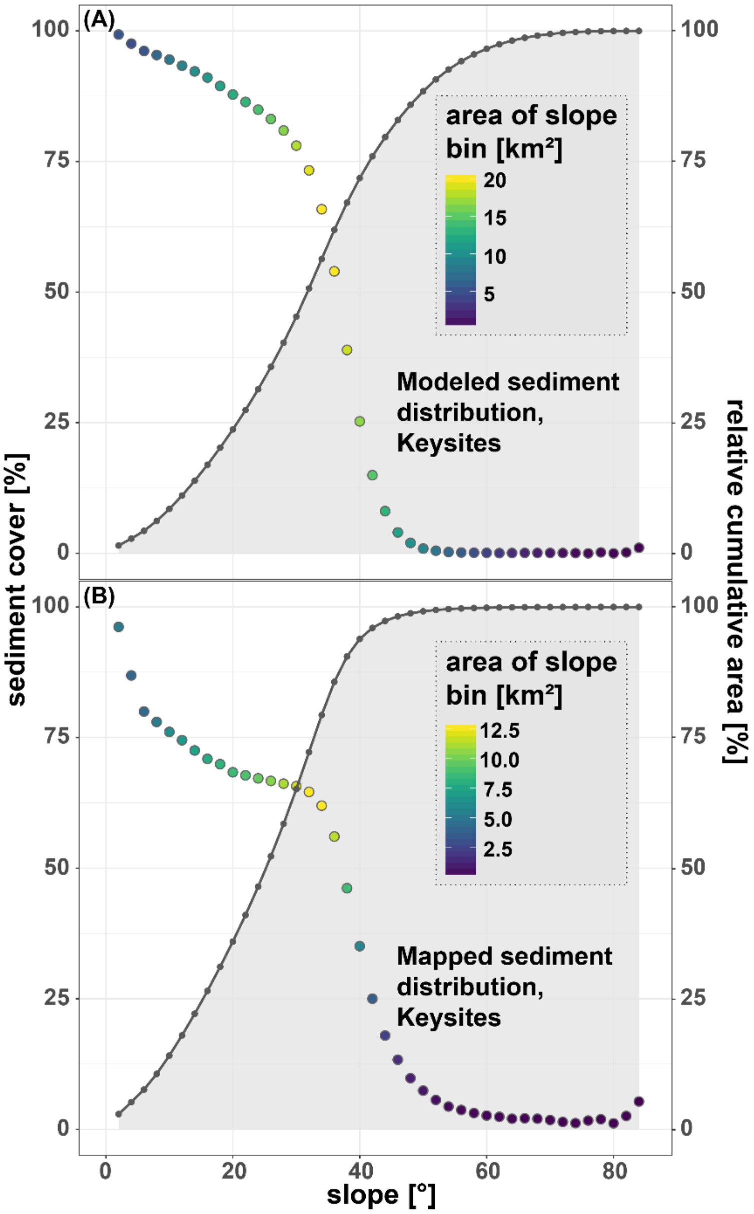

Figure 7-8: Sediment cover [%] as a function of slope (points) in the five key sites based on A: the modeled and B: the mapped sediment distribution. Points are color-coded by total area of each elevation bin. The cumulative sediment coverage is given by the gray line.

7.5.2.1 Sediment storage variability in the Upper Rhone Basin

Several factors potentially govern the spatial distribution of sediment storages and the great spatial variability of sediment cover, i.e. topography, connectivity, glacial imprint, lithology and tectonic uplift (chapter 7.5.1.2). Headwaters in the URB feature a very strong variability of sediment coverage (Figure 7-5). Watersheds with a high degree of sediment cover are located right next to watersheds with minor sediment coverage, i.e. it ranges from 0-100% in watersheds < 5 km^2. Previous studies investigating sediment storage in alpine catchments focus on one or several catchments (usually 10^0 to 10^2 km^2). In the Turtmanntal 75% of the hanging valleys are covered with sediment (Otto et al., 2009), whereas this portion is only 34% of Val Müschauns, located in the easternmost part of Switzerland (Messenzehl et al., 2014). In the Canadian Rocky Mountains sediment coverage in five catchments ranges between 44% and 82% (Hoffmann et al., 2013). However, the actual variability of sediment cover in headwaters in a large scale drainage basin, i.e. the URB, is much greater.

In general, relative sediment cover decreases with increasing elevations in the URB (Figure 7-9). Sediment cover as well as volume (e.g. Hinderer, 2001; Mey et al., 2015) is highest in elevations up to 500 m (80-92%) representing the valley fill of the Rhone Valley up to Sion. At elevations between 500-700 m the relative sediment cover is strongly reduced (52%), although this bin comprises mostly the valley fill of the Rhone Valley up to Brig but also partly the trough walls and the incised bedrock gorges of the tributaries of the lowermost URB, both featuring low sediment cover. Despite the general decreasing trend of sediment cover with rising height, the relative sediment cover increases steadily from 37-65% at elevations from 700-1300 m. These elevations represent the transition zones from the Rhone Valley to the tributaries, which are characterized by low sediment coverage and storage (Figure 7-4, Figure 7-9) due to steep gradients, V-shaped valleys or gorges (e.g. Schlunegger and Hinderer, 2003; Norton et al., 2010a; Valla et al., 2010a; Valla et al., 2010b). River incision and retreating knickpoints will continuously lower the valley floors and increase the connectivity to the channel and the catchment outlet.

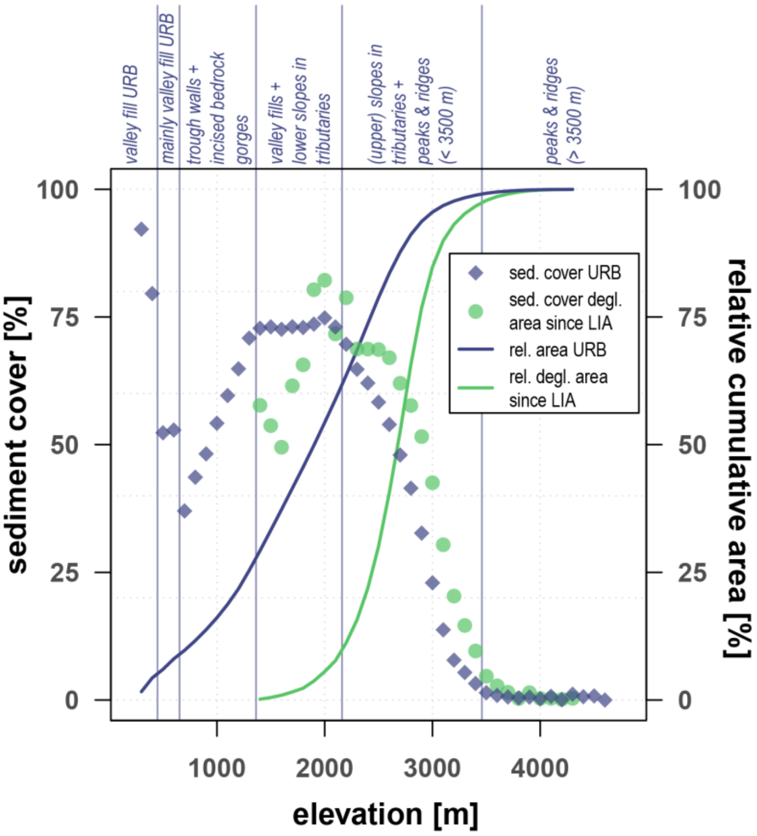

Figure 7-9: Sediment cover [%] as a function of elevation for the URB (blue diamonds) and the deglaciated area within the URB since the Little Ice Age (green dots). The area was stratified into 100 m-elevation bins (for location of bins see map in appendix B, Figure CC). The cumulative sediment coverage is given by the lines (blue=URB, green=deglaciated area). Deglaciated area since the Little Ice Age was delineated based on datasets by Maisch (2000) and Fischer (2013).

Currently, lots of sediment is stored further up in the tributaries above knickpoints. More than two thirds (70-73%) of the valley floors and lower slopes are covered with sediment due to the so far weak remobilization, the low sediment connectivity between hillslopes and channels and low transport capacities along channels of the now ice-free, wide, U-shaped and flat cirque floors (e.g. Schrott et al., 2003; Brardinoni and Hassan, 2006; Otto et al., 2009; Götz et al., 2013; Hoffmann et al., 2013). The upper slopes, peaks and ridges show a decreasing sediment cover with increasing elevation and the highest peaks and ridges (> 3500 m) are basically free of sediment. This points to the relevance of sediment cover and thus storage in the valley fills and at lower slopes of the tributaries of large scale drainage basins.

Based on an investigation of 57 headwaters, Hoffmann et al. (2013) concluded that erosion rates are higher in headwaters with distinct cirque morphology and yet the sediment delivery ratios are lower resulting in higher sediment storage. This pattern of sediment distribution is featured in the tributaries of the URB. It shows that the landscape and thus the low sediment connectivity and the sediment distribution in the URB is strongly inherited by the Pleistocene glacial imprint. However, fluvial and other post-glacial processes progressively reshape the alpine environment. Thus, the landscape is in a transient state adjusting to fluvial conditions (Brunsden and Thornes, 1979; Ballantyne, 2002b; Brardinoni and Hassan, 2006; Schlunegger and Norton, 2013; Hoffmann, 2015). Further studies should focus on the transition zones and their role in sediment dynamics (e.g. Valla et al., 2010a; van den Berg et al., 2012) and especially in the reworking of sediment storages. If sediment delivery ratios to the main valley increase, large amounts of sediment will potentially be mobilized, which might be a hazard in the future. However, the glacial imprint in the hanging valleys limiting sediment fluxes may persist until the onset of the next glaciation (Brardinoni and Hassan, 2006; Hoffmann, 2015), since fluvial adjustment of the transition zones is rather slow with incision rates on the order of several mm a^{-1} (e.g. Korup and Schlunegger, 2007; Valla et al., 2010a). Hoffmann (2015) demonstrates that paraglacial response times of sediment flux in mountain headwaters in the Canadian Rocky Mountains range in the order of 100–400 ka. Thus, the sediments stored above knickpoints will probably remain there for a long period of time.

7.5.2.2 Sediment cover in different topographic positions

For a more detailed analysis of the modeled spatial distribution of sediment storage in the URB, the areas covered with sediment were further classified according to six TSP (Weiss, 2000) (Figure 7-10) indicating the importance of different sediment storage types, which are typical for certain topographic positions. Excluding glaciated areas, sediments cover c. 60% of the URB. The broad valley of the Upper Rhone alone accounts for c. 9% of this area (260 km^2, 4.8% of URB) (Mey et al., 2015), leaving more than 90% covered with other types of sediment storage. These sediment storages outside the trunk valleys have often been neglected in large scale sediment budgets.

The ridges, upper and middle slopes constitute c. 55% of all sediment coverage, translating to 25% of the whole area of the URB. Despite their limited thickness (10^{-1} to 10^{1} m), Hoffmann et al. (2013) found these diffusive hillslope storages play a significant role in the sediment budgets of large scale alpine drainage basins. This is supported by other studies, where diffusive hillslope storages range between 25-35% of the sediment covered area (Otto et al., 2009; Messenzehl et al., 2014).

Sediments at the lower slopes and fringing the thalwegs of tributaries comprise c. 28% of sediment coverage in the URB. These sediments are deposited mainly by rock falls, debris flows and fluvial processes at locations with low slope gradients and transport capacity and their storages have greater thicknesses. Otto et al. (2009) lists depths up to 23.5 m for talus deposits in mountain headwaters and Götz et al. (2013) investigated even greater thicknesses for debris flow cones in the Gradenmoos basin, Austria. Talus and debris flow deposits have been identified as major sediment storages in several small scale mountain catchments. In the Reintal 72% of the sediment covered area is dominated by talus and debris flow deposits (Schrott et al., 2003), in the Val Müschauns they account for almost 50%

of the sediment covered area (Messenzehl et al., 2014), and talus deposits cover 20% of a hanging valley in the Turtmanntal (Otto et al., 2009). Although the relative areal extent of these storage forms is lower in large scale drainage basins, their role in large scale sediment budgets needs to be quantified (Sass, 2007). The last class comprises primarily the valley fill in the Upper Rhone Valley and fewer flat areas on slopes (total 12.4%). Some of the valley fills in the very large tributaries are also classified in this category. These two units cannot be further subdivided in this classification because of morphological similarities (Table 7-2). Glacial sediment storages, which constitute a significant portion in the hanging valleys of the Turtmanntal (Otto et al., 2009), are difficult to identify based on the approach using topographic slope positions since they are not deposited in one typical position. However, the presented model on the spatial sediment distribution has great potential to build the basis for a detailed sediment budget in a large scale drainage basin investigating quantitatively the importance of small scale sediment storages in comparison to large valley fills, e.g. in the Upper Rhone Valley. Detailed large scale sediment budgets are still rare (e.g. Jäckli, 1957; Jordan and Slaymaker, 1991; Tunnicliffe and Church, 2011; Tunnicliffe et al., 2012), as approaches to bridge the gap between scales are difficult to establish.

Earlier studies on large scale sediment storage in the URB focused on the Rhone Valley itself, while not including storage in small headwater basins or in talus and slope deposits. Volumetric estimates of the sediments stored in the wide, glacially overdeepened valley between Brig and Lake Geneva (Figure 3-1) range between 80 and 106 km^3 based on different approaches (Hinderer, 2001; Rosselli and Olivier, 2003; Jaboyedoff and Derron, 2005; Mey et al., 2015), with errors of up to ± 50% (Hinderer, 2001). Since the valley fill in the Rhone Valley accounts for 240 km^2 of the sediment coverage in the URB, the remaining c. 2600 km^2 must be covered with other sediment storages (Table 7-5). Conservatively assuming a mean depth of 1-5 m for these sediment storages, would translate to a volume of 2.6-13 km^3 (i.e. 2-16% of the sediment volume stored in the Rhone Valley between Brig and Lake Geneva), underscoring the significance of small scale sediment storages. We note that this is a very conservative estimate because sediment storages deposited at lower slopes or in thalweg positions in the tributaries, larger fans and valley fills have reportedly higher depth than 5 m (e.g. Schrott et al., 2003; Sass, 2006; Sass, 2007; Otto et al., 2009; Götz et al., 2013; Hoffmann et al., 2013). Thus, realistic estimations considering spatial scale effects on sediment thickness would yield much higher sediment volumes in small scales sediment storages.

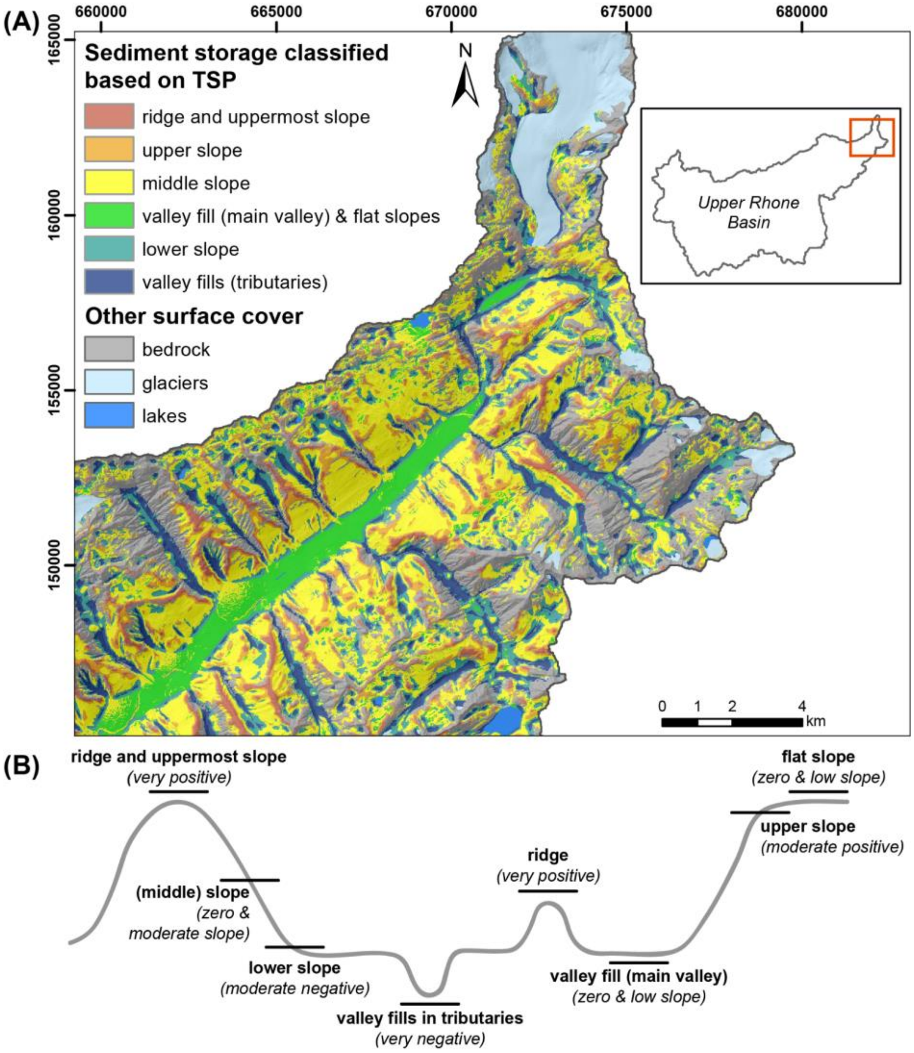

Figure 7-10: A: Modeled sediment distribution classified according to topographic slope position (TSP) based on the topographic position index (TPI) after Weiss (2000) in the Goms region, Upper Rhone valley. Glacier extent from Swiss glacier inventory 2010 (Fischer, 2013). Lakes classified based on digital elevation model (DEM) with a semi-automated surface classification model (Bowles and Cowgill, 2012) (DEM from swisstopo, projection: CH1903). B: Sketch of TSP and TPI and slope values after Weiss (2000).

Table 7-6: Sediment storage [km^2 and %] per topographic slope position (TSP) class based on the topographic position index (TPI) after Weiss (2000).

Topographic slope position (TSP)	Area [km^2]	Area [%]
ridge and uppermost slope	131.32	4.56
upper slope	255.20	8.87
(middle) slope	1328.01	46.16
valley fill (main valley) and flat slopes	356.08	12.38
lower slope	493.42	17.15
valley fills (tributaries)	312.90	10.88
total	**2876.93**	**100**

7.5.2.3 Sediment cover in deglaciated areas since the LIA

The rapid deglaciation in the European Alps since the Little Ice Age (Maisch, 2000; Zemp et al., 2008) and especially in the last decades (Haeberli et al., 2007; Fischer et al., 2014) exposed large areas that were previously buried beneath ice. With ongoing glacial melt, this trend will continue within the next decades (Huss et al., 2017). Studies focusing on sediment storage in deglaciated areas on a larger scale are so far missing. Thus, we will contribute to this research gap by investigating the sediment cover in the areas deglaciated since the Little Ice Age in a large scale catchment. In the URB an area of 355.8 km^2 has been deglaciated since the LIA (Maisch, 2000; Fischer, 2013), of which 201.4 km^2 (c. 56.6%) are covered with sediment, 152.7 km^2 (42.9%) with bedrock and the remaining parts (0.5%) with lakes. This is similar to the areal extents of sediment and bedrock cover in the URB, with c. 60% of the non-glaciated area covered with sediment and c. 40% with bedrock. The exposed areas, largely located in the glacier forefields between 1900 and 3000 m, are mainly covered with unconsolidated, barely vegetated and thus unstable sediments (Baewert and Morche, 2014; Lane et al., 2017). But also smaller areas surrounding the upper parts of glaciers will be deglaciated, where bedrock is exposed due to glacial thinning (Figure 7-9). These areas located above 3500 m amount to only 5% of the total deglaciated area and the sediment cover is less than 10%. The sediment coverage is characterized by a general decrease with increasing elevation in the deglaciated areas (Figure 7-9), a trend that also holds for the whole URB. However, in direct comparison to areas without recent glacial imprint, the relative sediment cover in the deglaciated areas is distinctly higher (up to 82%) at elevations ranging from 1900-3500 m. Deglaciated areas below 1900 m (cumulative area 2.5%) show a large scatter in the areal extent of sediment cover since these areas are located only in the proglacial area of two of the largest glaciers, the Aletsch and the Fiescher glaciers. Both glaciers are located in very narrow and steep valleys, hence their glacier forefields are bedrock-dominated. The sediment cover at these elevations is thus lower than at the same elevations in the whole URB.

Our data support that proglacial areas in the Alps feature an intense availability of sediment (Maisch et al., 1999). In comparison to most other areas, they are very young (exposure max. 170 years) and glacial erosion and thus sediment production has been recently active. If recently deglaciated areas are subject to increased geomorphic activity (Carrivick et al., 2013) the availability of glacial sediment, recently analyzed in this and several other studies (review given by Heckmann et al., 2016b), might pose a hazard through different geomorphic processes (Moore et al., 2009; Heckmann et al., 2016b). The modeled sediment distribution in the URB could be further used to analyze the sediment cover of individual glacier forefields to improve the classification of sedimentary, bedrock and mixed sedimentary-rocky glacier forefields and beds, which is especially important to gain information about future hazards due to the ongoing deglaciation (Maisch et al., 1999; Zemp et al., 2005).

7.6 Conclusion

Bridging the gap between different spatial scales remains a major challenge in geomorphic research. This is especially true for the field of sediment budgets, where small scale (< 10^2 km^2) investigations are primarily based on field work in individual headwater catchments, whereas large scale studies focus on the role of macro-sedimentary landforms in a regional context. Here we applied a combined field mapping and statistical modeling approach to fill this gap and to predict the location and spatial distribution of sediment and bedrock cover in the URB.

- **Modeling approach and transferability**: We compared different predictive modeling approaches, namely logistic regression, principal component logistic regression, and generalized additive models. All tested models performed well, best prediction results with a high spatial and non-spatial transferability were achieved by a generalized additive model with five degrees of freedom. Our approach to train one model for a large scale, heterogeneous, mountain drainage basin, with a dataset representing this heterogeneity shows to be a suitable way to bridge the gap between large and small scale sediment budgets studies. However, the reference area mapped in the field has to represent the spatial heterogeneity of the large scale drainage basin, but we show that as few as c. 50 km^2 of manual mapping could be sufficient.
- **High-resolution model and its benefits**: Our model of the spatial distribution of sediment and bedrock reveals that 53.5 ± 21.7% of the URB are covered with sediment and predicts its location with 2 m ground resolution. This dataset can serve as an important input for models of seismic wave propagation, hydropower management, and the assessment of sediment-related natural hazards in the URB. Moreover, future sediment budget studies will benefit from this data and might further explore its potential in estimating sedimentary volumes of individual landforms. In addition, the high spatial and non-spatial transferability of the model calls for an application to an even larger scale, e.g. to the entire Alps. This might reveal larger patterns of sediment distribution which are not discernible on the scale of one large scale catchment.
- **Importance of small scale storage**: Assuming a very conservative mean depth of 1-5 m for all sediment covered areas outside the main valley, we estimate that a volume of 2.6-13 km^3 is trapped in low-order catchments. This finding underscores the relevance of small scale sediment storage in large scale sediment budgets. In the URB shallow diffusive hillslope storages at the ridges, upper and middle slopes alone constitute more than 50% of all sediment coverage. Sediment cover deposited mainly by rock falls, debris flows and fluvial processes at the lower slopes and the thalweg of tributaries comprises one third of relative sediment coverage. These results warrant a detailed volumetric quantification of the sediments stored in the large scale drainage basins that better include the entire spectrum of sedimentary landforms.

- **Deglaciated areas and hazard**: Areas that have deglaciated since the Little Ice Age show an elevated relative sediment coverage compared to the remaining catchment at similar elevations. Due to their recent exposure, these glacier forefields are characterized by low vegetation cover, and hence a reduced stability of the sediments trapped. Our data ultimately help assessing the natural hazard potential in a large alpine drainage basin, pinpointing the locations of loose sediments that might nourish catastrophic processes.

8 Synthesis

Major findings and conclusions of the three investigated scales based on the objectives and aims introduced in chapter 1 are summarized in this chapter (Figure 8-1). Since the issue of transferring knowledge between systems of various spatial scales is regarded as one of the most relentless problems in geomorphology (Church, 1996), scale linkages and contributions of this thesis to resolving scaling issues in sediment storage analysis are pointed out explicitly. Finally, difficulties and future research needs are discussed.

In this thesis, I used a multi-scale and multi-method approach, which is based on the application of different, well-chosen methods on specific scales. In the process, the nested hierarchy structure of geomorphic systems (de Boer, 1992), which is the basis for the chosen upscaling framework, is acknowledged and emphasized. The study area of the URB is an ideal setting to study Postglacial sediment storage, since it is a closed system for clastic and suspended sediment transport with Lake Geneva acting as a final sink. Moreover, it is one of the largest inner-alpine basins. A relatively large amount of scientific studies and (geomorphic) data is available, thus also valuable knowledge on sediment storage and distribution on individual spatial scales exists (e.g. Welten, 1982; Pfiffner et al., 1997; Hinderer, 2001; Ivy-Ochs et al., 2006b; Kelly et al., 2006; Otto et al., 2009; Mey et al., 2015).

8.1 Major findings and conclusions on the investigated scales

Objective 1: Understanding and analyzing the formation of Postglacial landforms on a small scale using the examples of outsize fans in the Upper Rhone valley, Switzerland

Sedimentary fans are ubiquitous landforms, especially in mountainous terrain. Nonetheless, outsize fans that are characterized by a seemingly disproportional, small feeder catchment, and their formation have rarely been examined in detail. In this thesis, three outsize fans in the Upper Rhone Valley were studied to contribute to a better understanding of formation processes, timing and the sedimentology of these potentially indicative landforms. The focus lies thereby on their formation, showcasing that even on the small scale knowledge to understand sediment storage in high-mountain environments is still lacking.

The applied multi-method approach revealed the following results and conclusions:

- The three GOFs feature small catchments, roughly of equal size as the respective fan areas, are cut into sheer bedrock. Hence, no unconsolidated material, let alone a pre-existing catchment was in place before deglaciation. This is backed up by the geomorphometric volume estimation of fan deposit and eroded material from the catchment: The majority of the eroded material is stored within the fans (only GOF #2 was subject to erosion by the Rhone). Our geomorphic analysis further sharpens the definition and characteristics of outsize fans: They can have fan-to-source area ratios close to or even larger than one, steep gradients and a bottle-neck transition between fan surface and feeder basin. The fans are Postglacial landforms deposited mostly on top of a Late- and Postglacial valley fill with only small portions (c. 30 m of total thickness) of the described features being buried. Mapping of sedimentary fans within the URB (n=186, min. area: 0.015 km^2) revealed the distinctiveness of the three investigated fans. However, it is also clear that these are not singular cases.

- The sedimentary architecture of GOF #3, investigated with GPR and ERT profiles, reveals two sedimentary units dominated by debris flow deposits, since we interpret the high resistivities and strong reflectors present in our ERT and GPR sections of both units as indicators for a heterogeneous texture with large boulders in a finer matrix. The bulk of the fan (lower sedimentary unit) consists of material featuring very strong and more heterogeneously appearing reflectors and resitivities up to 20 kΩm. The second sedimentary unit constituting the upper 5-10 m has less pronounced reflectors, which appear more steady with lower angles and show larger structures. Resistivities largely remain below 5 kΩm.
- Apparent ^{10}Be and ^{26}Al exposure ages from boulders on GOF #3 surface and from bedrock outcrops in its feeder basin in combination with the geophysical data reveal a fan formation in three phases. During Phase I that ceased with the full development of the catchment around ~6.0 ka, the fan interior (lower sedimentary unit) was built up by the deposits of massive high-energy, high-magnitude debris flows sourced from the feeder catchment. In Phase II lasting until c. 0.8 ka, the feeder basin was affected by comparatively lower-magnitude debris flows that deposited the upper sedimentary unit characterized by debris flow channels, snouts and large boulders on the initial fan. During the most recent Phase III, the fan-feeder basin transport system seized up with only isolated cases of geomorphic activity within the catchment not reaching the fan. Therefore, our quantitative data point to a rapid, but incremental and non-catstrophic formation of outsize fans in the Upper Rhone valley.
- The magnitude of averaged denudation rates in Phase I of fan formation were exceptionally high, ranging 45- to 75-times higher than median basin wide denudation rates from the Goms region and Upper Rhone valley, respectively. This extreme activity following deglaciation is at least comparable to the current Illgraben activity producing several large debris flows per year and extremely high basin wide denudation rates. These findings are in agreement with models of Postglacial landscape evolution. Erosion and sedimentation rates of the fan systems were elevated soon after deglaciation and then decreased or ceased over time during the Holocene.

This aspect is a core notion of paraglacial sedimentation theory in fan environments. However, besides paraglacial rock slope instabilities we acknowledge that tectonic and/or climatic conditioning of catchment initiation and fan formation might have (also) conditioned initially high rates of sediment production.

- Outsize fans are outstanding landforms, rapidly evolving from small feeder basins that export material at extremely high rates. They are capable of disrupting longitudinal sediment connectivity in mountain regions, which is well shown by the analysis of the longitudinal profile in the Goms region. Rapid delivery of material from the GOF #3 feeder catchment induced upstream aggradation in the main valley and strongly interrupted the sediment cascade on a much larger spatial scale.

Scale linkages

These findings clearly show that we have to understand sediment storage and dynamics on small scales to further investigate sediment storage and dynamics on a larger scale. Only on the “landform scale”, it is possible to investigate the details, initiation and period of landform formation, which are further need to analyze sediment storage adequately on the regional scale. Solely through this scale linkage it is possible to explain more complex landform assemblages and the disruption or amplification of sediment fluxes. Even if it is difficult to directly or quantitatively use this knowledge on higher hierarchy levels in geomorphic systems, I point out that also indirect, qualitative scale linkages are major components in understanding and investigating large scale geomorphic systems regarding their sediment storage distribution.

Objective 2: Investigating the landform assemblage in medium-sized tributaries within the Upper Rhone Basin

On a regional scale, we mapped the distribution of sediment cover and bedrock in great detail in five key sites: Val d’Illiez, Val de la Liène, Turtmanntal, Lötschental and Goms with areal extents of c. 90-230 km^2. Data for the Turtmanntal hanging valleys was provided by Otto et al. (2009) and supplemented with data from the main valley and the glacier forefield. In total ~360 km^2 were mapped with combined geomorphic mapping methods in the field and from high resolution remote sensing data. The five key sites were chosen to cover the full width of morphological, geological, climatological and glacial imprint characteristics within the URB. It is important to acknowledge the invariance of properties on a certain scale and how ignoring this results in problematic upscaling attempts with poor results (chapter 7.5.1). Furthermore, 186 sedimentary fans are mapped from digital topographic data and remote sensing imagery.

Since the regional scale is not the focus of this dissertation and has been addressed in many other studies before (e.g. Schrott et al., 2003; Otto et al., 2009; Götz et al., 2013), sediment distribution, storage and connectivity was not examined in further detail on this scale.

Scale linkages

The data gathered on this scale was used in a direct upscaling technique based on predictive mapping. This technique aims at incorporating small scale sediment storages in the analysis of sediment storage on a large scale as including data on landform assemblage, sediment distribution and thus the characteristics of sediment storages from a smaller scale is crucial to the sensible modeling of sediment distribution in a large scale drainage basin. For example, knowledge from headwaters and lower-order catchments needs to be included to produce a realistic model outcome. Highly resolved data represents one important scale linkage, since it allows the modeling of sediment distribution with the same accuracy and level of detail. Furthermore, the analysis of the spatial distribution and frequency of certain sediment storage forms in a large scale system (i.e. the mapping of all sedimentary fans in the URB and their morphometric analysis) reveals important quantitative information on their importance and prevalence within the higher-order system as well as their characteristics on a more general basis.

Objective 3: Creating scale linkages for sediment distribution between smaller scales and a large catchment scale through a hierarchical upscaling approach based on predictive mapping

Bridging the gap between different spatial scales remains a major challenge in geomorphic research and especially in the field of sediment budgets. Small scale (< 10^2 km^2) investigations are primarily based on field work in individual headwater catchments, whereas large scale studies focus on the role of macro-sedimentary landforms. Hence, a combination of field-based data from smaller scales with remote-sensing and modeling data from larger scales proves useful: A combined geomorphic mapping and statistical modeling approach was applied to create scale linkages between smaller scale key sites and a large catchment scale to predict the location and spatial distribution of sediment and bedrock cover in the URB.

- Four predictive modeling approaches (logistic regression, principal component logistic regression, and generalized additive models) performed well. However, the best prediction results with a high spatial and non-spatial transferability were achieved through a generalized additive model with five degrees of freedom. The approach to train one model for a large scale, heterogeneous, mountain drainage basin, with a dataset representing this heterogeneity on the regional scale, and thus acknowledging scale invariance, proofs to be a suitable means to bridge the gap between small and large scale sediment budgets studies. We can show that as few as c. 50 km^2 of manual mapping could be sufficient as long as spatial heterogeneity is taken into account.

- The predictive model of the spatial distribution of sediment and bedrock reveals that 53.5 ± 21.7% of the URB is covered with sediment and predicts its location with 2x2 m ground resolution. The presented dataset can serve as an important input for models of seismic wave propagation, hydropower management, and the assessment of sediment-related natural hazards in this catchment.
- Our results underscore the importance of small scale storage. Assuming a very conservative mean depth of 1-5 m for all sediment covered areas outside the main valley, we estimate that a volume of 2.6-13.0 km^3 is trapped in low-order catchments. Since the valley fill in the Rhone Valley accounts for only 240 km^2 of the sediment coverage in the URB, the remaining c. 2600 km^2 must be covered with other sediment storages. These findings highlight the relevance of small scale sediment storage in large scale sediment budgets, where often only the largest macro-scale sediment storages are factored in. In the URB, shallow diffusive hillslope storages at the ridges, upper and middle slopes alone constitute more than 50% of all sediment coverage. Sediment cover deposited mainly by rock falls, debris flows and fluvial processes at the lower slopes and the thalweg of tributaries comprises one third of relative sediment coverage. These results warrant a detailed volumetric quantification of the sediments stored in the large scale drainage basin that better includes the entire spectrum of sedimentary landforms. We conclude that an urgently needed, realistic estimation considering spatial scale effects on sediment thickness would yield much higher sediment volumes in small scales sediment storages than the conservative estimate based on a mean thickness of 1-5 m.
- Proglacial areas that have been deglaciated since the Little Ice Age show an elevated relative sediment coverage compared to the remaining catchment at similar elevations, thus providing relatively large amount of sediment. Due to their recent exposure, these glacier forefields are characterized by low vegetation cover, and hence a reduced stability of the sediments trapped. Our data ultimately help assessing the natural hazard potential in a large alpine drainage basin, pinpointing the locations of loose sediments that might nourish catastrophic processes.

Scale linkages

These findings demonstrate that quantitative scale linkages facilitate a detailed sediment budget even in a large scale drainage basin. Predictive mapping approaches based on statistical models or machine learning methods are the basis for a successful hierarchical upscaling approach. This methodology should be further exploited to get even more detailed insights into sediment distribution, storage volumes and dynamics in alpine systems. The general upscaling of sediment cover as opposed to modeling the spatial distribution of different landforms (e.g. talus or moraine deposits) has proven to be a powerful approach, since the characteristics of some landforms are highly variable and/or not clearly delimitable from other forms (convergence or equifinality). Thus, I recommend this procedure and the ensuing geomorphometric analysis, e.g. based on the topographic slope position (Weiss, 2000).

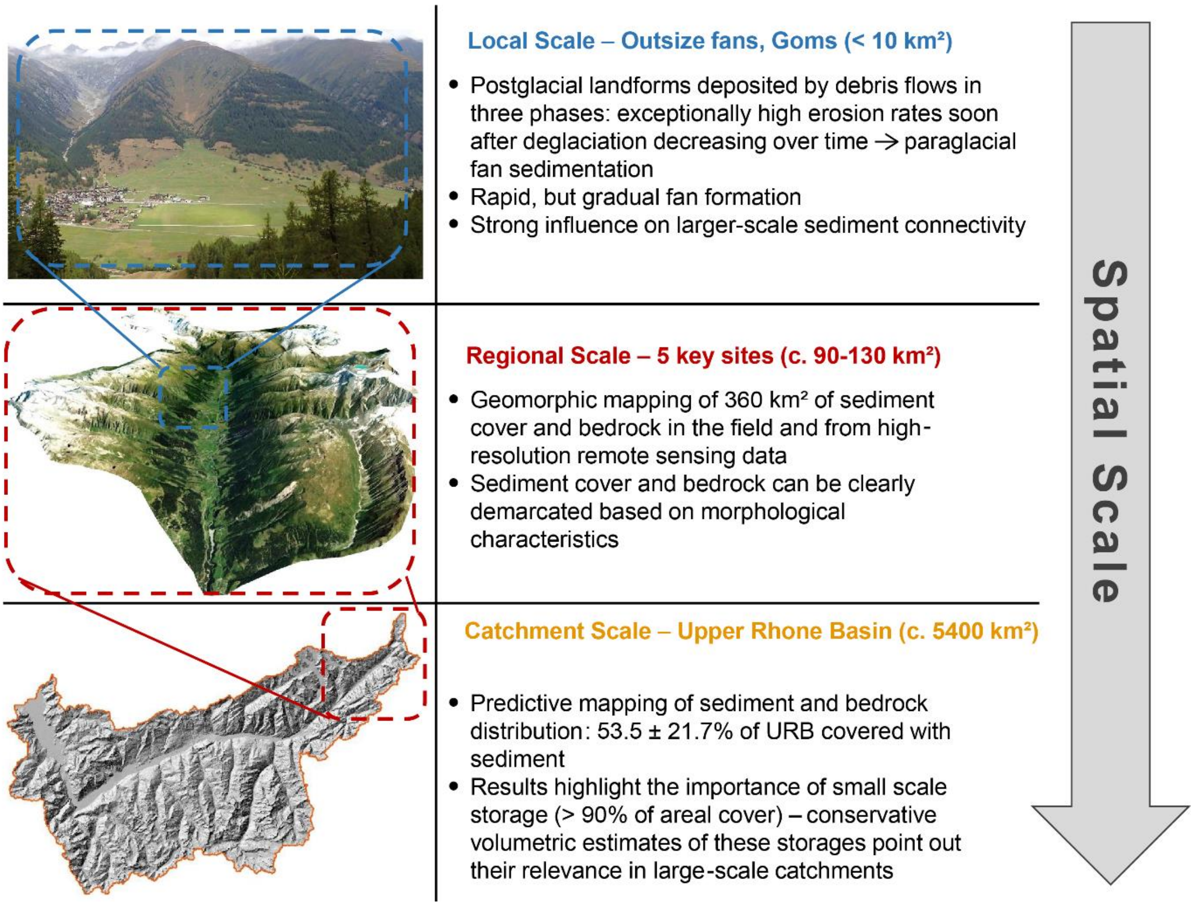

Local Scale – Outsize fans, Goms (< 10 km²)

- Postglacial landforms deposited by debris flows in three phases: exceptionally high erosion rates soon after deglaciation decreasing over time → paraglacial fan sedimentation
- Rapid, but gradual fan formation
- Strong influence on larger-scale sediment connectivity

Regional Scale – 5 key sites (c. 90-130 km²)

- Geomorphic mapping of 360 km² of sediment cover and bedrock in the field and from high-resolution remote sensing data
- Sediment cover and bedrock can be clearly demarcated based on morphological characteristics

Catchment Scale – Upper Rhone Basin (c. 5400 km²)

- Predictive mapping of sediment and bedrock distribution: 53.5 ± 21.7% of URB covered with sediment
- Results highlight the importance of small scale storage (> 90% of areal cover) – conservative volumetric estimates of these storages point out their relevance in large-scale catchments

Figure 8-1: Summary of major findings and conclusions from the three investigated scales.

8.2 A framework to resolving scaling issues in sediment storage analysis

The following framework is intended to provide a structure for further large-scale sediment budget studies and sediment storage analysis. I present conceptual as well as applied ideas that should be considered when resolving scaling issues.

Ordering the investigated systems and thinking across scales

We need to order the geomorphic system of interest, i.e. the sediment storage in the large-scale inner-alpine URB, into subsystems of different spatial scales. However, we cannot stop here and regard each scale individually, but we need to think across these scales, identify the strengths of each one and the respective properties of sediment storage, which can be observe with appropriate methods.

Finding and identifying the linkages between scales
Moreover, and most importantly, we have to find and identify the scale linkages and use them to transfer and thus upscale our findings. These linkages can be qualitative or quantitative while facilitating the understanding of a large scale system. Not knowing the scale linkages has been deemed a major problem in sediment budget studies (Slaymaker, 2006) and in mountain geomorphology in general (Church, 1996).

Multi-scale and multi-method approach
The results presented in this thesis indicate that scaling issues in sediment storage analysis and thus in sediment budget studies can only be overcome by applying a multi-scale and multi-method approach. Every scale has certain related strengths and geomorphic characteristics as well as applicable methods, which are pointed out above. I produced data and therefore knowledge on three different scales and linked them through appropriate methods quantitatively and qualitatively with higher scales. Data from different smaller scales or geomorphic subsystems is needed to understand the distribution of sediment storage in a large scale geomorphic system. This approach is based on the nested, hierarchical structure of geomorphic systems (de Boer, 1992), which allows to incorporate emergent properties and recognizes the increasing complexity of sediment storage forms with increasing spatial scale (Figure 4-1). Furthermore, one can incorporate steps to overcome the challenge of scale invariance by acknowledging the spatial heterogeneity of certain properties on each scale.

Bringing together spatial scales – process, observation and modeling
The presented framework is based on the idea that, on the one hand, the observation scale and the targeted modeling scale need to be brought together by overcoming the discrepancies between these two scales. On the other hand, the observation scale needs to fit the process scale, i.e. the scale at which processes operate (Blöschl and Sivapalan, 1995; Zhang et al., 2004; Schlummer et al., 2014). Thus, I collected data on the sediment storage distribution on the regional scale from high-resolution remote sensing data and in the field, where the assemblage of geomorphic landforms can be investigated in detail. The discrepancy between the observation scale and the modeling scale was overcome by keeping the same spatial resolution of data on the larger, modeling scale.

Incorporation of existing data
Existing data, such as the mapping results by Otto et al. (2009) or dating results by Kelly et al. (2006) and Ivy-Ochs et al. (2006b) for this thesis, should be incorporated and used, since more information in general leads to better upscaling results. Furthermore, they lead to higher data independence, since the data has been acquired in separate, unattached studies.

The important role of high-resolution data and computational power

High-resolution remote sensing data and computational power (Church, 2010b; Tarolli, 2014) enable the above mentioned scale linkage. The lack of data availability has been described as a problem in earlier publications (Harvey, 2000; Tunnicliffe and Church, 2011).

The presented framework can be further improved and adjusted to the objectives and needs of other studies, but at the same time may lead through their analysis as a guiding concept. Considering the future research needs mentioned below, I propose the nested hierarchy approach presented and elaborated in this thesis as a golden thread and not as a single, encompassing tool for further analysis of the full spectrum of sediment storage in a large-scale catchment or on even larger scales.

8.3 Future research needs

Finally, I point out the needs for further research on the individual scales and in particular on the scale linkages tackled in this dissertation. I stress that outsize fans on the small scale deserve more attention in future research. Based on the collected data, I was able to advance the definition of outsize fans and to suggest a first model of outsize fan formation. However, a larger dataset (e.g. orogen scale) on their spatial distribution and geomorphometric characteristics in comparison to other alpine, 'allometric' fans (Crosta and Frattini, 2004) is needed. This would enable a more concise definition for this landform and an additional investigation of formative differences between outsize fans of different scales (i.e. vague distinction into outsize vs. megafans in Jarman et al., 2011). To better understand timing and processes of fan formation, quantitative data from different outsize fan sites is necessary. These data should be used to establish a general model of outsize fan formation. Furthermore, a comparison to alpine, alluvial fan formation (e.g. Hornung et al., 2010; Franke et al., 2015; Brardinoni et al., 2018; Kober et al., 2019; Ratnayaka et al., 2019) would shed light on the question if outsize fan formation differentiates fundamentally. For the three GOFs in the Upper Rhone valley, other quantitative dating approaches based on ^{14}C in organic material could allow for a better constraint of the timing of fan initiation. This material could be extracted from core drillings on the fan and upstream of GOF #3. Investigating the upstream valley deposits facilitates further investigation of their influence on the large-scale sediment cascade. Determining the exact controls on outsize fan formation is a big research intention, which might be solved either with a larger, quantitative dataset on outsize fans or a detailed statistical analysis on potential controlling factors (e.g. tectonics, lithology, glacial imprint, climatic triggers) for a specific study site.

On the regional scale, the large dataset on sediment storages in five key sites within the URB was mainly used as an input-dataset for predictive modeling. Nevertheless, it could also be used to better understand sediment storage assemblages in different settings or subregions, e.g. with a focus on (dis)connectivity along the sediment cascade. However, since this scale has not been the focus, this reaches beyond the scope of the presented dissertation.

Based on the nested, hierarchical scaling approach, I was able to predict the spatial distribution of sediment storage and cover in great detail for the large-scale alpine Upper Rhone catchment. A first conservative estimation of sediment storage volume reveals the importance of headwater storage not only within the URB tributaries, but also on the larger scale. Future sediment budget studies will benefit from the data presented in this thesis and might further explore its potential in estimating sedimentary volumes of individual landform types. In a further refinement of the predictive mapping approach, the method could be applied to model the spatial distribution of certain sediment storage types or process domains with distinct topographic/geomorphometric characteristics (e.g. talus deposits). However, this methodology reaches its limits, when the targeted sediment storage types have more variable properties (e.g. moraine deposits or complex deposits, i.e. built up by more than one process).

The detailed, volumetric quantification of sediment storage in a large scale catchment poses additional challenges. Predictive mapping of different sediment storage types remains a challenge and is still linked with a relatively low accuracy (Seijmonsbergen et al., 2011; Otto and Smith, 2013). The determination of mean thickness values for certain sediment storage types based on e.g. geophysical surveying (Otto et al., 2009) is associated with high work effort and the general accuracy needs to be questioned. These uncertainties combined and thus the error propagation from smaller to larger scales lead to a hardly quantifiable error of the final quantification. Therefore, I propose that a more general approach based on the detailed distribution of sediment storage and cover, such as the one presented in this thesis, and a data-based quantification of general sediment storage thickness with different scenarios would lead to a better, more robust and more reliable result. These estimates on small scale sediment storages in headwaters and lower-order catchments should then be combined with existing data on macro-scale sediment storages, i.e. in valley fills or lakes (e.g. Hinderer, 2001; Jaboyedoff and Derron, 2005; Straumann and Korup, 2009).

The presented upscaling framework for sediment storage distribution could also be applied to the orogeny scale (e.g. the entire Alps) or another study area with limited data availability due to the high spatial and non-spatial transferability of the model. This might reveal larger patterns of sediment distribution which are not discernible on the scale of one large-scale catchment. It would be interesting to study the impact inherent to different degrees of spatial resolution, as I suggest that high-resolution data availability renders the detailed prediction of spatial sediment distribution possible.

References

Aguilera, A.M., Escabias, M., Valderrama, M.J., 2006. Using principal components for estimating logistic regression with high-dimensional multicollinear data. Computational Statistics & Data Analysis, 50(8), 1905-1924.

Akaike, H., 1974. A new look at the statistical model identification. IEEE transactions on automatic control, 19(6), 716-723.

Allen, T.I., Wald, D.J., 2009. On the use of high-resolution topographic data as a proxy for seismic site conditions (VS30). Bulletin of the Seismological Society of America, 99(2A), 935-943.

Andersen, K.K., Azuma, N., Barnola, J.M., Bigler, M., Biscaye, P., Caillon, N., Chappellaz, J., Clausen, H.B., DahlJensen, D., Fischer, H., Fluckiger, J., Fritzsche, D., Fujii, Y., Goto-Azuma, K., Gronvold, K., Gundestrup, N.S., Hansson, M., Huber, C., Hvidberg, C.S., Johnsen, S.J., Jonsell, U., Jouzel, J., Kipfstuhl, S., Landais, A., Leuenberger, M., Lorrain, R., Masson-Delmotte, V., Miller, H., Motoyama, H., Narita, H., Popp, T., Rasmussen, S.O., Raynaud, D., Rothlisberger, R., Ruth, U., Samyn, D., Schwander, J., Shoji, H., Siggard-Andersen, M.L., Steffensen, J.P., Stocker, T., Sveinbjornsdottir, A.E., Svensson, A., Takata, M., Tison, J.L., Thorsteinsson, T., Watanabe, O., Wilhelms, F., White, J.W.C., 2004. High-resolution record of Northern Hemisphere climate extending into the last interglacial period. Nature, 431(7005), 147-151.

Antoniazza, G., Lane, S.N., 2021. Sediment yield over glacial cycles: a conceptual model. Progress in Physical Geography: Earth and Environment.

Atkinson, P., Jiskoot, H., Massari, R., Murray, T., 1998. Generalized linear modelling in geomorphology. Earth Surface Processes and Landforms, 23(13), 1185-1195.

Baewert, H., Morche, D., 2014. Coarse sediment dynamics in a proglacial fluvial system (Fagge River, Tyrol). Geomorphology, 218, 88-97.

Balco, G., 2020. Technical note: A prototype transparent-middle-layer data management and analysis infrastructure for cosmogenic-nuclide exposure dating. Geochronology, 2(2), 169-175.

Balco, G., Stone, J.O., Lifton, N.A., Dunai, T.J., 2008. A complete and easily accessible means of calculating surface exposure ages or erosion rates from ^{10}Be and 26^{Al} measurements. Quaternary Geochronology, 3(3), 174-195.

Ballantyne, C.K., 2002a. A general model of paraglacial landscape response. Holocene, 12(3), 371-376.

Ballantyne, C.K., 2002b. Paraglacial geomorphology. Quaternary Science Reviews, 21(18-19), 1935-2017.

Ballantyne, C.K., Harris, C., 1994. The Periglaciation of Great Britain. Cambridge University Press, Cambridge.

Barsch, D., Caine, N., 1984. The nature of mountain geomorphology. Mountain Research and Development, 4(4), 287-298.

Berger, A., Mercolli, I.P., Herwegh, M., Gnos, E., 2017. Geological map of the Aar massif, Tavetsch and Gotthard nappe. Geol. Spec. Map 1:100 000, map sheet 129 with explanatory notes. Federal Office of Topography swisstopo.

Beven, K.J., Kirkby, M.J., 1979. A physically based, variable contributing area model of basin hydrology/Un modèle à base physique de zone d'appel variable de l'hydrologie du bassin versant. Hydrological Sciences Journal, 24(1), 43-69.

Bini, A., Buoncristani, J.-F., Couterrand, S., Ellwanger, D., Felber, M., Florineth, D., Graf, H.R., Keller, O., Kelly, M., Schlüchter, C., Schoeneich, P., 2009. Switzerland during the Last Glacial Maximum (LGM) 1:500 000. Federal Office of Topography swisstopo, Wabern.

Binnie, S.A., Dewald, A., Heinze, S., Voronina, E., Hein, A., Wittmann, H., von Blanckenburg, F., Hetzel, R., Christl, M., Schaller, M., 2019. Preliminary results of CoQtz-N: a quartz reference material for terrestrial in-situ cosmogenic ^{10}Be and ^{26}Al measurements. Nuclear Instruments and Methods in Physics Research Section B: Beam Interactions with Materials and Atoms, 456, 203-212.

Bishop, C.M., 1995. Neural Networks for Pattern Recognition. Oxford University Press, Oxford.

Blahut, J., van Westen, C.J., Sterlacchini, S., 2010. Analysis of landslide inventories for accurate prediction of debris-flow source areas. Geomorphology, 119(1-2), 36-51.

Blair, T.C., McPherson, J.G., 2009. Processes and forms of alluvial fans. In: A.J. Parsons, A.D. Abrahams (Eds.), Geomorphology of Desert Environments. Springer, Dordrecht, pp. 413-467.

Blaschke, T., 2010. Object based image analysis for remote sensing. ISPRS Journal of Photogrammetry and Remote Sensing, 65(1), 2-16.

Blöschl, G., Sivapalan, M., 1995. Scale issues in hydrological modeling – a review. Hydrological Processes, 9(3-4), 251-290.

Blöthe, J.H., Korup, O., 2013. Millennial lag times in the Himalayan sediment routing system. Earth and Planetary Science Letters, 382, 38-46.

Blöthe, J.H., Munack, H., Korup, O., Fulling, A., Garzanti, E., Resentini, A., Kubik, P.W., 2014. Late Quaternary valley infill and dissection in the Indus River, Western Tibetan Plateau margin. Quaternary Science Reviews, 94, 102-119.

Bögli, A., 1941. Morphologische Untersuchungen im Goms. Mitteilungen der Naturforschenden Gesellschaft Freiburg (Schweiz), 11(2), 97-159.

Borchers, B., Marreo, S., Balco, G., Caffee, M., Goehring, B., Lifton, N., Nishiizumi, K., Phillips, F., Schaefer, J., Stone, J., 2016: Geological calibration of spallation production rates in the CRONUS-Earth project. Quaternary Geochronology, 31, 188-198.

Borselli, L., Cassi, P., Torri, D., 2008. Prolegomena to sediment and flow connectivity in the landscape: a GIS and field numerical assessment. Catena, 75(3), 268-277.

Bowles, C.J., Cowgill, E., 2012. Discovering marine terraces using airborne LiDAR along the Mendocino-Sonoma coast, Northern California. Geosphere, 8(2), 386-402.

Bowman, D., 2019. Principles of Alluvial Fan Morphology. Springer, Dordrecht.

Brardinoni, F., Grischott, R., Kober, F., Morelli, C., Christl, M., 2020. Evaluating debris-flow and anthropogenic disturbance on ^{10}Be concentration in mountain drainage basins: implications for functional connectivity and denudation rates across time scales. Earth Surface Processes and Landforms, 45(15), 3955-3974.

Brardinoni, F., Hassan, M.A., 2006. Glacial erosion, evolution of river long profiles, and the organization of process domains in mountain drainage basins of coastal British Columbia. Journal of Geophysical Research-Earth Surface, 111(F1).

Brardinoni, F., Picotti, V., Maraio, S., Bruno, P.P., Cucato, M., Morelli, C., Mair, V., 2018. Postglacial evolution of a formerly glaciated valley: reconstructing sediment supply, fan building, and confluence effects at the millennial time scale. Geological Society of America Bulletin, 130(9-10), 1457-1473.

Brenning, A., 2005. Spatial prediction models for landslide hazards: review, comparison and evaluation. Natural Hazards and Earth System Sciences, 5(6), 853-862.

Brenning, A., 2008. Statistical geocomputing combining R and SAGA: the example of landslide susceptibility analysis with generalized additive models. Hamburger Beiträge zur Geographie und Landschaftsökologie, 19, 23-32.

Brenning, A., 2009. Benchmarking classifiers to optimally integrate terrain analysis and multispectral remote sensing in automatic rock glacier detection. Remote Sensing of Environment, 113(1), 239-247.

Brenning, A., 2012. Spatial cross-validation and bootstrap for the assessment of prediction rules in remote sensing: the R package sperrorest, 2012 IEEE International Geoscience and Remote Sensing Symposium, pp. 5372-5375.

Brierley, G., Fryirs, K., Jain, V., 2006. Landscape connectivity: the geographic basis of geomorphic applications. Area, 38(2), 165-174.

Brocklehurst, S.H., Whipple, K.X., 2002. Glacial erosion and relief production in the Eastern Sierra Nevada, California. Geomorphology, 42(1-2), 1-24.

Brocklehurst, S.H., Whipple, K.X., 2004. Hypsometry of glaciated landscapes. Earth Surface Processes and Landforms, 29(7), 907-926.

Brunsden, D., Thornes, J.B., 1979. Landscape sensitivity and change. Transactions of the Institute of British Geographers, 4(4), 463-484.

Buechi, M.W., Kober, F., Ivy-Ochs, S., Salcher, B., Kubik, P.W., Christl, M., 2014. Denudation rates of small transient catchments controlled by former glaciation: the Hornli nunatak in the Northeastern Swiss Alpine Foreland. Quaternary Geochronology, 19, 135-147.

Bull, W.B., 1977. The alluvial-fan environment. Progress in Physical Geography: Earth and Envioronment, 1(2), 222-270.

Burt, T., Allison, R.J., 2010. Sediment Cascades: An Integrated Approach. John Wiley & Sons, Chichester.

Caine, N., 1974. The geomorphic processes of the alpine environment. In: J.D. Ives, R.G. Barry (Eds.), Arctic and Alpine Environments. Methuen, London, pp. 721-748.

Caine, N., Swanson, F., 1989. Geomorphic coupling of hillslope and channel systems in two small mountain basins. Zeitschrift für Geomorphologie, 33(2), 189-203.

Carrivick, J.L., Geilhausen, M., Warburton, J., Dickson, N.E., Carver, S.J., Evans, A.J., Brown, L.E., 2013. Contemporary geomorphological activity throughout the proglacial area of an alpine catchment. Geomorphology, 188, 83-95.

Cassidy, N.J., 2009. Ground penetrating radar data processing, modelling and analysis. In: H.M. Jol (Ed.), Ground Penetrating Radar: Theory and Applications. Elsevier, Amsterdam, pp. 141-176.

Cavalli, M., Heckmann, T., Marchi, L., 2019. Sediment connectivity in proglacial areas. In: T. Heckmann, D. Morche (Eds.), Geomorphology of Proglacial Systems. Landform and Sediment Dynamics in Recently Deglaciated Alpine Landscapes. Springer, Cham, pp. 271-287.

Cavalli, M., Trevisani, S., Comiti, F., Marchi, L., 2013. Geomorphometric assessment of spatial sediment connectivity in small Alpine catchments. Geomorphology, 188, 31-41.

Champagnac, J.D., Molnar, P., Sue, C., Herman, F., 2012. Tectonics, climate, and mountain topography. Journal of Geophysical Research-Solid Earth, 117.

Champagnac, J.D., Schlunegger, F., Norton, K., von Blanckenburg, F., Abbuhl, L.M., Schwab, M., 2009. Erosion-driven uplift of the modern Central Alps. Tectonophysics, 474(1-2), 236-249.

Chander, G., Markham, B.L., Helder, D.L., 2009. Summary of current radiometric calibration coefficients for Landsat MSS, TM, ETM+, and EO-1 ALI sensors. Remote Sensing of Environment, 113(5), 893-903.

Chen, J., Dai, F.C., Yao, X., 2008. Holocene debris-flow deposits and their implications on the climate in the upper Jinsha River valley, China. Geomorphology, 93(3-4), 493-500.

Child, D., Elliott, G., Mifsud, C., Smith, A.M., Fink, D., 2000. Sample processing for earth science studies at ANTARES. Nuclear Instruments & Methods in Physics Research Section B-Beam Interactions with Materials and Atoms, 172, 856-860.

Chmeleff, J., von Blanckenburg, F., Kossert, K., Jakob, D., 2010. Determination of the ^{10}Be half-life by multicollector ICP-MS and liquid scintillation counting. Nuclear Instruments and Methods in Physics Research Section B: Beam Interactions with Materials and Atoms, 268(2), 192-199.

Chorley, R.J., 1962. Geomorphology and General Systems Theory. US Geological Survey Professional Paper, 500-B. US Geological Survey, Washington, DC.

Chorley, R.J., Kennedy, B.A., 1971. Physical Geography: A Systems Approach. Prentice-Hall, London.

Chorley, R.J., Schumm, S.A., Sugden, D.E., 1985. Geomorphology. Methuen, London.

Church, M., 1996. Space, time and the mountain–how do we order what we see? In: B.L. Rhoads, C.E. Thorn (Eds.), The Scientific Nature of Geomorphology: Proceedings of the 27th Binghamton Symposium in Geomorphology. The Binghamton Symposia in Geomorphology. John Wiley & Sons, pp. 147-170.

Church, M., 2010a. Mountains and montane channels. In: T. Burt, R.J. Allison (Eds.), Sediment Cascades: An Integrated Approach. John Wiley & Sons, Chichester, pp. 17-53.

Church, M., 2010b. The trajectory of geomorphology. Progress in Physical Geography-Earth and Environment, 34(3), 265-286.

Church, M., Ryder, J.M., 1972. Paraglacial sedimentation: a consideration of fluvial processes conditioned by glaciation. Geological Society of America Bulletin, 83(10), 3059-3072.

Church, M., Slaymaker, O., 1989. Disequilibrium of Holocene sediment yield in glaciated British Columbia. Nature, 337(6206), 452-454.

Codilean, A.T., 2006. Calculation of the cosmogenic nuclide production topographic shielding scaling factor for large areas using DEMs. Earth Surface Processes and Landforms, 31(6), 785-794.

Codilean, A.T., Munack, H., Cohen, T.J., Saktura, W.M., Gray, A., Mudd, S.M., 2018. OCTOPUS: an open cosmogenic isotope and luminescence database. Earth System Science Data, 10(4), 2123-2139.

Costa, J.E., 1984. Physical geomorphology of debris flows. In: J.E. Costa, P.J. Fleisher (Eds.), Developments and Applications of Geomorphology. Springer, Berlin, pp. 268-317.

Costa, J.E., Schuster, R.L., 1988. The formation and failure of natural dams. Geological Society of America Bulletin, 100(7), 1054-1068.

Crosta, G.B., Frattini, P., 2004. Controls on modern alluvial fan processes in the central Alps, Northern Italy. Earth Surface Processes and Landforms, 29(3), 267-293.

Cruden, D., Hu, X., 1993. Exhaustion and steady state models for predicting landslide hazards in the Canadian Rocky Mountains. Geomorphology, 8(4), 279-285.

Cruden, D.M., Varnes, D.J., 1996. Landslide types and processes. In: A.K. Turner, R.L. Schuster (Eds.), Landslides Investigation and Mitigation. Special Report. Transportation Research Board, US National Research Council, Washington, DC, pp. 36-75.

D'Arcy, M. K., Schildgen, T. F., Turowski, J. M., DiNezio, P., 2019. Inferring the timing of abandonment of aggraded alluvial surfaces dated with cosmogenic nuclides, Earth Surface Dynamics, 7, 755–771.

Davies, T.R., Korup, O., 2010. Sediment cascades in active landscapes. In: T. Burt, R.J. Allison (Eds.), Sediment Cascades: An Integrated Approach. John Wiley & Sons, Chichester, pp. 89-115.

de Boer, D.H., 1992. Hierarchies and spatial scale in process geomorphology – a review. Geomorphology, 4(5), 303-318.

de Boer, D.H., 2001. Self-organization in fluvial landscapes: sediment dynamics as an emergent property. Computers & Geosciences, 27(8), 995-1003.

De Finis, E., Gattinoni, P., Marchi, L., Scesi, L., 2018. Anomalous Alpine fans: from the genesis to the present hazard. Landslides, 15(4), 683-694.

de Vente, J., Poesen, J., Arabkhedri, M., Verstraeten, G., 2007. The sediment delivery problem revisited. Progress in Physical Geography, 31(2), 155-178.

Delunel, R., Schlunegger, F., Valla, P.G., Dixon, J., Glotzbach, C., Hippe, K., Kober, F., Molliex, S., Norton, K.P., Salcher, B., Wittmann, H., Akcar, N., Christl, M., 2020. Late-Pleistocene catchment-wide denudation patterns across the European Alps. Earth-Science Reviews, 211, 103407.

Densmore, A.L., Allen, P.A., Simpson, G., 2007. Development and response of a coupled catchment fan system under changing tectonic and climatic forcing. Journal of Geophysical Research-Earth Surface, 112(F1).

Derbyshire, E., Owen, L.A., 1990. Quaternary alluvial fans in the Karakoram Mountains. In: A.H. Rachoki, M. Chruch (Eds.), Alluvial Fans: A Field Approach. John Wiley & Sons, Chichester, pp. 27-53.

Dielforder, A., Hetzel, R., 2014. The deglaciation history of the Simplon region (Southern Swiss Alps) constrained by ^{10}Be exposure dating of ice-molded bedrock surfaces. Quaternary Science Reviews, 84, 26-38.

Dietrich, A., Krautblatter, M., 2017. Evidence for enhanced debris-flow activity in the Northern Calcareous Alps since the 1980s (Plansee, Austria). Geomorphology, 287, 144-158.

Dietrich, W.E., Dunne, T., Humphrey, N.F., Reid, L.M., 1982. Construction of sediment budgets for drainage basins, Proceedings of the Symposium; 31 May-1 June 1982; Corvallis, Oregon. Gen. Tech. Rep. PNW-141.Pacific Northwest Forest and Range Experiment Station, Forest Service, US Department of Agriculture, pp. 5-23.

Dragut, L., Blaschke, T., 2006. Automated classification of landform elements using object-based image analysis. Geomorphology, 81(3-4), 330-344.

Dramisa, F., Guidab, D., Cestaric, A., 2011. Nature and aims of geomorphological mapping. In: M.J. Smith, P. Paron, J.S. Griffiths (Eds.), Geomorphological Mapping: Methods and Applications. Developments in Earth Surface Processes. Elsevier, Amsterdam, pp. 39-72.

Dühnforth, M., Densmore, A.L., Ivy-Ochs, S., Allen, P.A., Kubik, P.W., 2007. Timing and patterns of debris flow deposition on Shepherd and Symmes creek fans, Owens Valley, California, deduced from cosmogenic ^{10}Be. Journal of Geophysical Research-Earth Surface, 112(F3).

Dunai, T.J., 2010. Cosmogenic Nuclides: Principles, Concepts and Applications in the Earth Surface Sciences. Cambridge University Press, New York.

Dunning, S.A., Rosser, N.J., Petley, D.N., Massey, C.R., 2006. Formation and failure of the Tsatichhu landslide dam, Bhutan. Landslides, 3(2), 107-113.

Ekes, C., Friele, P., 2003. Sedimentary architecture and post-glacial evolution of Cheekye fan, Southwestern British Columbia, Canada. In: C.S. Bristow, H.M. Jol (Eds.), Ground Penetrating Radar in Sediments. Special Publications. Geological Society, London, pp. 87-98.

Evans, I.S., 2006. Allometric development of glacial cirque form: geological, relief and regional effects on the cirques of Wales. Geomorphology, 80(3-4), 245-266.

Fawcett, T., 2006. An introduction to ROC analysis. Pattern Recognition Letters, 27(8), 861-874.

Finckh, P., Frei, W., 1991. Seismic-reflection profiling in the Swiss Rhone Valley: 1. Seismic-reflection field work, seismic processing and seismic results of the Roche-Vouvry and Turtmann and Agarn lines. Eclogae Geologicae Helvetiae, 84(2), 345-357.

Fischer, M., 2013. GLIMS Glacier Database. National Snow and Ice Data Center, Boulder, CO.

Fischer, M., Huss, M., Barboux, C., Hoelzle, M., 2014. The new Swiss Glacier Inventory SGI2010: relevance of using high-resolution source data in areas dominated by very small glaciers. Arctic Antarctic and Alpine Research, 46(4), 933-945.

Florineth, D., Schlüchter, C., 1998. Reconstructing the Last Glacial Maximum (LGM) ice surface geometry and flowlines in the central Swiss Alps. Eclogae Geologicae Helvetiae, 91(3), 391-407.

Franke, D., Hornung, J., Hinderer, M., 2015. A combined study of radar facies, lithofacies and three-dimensional architecture of an alpine alluvial fan (Illgraben fan, Switzerland). Sedimentology, 62(1), 57-86.

Frei, C., 2014. Interpolation of temperature in a mountainous region using nonlinear profiles and non-Euclidean distances. International Journal of Climatology, 34(5), 1585-1605.

Frei, C., Schar, C., 1998. A precipitation climatology of the Alps from high-resolution rain-gauge observations. International Journal of Climatology, 18(8), 873-900.

Fryirs, K., 2013. (Dis)Connectivity in catchment sediment cascades: a fresh look at the sediment delivery problem. Earth Surface Processes and Landforms, 38(1), 30-46.

Fryirs, K.A., Brierley, G.J., Preston, N.J., Kasai, M., 2007. Buffers, barriers and blankets: the (dis)connectivity of catchment-scale sediment cascades. Catena, 70(1), 49-67.

Fujioka, T., Fink, D., Mifsud, C., 2015. Towards improvement of aluminium assay in quartz for in situ cosmogenic ^{26}Al analysis at ANSTO. Nuclear Instruments and Methods in Physics Research Section B: Beam Interactions with Materials and Atoms, 361, 346-353.

Gao, J., 2019. Global population projection grids based on Shared Socioeconomic Pathways (SSPs), downscaled 1-km grids, 2010-2100, National Center for Atmospheric Research, Boulder, CO, USA. NASA Socioeconomic Data and Applications Center (SEDAC), Palisades, NY.

Gemeinde Münster, V., 1992. Münster – Als der Bach kam. Gemeinde Münster VS.

Giles, P.T., 2010. Investigating the use of alluvial fan volume to represent fan size in morphometric studies. Geomorphology, 121(3-4), 317-328.

Glade, T., 2005. Linking debris-flow hazard assessments with geomorphology. Geomorphology, 66(1-4), 189-213.

Goetz, J.N., Brenning, A., Petschko, H., Leopold, P., 2015. Evaluating machine learning and statistical prediction techniques for landslide susceptibility modeling. Computers & Geosciences, 81, 1-11.

Goetz, J.N., Guthrie, R.H., Brenning, A., 2011. Integrating physical and empirical landslide susceptibility models using generalized additive models. Geomorphology, 129(3-4), 376-386.

Gosse, J.C., Phillips, F.M., 2001. Terrestrial in situ cosmogenic nuclides: theory and application. Quaternary Science Reviews, 20(14), 1475-1560.

Götz, J., Otto, J.-C., Schrott, L., 2013. Postglacial sediment storage and rockwall retreat in a semi-closed inner-alpine sedimentary basin (Gradenmoos, Hohe Tauern, Austria). Geografia Fisica e Dinamica Quaternaria, 36, 63-80.

Granger, D.E., Muzikar, P.F., 2001. Dating sediment burial with in situ-produced cosmogenic nuclides: theory, techniques, and limitations. Earth and Planetary Science Letters, 188(1-2), 269-281.

Grove, J.M., 2004. Little Ice Ages: Ancient and Modern, 1. Routledge, London, New York.

Gudmundsson, G., 1994. An order-of-magnitude estimate of the current uplift-rates in Switzerland caused by the Würm Alpine deglaciation. Eclogae Geologicae Helvetiae, 87(2), 545-557.

Guisan, A., Weiss, S.B., Weiss, A.D., 1999. GLM versus CCA spatial modeling of plant species distribution. Plant Ecology, 143(1), 107-122.

Guzzetti, F., Reichenbach, P., Ardizzone, F., Cardinali, M., Galli, M., 2006. Estimating the quality of landslide susceptibility models. Geomorphology, 81(1-2), 166-184.

Haas, J.N., Richoz, I., Tinner, W., Wick, L., 1998. Synchronous Holocene climatic oscillations recorded on the Swiss Plateau and at timberline in the Alps. Holocene, 8(3), 301-309.

Hack, J.T., 1960. Interpretation of erosional topography in humid temperate regions. American Journal of Science, 258-A, 80-97.

Haeberli, W., Hoelzle, M., Paul, F., Zemp, M., 2007. Integrated monitoring of mountain glaciers as key indicators of global climate change: the European Alps. Annals of Glaciology, 46(1), 150-160.

Haeberli, W., Linsbauer, A., Cochachin, A., Salazar, C., Fischer, U.H., 2016. On the morphological characteristics of overdeepenings in high-mountain glacier beds. Earth Surface Processes and Landforms, 41(13), 1980-1990.

Haeberli, W., Rickenmann, D., Zimmermann, M., 1990. Investigation of 1987 debris flows in the Swiss Alps: general concept and geophysical soundings. In: R.O. Sinnige, M. Monbaron (Eds.), Hydrology in Mountainous Regions II Artificial Reservoirs, Water and Slopes. IAHS Publication. IAHS, Lausanne, pp. 303-310.

Hallet, B., Hunter, L., Bogen, J., 1996. Rates of erosion and sediment evacuation by glaciers: a review of field data and their implications. Global and Planetary Change, 12(1-4), 213-235.

Harbor, J., Warburton, J., 1993. Relative rates of glacial and nonglacial erosion in alpine environments. Arctic and Alpine Research, 1-7.

Harvey, A.M., 2011. Dryland alluvial fans. In: D.S.G. Thomas (Ed.), Arid Zone Geomorphology: Process, Form and Change in Drylands. John Wiley & Sons, Chichester, pp. 333-371.

Harvey, A.M., Mather, A.E., Stokes, M. (Eds.), 2005. Alluvial Fans: Geomorphology, Sedimentology, Dynamics. Special Publications, 251. Geological Society.

Harvey, A.M., Wigand, P.E., Wells, S.G., 1999. Response of alluvial fan systems to the late Pleistocene to Holocene climatic transition: contrasts between the margins of pluvial Lakes Lahontan and Mojave, Nevada and California, USA. Catena, 36(4), 255-281.

Harvey, L.D.D., 2000. Upscaling in global change research. Climatic Change, 44(3), 223-223.

Hastie, T., 2015. gam: Generalized Additive Models.

Hastie, T., Tibshirani, R., 1990. Generalized Additive Models. Monographs on Statistics and Applied Probability, 43. Chapman & Hall/CRC, London.

Hastie, T., Tibshirani, R., Friedman, J., 2009. The elements of statistical learning – additive models, trees, and related methods. In: T. Hastie, J. Friedman, R. Tibshirani (Eds.), The Elements of Statistical Learning. Springer Series in Statistics. Springer, New York, pp. 257-298.

Heckmann, T., Gegg, K., Gegg, A., Becht, M., 2014. Sample size matters: investigating the effect of sample size on a logistic regression susceptibility model for debris flows. Natural Hazards and Earth System Sciences, 14(2), 259-278.

Heckmann, T., Hilger, L., Vehling, L., Becht, M., 2016a. Integrating field measurements, a geomorphological map and stochastic modelling to estimate the spatially distributed rockfall sediment budget of the Upper Kaunertal, Austrian Central Alps. Geomorphology, 260, 16-31.

Heckmann, T., McColl, S., Morche, D., 2016b. Retreating ice: research in pro-glacial areas matters. Earth Surface Processes and Landforms, 41(2), 271-276.

Heckmann, T., Morche, D., Becht, M., 2019. Introduction. In: T. Heckmann, D. Morche (Eds.), Geomorphology of Proglacial Systems. Landform and Sediment Dynamics in Recently Deglaciated Alpine Landscapes. Springer, Cham, pp. 1-19.

Heckmann, T., Schwanghart, W., 2013. Geomorphic coupling and sediment connectivity in an alpine catchment – exploring sediment cascades using graph theory. Geomorphology, 182, 89-103.

Heckmann, T., Schwanghart, W., Phillips, J.D., 2015. Graph theory – recent developments of its application in geomorphology. Geomorphology, 243, 130-146.

Hengl, T., Heuvelink, G.B.M., Stein, A., 2004. A generic framework for spatial prediction of soil variables based on regression-kriging. Geoderma, 120(1-2), 75-93.

Hewitt, K., 1992. Mountain hazards. GeoJournal, 27(1), 47-60.

Hewitt, K., 2002a. Introduction: landscape assemblages and transitions in cold regions. In: K. Hewitt, M.-L. Byrne, M. English, G. Young (Eds.), Landscapes of Transition – Landform Assemblages and Transformations in Cold Regions. The GeoJournal Library. Springer, Dordrecht, pp. 1-8.

Hewitt, K., 2002b. Postglacial landform and sediment associations in a landslide-fragmented river system: the Transhimalayan Indus streams, central Asia. In: K. Hewitt, M.-L. Byrne, M. English, G. Young (Eds.), Landscapes of Transition – Landform Assemblages and Transformations in Cold Regions. The GeoJournal Library. Springer, Dordrecht, pp. 63-91.

Hewitt, K., 2004. Geomorphic hazards in mountain environments. In: P.N. Owens, O. Slaymaker (Eds.), Mountain Geomorphology. Arnold, London, pp. 187-218.

Hijmans, R.J., 2014. raster: Geographic data analysis and modeling.

Hilbich, C., Marescot, L., Hauck, C., Loke, M.H., Mäusbacher, R., 2009. Applicability of electrical resistivity tomography monitoring to coarse blocky and ice-rich permafrost landforms. Permafrost and Periglacial Processes, 20(3), 269-284.

Hilger, L., Beylich, A.A., 2019. Sediment budgets in high-mountain areas: review and challenges. In: T. Heckmann, D. Morche (Eds.), Geomorphology of Proglacial Systems. Landform and Sediment Dynamics in Recently Deglaciated Alpine Landscapes. Geography of the Physical Environment. Springer, Cham, pp. 251-269.

Hilger, L., Dusik, J.-M., Heckmann, T., Haas, F., Glira, P., Pfeifer, N., Vehling, L., Rohn, J., Morche, D., Baewert, H., 2019. A sediment budget of the Upper Kaunertal. In: T. Heckmann, D. Morche (Eds.), Geomorphology of Proglacial Systems. Landform and Sediment Dynamics in Recently Deglaciated Alpine Landscapes. Springer, Cham, pp. 289-312.

Hilger, P., Hermanns, R.L., Gosse, J.C., Jacobs, B., Etzelmuller, B., Krautblatter, M., 2018. Multiple rock-slope failures from Mannen in Romsdal Valley, western Norway, revealed from Quaternary geological mapping and ^{10}Be exposure dating. Holocene, 28(12), 1841-1854.

Hinderer, M., 2001. Late Quaternary denudation of the Alps, valley and lake fillings and modern river loads. Geodinamica Acta, 14(4), 231-263.

Hinderer, M., 2012. From gullies to mountain belts: a review of sediment budgets at various scales. Sedimentary Geology, 280, 21-59.

Hinderer, M., Kastowski, M., Kamelger, A., Bartolini, C., Schlunegger, F., 2013. River loads and modern denudation of the Alps – a review. Earth-Science Reviews, 118, 11-44.

Hock, R., Rasul, G., Adler, C., Cáceres, B., Gruber, S., Hirabayashi, Y., Jackson, M., Kääb, A., Kang, S., Kutuzov, S., 2019. High mountain areas. In: H.-O. Pörtner, D.C. Roberts, V. Masson-Delmotte, P. Zhai, M. Tignor, E. Poloczanska, K. Mintenbeck, A. Alegría, M. Nicolai, A. Okem, J. Petzold, B.

Rama, N.M. Weyer (Eds.), IPCC Special Report on the Ocean and Cryosphere in a Changing Climate, pp. 131-202.

Hoffmann, T., 2015. Sediment residence time and connectivity in non-equilibrium and transient geomorphic systems. Earth-Science Reviews, 150, 609-627.

Hoffmann, T., Müller, T., Johnson, E.A., Martin, Y.E., 2013. Postglacial adjustment of steep, low-order drainage basins, Canadian Rocky Mountains. Journal of Geophysical Research-Earth Surface, 118(4), 2568-2584.

Hoffmann, T., Schrott, L., 2002. Modelling sediment thickness and rockwall retreat in an Alpine valley using 2D-seismic refraction (Reintal, Bavarian Alps). Zeitschrift für Geomorphologie Supplementband, 153-173.

Hoffmann, U., Hoffmann, T., Jurasinski, G., Glatzel, S., Kuhn, N.J., 2014. Assessing the spatial variability of soil organic carbon stocks in an alpine setting (Grindelwald, Swiss Alps). Geoderma, 232, 270-283.

Hollander, M., Wolfe, D.A., Chicken, E., 1999. Nonparametric Statistical Methods. Wiley Series in Probability and Statistics. John Wiley & Sons, Hoboken.

Hooke, R.L., 1968. Steady-state relationships on arid-region alluvial fans in closed basins. American Journal of Science, 266(8), 609-629.

Hooke, R.L., 1991. Positive feedbacks associated with erosion of glacial cirques and overdeepenings. Geological Society of America Bulletin, 103(8), 1104-1108.

Hornung, J., Pflanz, D., Hechler, A., Beer, A., Hinderer, M., Maisch, M., Bieg, U., 2010. 3-D architecture, depositional patterns and climate triggered sediment fluxes of an alpine alluvial fan (Samedan, Switzerland). Geomorphology, 115(3-4), 202-214.

Hosmer, D.W., Lemeshow, S., Sturdivant, R.X., 2013. Applied Logistic Regression. Wiley Series in Probability and Statistics. John Wiley & Sons, New York.

Huss, M., Bookhagen, B., Huggel, C., Jacobsen, D., Bradley, R.S., Clague, J.J., Vuille, M., Buytaert, W., Cayan, D.R., Greenwood, G., Mark, B.G., Millner, A.M., Weingartner, R., Winder, M., 2017. Toward mountains without permanent snow and ice. Earth's Future, 5, 1-18.

Ivy-Ochs, S., Dühnforth, M., Densmore, A.L., Alfimov, V., 2013. Dating fan deposits with cosmogenic nuclides. In: M. Schneuwly-Bollschweiler, M. Stoffel, F. Rudolf-Miklau (Eds.), Dating Torrential Processes on Fans and Cones: Methods and their Application for Hazard and Risk Assessment Advances in Global Change Research. Springer, Dordrecht, pp. 243-263.

Ivy-Ochs, S., Kerschner, H., Kubik, P.W., Schlüchter, C., 2006a. Glacier response in the European Alps to Heinrich Event 1 cooling: the Gschnitz stadial. Journal of Quaternary Science, 21(2), 115-130.

Ivy-Ochs, S., Kerschner, H., Maisch, M., Christl, M., Kubik, P.W., Schlüchter, C., 2009a. Latest Pleistocene and Holocene glacier variations in the European Alps. Quaternary Science Reviews, 28(21-22), 2137-2149.

Ivy-Ochs, S., Kerschner, H., Reuther, A., Maisch, M., Sailer, R., Schäfer, J., Kubik, P.W., Synal, H.-A., Schlüchter, C., 2006b. The timing of glacier advances in the northern European Alps based on surface exposure dating with cosmogenic ^{10}Be, ^{26}Al, ^{36}Cl, and ^{21}Ne. Geological Society of America Special Papers, 415, 43-60.

Ivy-Ochs, S., Kerschner, H., Reuther, A., Preusser, F., Heine, K., Maisch, M., Kubik, P.W., Schlüchter, C., 2008. Chronology of the last glacial cycle in the European Alps. Journal of Quaternary Science, 23(6-7), 559-573.

Ivy-Ochs, S., Kober, F., 2008. Surface exposure dating with cosmogenic nuclides. Quaternary Science Journal, 57(1-2), 179-209.

Ivy-Ochs, S., Poschinger, A.V., Synal, H.A., Maisch, M., 2009b. Surface exposure dating of the Flims landslide, Graubünden, Switzerland. Geomorphology, 103(1), 104-112.

Ivy-Ochs, S., Schäfer, J., Kubik, P.W., Synal, H.A., Schluchter, C., 2004. Timing of deglaciation on the Northern Alpine foreland (Switzerland). Eclogae Geologicae Helvetiae, 97(1), 47-55.

Jaboyedoff, M., Derron, M.-H., 2005. A new method to estimate the infilling of alluvial sediment of glacial valleys using a sloping local base level. Geografia Fisica e Dinamica Quaternaria, 28(1), 37-46.

Jäckli, H., 1957. Gegenwartsgeologie des bündnerischen Rheingebietes: ein Beitrag zur exogenen Dynamik alpiner Gebirgslandschaften. Beiträge zur Geologie der Schweiz, 36. Kümmerly & Frey, Bern.

James, G., Witten, D., Hastie, T., Tibshirani, R., 2013. An Introduction to Statistical Learning: With Applications in R. Springer Texts in Statistics, 6. Springer, New York.

Jarman, D., Agliardi, F., Crosta, G.B., 2011. Megafans and outsize fans from catastrophic slope failures in Alpine glacial troughs: the Malser Haide and the Val Venosta cluster, Italy. In: M. Jaboyedoff (Ed.), Slope Tectonics. Geological Society. Special Publications, London, pp. 253-277.

Joerin, U.E., Stocker, T.F., Schlüchter, C., 2006. Multicentury glacier fluctuations in the Swiss Alps during the Holocene. Holocene, 16(5), 697-704.

Jol, H.M., Bristow, C.S., 2003. GPR in sediments: advice on data collection, basic processing and interpretation, a good practice guide. In: C.S. Bristow, H.M. Jol (Eds.), Ground Penetrating Radar in Sediments. Special Publications. Geological Society, London, pp. 9-27.

Jones, B., O'Neill, B.C., 2016. Spatially explicit global population scenarios consistent with the Shared Socioeconomic Pathways. Environmental Research Letters, 11(8).

Jordan, P., Slaymaker, O., 1991. Holocene sediment production in Lillooet River basin, British Colombia: a sediment budget approach. Géographie physique et Quaternaire, 45(1), 45-57.

Jull, A.J.T., Scott, E.M., Bierman, P., 2015. The CRONUS-Earth inter-comparison for cosmogenic isotope analysis. Quaternary Geochronology, 26, 3-10.

Kahle, H.G., Geiger, A., Bürki, B., Gubler, E., Marti, U., Wirth, B., Rothacher, M., Gurtner, W., Beutler, G., Bauersima, I., 1997. Recent crustal movements, geoid and density distribution: contribution from integrated satellite and terrestrial measurements. Results of the National Research Program, 20, 251-259.

Kaiser, H.F., 1958. The varimax criterion for analytic rotation in factor-analysis. Psychometrika, 23(3), 187-200.

Kelly, M.A., Buoncristiani, J.F., Schlüchter, C., 2004. A reconstruction of the Last Glacial Maximum (LGM) ice-surface geometry in the Western Swiss Alps and contiguous Alpine regions in Italy and France. Eclogae Geologicae Helvetiae, 97(1), 57-75.

Kelly, M.A., Ivy-Ochs, S., Kubik, P.W., von Blanckenburg, F., Schlüchter, C., 2006. Chronology of deglaciation based on ^{10}Be dates of glacial erosional features in the Grimsel Pass region, central Swiss Alps. Boreas, 35(4), 634-643.

Kirchner, J.W., Finkel, R.C., Riebe, C.S., Granger, D.E., Clayton, J.L., King, J.G., Megahan, W.F., 2001. Mountain erosion over 10 yr, 10 k.y., and 10 m.y. time scales. Geology, 29(7), 591-594.

Klingseisen, B., Metternicht, G., Paulus, G., 2008. Geomorphometric landscape analysis using a semi-automated GIS-approach. Environmental Modelling & Software, 23(1), 109-121.

Knapp, S., Mamot, P., Lempe, B., Krautblatter, M., 2021. Impact of an 0.2 km^3 rock avalanche on Lake Eibsee (Bavarian Alps, Germany) – Part I: reconstruction of the paleolake and effects of the impact. Earth Surface Processes and Landforms, 46(1), 296-306.

Kneisel, C., Hauck, C., 2008. Electrical methods. In: C. Hauck, C. Kneisel (Eds.), Applied Geophysics in Periglacial Environments. Cambridge University Press, Cambridge.

Knight, J., Harrison, S., 2014. Mountain glacial and paraglacial environments under global climate change: lessons from the past, future directions and policy implications. Geografiska Annaler Series A, Physical Geography, 96(3), 245-264.

Knödel, K., Krummel, H., Lange, G., 2005. Handbuch zur Erkundung des Untergrundes von Deponien und Altlasten – Band 3: Geophysik. Springer, Berlin.

Kober, F., Hippe, K., Salcher, B., Grischott, R., Zurfluh, R., Hajdas, I., Wacker, L., Christl, M., Ivy-Ochs, S., 2019. Postglacial to Holocene landscape evolution and process rates in steep alpine catchments. Earth Surface Processes and Landforms, 44(1), 242-258.

Kohl, C., Nishiizumi, K., 1992. Chemical isolation of quartz for measurement of in-situ-produced cosmogenic nuclides. Geochimica Et Cosmochimica Acta, 56(9), 3583-3587.

Korschinek, G., Bergmaier, A., Faestermann, T., Gerstmann, U.C., Knie, K., Rugel, G., Wallner, A., Dillmann, I., Dollinger, G., Gostomski, v., C.L., Kossert, K., Maiti, M., Poutivtsev, M., Remmert, A., 2010. A new value for the half-life of ^{10}Be by heavy-ion elastic recoil detection and liquid scintillation counting. Nuclear Instruments and Methods in Physics Research Section B: Beam Interactions with Materials and Atoms, 268(2), 187-191.

Korup, O., 2012. Earth's portfolio of extreme sediment transport events. Earth-Science Reviews, 112(3-4), 115-125.

Korup, O., Schlunegger, F., 2007. Bedrock landsliding, river incision, and transience of geomorphic hillslope-channel coupling: evidence from inner gorges in the Swiss Alps. Journal of Geophysical Research-Earth Surface, 112(F3).

Kraal, E.R., Asphaug, E., Moore, J.M., Howard, A., Bredt, A., 2008. Catalogue of large alluvial fans in martian impact craters. Icarus, 194(1), 101-110.

Kühni, A., Pfiffner, O.A., 2001. The relief of the Swiss Alps and adjacent areas and its relation to lithology and structure: topographic analysis from a 250-m DEM. Geomorphology, 41(4), 285-307.

Kummu, M., Varis, O., 2007. Sediment-related impacts due to upstream reservoir trapping, the Lower Mekong River. Geomorphology, 85(3-4), 275-293.

Labhart, T.P., 1977. Aarmassiv und Gotthardmassiv. Sammlung Geologischer Führer, 63. Gebr. Bornträger, Berlin.

Lambiel, C., Maillard, B., Kummert, M., Reynard, E., 2016. Geomorphology of the Hérens valley (Swiss Alps). Journal of Maps, 12(1), 160-172.

Lane, S.N., Bakker, M., Gabbud, C., Micheletti, N., Saugy, J.N., 2017. Sediment export, transient landscape response and catchment-scale connectivity following rapid climate warming and Alpine glacier recession. Geomorphology, 277, 210-227.

Lang, A., Moya, J., Corominas, J., Schrott, L., Dikau, R., 1999. Classic and new dating methods for assessing the temporal occurrence of mass movements. Geomorphology, 30(1-2), 33-52.

Lang, N., Wolff, E.W., 2011. Interglacial and glacial variability from the last 800 ka in marine, ice and terrestrial archives. Climate of the Past, 7(2), 361-380.

Lecce, S.A., 1990. The alluvial fan problem. In: A.H. Rachocki, M. Church (Eds.), Alluvial Fans: A Field Approach. John Wiley & Sons, Chichester, pp. 3-24.

Lecce, S. A. 1991. Influence of lithologic erodibility on alluvial fan area, western White Mountains, California and Nevada. Earth Surface Processes and Landforms, 16(1), 11-18.

Lenzi, M.A., Mao, L., Comiti, F., 2003. Interannual variation of suspended sediment load and sediment yield in an alpine catchment. Hydrological Sciences Journal-Journal Des Sciences Hydrologiques, 48(6), 899-915.

Lifton, N., Sato, T., Dunai, T.J., 2014. Scaling in situ cosmogenic nuclide production rates using analytical approximations to atmospheric cosmic-ray fluxes. Earth and Planetary Science Letters, 386, 149-160.

Lisiecki, L.E., Raymo, M.E., 2005. A Pliocene-Pleistocene stack of 57 globally distributed benthic $\delta^{18}O$ records. Paleoceanography, 20(1).

Loke, M.H., 2017. RES2DINVx64 ver. 4.07 with multicore and 64-bit support for Windows XP/Vista/7/8/10. Rapid 2-D Resistivity & IP inversion using the least-squares method. Geotomo Software.

Loke, M.H., Acworth, I., Dahlin, T., 2003. A comparison of smooth and blocky inversion methods in 2D electrical imaging surveys. Exploration Geophysics, 34(3), 182-187.

Loke, M.H., Barker, R.D., 1995. Least-squares deconvolution of apparent resistivity pseudosections. Geophysics, 60(6), 1682-1690.

Loke, M.H., Barker, R.D., 1996. Rapid least-squares inversion of apparent resistivity pseudosections by a quasi-Newton method. Geophysical Prospecting, 44(1), 131-152.

Loke, M.H., Dahlin, T., 2002. A comparison of the Gauss-Newton and quasi-Newton methods in resistivity imaging inversion. Journal of Applied Geophysics, 49(3), 149-162.

Luoto, M., Hjort, J., 2004. Generalized linear modelling in periglacial studies: terrain parameters and patterned ground. Permafrost and Periglacial Processes, 15(4), 327-338.

Luoto, M., Hjort, J., 2005. Evaluation of current statistical approaches for predictive geomorphological mapping. Geomorphology, 67(3-4), 299-315.

Maisch, M., 1987. Zur Gletscher- und Klimageschichte des alpinen Spätglazials: Analyse und Interpretation von Schneegrenzdaten. Geographica Helvetica, 42, 63-71.

Maisch, M., 2000. Die Gletscher der Schweizer Alpen: Gletscherhochstand 1850, aktuelle Vergletscherung, Gletscherschwund-Szenarien. vdf, Zürich.

Maisch, M., Haeberli, W., Hoelzle, M., Wenzel, J., 1999. Occurrence of rocky and sedimentary glacier beds in the Swiss Alps as estimated from glacier-inventory data. Annals of Glaciology, 28(1), 231-235.

Mann, M.E., 2002. Little Ice Age. In: M.C. MacCracken, J.S. Perry (Eds.), Encyclopedia of Global Environmental Change, Volume 1, The Earth System: Physical and Chemical Dimensions of Global Environmental Change. Encyclopedia of Global Environmental Change. John Wiley & Sons, Chichester, pp. 504-509.

Marescot, L., Loke, M.H., Chapellier, D., Delaloye, R., Lambiel, C., Reynard, E., 2003. Assessing reliability of 2D resistivity imaging in mountain permafrost studies using the depth of investigation index method. Near Surface Geophysics, 1(2), 57-67.

Marmion, M., Hjort, J., Thuiller, W., Luoto, M., 2008. A comparison of predictive methods in modelling the distribution of periglacial landforms in Finnish Lapland. Earth Surface Processes and Landforms, 33(14), 2241-2254.

McArdell, B.W., Hirschberg, J., 2020. Debris-flow volumes at the Illgraben 2000-2017. EnviDat.

McColl, S.T., 2012. Paraglacial rock-slope stability. Geomorphology, 153, 1-16.

Mellett, C.L., 2013. Luminescence dating. In: S.J. Cook, L.E. Clarke, J.M. Nield (Eds.), Geomorphological Techniques (Online Edition). British Society for Geomorphology, London.

Messenzehl, K., Hoffmann, T., Dikau, R., 2014. Sediment connectivity in the high-alpine valley of Val Muschauns, Swiss National Park – linking geomorphic field mapping with geomorphometric modelling. Geomorphology, 221, 215-229.

Messenzehl, K., Meyer, H., Otto, J.-C., Hoffmann, T., Dikau, R., 2017. Regional-scale controls on the spatial activity of rockfalls (Turtmann Valley, Swiss Alps) – a multivariate modeling approach. Geomorphology, 287, 29-45.

Mey, J., Scherler, D., Wickert, A.D., Egholm, D.L., Tesauro, M., Schildgen, T.F., Strecker, M.R., 2016. Glacial isostatic uplift of the European Alps. Nature Communications, 7.

Mey, J., Scherler, D., Zeilinger, G., Strecker, M.R., 2015. Estimating the fill thickness and bedrock topography in intermontane valleys using artificial neural networks. Journal of Geophysical Research-Earth Surface, 120(7), 1301-1320.

Meybeck, M., Green, P., Vörösmarty, C., 2001. A new typology for mountains and other relief classes: an application to global continental water resources and population distribution. Mountain Research and Development, 21(1), 34-45.

Milliman, J.D., Syvitski, J.P.M., 1992. Geomorphic/tectonic control of sediment discharge to the ocean: the importance of small mountainous rivers. The Journal of Geology, 525-544.

Milsom, J., 2003. Field Geophysics. The Geological Field Guide Series. John Wiley & Sons, Chichester.

Mitchum, R.M., Vail, R.R., Sangree, J.B., 1977. Stratigraphic interpretation of seismic reflection patterns in depositional sequences. In: C.E. Payton (Ed.), Seismic Stratigraphy – Applications to Hydrocarbon Exploration. American Association of Petroleum Geologists, Tulsa, pp. 117-134.

Molnar, P., 2009. The state of interactions among tectonics, erosion, and climate: a polemic. GSA Today, 19(7), 44-45.

Molnar, P., England, P., 1990. Late Cenozoic uplift of mountain ranges and global climate change: chicken or egg? Nature, 346, 29-34.

Montgomery, D.R., 2002. Valley formation by fluvial and glacial erosion. Geology, 30(11), 1047-1050.

Moore, J.M., Howard, A.D., 2005. Large alluvial fans on Mars. Journal of Geophysical Research-Planets, 110(E4).

Moore, R.D., Fleming, S.W., Menounos, B., Wheate, R., Fountain, A., Stahl, K., Holm, K., Jakob, M., 2009. Glacier change in Western North America: influences on hydrology, geomorphic hazards and water quality. Hydrological Processes, 23(1), 42-61.

Neal, A., 2004. Ground-penetrating radar and its use in sedimentology: principles, problems and progress. Earth-Science Reviews, 66(3-4), 261-330.

Nicolussi, K., Kaufmann, M., Melvin, T.M., van der Plicht, J., Schiessling, P., Thurner, A., 2009. A 9111 year long conifer tree-ring chronology for the European Alps: a base for environmental and climatic investigations. Holocene, 19(6), 909-920.

Nishiizumi, K., 2004. Preparation of ^{26}Al AMS standards. Nuclear Instruments and Methods in Physics Research Section B: Beam Interactions with Materials and Atoms, 223, 388-392.

Nishiizumi, K., Imamura, M., Caffee, M.W., Southon, J.R., Finkel, R.C., McAninch, J., 2007. Absolute calibration of ^{10}Be AMS standards. Nuclear Instruments and Methods in Physics Research Section B: Beam Interactions with Materials and Atoms, 258(2), 403-413.

Nishiizumi, K., Kohl, C.P., Arnold, J.R., Dorn, R., Klein, I., Fink, D., Middleton, R., Lal, D., 1993. Role of in situ cosmogenic nuclides ^{10}Be and ^{26}Al in the study of diverse geomorphic processes. Earth Surface Processes and Landforms, 18(5), 407-425.

Norton, K.P., Abbuhl, L.M., Schlunegger, F., 2010a. Glacial conditioning as an erosional driving force in the Central Alps. Geology, 38(7), 655-658.

Norton, K.P., von Blanckenburg, F., Kubik, P.W., 2010b. Cosmogenic nuclide-derived rates of diffusive and episodic erosion in the glacially sculpted upper Rhone Valley, Swiss Alps. Earth Surface Processes and Landforms, 35(6), 651-662.

Nussbaumer, S.U., Steinhilber, F., Trachsel, M., Breitenmoser, P., Beer, J., Blass, A., Grosjean, M., Hafner, A., Holzhauser, H., Wanner, H., Zumbuhl, H.J., 2011. Alpine climate during the Holocene: a comparison between records of glaciers, lake sediments and solar activity. Journal of Quaternary Science, 26(7), 703-713.

Nyenhuis, M., 2006. Permafrost und Sedimenthaushalt in einem alpinen Geosystem. Bonner Geographische Abhandlungen, 116. Asgard-Verlag, Sankt Augustin.

O'Callaghan, J.F., Mark, D.M., 1984. The extraction of drainage networks from digital elevation data. Computer Vision Graphics and Image Processing, 28(3), 323-344.

Oldenburg, D.W., Li, Y.G., 1999. Estimating depth of investigation in DC resistivity and IP surveys. Geophysics, 64(2), 403-416.

Otto, J.-C., 2006. Paraglacial Sediment Storage Quantification in the Turtmann Valley, Swiss Alps. PhD thesis, University of Bonn, Bonn.

Otto, J.-C., Dikau, R., 2004. Geomorphologic system analysis of a high mountain valley in the Swiss Alps. Zeitschrift für Geomorphologie, 48(3), 323-341.

Otto, J.-C., Götz, J., Schrott, L., 2008. Sediment storage in Alpine sedimentary systems – quantification and scaling issues, Sediment Dynamics in Changing Environments – 2008 Symposium of the International Commission on Continental Erosion. IAHS Publication, Christchurch, pp. 258-265.

Otto, J.-C., Prasicek, G., Blöthe, J., Schrott, L., 2018. GIS applications in geomorphology. In: B. Huang (Ed.), Comprehensive Geographic Information Systems. Elsevier, Amsterdam, pp. 81-111.

Otto, J.-C., Sass, O., 2006. Comparing geophysical methods for talus slope investigations in the Turtmann Valley (Swiss Alps). Geomorphology, 76(3-4), 257-272.

Otto, J.-C., Schrott, L., Jaboyedoff, M., Dikau, R., 2009. Quantifying sediment storage in a high alpine valley (Turtmanntal, Switzerland). Earth Surface Processes and Landforms, 34(13), 1726-1742.

Otto, J.-C., Smith, M.J., 2013. Geomorphological mapping. In: S.J. Cook, L.E. Clarke, J.M. Nield (Eds.), Geomorphological Techniques (Online Edition). British Society for Geomorphology, London.

Penck, A., 1905. Glacial features in the surface of the Alps. The Journal of Geology, 13(1), 1-19.

Persaud, M., Pfiffner, O.A., 2004. Active deformation in the eastern Swiss Alps: post-glacial faults, seismicity and surface uplift. Tectonophysics, 385(1-4), 59-84.

Petschko, H., Bell, R., Glade, T., Brenning, A., 2012. Landslide susceptibility modeling with generalized additive models – facing the heterogeneity of large regions. In: E. Eberhardt, C. Froese, K. Turner, S. Leroueil (Eds.), Landslides and Engineered Slopes: Protecting Society through Improved Understanding. CRC Press London, pp. 769-775.

Petschko, H., Brenning, A., Bell, R., Goetz, J., Glade, T., 2014. Assessing the quality of landslide susceptibility maps – case study Lower Austria. Natural Hazards and Earth System Sciences, 14(1), 95-118.

Pfiffner, O.A., 2021. The geology of Switzerland. In: E. Reynard (Ed.), Landscapes and Landforms of Switzerland. World Geomorphological Landscapes. Springer, Cham, pp. 7-30.

Pfiffner, O.A., Heitzmann, P., Lehner, P., Frei, W., Pugin, A., Felber, M., 1997. Incision and Backfilling of Alpine Valleys: Pliocene, Pleistocene and Holocene Processes. Deep Structure of the Swiss Alps: results of NRP, 20, 265-288.

Phartiyal, B., Sharma, A., Upadhyay, R., Ram-Awatar, Sinha, A.K., 2005. Quaternary geology, tectonics and distribution of palaeo- and present fluvio/glacio lacustrine deposits in Ladakh, NW Indian Himalaya – a study based on field observations. Geomorphology, 65(3-4), 241-256.

Phillips, J.D., 1986. Sediment storage, sediment yield, and time scales in landscape denudation studies. Geographical Analysis, 18(2), 161-167.

Phillips, J.D., 1991. Fluvial sediment budgets in the North Carolina Piedmont. Geomorphology, 4(3), 231-241.

Phillips, J.D., 1992. The End of Equilibrium. Geomorphology, 5(3-5), 195-201.

Phillips, J.D., 1999. Earth Surface Systems: Complexity, Order, and Scale. The Natural Environment. Blackwell, Malden.

Phillips, J.D., 2001. Contingency and generalization in pedology, as exemplified by texture-contrast soils. Geoderma, 102(3-4), 347-370.

Phillips, J.D., 2003a. Alluvial storage and the long-term stability of sediment yields. Basin Research, 15(2), 153-163.

Phillips, J.D., 2003b. Sources of nonlinearity and complexity in geomorphic systems. Progress in Physical Geography, 27(1), 1-23.

Phillips, J.D., 2011. Emergence and pseudo-equilibrium in geomorphology. Geomorphology, 132(3-4), 319-326.

Prasicek, G., Otto, J.-C., Montgomery, D.R., Schrott, L., 2014. Multi-scale curvature for automated identification of glaciated mountain landscapes. Geomorphology, 209, 53-65.

Preusser, F., Blei, A., Graf, H., Schluchter, C., 2007. Luminescence dating of Wurmian (Weichselian) proglacial sediments from Switzerland: methodological aspects and stratigraphical conclusions. Boreas, 36(2), 130-142.

Preusser, F., Reitner, J.M., Schlüchter, C., 2010. Distribution, geometry, age and origin of overdeepened valleys and basins in the Alps and their foreland. Swiss Journal of Geosciences, 103(3), 407-426.

Radebaugh, J., Lorenz, R.D., Farr, T.G., Kirk, R.L., Lunine, J.I., Ventra, D., Le Gall, A., Lopes, R.M.C., Barnes, J.W., Hayes, A.G., 2013. Alluvial fans on Titan reveal materials, processes and regional conditions, 44th Lunar and Planetary Science Conference. Lunar Planetary Institute.

Rapp, A., 1960. Recent development of mountain slopes in Kärkevagge and surroundings, Northern Scandinavia. Geografiska Annaler, 42(2-3), 65-200.

Rasemann, S., 2004. Geomorphometrische Struktur eines mesoskaligen alpinen Geosystems. Bonner Geographische Abhandlungen, 111. Asgard-Verlag, Sankt Augustin.

Ratnayaka, K., Hetzel, R., Hornung, J., Hampel, A., Hinderer, M., Frechen, M., 2019. Postglacial alluvial fan dynamics in the Cordillera Oriental, Peru, and palaeoclimatic implications. Quaternary Research, 91(1), 431-449.

Raymo, M.E., Ruddiman, W.F., 1992. Tectonic forcing of Late Cenozoic climate. Nature, 359(6391), 117-122.

Reid, L.M., Dunne, T., 1996. Rapid Evaluation of Sediment Budgets, GeoEcology paperback. Catena, Reiskirchen.

Revelle, W., 2015. psych: Procedures for Personality and Psychological Research. Northwestern University, Evanston.

Reynolds, J.M., 1997. An Introduction to Applied and Environmental Geophysics. John Wiley & Sons, Chichester.

RGI-Consortium, 2017. Randolph Glacier Inventory – A Dataset of Global Glacier Outlines: Version 6.0: Technical Report, Global Land Ice Measurements from Space, Colorado.

Rosselli, A., Olivier, R., 2003. Modélisation gravimétrique 2.5 D et cartes des isohypses au 1: 100'000 du substratum rocheux de la Vallée du Rhône entre Villeneuve et Brig (Suisse). Eclogae Geologicae Helvetiae, 96(1), 399-423.

Sass, O., 2006. Determination of the internal structure of alpine talus deposits using different geophysical methods (Lechtaler Alps, Austria). Geomorphology, 80(1-2), 45-58.

Sass, O., 2007. Bedrock detection and talus thickness assessment in the European Alps using geophysical methods. Journal of Applied Geophysics, 62(3), 254-269.

Sass, O., Krautblatter, M., 2007. Debris flow-dominated and rockfall-dominated talus slopes: genetic models derived from GPR measurements. Geomorphology, 86(1-2), 176-192.

Savi, S., Tofelde, S., Wickert, A.D., Bufe, A., Schildgen, T.F., Strecker, M.R., 2020. Interactions between main channels and tributary alluvial fans: channel adjustments and sediment-signal propagation. Earth Surface Dynamics, 8(2), 303-322.

Schlatter, A., Schneider, D., Geiger, A., Kahle, H.G., 2005. Recent vertical movements from precise levelling in the vicinity of the city of Basel, Switzerland. International Journal of Earth Sciences, 94(4), 507-514.

Schlüchter, C., 1988. The deglaciation of the Swiss Alps: a paleoclimatic event with chronological problems. Quaternaire, 25(2-3), 141-145.

Schlüchter, C., 2004a. The Swiss glacial record – a schematic summary. In: J. Ehlers, P.L. Gibbard (Eds.), Quaternary Glaciations Extent and Chronology Part I: Europe. Developments in Quaternary Sciences. Elsevier, Amsterdam, pp. 413-418.

Schlüchter, C., 2004b. The Swiss glacial record: a schematic summary. In: J. Ehlers, P.L. Gibbard (Eds.), Quaternary Glaciations – Extent and Chronology. Part I: Europe. Developments in Quaternary Science. Elsevier, Amsterdam, pp. 413-418.

Schlüchter, C., Akçar, N., Ivy-Ochs, S., 2021. The Quaternary period in Switzerland. In: E. Reynard (Ed.), Landscapes and Landforms of Switzerland. World Geomorphological Landscapes. Springer, Cham, pp. 47-69.

Schlummer, M., Hoffmann, T., Dikau, R., Eickmeier, M., Fischer, P., Gerlach, R., Holzkamper, J., Kalis, A.J., Kretschmer, I., Lauer, F., Maier, A., Meesenburg, J., Meurers-Balke, J., Munch, U., Patzold, S., Steininger, F., Stobbe, A., Zimmermann, A., 2014. From point to area: upscaling approaches for Late Quaternary archaeological and environmental data. Earth-Science Reviews, 131, 22-48.

Schlunegger, F., Badoux, A., McArdell, B.W., Gwerder, C., Schnydrig, D., Rieke-Zapp, D., Molnar, P., 2009. Limits of sediment transfer in an alpine debris-flow catchment, Illgraben, Switzerland. Quaternary Science Reviews, 28(11-12), 1097-1105.

Schlunegger, F., Hinderer, M., 2003. Pleistocene/Holocene climate change, re-establishment of fluvial drainage network and increase in relief in the Swiss Alps. Terra Nova, 15(2), 88-95.

Schlunegger, F., Norton, K.P., 2013. Water versus ice: the competing roles of modern climate and Pleistocene glacial erosion in the Central Alps of Switzerland. Tectonophysics, 602, 370-381.

Schmid, S.M., Fügenschuh, B., Kissling, E., Schuster, R., 2004. Tectonic map and overall architecture of the Alpine orogen. Eclogae Geologicae Helvetiae, 97(1), 93-117.

Schneevoigt, N.J., van der Linden, S., Thamm, H.P., Schrott, L., 2008. Detecting Alpine landforms from remotely sensed imagery. A pilot study in the Bavarian Alps. Geomorphology, 93(1-2), 104-119.

Schoch, A., Blöthe, J.H., Hoffmann, T., Schrott, L., 2018. Multivariate geostatistical modeling of the spatial sediment distribution in a large scale drainage basin, Upper Rhone, Switzerland. Geomorphology, 303, 375-392.

Schoch-Baumann, A., Blöthe, J. H., Munack, H., Hornung, J., Codilean, A. T., Fülöp, R.-H., & Schrott, L., 2022. Postglacial outsize fan formation in the Upper Rhone Valley, Switzerland – gradual or catastrophic?. Earth Surface Processes and Landforms, 47(4), 1032-1053.

Schön, J.H., 2004. Physical properties of rocks: fundamentals and principles of petrophysics. Handbook of geophysical exploration. Elsevier, Amsterdam.

Schrott, L., Adams, T., 2002. Quantifying sediment storage and Holocene denudation in an Alpine basin, Dolomites, Italy. Zeitschrift für Geomorphologie Supplementband, 129-145.

Schrott, L., Hufschmidt, G., Hankammer, M., Hoffmann, T., Dikau, R., 2003. Spatial distribution of sediment storage types and quantification of valley fill deposits in an alpine basin, Reintal, Bavarian Alps, Germany. Geomorphology, 55(1), 45-63.

Schrott, L., Niederheide, A., Hankammer, M., Hufschmidt, G., Dikau, R., 2002. Sediment storage in a mountain catchment: geomorphic coupling and temporal variability (Reintal, Bvarian Alps, Germany). Zeitschrift für Geomorphologie Supplementband, 127, 175-196.

Schrott, L., Sass, O., 2008. Application of field geophysics in geomorphology: advances and limitations exemplified by case studies. Geomorphology, 93(1-2), 55-73.

Schumm, S.A., 1977. The Fluvial System. John Wiley & Sons, New York.

Schumm, S.A., 1991. To Interpret the Earth: Ten Ways to be Wrong. Cambridge University Press, Cambridge.

Schürch, P., Densmore, A.L., Ivy-Ochs, S., Rosser, N.J., Kober, F., Schlunegger, F., McArdell, B., Alfimov, V., 2016. Quantitative reconstruction of late Holocene surface evolution on an alpine debris-flow fan. Geomorphology, 275, 46-57.

Schwanghart, W., Bernhardt, A., Stolle, A., Hoelzmann, P., Adhikari, B.R., Andermann, C., Tofelde, S., Merchel, S., Rugel, G., Fort, M., Korup, O., 2016. Repeated catastrophic valley infill following medieval earthquakes in the Nepal Himalaya. Science, 351(6269), 147-150.

Schwarb, M., 2000. The Alpine Precipitation Climate: Evaluation of a High-resolution Analysis Scheme Using Comprehensive Rain-gauge Data. PhD thesis, ETH Zürich, Zürich.

Schwarb, M., Daly, C., Frei, C., Schär, C., 2001. Mean annual and seasonal precipitation in the European Alps 1971–1990, Hydrological Atlas of Switzerland.

Seijmonsbergen, A.C., Hengl, T., Anders, N.S., 2011. Semi-automated identification and extraction of geomorphological features using digital elevation data. In: M.J. Smith, P. Paron, J.S. Griffiths (Eds.), Geomorphological Mapping: Methods and Applications. Developments in Earth Surface Processes. Elsevier, Amsterdam, pp. 297-335.

Silhan, K., Panek, T., 2010. Fossil and recent debris flows in medium-high mountains (Moravskoslezske Beskydy Mts, Czech Republic). Geomorphology, 124(3-4), 238-249.

Sing, T., Sander, O., Beerenwinkel, N., Lengauer, T., 2005. ROCR: visualizing classifier performance in R. Bioinformatics, 21(20), 3940-3941.

Slaymaker, O., 1991. Mountain geomorphology: a theoretical framework for measurement programmes. Catena, 18(5), 427-437.

Slaymaker, O., 2003. The sediment budget as conceptual framework and management tool. Hydrobiologia, 494(1-3), 71-82.

Slaymaker, O., 2006. Towards the identification of scaling relations in drainage basin sediment budgets. Geomorphology, 80(1-2), 8-19.

Slaymaker, O., 2009. Proglacial, periglacial or paraglacial? In: J. Knight, S. Harrison (Eds.), Periglacial and Paraglacial Processes and Environments. Special Publications. The Geological Society, London, pp. 71-84.

Small, E.E., Anderson, R.S., 1998. Pleistocene relief production in Laramide mountain ranges, Western United States. Geology, 26(2), 123-126.

Smith, M.J., Paron, P., Griffiths, J.S., 2011. Geomorphological Mapping: Methods and Applications. Developments in Earth Surface Processes, 15. Elsevier, Amsterdam.

Steger, S., Bell, R., Petschko, H., Glade, T., 2015. Evaluating the effect of modelling methods and landslide inventories used for statistical susceptibility modelling. In: G. Lollino, D. Giordan, G.B. Crosta, J. Corominas, R. Azzam, J. Wasowski, N. Sciarra (Eds.), Engineering Geology for Society and Territory. Springer, Cham, pp. 201-204.

Steger, S., Brenning, A., Bell, R., Petschko, H., Glade, T., 2016. Exploring discrepancies between quantitative validation results and the geomorphic plausibility of statistical landslide susceptibility maps. Geomorphology, 262, 8-23.

Sternai, P., Herman, F., Fox, M.R., Castelltort, S., 2011. Hypsometric analysis to identify spatially variable glacial erosion. Journal of Geophysical Research-Earth Surface, 116.

Stoffel, M., Mendlik, T., Schneuwly-Bollschweiler, M., Gobiet, A., 2014. Possible impacts of climate change on debris-flow activity in the Swiss Alps. Climatic Change, 122, 141-155.

Stokes, S., 1999. Luminescence dating applications in geomorphological research. Geomorphology, 29(1-2), 153-171.

Stolle, A., Langer, M., Blothe, J.H., Korup, O., 2015. On predicting debris flows in arid mountain belts. Global and Planetary Change, 126, 1-13.

Straumann, R.K., Korup, O., 2009. Quantifying postglacial sediment storage at the mountain-belt scale. Geology, 37(12), 1079-1082.

Stutenbecker, L., Delunel, R., Schlunegger, F., Silva, T.A., Segvic, B., Girardclos, S., Bakker, M., Costa, A., Lane, S.N., Loizeau, J.L., Molnar, P., Akcar, N., Christl, M., 2018. Reduced sediment supply in a fast eroding landscape? A multi-proxy sediment budget of the upper Rhone basin, Central Alps. Sedimentary Geology, 375, 105-119.

swisstopo, 2005. Geologic Map of Switzerland 1:500 000. Federal Office of Topography swisstopo.

swisstopo, 2011. Tectonic Map of Switzerland 1:500 000. Federal Office of Topography swisstopo.

swisstopo, 2013. GeoCover – Geologische Vektordaten 1:25 000, map sheet 1250 Ulrichen. Federal Office of Topography swisstopo.

Syvitski, J.P.M., Milliman, J.D., 2007. Geology, geography, and humans battle for dominance over the delivery of fluvial sediment to the coastal ocean. Journal of Geology, 115(1), 1-19.

Tarolli, P., 2014. High-resolution topography for understanding Earth surface processes: opportunities and challenges. Geomorphology, 216, 295-312.

Telford, W.M., Geldart, L.P., Sheriff, R.E., 1990. Applied Geophysics. Cambridge University Press, Cambridge.

Theler, D., Reynard, E., Lambiel, C., Bardou, E., 2010. The contribution of geomorphological mapping to sediment transfer evaluation in small alpine catchments. Geomorphology, 124(3-4), 113-123.

Thorn, C.E., 1988. An Introduction to Theoretical Geomorphology. Unwin Hyman, Boston.

Tinner, W., Theurillat, J.P., 2003. Uppermost limit, extent, and fluctuations of the timberline and treeline ecocline in the Swiss Central Alps during the past 11,500 years. Arctic Antarctic and Alpine Research, 35(2), 158-169.

Tonini, M., Pedrazzini, A., Penna, I., Jaboyedoff, M., 2014. Spatial pattern of landslides in Swiss Rhone Valley. Natural Hazards, 73(1), 97-110.

Tunnicliffe, J., Church, M., Clague, J.J., Feathers, J.K., 2012. Postglacial sediment budget of Chilliwack Valley, British Columbia. Earth Surface Processes and Landforms, 37(12), 1243-1262.

Tunnicliffe, J.F., Church, M., 2011. Scale variation of post-glacial sediment yield in Chilliwack Valley, British Columbia. Earth Surface Processes and Landforms, 36(2), 229-243.

Valla, P.G., Shuster, D.L., van der Beek, P.A., 2011. Significant increase in relief of the European Alps during mid-Pleistocene glaciations. Nature Geoscience, 4(10), 688-692.

Valla, P.G., van der Beek, P.A., Carcaillet, J., 2010a. Dating bedrock gorge incision in the French Western Alps (Ecrins-Pelvoux massif) using cosmogenic ^{10}Be. Terra Nova, 22(1), 18-25.

Valla, P.G., van der Beek, P.A., Lague, D., 2010b. Fluvial incision into bedrock: Insights from morphometric analysis and numerical modeling of gorges incising glacial hanging valleys (Western Alps, France). Journal of Geophysical Research-Earth Surface, 115.

van Asselen, S., Seijmonsbergen, A.C., 2006. Expert-driven semi-automated geomorphological mapping for a mountainous area using a laser DTM. Geomorphology, 78(3-4), 309-320.

van den Berg, F., Schlunegger, F., Akcar, N., Kubik, P., 2012. ^{10}Be-derived assessment of accelerated erosion in a glacially conditioned inner gorge, Entlebuch, Central Alps of Switzerland. Earth Surface Processes and Landforms, 37(11), 1176-1188.

van der Knaap, W.O., van Leeuwen, J.F.N., Fankhauser, A., Ammann, B., 2000. Palynostratigraphy of the last centuries in Switzerland based on 23 lake and mire deposits: chronostratigraphic pollen markers, regional patterns, and local histories. Review of Palaeobotany and Palynology, 108(1-2), 85-142.

Vernon, A.J., van der Beek, P.A., Sinclair, H.D., Rahn, M.K., 2008. Increase in late Neogene denudation of the European Alps confirmed by analysis of a fission-track thermochronology database. Earth and Planetary Science Letters, 270(3-4), 316-329.

Vogelmann, J.E., Howard, S.M., Yang, L.M., Larson, C.R., Wylie, B.K., Van Driel, N., 2001. Completion of the 1990s National Land Cover Dataset for the conterminous United States from Landsat Thematic Mapper data and ancillary data sources. Photogrammetric Engineering and Remote Sensing, 67(6), 650-662.

von Blanckenburg, F., Belshaw, N.S., O'Nions, R.K., 1996. Separation of ^{9}Be and cosmogenic ^{10}Be from environmental materials and SIMS isotope dilution analysis. Chemical Geology, 129(1-2), 93-99.

von Grafenstein, U., Erlenkeuser, H., Brauer, A., Jouzel, J., Johnsen, S.J., 1999. A mid-European decadal isotope-climate record from 15,500 to 5000 years BP. Science, 284(5420), 1654-1657.

Vörösmarty, C.J., Meybeck, M., Fekete, B., Sharma, K., Green, P., Syvitski, J.P.M., 2003. Anthropogenic sediment retention: major global impact from registered river impoundments. Global and Planetary Change, 39(1-2), 169-190.

Wainwright, J., Mulligan, M., 2004. Environmental Modelling: Finding Simplicity in Complexity. John Wiley & Sons, Chichester.

Walker, M., 2005. Quaternary Dating Methods. John Wiley & Sons, Chichester.

Walling, D.E., 1983. The sediment delivery problem. Journal of Hydrology, 65(1-3), 209-237.

Weiss, A.D., 2000. Topographic position and landforms analysis. Poster Presentation, ESRI Users Conference, San Diego, CA.

Welten, M., 1982. Vegetationsgeschichtliche Untersuchungen in den westlichen Schweizer Alpen: Bern-Wallis. Denkschriften der Schweizerischen Naturforschenden Gesellschaft, 95.

Whipple, K.X., 2009. The influence of climate on the tectonic evolution of mountain belts. Nature Geoscience, 2(2), 97-104.

Whipple, K.X., Kirby, E., Brocklehurst, S.H., 1999. Geomorphic limits to climate-induced increases in topographic relief. Nature, 401(6748), 39-43.

Wilcken, K.M., Fujioka, T., Fink, D., Fulop, R.H., Codilean, A.T., Simon, K., Mifsud, C., Kotevski, S., 2019. SIRIUS Performance: ^{10}Be, ^{26}Al and ^{36}Cl measurements at ANSTO. Nuclear Instruments & Methods in Physics Research Section B-Beam Interactions with Materials and Atoms, 455, 300-304.

Winkler, S., Bell, D., Hemmingsen, M., Pedley, K., & Schoch, A., 2018. Disestablishing “Glacial Lake Speight”, New Zealand? An example for the validity of detailed geomorphological assessment with the study of mountain glaciations. E&G Quaternary Science Journal, 67(1), 25-31.

Wittmann, H., von Blanckenburg, F., Kruesmann, T., Norton, K.P., Kubik, P.W., 2007. Relation between rock uplift and denudation from cosmogenic nuclides in river sediment in the Central Alps of Switzerland. Journal of Geophysical Research-Earth Surface, 112(F4).

Wolman, M.G., Miller, J.P., 1960. Magnitude and frequency of forces in geomorphic processes. Journal of Geology, 68(1), 54-74.

Zemp, M., Frey, H., Gartner-Roer, I., Nussbaumer, S.U., Hoelzle, M., Paul, F., Haeberli, W., Denzinger, F., Ahlstrom, A.P., Anderson, B., Bajracharya, S., Baroni, C., Braun, L.N., Caceres, B.E., Casassa, G., Cobos, G., Davila, L.R., Granados, H.D., Demuth, M.N., Espizua, L., Fischer, A., Fujita, K., Gadek, B., Ghazanfar, A., Hagen, J.O., Holmlund, P., Karimi, N., Li, Z.Q., Pelto, M., Pitte, P., Popovnin, V.V., Portocarrero, C.A., Prinz, R., Sangewar, C.V., Severskiy, I., Sigurosson, O., Soruco, A., Usubaliev, R., Vincent, C., 2015. Historically unprecedented global glacier decline in the early 21st century. Journal of Glaciology, 61(228), 745-762.

Zemp, M., Kääb, A., Hoelzle, M., Haeberli, W., 2005. GIS-based modelling of glacial sediment balance. Zeitschrift für Geomorphologie Supplementband, 138, 113-129.

Zemp, M., Paul, F., Hoelze, M., Haeberli, W., 2008. Glacier fluctuations in the European Alps, 1850–2000. In: B. Orlove, E. Wiegandt, B.H. Luckman (Eds.), Darkening Peaks – Glacier Retreat, Science, and Society. University of California Press, Berkeley, pp. 152-167.

Zhang, X., Drake, N.A., Wainwright, J., 2004. Scaling issues in environmental modelling. In: J. Wainwright, M. Mulligan (Eds.), Environmental Modelling: Finding Simplicity in Complexity. John Wiley & Sons, London, pp. 319-334.

Zimmermann, M., Haeberli, W., 1993. Climatic change and debris flow activity in high-mountain areas- a case study in the Swiss Alps. Catena Supplement, 22, 59-59.

Zweck, C., Zreda, M., Desilets, D., 2013. Snow shielding factors for cosmogenic nuclide dating inferred from Monte Carlo neutron transport simulations. Earth and Planetary Science Letters, 379, 64-71.

Appendix

A Supplementary material for chapter 5: Postglacial outsize fan formation in the Upper Rhone valley, Switzerland – gradual or catastrophic?

B Supplementary material for chapter 7: Multivariate geostatistical modeling of the spatial sediment distribution in a large scale drainage basin, Upper Rhone, Switzerland

List of Figures and Tables in Appendix

A. Supplementary material for chapter 5: Postglacial outsize fan formation in the Upper Rhone valley, Switzerland – gradual or catastrophic?

The tables and figures in the supplement are referred to in the corresponding chapter.

Underlying geology of GOF #3 and its catchment

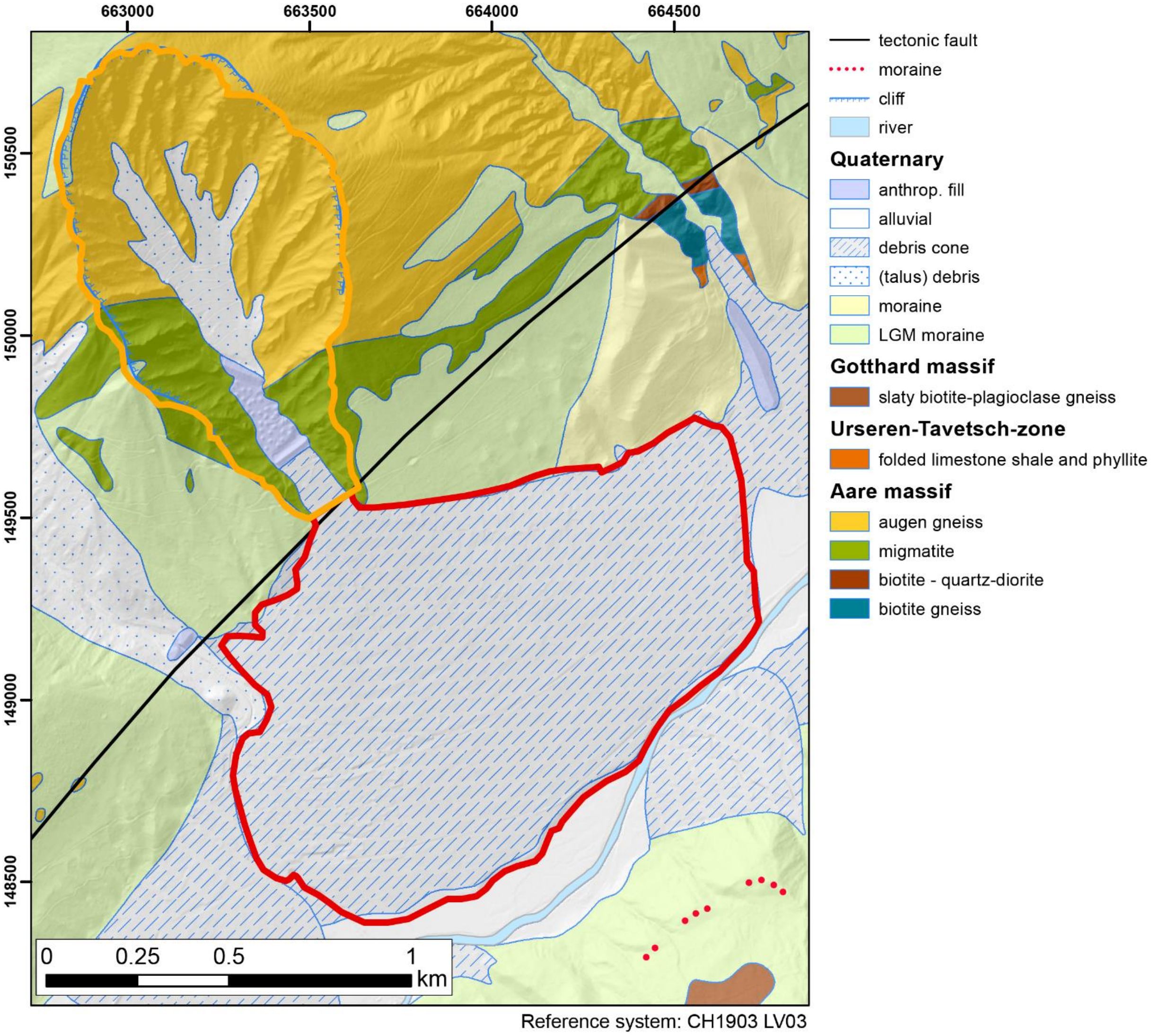

Figure A: Geologic map of GOF #3 and source area (swisstopo, 2011; swisstopo, 2013) (swisstopo DEM, EPSG:21781).

Geophysical surveying

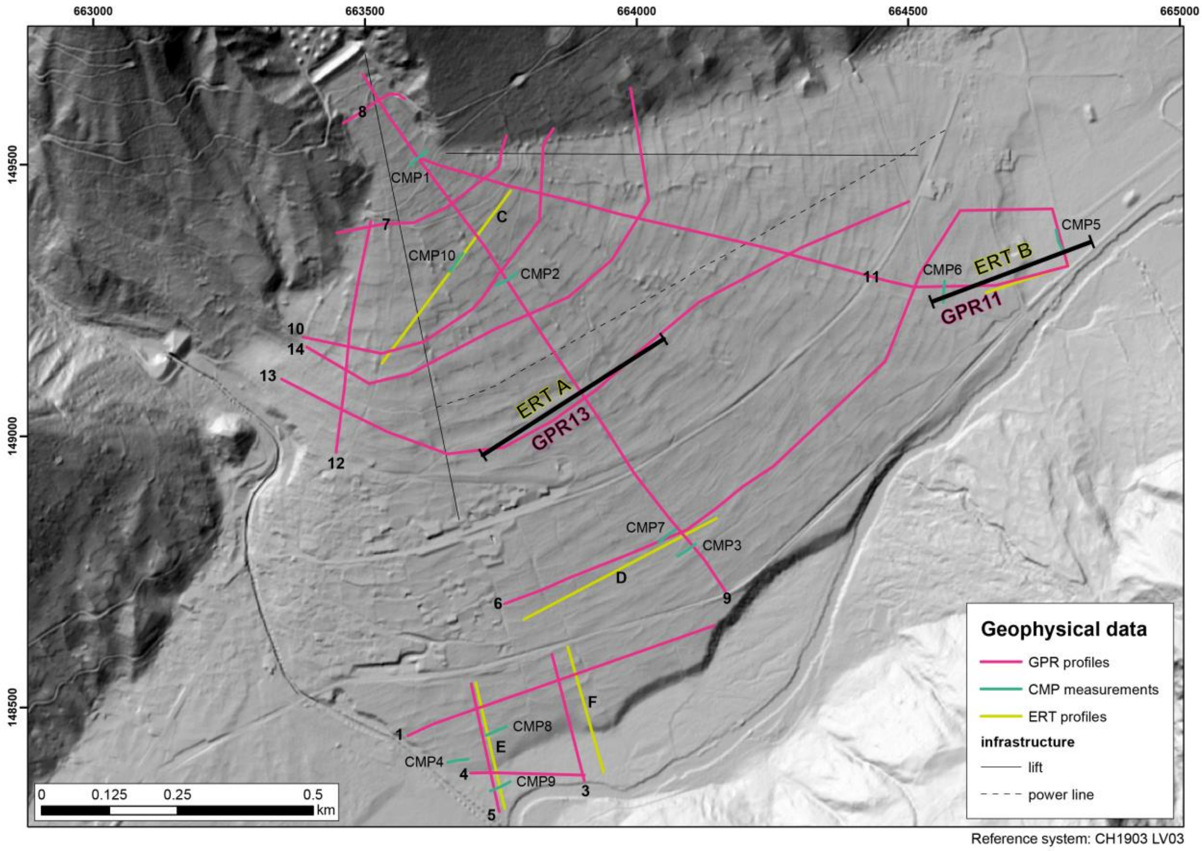

Figure B: Surface of GOF #3 with the location of GPR and ERT transects in pink and yellow, respectively. Common midpoint (CMP) measurents shown in green. Transects shown in the paper are highlighted (swisstopo DEM, EPSG:21781).

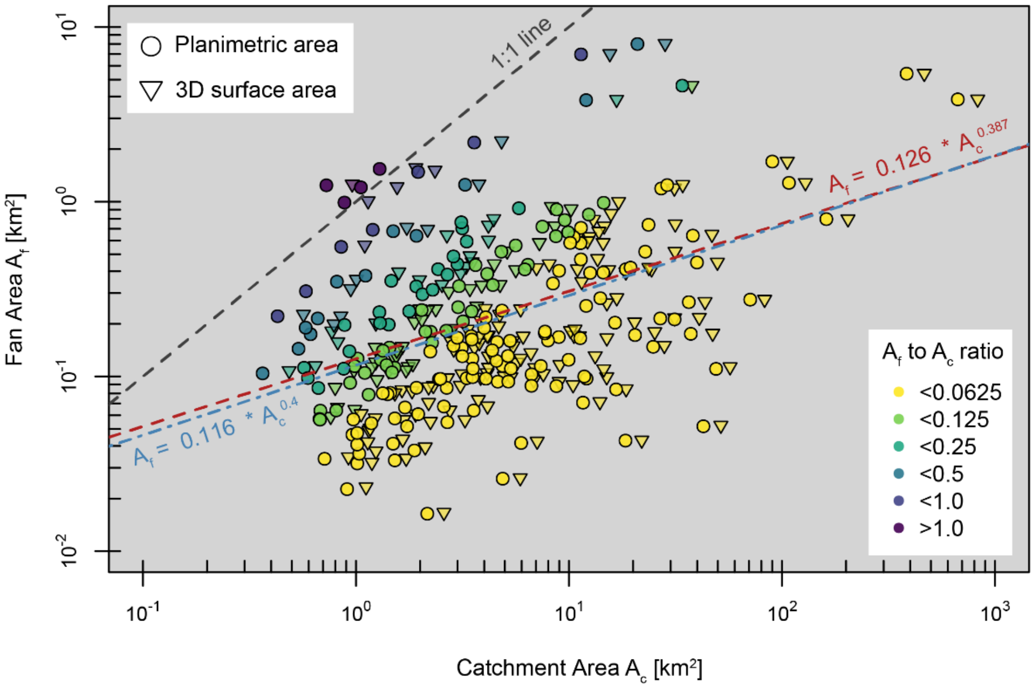

Figure C: Log-log plot of fan area versus catchment area for 186 fans located in the Upper Rhone catchment. Circles indicate planimetric, triangles show 3D surface areas of fan and catchment areas, respectively, color-coded to their fan-to-catchment area ratio. Regression lines and formulas are shown in red and blue for the planimetric and 3D surface areas, respectively. Grey dashed line shows 1:1 line (see Figure 6-8 for map showing the locations of all mapped fans).

Ground penetrating radar

Table D: Overview of measured ground penetrating radar (GPR) profiles on GOF #3.

Profile	Length [m]	Orientation & description	SIR & Antenna	SIR & Antenna (2)
#1	600	cross profile, lowermost fan	SIR3000, 40 MHz	
#3	241	long profile, distal fan & valley fill fluvial	SIR3000, 40 MHz	
#4	210	cross profile, valley fill fluvial	SIR3000, 40 MHz	
#5	241	long profile, distal fan & valley fill fluvial	SIR3000, 40 MHz	
#6	1322	cross profile, lower fan, incl. distal fan and valley fill fluvial	SIR3000, 40 MHz	
#7	390	cross profile, uppermost fan	SIR3000, 40 MHz	
#8	131	cross profile, apex	SIR3000, 40 MHz	SIR4000, 100 MHz
#9	1164	long profile center	SIR4000, 40 MHz	SIR3000, 100 MHz
#10	716	cross profile center	SIR4000, 40 MHz	SIR3000, 100 MHz
#11	1231	long profile left, incl. distal fan and valley fill fluvial	SIR4000, 40 MHz	SIR3000, 100 MHz
#12	430	long profile right	SIR4000, 40 MHz	SIR3000, 200 MHz
#13	1318	cross profile center	SIR4000, 40 MHz	SIR3000, 200 MHz
#14	978	cross profile center	SIR4000, 40 MHz	
CMP1	40	uppermost fan	SIR4000, 40 MHz	
CMP2	40	center fan	SIR4000, 40 MHz	
CMP3	40	lower fan	SIR4000, 40 MHz	
CMP4	40	Distal/lowermost fan	SIR4000, 40 MHz	
CMP5	40	valley fill (upstream of fan)	SIR4000, 40 MHz	
CMP6	40	lower fan	SIR4000, 40 MHz	
CMP7	40	lower fan	SIR4000, 40 MHz	
CMP8	40	lower fan	SIR4000, 40 MHz	
CMP9	40	valley fill (downstream of fan)	SIR4000, 40 MHz	
CMP10	40	upper fan	SIR3000, 40 MHz	

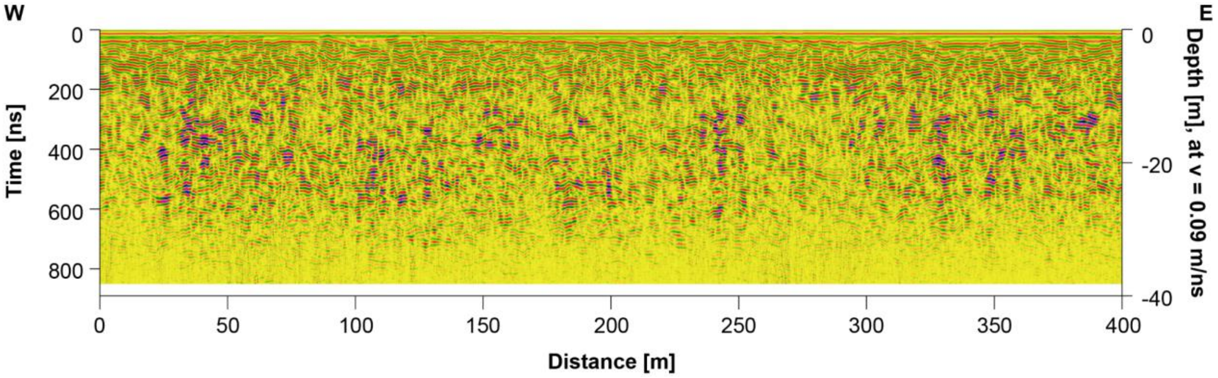

Figure E: GPR profile #13 measured with a 40 MHz antenna in the center of GOF #3 without marks (see Figure B for location).

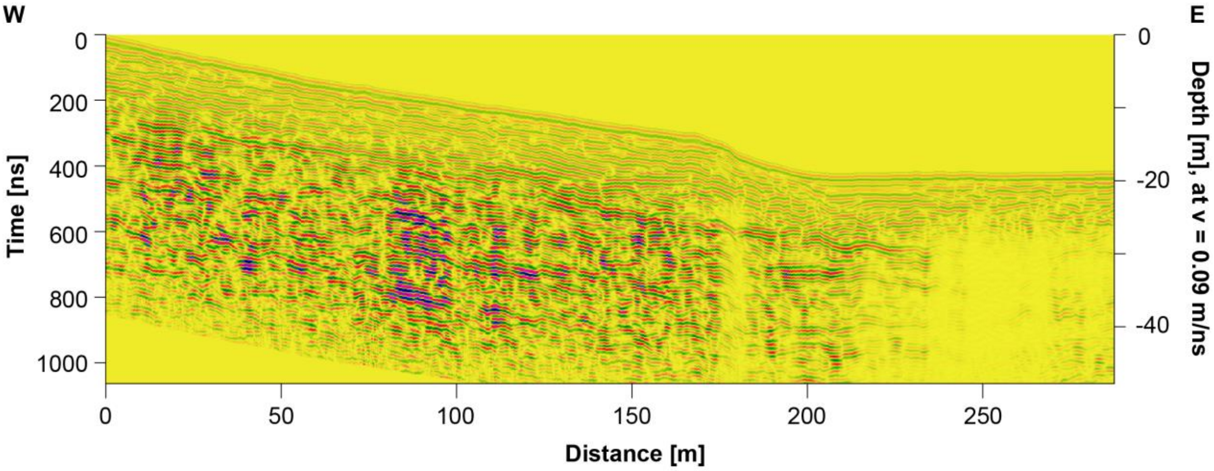

Figure F: GPR profile #11 measured with a 40 MHz antenna at the interface between GOF #3 and fluvial deposit of the Rhone without marks (see Figure B for location).

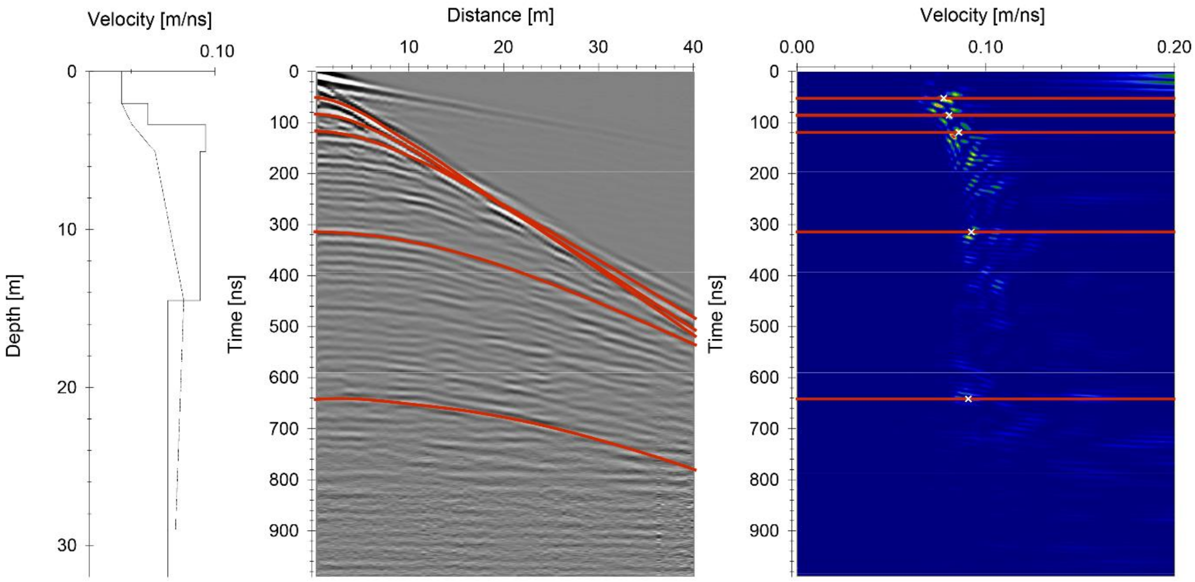

Figure G: CMP1 on the uppermost GOF #3 (see Figure B for location).

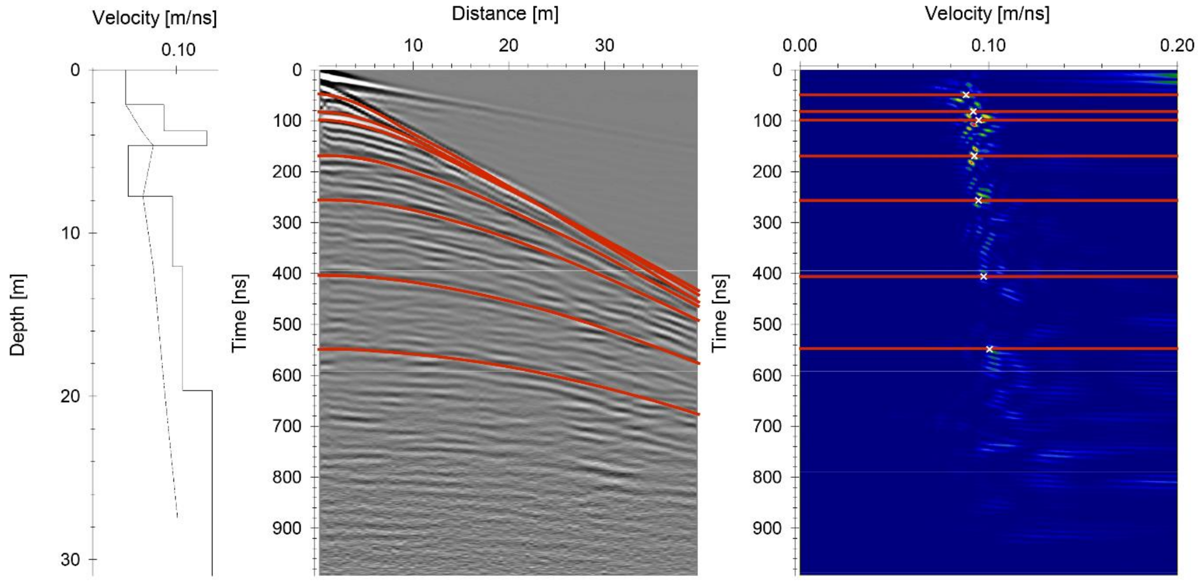

Figure H: CMP2 on the center GOF #3 (see Figure B for location).

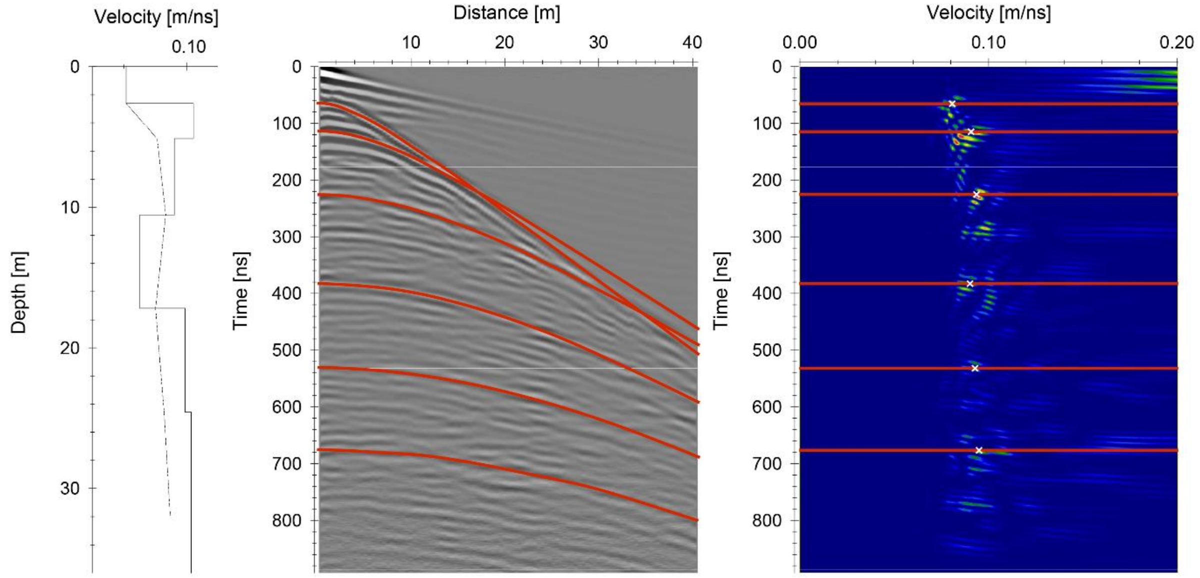

Figure I: CMP3 on the lower GOF #3 (see Figure B for location).

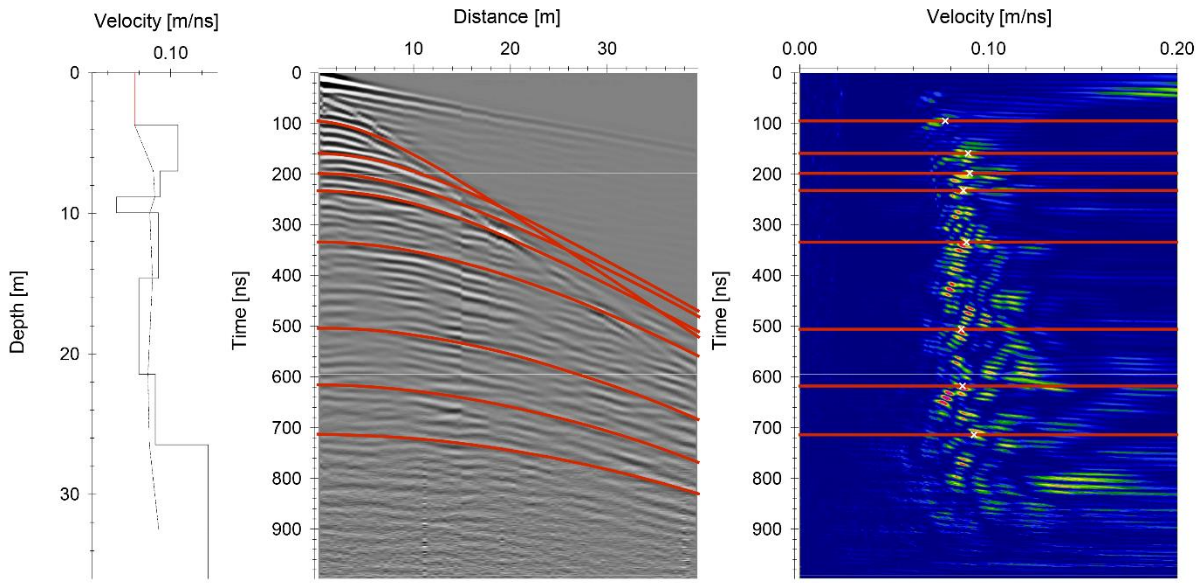

Figure J: CMP4 on the distal/lowermost GOF #3 (see Figure B for location).

Table K: Processing sequences for the different combinations of antennas and control units performed with ReflexW (Sandmeier Scientific).

SIR 3000, 40 MHz (automated, preprocessed data)	**SIR 3000, 200 MHz (automated, preprocessed data)**	**SIR 4000, 40 MHz (raw data)**	**CMP (SIR 4000, 40 MHz) (raw data)**
Remove header gain	Remove header gain	Move start time	Move start time
Move start time	Move start time	Dewow	Dewow
Editing (e.g. insert profiles)	Editing (e.g. insert profiles)	Energy decay	Energy decay
Energy decay	Kirchhoff 2D-velocity	Average xy-filter	
Average xy-filter	Energy decay	Bandpass butterworth filter (upper: 10; lower: 80)	
Bandpass butterworth filter (upper: 10; lower: 80)	Average xy-filter	Editing (XFlip profile)	
Subtracting average	Bandpass butterworth filter (upper: 400; lower: 40)	Correct 3D topography	
Editing (XFlip profile)	Editing (XFlip profile)	Time cut	
Correct 3D topography	Correct 3D topography	Editing (remove)	
Time cut	Time cut		
Editing (remove)	Editing (remove)		

Electrical Resistivity tomography

Table L: Overview of measured electrical resistivity tomography (ERT) profiles GOF #3.

Profile	Position [m]	Array	Spacing [m]	RMS error [%]	# of iterations	Orig. # of data points	Final # of data points	Filtered data points [%]	Orientation & description
A	0-400	Wenner	5	7.1	5	437	418	4.35%	cross profile, center fan
B	0-160	Gradient	2	4.5	5	960	928	3.33%	long profile, distal fan & valley fill fluvial
B	40-120	Gradient	1	3.7	5	883	856	3.06%	long profile, distal fan & valley fill fluvial
B	0-320	Gradient	4	6.5	5	995	886	10.95%	long profile, distal fan & valley fill fluvial
C	0-400	Wenner	5	7.6	5	432	382	11.57%	cross profile, upper fan
C	120-280	Wenner	2	11.1	5	445	421	5.39%	cross profile, upper fan
D	0-400	Wenner	5	8.5	5	445	426	4.27%	cross profile, lower fan
E	0-240	Gradient	3	3.7	5	1072	980	8.58%	long profile, distal fan & valley fill fluvial
E	50-130	Wenner	1	10.9	5	433	402	7.16%	long profile, distal fan & valley fill fluvial
F	0-240	Wenner	3	11.2	5	445	419	5.84%	long profile, distal fan & valley fill fluvial
F	50-130	Wenner	1	10.1	5	445	418	6.07%	long profile, distal fan & valley fill fluvial

Depth of investigation

A challenge for the interpretation of ERT results are high resistivity contrasts between materials, which makes inversion and interpretation difficult and problematic (Marescot et al., 2003). We use the depth of investigation index (DOI) to identify unreliable resistivity areas in the model, which are not confined by the measured data, and to avoid over-interpretation (Oldenburg and Li, 1999). To calculate the DOI, two inversions of the same data set with two different reference models with homogeneous resistivity values are performed.

$$DOI\ (x,z) = \frac{m_1\ (x,z) - \ m_2\ (x,z)}{DOI_{max}\ (m_{01} - \ m_{02})} \tag{6}$$

m1 and m2 are model cell resistivities obtained from the first and second inversion and m01 and m02 are the resistivities of the first and second reference models. The DOI is normalized with the maximum, calculated DOI, thus the DOI values will be close to 0 where the models are well constrained by the data as the two inversions show the same results. The DOI value approaches 1.0 where the result is controlled by the reference models. Both reference models are set at one tenth and ten times the average observed apparent resistivity (Oldenburg and Li, 1999; Marescot et al., 2003; Hilbich et al., 2009). We calculated the smoothed normalized DOI in RES2DINV, which takes a weighted average of the DOI value for a specific model call with the DOI values for the neighboring cells (Loke, 2017). The depth range of the models was extended to five times the median depth of investigation for the used spacing. At this depth the inversion model is thus close to the reference model and the DOI value close to unity. We used a cut-off value of the DOI of > 0.2 to identify unreliable model regions (as suggested by Oldenburg and Li, 1999) and set the number of iterations to 4 for each DOI calculation.

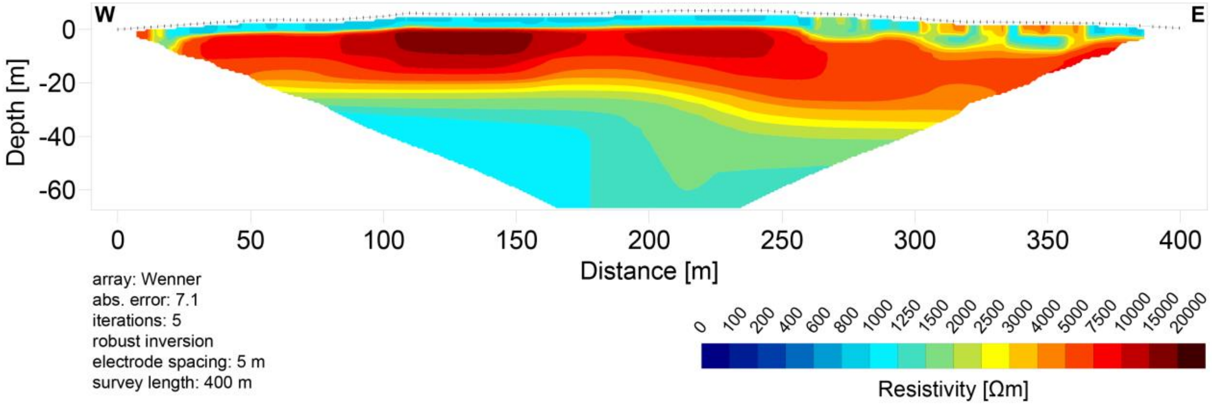

Figure M: ERT cross profile in the center of GOF #3 (Profile A, see Figure B for location, 0-400 m). DOI for this profile is shown in Figure N.

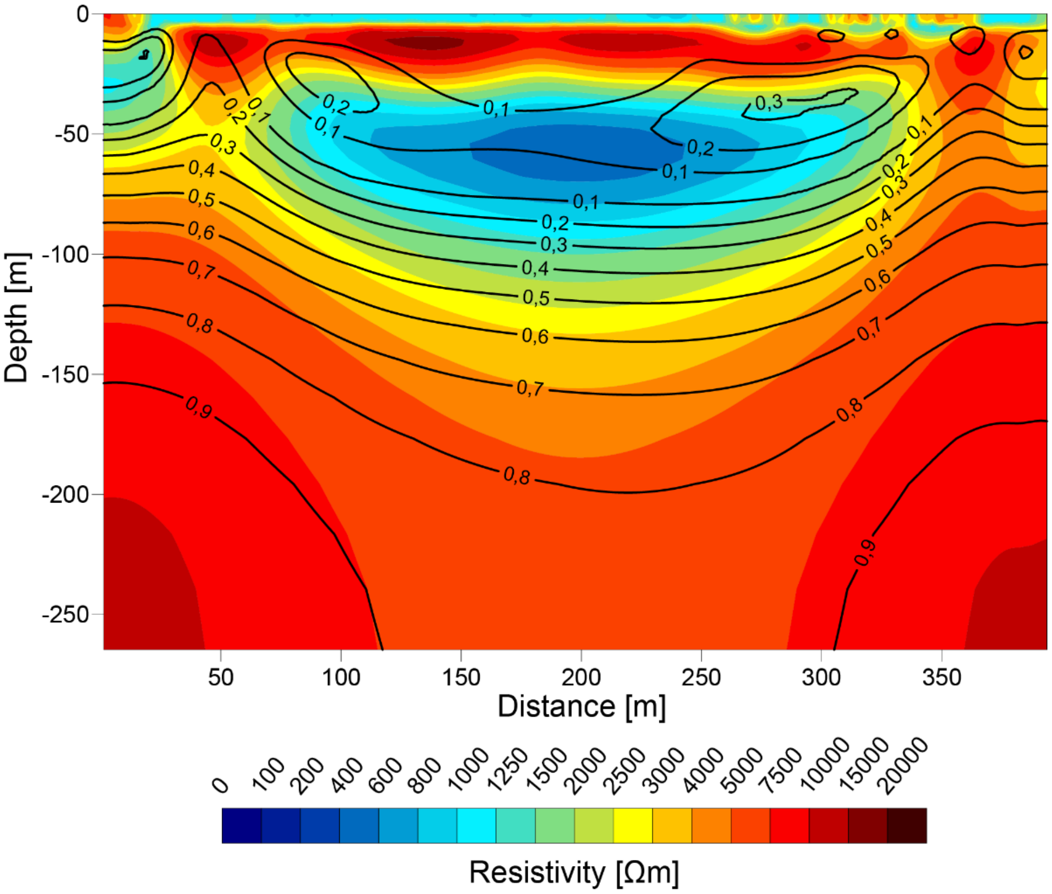

Figure N: DOI (contour lines in figure) for ERT profile A (cross profile in the center of GOF #3, see Figure B for location, 0-400 m).

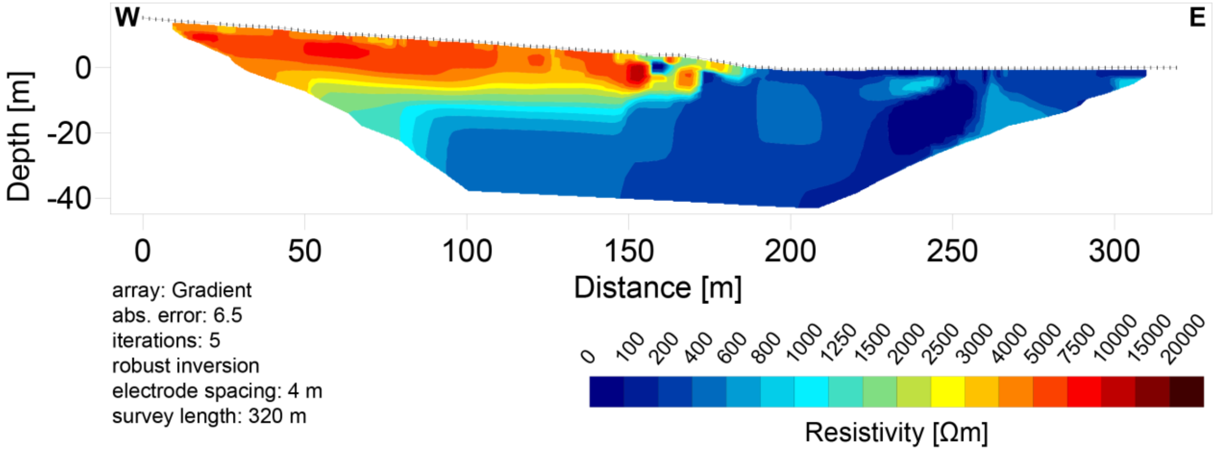

Figure O: ERT profile at the interface between GOF #3 and fluvial deposit of the Rhone (Profile B, see Figure B for location, 0-320 m). DOI for this profile is shown in Figure P.

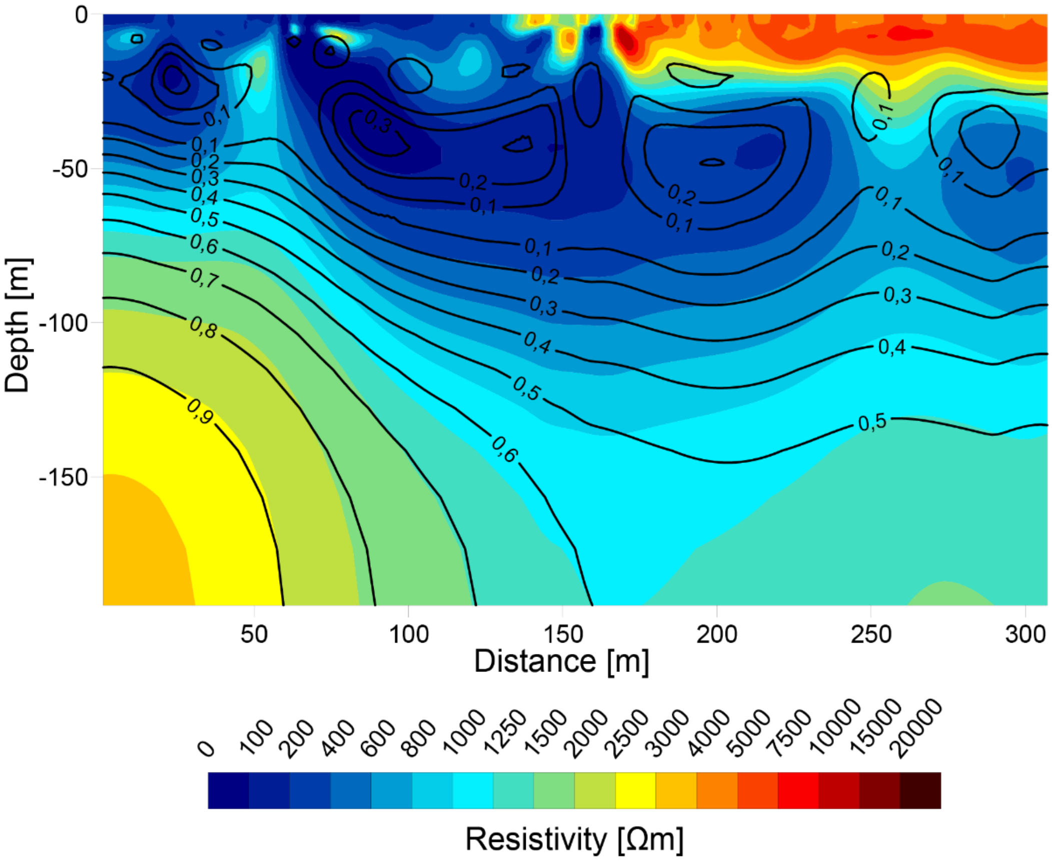

Figure P: DOI (contour lines in figure) for ERT profile B (intersection zone of GOF #3 and fluvial deposit of the Rhone, see Figure B for location, 0-320 m).

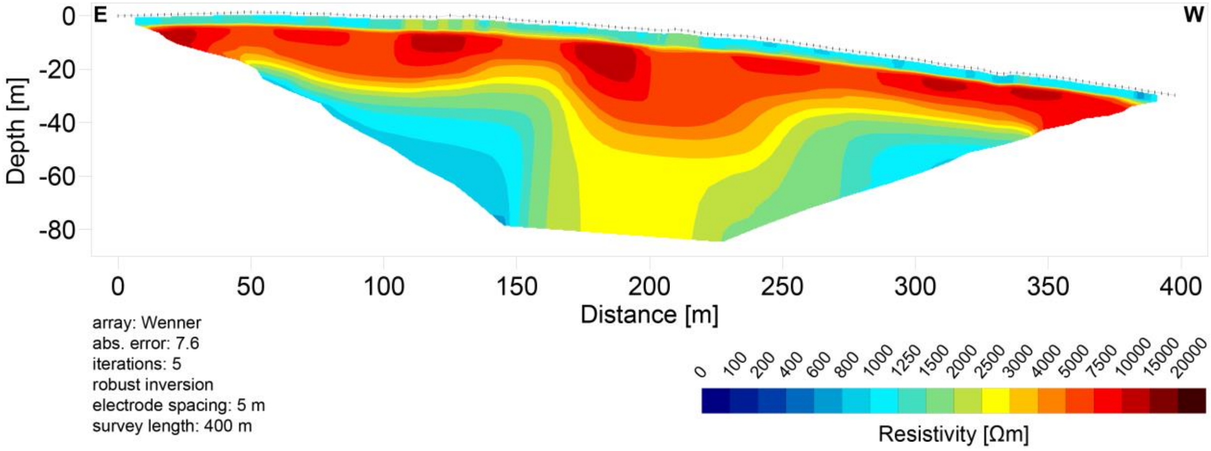

Figure Q: ERT cross profile on the upper GOF #3 (Profile C, see Figure B for location, 0-400 m). DOI for this profile is shown in Figure R.

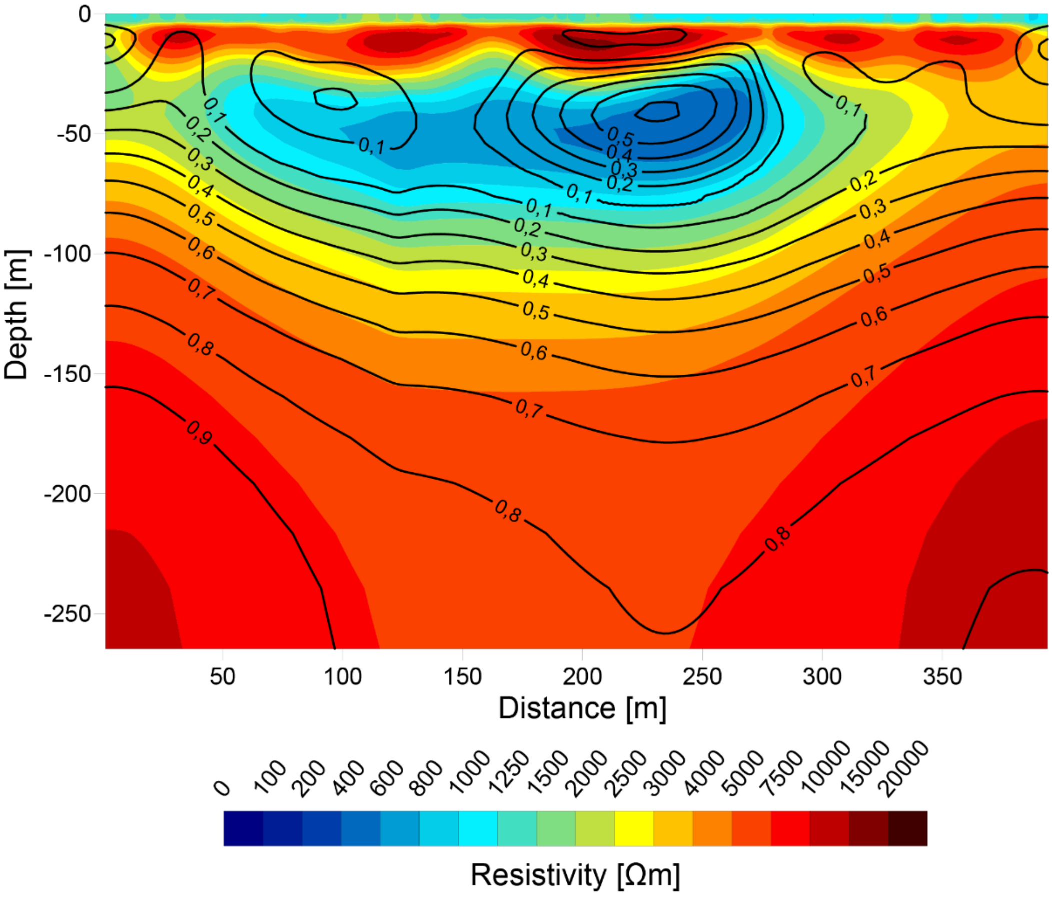

Figure R: DOI (contour lines in figure) for ERT profile C (cross profile on the upper GOF #3, see Figure B for location, 0-400 m).

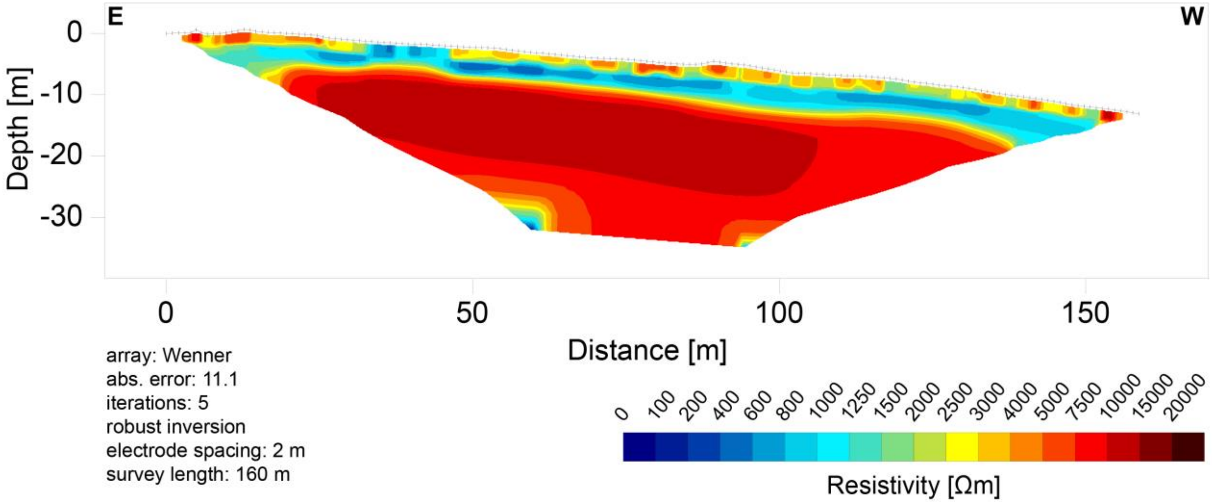

Figure S: ERT cross profile on the upper GOF #3 (Profile C, see Figure B for location, 120-280 m). DOI for this profile is shown in Figure T.

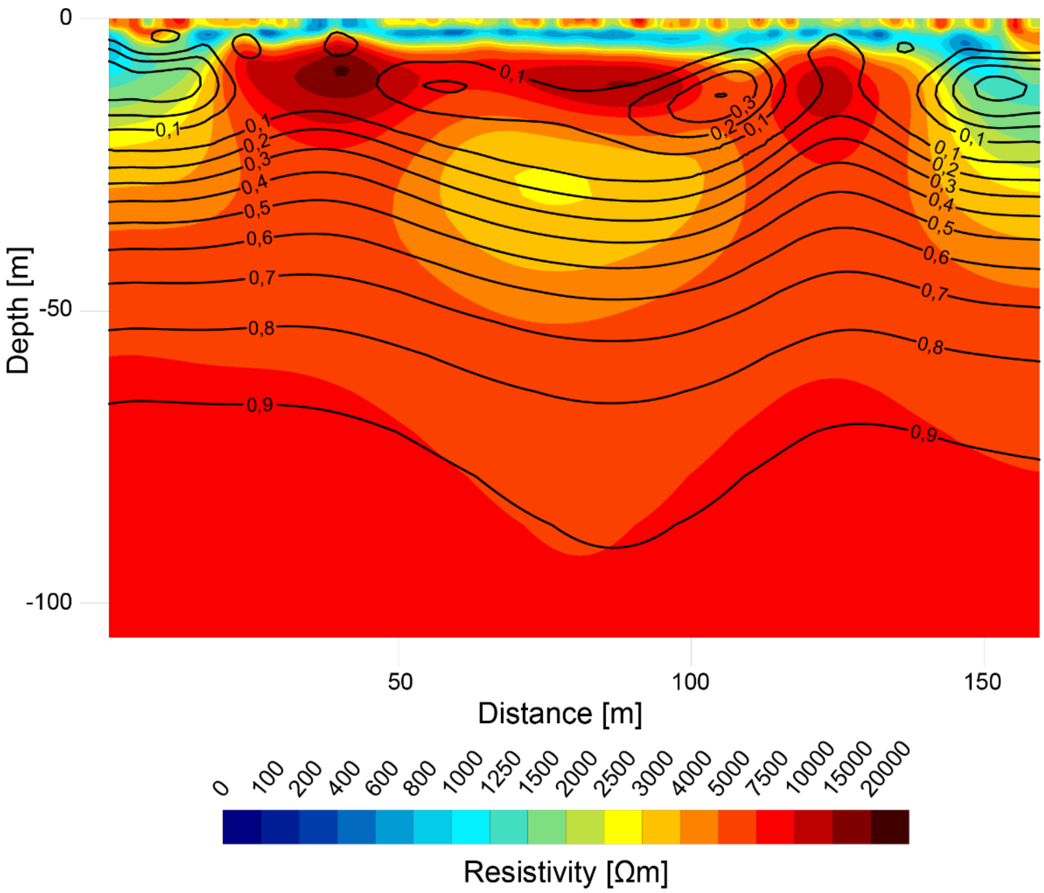

Figure T: DOI (contour lines in figure) for ERT profile C (cross profile on the upper GOF #3, see Figure B for location, 120-280 m).

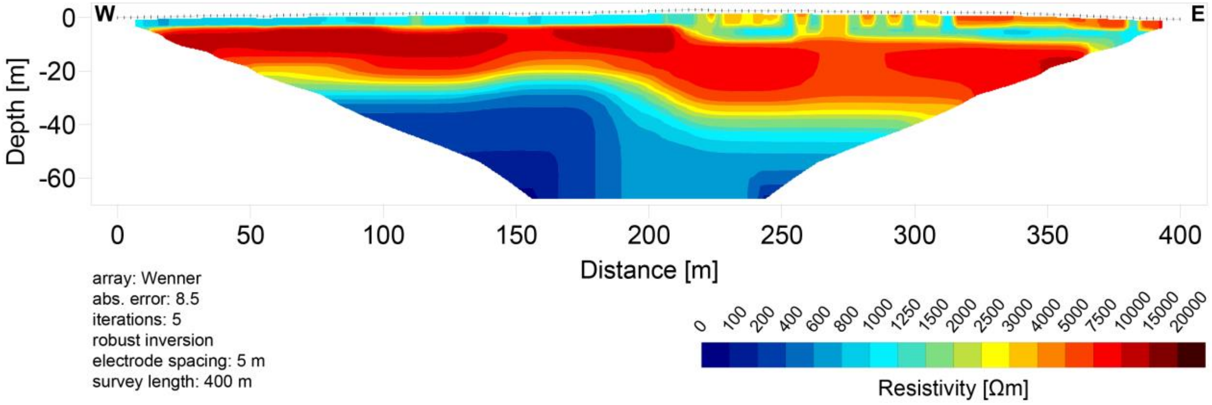

Figure U: ERT cross profile on the lower GOF #3 (Profile D, see Figure B for location, 0-400 m). DOI for this profile is shown in Figure V.

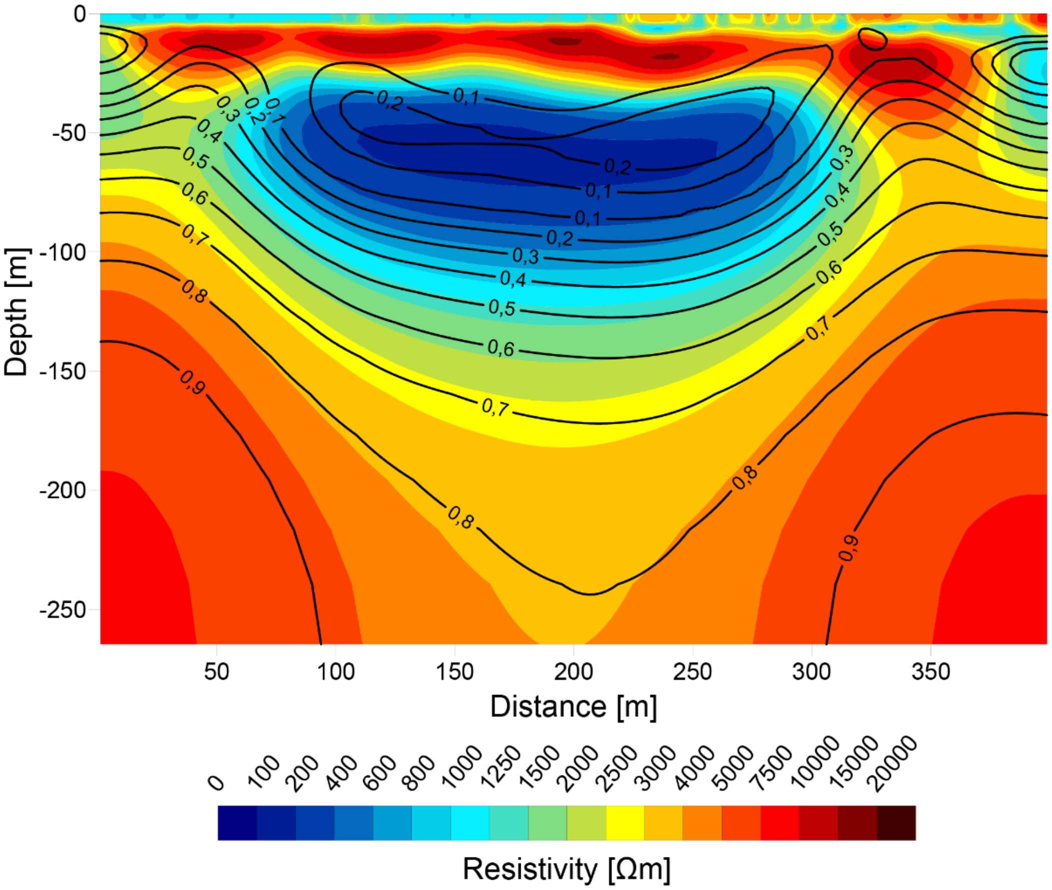

Figure V: DOI (contour lines in figure) for ERT profile D (cross profile on the lower GOF #3, see Figure B for location, 0-400 m).

Table W: Range of resistivities for different materials (compiled from different sources).

Material	**Range of resistivity [Ωm]**
Sediments with distinct grain sizes	
Clay (Telford et al., 1990; Milsom, 2003; Knödel et al., 2005)	1 - 100
Clay (moist) (Knödel et al., 2005)	3 - 30
Clay (dry) (Knödel et al., 2005)	> 1,000
Quaternary/recent sands (Reynolds, 1997)	50 - 100
Dry sandy soil (Reynolds, 1997)	80 - 1,050
Sand (dry) (Knödel et al., 2005)	> 10,000
Sand (saturated) (Knödel et al., 2005)	50
Sand and gravel (Reynolds, 1997)	30 - 225
Loose sand (Milsom, 2003)	500 - 5,000
Gravel (Milsom, 2003)	100 - 600
Gravel (dry) (Reynolds, 1997)	1,400
Gravel (saturated) (Reynolds, 1997)	100
Gravel (dry) (Knödel et al., 2005)	> 10,000
Gravel (saturated) (Knödel et al., 2005)	50
Other material	
Groundwater (natural waters) (Knödel et al., 2005)	10 - 300
Air (Kneisel and Hauck, 2008)	Infinity
Surface waters (sediments)/Natural waters (sediment)/Soil waters (Telford et al., 1990)	10 - 100
Landforms/unsorted sediments	
Alluvium and sand (Reynolds, 1997)	10 - 800
Till (Sass, 2007)	500 - 3,000
Moraine (Reynolds, 1997)	10 - 5,000
Moraine (veg. covered, Egesen) (Sass, 2006)	500 - 3,000
Moraines, consolidated/wet (Haeberli et al., 1990)	1,000 - 10,000
Groundwater in debris/moraine (Haeberli et al., 1990)	500 - 2,000
Debris (coarse, loose) (Sass, 2006)	8,000 - >20,000
Coarse, dry debris (Haeberli et al., 1990)	1,000 - 10,000
Debris (consolidated) (Sass, 2006)	6,000 - 15,000
Debris (fine or veg. covered) (Sass, 2006)	2,000 - 8,000
Debris (fluvially reassorted) (Sass, 2006)	1,000 - 4,000
Loose debris (Sass, 2007)	1,000 - 20,000
Compacted, wet debris (Sass, 2007)	1,000 - 15,000
debris flow deposits (normal size/magnitude) (Dietrich and Krautblatter, 2017)	up to 10,000
debris flow deposits (Sass, 2006)	up to 10,000
debris flow deposits (Silhan and Panek, 2010)	up to 7,000
debris flow deposits (Haeberli et al., 1990)	up to 2,500
talus slopes in alpine valley with dry coarse debris (higher resistivities at bottom of talus where boulders are largest) (Otto and Sass, 2006)	up to 20,000
rock avalanche deposits with large boulders (Knapp et al., 2021)	> 2,000
(catastrophic) rock slope failure deposits (coarse grained dry sediments) (Hilger et al., 2018)	14,000 - > 36,000

Material	**Range of resistivity [Ωm]**
Bedrock (exposed in feeder basin of fan 3)	
Gneiss (Telford et al., 1990) (Kneisel and Hauck, 2008)	68,000 (wet) - 3,000,000 (dry) 100 - 1,000
Magmatites, metamorphites (Reynolds, 1997)	150 (weathered, moist) - > 1,000,000 (compact)

Snow depth analysis for surface exposure dating

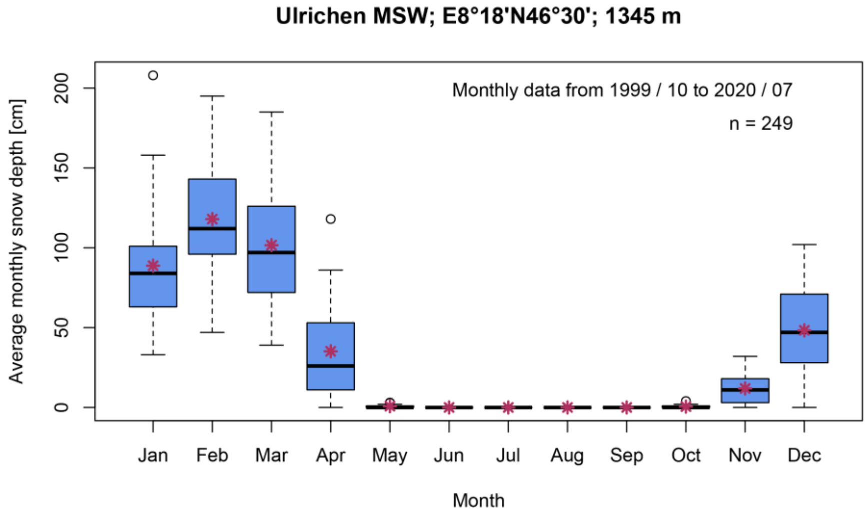

Figure X: Boxplots of monthly averaged snow depth as measured at the MeteoSwiss station Ulrichen between October 2010 and July 2020; mean monthly averages are indicated by the red stars. Data kindly provided through MeteoSwiss IDAWEB portal.

Borehole data

Borehole data for the canton Valais is available via https://geocadast.crealp.ch/. 35 boreholes were drilled and recorded upstream of GOF #3 with depth ranging mostly between 6-8.5 m, but several boreholes are up to 20 m in depth. Further borehole data is available for the fans and their very close vicinity. 14 boreholes are located on and near GOF #3, six boreholes are located on or near GOF #2 and eight boreholes on GOF #1. These have depth of 60-114 m and in 11 cases reach bedrock.

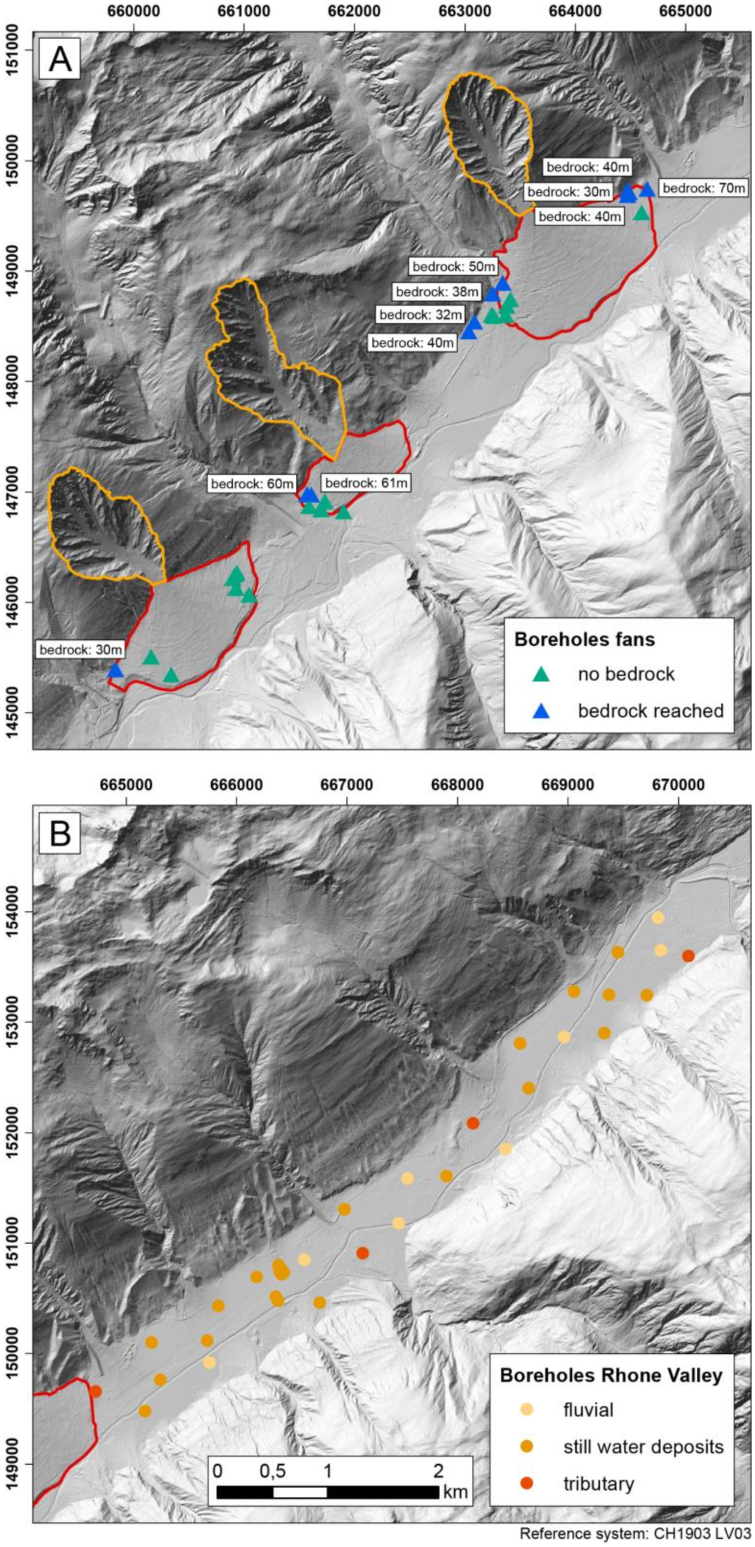

Figure Y: A: Locations of 28 boreholes on or near GOFs. Labels: depth at which bedrock is reached [m]. B: Locations of 35 boreholes in the Upper Rhone Valley upstream of GOF #3 (data: https://geocadast.crealp.ch; swisstopo DEM, EPSG:21781).

B. Supplementary material for chapter 7: Multivariate geostatistical modeling of the spatial sediment distribution in a large scale drainage basin, Upper Rhone, Switzerland

The tables and figures in the supplement are referred to in the corresponding chapter.

Table Z: Dates and specifications of Landsat scenes used to compute the maximum normalized difference vegetation index (NDVI) of each cell. The scenes were selected based on a minimal snow and cloud cover within the study area and a high image quality.

Acquisition date	Spacecraft	Sensor	Path	Row	Cloud cover [%]	Image quality
1986-10-17	LANDSAT_5	TM	195	028	20	7
1987-08-17	LANDSAT_5	TM	195	028	30	9
1999-07-25	LANDSAT_7	ETM	195	028	4	9
2001-07-30	LANDSAT_7	ETM	195	028	8	9
2003-08-13	LANDSAT_5	TM	195	028	0	9
2003-09-14	LANDSAT_5	TM	195	028	0	9
2004-07-14	LANDSAT_5	TM	195	028	24	9
2006-09-22	LANDSAT_5	TM	195	028	23	9
2009-09-30	LANDSAT_5	TM	195	028	15	9
2010-07-31	LANDSAT_5	TM	195	028	14	7
2010-09-01	LANDSAT_5	TM	195	028	1	9

Table AA: Variance inflation factor (VIF) values of the original input variables and of selected variables based on the results of the first analysis. VIF values larger than 10 indicate a problematic amount of collinearity. For abbreviations of variables refer to Table 7-1 in chapter 5

Variables	Test 1: VIF values	Test 2: VIF values
dem	3.566	3.404
slp	3.926	3.367
slp25	28.838	3.675
acclog	13.003	1.207
accslp	3.884	4.244
asp_ns	1.125	1.328
asp_ew	1.027	1.030
plc10	243437817695703	1.971
prc10	360287970189640	2.316
cur10	1000799917193440	
plc25	128674275067728	2.330
prc25	166799986198907	3.273
cur25	450359962737050	
ndr	3.050	3.042
sr	1.620	1.643
rou	1.183	1.144
rou25	1.327	1.212
rel40	26.238	
hi40	1.679	1.587
ndvi	2.729	2.614
vdc	3.231	3.300
twi	15.047	

Table BB: Thematic consistency of generalized additive model with input variables transformed with a smoothing spline with two degrees of freedom (GAM2df) for different sample sizes based on 10 individual models build. Relative variable selection frequencies (VF) as well as the variable selection frequencies of non-transformed (N) and transformed (S) variables are calculated for each independent input variable. For abbreviations of variables refer to Table 7-1 in chapter 5.

Samp. size	100			200			400			800			1600			3200			6400			12800			25600			51200		
	VF [%]	N	S	VF [%]	N	S	VF [%]	N	S	VF [%]	N	S	VF [%]	N	S	VF [%]	N	S	VF [%]	N	S	VF [%]	N	S	VF [%]	N	S	VF [%]	N	S
acclog	30	2	1	40	1	3	30	2	1	10	1	-	10	-	1	30	3	-	10	1	-	30	3	-	90	3	6	100	3	7
accslp	20	2	-	30	3	-	20	2	-	0	-	-	50	3	2	50	4	1	30	3	-	60	-	6	30	-	3	50	-	5
asp_ew	10	1	-	30	2	1	30	2	1	80	5	3	90	6	3	100	8	2	100	5	5	100	1	9	100	1	9	100	-	10
asp_ns	30	1	2	20	2	-	50	1	4	60	1	5	90		9	100	-	10	100	-	10	100	-	10	100	-	10	100	-	10
dem	20	2	-	10	1	-	10	1	-	30	1	2	30		3	30	-	3	60	-	6	100	-	10	100	-	10	100	-	10
hi40	40	2	2	40	-	4	60	6	-	80	5	3	80	2	6	100	2	8	100	1	9	100	-	10	100	-	10	100	-	10
ndr	10	1	-	30	1	2	30	2	1	80	4	4	100	1	9	100	1	9	100	-	10	100	-	10	100	-	10	100	-	10
ndvi	20	1	1	90	6	3	100	4	6	100	2	8	100		10	100	-	10	100	-	10	100	-	10	100	-	10	100	-	10
plc10	30	3	-	10	1	-	10	1	-	10	-	1	20		2	0	-	-	10	-	1	40	-	4	30	-	3	90	-	9
plc25	20	2	-	0	-	-	40	-	4	30	-	3	60	1	5	40	-	4	50	-	5	90	-	9	90	-	9	100	-	10
prc10	10	1	-	20	2	-	0	-	-	20	-	2	10		1	30	-	3	20	-	2	0	-	-	50	-	5	60	-	6
prc25	30	3	-	30	2	1	40	3	1	60	4	2	50	4	1	70	2	5	80	1	7	100	1	9	100	-	10	100	-	10
rou	20	1	1	50	3	2	90	7	2	100	7	3	100	3	7	100	2	8	100	-	10	100	-	10	100	-	10	100	-	10
rou25	30	2	1	60	5	1	30	1	2	60	1	5	70		7	100	-	10	100	-	10	100	-	10	100	-	10	100	-	10
slp	70	2	5	70	3	4	60	1	5	90	1	8	100	1	9	100	-	10	100	-	10	100	-	10	100	-	10	100	-	10
slp25	70	2	5	90	2	7	100	2	8	100	-	10	100		10	100	-	10	100	-	10	100	-	10	100	-	10	100	-	10
sr	60	5	1	20	2	-	40	2	2	30	1	2	40	1	3	90	1	8	60	-	6	100	-	10	100	-	10	100	-	10
vdc	40	4	-	60	3	3	40	3	1	70	4	3	100	2	8	100	-	10	100	-	10	100	-	10	100	-	10	100	-	10

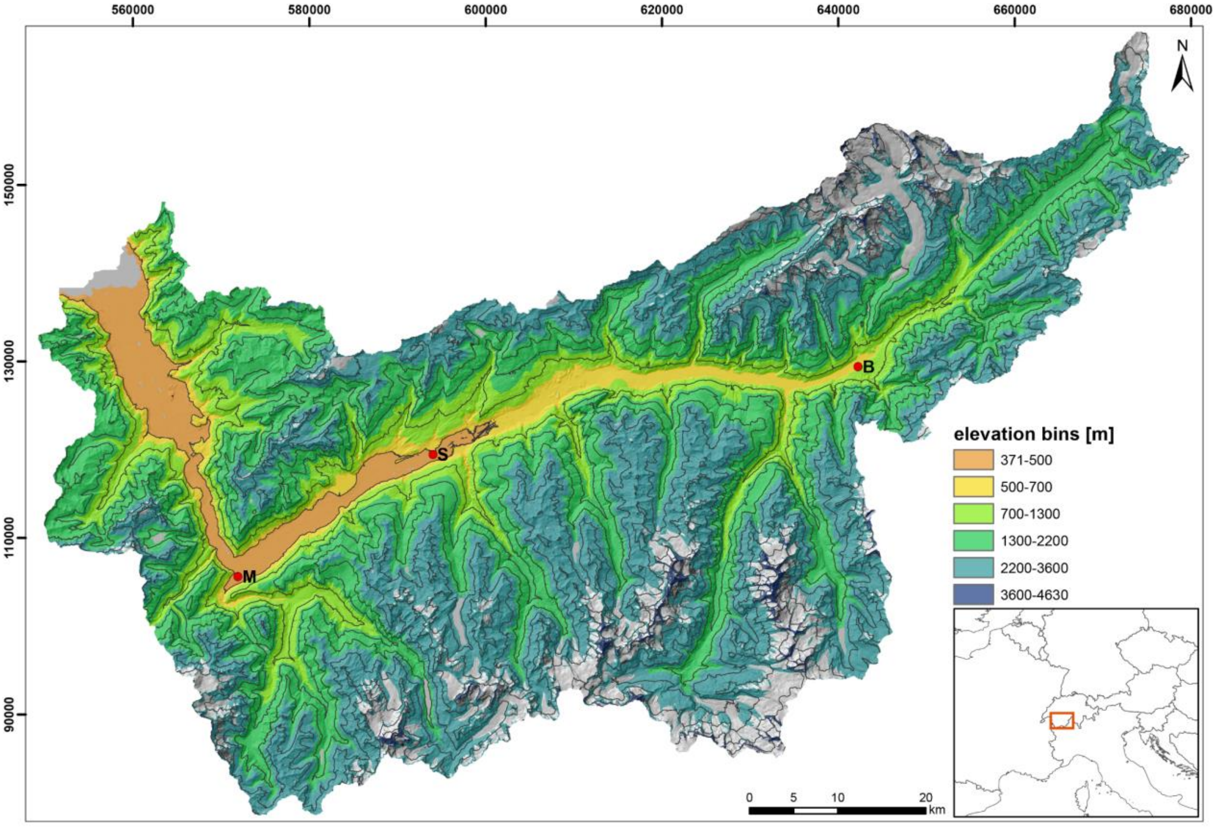

Figure CC: Elevation bins in the URB (M=Martigny, S=Sion, B=Brig) referred to in Figure 7-7 in chapter 7. 500 m contour line are shown (DEM from swisstopo, projection: CH1903).